Integrative analysis of the mineralogical and chemical composition of modern microbialites from ten Mexican lakes: What do we learn about their formation?

Nina Zeyen, Karim Benzerara, Olivier Beyssac, Damien Daval, Elodie Muller, Christophe Thomazo, Rosaluz Tavera, Purificación López-García, David Moreira, Elodie Duprat

Integrative analysis of the mineralogical and chemical composition of modern microbialites from ten Mexican lakes: what do we learn about their formation?

Nina Zeyen[a+], Karim Benzerara*[a], Olivier Beyssac[a], Damien Daval[b], Elodie Muller[a], Christophe Thomazo[c,d], Rosaluz Tavera[e], Purificación López-García[f], David Moreira[f] and Elodie Duprat[a]

[a] *Sorbonne Université, Muséum National d'Histoire Naturelle, UMR CNRS 7590. Institut de Minéralogie, de Physique des Matériaux et de Cosmochimie (IMPMC), 4 Place Jussieu, 75005 Paris, France.*

[b] *Laboratoire d'Hydrologie et de Géochimie de Strasbourg, EOST-ENGEES, Univ Strasbourg, EOST CNRS UMR 7517, 67084 Strasbourg, France*

[c] *UMR CNRS/uB6282 Biogéosciences, Université de Bourgogne Franche-Comté, 6 Bd Gabriel, 21000, Dijon, France*

[d] *Institut Universitaire de France*

[e] *Departamento de Ecología y Recursos Naturales, Universidad Nacional Autónoma de México, DF México, México*

[f] *Ecologie, Systématique et Evolution, CNRS, Université Paris-Saclay, AgroParisTech, Orsay, France*

* Corresponding author

Tel.: +33(0)144277542

E-mail address: karim.benzerara@upmc.fr

[+] *Now at Department of Earth and Atmospheric Sciences, University of Alberta, Edmonton, AB T6G 2E3, Canada*

Keywords: microbialites; crater lake; alkalinity; monohydrocalcite; (Mg-)calcite; aragonite; hydromagnesite; kerolite; REE+Y

Submitted to Geochimica et Cosmochimica Acta – Second revised Version

ABSTRACT

Interpreting the environmental conditions under which ancient microbialites formed relies upon comparisons with modern analogues. This is why we need a detailed reference framework relating the chemical and mineralogical compositions of modern microbialites to the physical and chemical parameters prevailing in the environments where they form. Here, we measured the chemical, including major and trace elements, and mineralogical composition of microbialites from ten Mexican lakes as well as the chemical composition of the surrounding waters. Saturation states of lakes with different mineral phases were systematically determined and correlations between solution and solid chemical analyses were assessed using multivariate analyses. A large diversity of microbialites was observed in terms of mineralogical composition, with occurrence of diverse carbonate phases such as (Mg-)calcite, monohydrocalcite, aragonite, hydromagnesite, and dolomite as well as authigenic Mg-silicate phases (kerolite and/or stevensite). All lakes harbouring microbialites were saturated or supersaturated with monohydrocalcite, suggesting that such a saturation state might be required for the onset of microbialite formation and that precursor soluble phases such as amorphous calcium carbonate and monohydrocalcite play a pivotal role in these lakes. Subsequently, monohydrocalcite transforms partly or completely to aragonite or Mg-calcite, depending on the lake $(Mg/Ca)_{aq}$. Moreover, lakes harbouring hydromagnesite-containing microbialites were saturated with an amorphous magnesium carbonate phase, supporting again the involvement of precursor carbonate phases. Last, authigenic Mg-silicates formed by homogenous or heterogenous nucleation in lakes saturated or supersaturated with a phase reported in the literature as "amorphous sepiolite" and with a H_4SiO_4 concentration superior to 0.2 mM. A strong correlation between the alkalinity and the salinity of all the lakes was observed. The observed large variations of alkalinity between the lakes relate to varying concentration stages of an initial alkaline dilute water, due to a varying hydrochemical functioning. In all cases, the size of microbialites in the lakes correlated positively with salinity, $(Mg/Ca)_{aq}$ ratio and alkalinity. The trace element compositions of the microbialites also varied significantly between the lakes. Detrital contamination of the studied microbialites was the major factor affecting their rare earth elements (REE)+Y patterns. In particular, the microbialites highly affected by detrital contamination showed a high (REE+Y) content and flat (REE+Y) patterns. In contrast, some microbialites poorly affected by detrital contamination showed (REE+Y) patterns with features commonly reported for marine microbialites, such as a superchondritic Y/Ho ratio, enrichment in heavy REE and a negative Ce anomaly. This last observation

questions the possibility to infer the marine *versus* lacustrine origin of a microbialite only based on (REE+Y) patterns. Overall, while microorganisms can impact nucleation processes and textural arrangements in microbialites, we observe that the hydrogeochemical evolution of lakes exerts a primary control over the onset of microbialite formation and the evolution of their chemical and mineralogical composition. Moreover, while changes of all these chemical and mineralogical features upon diagenesis and metamorphism will need to be assessed, the present study, together with recent meta-analyses of modern microbialites, broadens the set of modern references available for comparisons with geological archives.

INTRODUCTION

Microbialites are organo-sedimentary rocks formed by the trapping and binding of detrital sediments and/or the precipitation of authigenic minerals by benthic microbial communities (Burne and Moore, 1987). These rocks are abundant in the geological record and are considered as being among the oldest traces of life (Allwood et al., 2006; Van Kranendonk et al., 2008; Nutman et al., 2016). Both marine and lacustrine microbialites have been found in the geological record (Kamber et al., 2004; Awramik and Buchheim, 2009). Yet, it has been sometimes difficult to determine the environmental conditions in which they formed. For instance, stromatolites from the 2.7 Ga old Tumbiana Formation have been interpreted either as shallow marine (Thorne and Trendall, 2001; Sakurai et al., 2005) or lacustrine (Buick, 1992; Bolhar and Van Kranendonk, 2007; Awramik and Buchheim, 2009; Stüeken et al., 2015) deposits. This calls for establishing diagnostic criteria, which could help discriminate between different formation environments for these sedimentary archives.

Unlike their marine counterparts, modern lacustrine microbialites form under a wide diversity of conditions obscuring the search for analogues of ancient lacustrine settings and requesting a good appraisal of this diversity. For example, lakes populated by modern microbialites show a broad range of pH from 7.5 in the Cuatro Ciénegas basin located in Mexico, to 10.5 in Lake Bogoria and Lake Magadi in Kenya (Centeno et al., 2012; Harris et al., 2013). Many of these lakes are hypersaline, with salinity values up to 200 g/l for Lake Big Pond (Eleuthera, Bahamas) (Glunk et al., 2011), while some lakes are characterized by moderate salinity, including Lake Tanganyika with a salinity as low as 0.5 g/l (Harris et al., 2013). Microbialites are formed in lakes showing a large range of $(Mg/Ca)_{aq}$ ratios ranging between 0.5 for the Ruidera Pool in Spain (Souza-Egipsy et al., 2006), up to 90 for Lake Walyungup in Western Australia (Coshell et al., 1998). In association with this environmental

diversity, modern lacustrine microbialites show a large range of morphologies and microfabrics (*e.g.*, Kempe et al., 1991; López-García et al., 2005; Harris et al., 2013). There is also a broad diversity of mineralogical compositions, including various carbonate phases such as hydromagnesite (*e.g.*, Braithwaite and Zedef, 1994), aragonite and calcite (*e.g.*, Arp et al., 1999a; Guo and Chafetz, 2012), aragonite and dolomite (*e.g.*, Last et al., 2012), or monohydrocalcite (MHC; *e.g.*, Rosen et al., 2004). In addition to carbonates, authigenic Mg-silicates such as smectites (saponite, stevensite), kerolite or sepiolite, have been detected as sometimes abundant phases in several lacustrine microbialites from different localities (Arp et al., 2003; Souza-Egipsy et al., 2005; Reimer et al., 2009; Benzerara et al., 2010; Burne et al., 2014; Zeyen et al., 2015; Pace et al., 2016; Gérard et al., 2018).

Overall, there is a need to link the diversity of microbialite features with their formation conditions. For example, the macroscopic morphology, size and spatial distribution of microbialites have been used to infer the distance to the coast, the water lake level, the presence of groundwater seepage or the impact of tectonic activity (*e.g.,* gravity deposits) (Cohen et al., 1997; Sarg et al., 2013; Bahniuk et al., 2015; Bouton et al., 2016). A recent study emphasized the importance of the chemistry and geometry of the substrates and the seasonal variations on the morphology of microbialites (Roche et al., 2019). The macro and/or micro-textures of microbialites have been used to assess the potential involvement of microorganisms in their formation (Arp et al., 1998; Knoll et al., 2013; Theisen et al., 2015). Isotopic compositions (*e.g.,* nitrogen and/or sulfur isotopes) of organic matter (kerogen) and/or bulk composition of ancient microbialites have been used to infer past metabolic activities of diverse microorganisms and/or the environmental conditions prevailing on the early Earth (*e.g.,* Bontognali et al., 2012; Thomazo et al., 2011; Stüeken et al., 2015). Finally, rare earth element (REE) patterns of some ancient stromatolites have been used to determine their formation environment, in particular marine or lacustrine (*e.g.*, Kamber and Webb, 2001; Bolhar and Van Kranendonk, 2007; Siahi et al., 2018). However, REE+Y patterns of modern marine or continental microbialites remain surprisingly scarce in the literature (*e.g.*, Chagas et al., 2016).

Several studies have coupled analyses of the mineralogical and chemical composition of microbialites with the lake water chemistry at one single locality/lake (*e.g.*, Lim et al., 2009; Power et al., 2011). Only recently, Chagas et al. (2016) developed a meta-analysis including such data from a larger number (n=21) of lakes. In addition, Valdespino-Castillo et al. (2018) and Iniesto et al. (2021) used a similar approach with a focus on the links between microbial diversity and microbialite or water chemistry, from five and ten locations, respectively, including several lakes in Mexico. These recent studies significantly improve our capability to

grasp the relationships between environmental conditions prevailing during microbialite formation and their chemical and mineralogical composition.

Here, we present an integrative analysis (defined as a comparative study integrating different data acquired on samples from different locations by a single research group and using a single set of protocols) of microbialites from ten Mexican volcanic lakes located in the trans-Mexican volcanic belt (TMVB) (Ferrari et al., 2012; Sigala et al., 2017). Some of these lakes were already included in the meta-analysis by Chagas et al. (2016). However, the present contribution adds (1) a novel dataset on three lakes in which microbialites had never been described before (Lakes Alberca de Guadalupe, Tecuitlapa and Aljojuca), and (2) new measurements for all sites, including bulk analyses of the major and trace elements (together with REE+Y) concentrations in the microbialites. The structure of prokaryotic and eukaryotic communities associated with the same microbialites was analyzed by Iniesto et al. (2021) based on massive 16S/18S rRNA gene amplicon sequencing. It was found that they all harbor a high diversity of microorganisms. Importantly, despite interlake community variations, a microbial core consisting of 247 operational taxonomic units was shown to be conserved across lake microbialites. Iniesto et al. (2021) suggested that this microbial core might be particularly important for carbonatogenesis. The present study focuses on a complementary piece of information, *i.e.*, relationships between microbialite chemistry/mineralogy and water chemistry. We uncover new relationships between the chemical/mineralogical composition of the lacustrine microbialites and their formation conditions and explore potential scenarios that could account for 1) the conditions necessary for microbialite formation in lakes and 2) the chemical and mineralogical diversity of Mexican lacustrine microbialites.

MATERIALS AND METHODS

1. Geological Setting

The ten lakes investigated in this study belong to the trans-Mexican volcanic belt (TMVB), a continental volcanic arc following an East-West orientation located in Central Mexico. It spans over almost 1000 km in length and 20 to 100 km in width, covering an area of about 160 000 km^2 (Ferrari et al., 2012) (Fig. 1a). The TMVB results from the subduction of the Rivera and Cocos plates beneath North America at the Middle American Trench during the Neogene period (Ferrari et al., 2012). Two types of volcanic rocks are generally described in this zone: (1) calc-alkaline rocks compatible with a subduction environment and (2) alkaline or transitional rocks with compositions similar to oceanic island basalts (Gómez-Tuena et al.,

2003). The TMVB hosts numerous monogenetic and shield volcanoes, lava domes and phreato-magmatic vents, sometimes leading to maar formation (Alcocer and Bernal-Brooks, 2010; Siebe et al., 2014). Six studied maar lakes are located on the eastern part of the TMVB in the Cuenca de Oriental basin (Puebla State): four of them (Lakes Alchichica, La Preciosa, Quechulac and Atexcac) are located in the Los Llanos de San Juan region (Fig. 1e) and two of them (Lakes Tecuitlapa and Aljojuca), in the Los Llanos de San Andrés region (Fig. 1f). Four other lakes are located in the central part of the TMVB in the Michoacán-Guanajuato volcanic field (MGVF). Two of them are maars (Lakes La Alberca de los Espinos and Alberca de Guadalupe – also called Alberca de Michoacan –, Fig. 1b and c, respectively) and the other two are lava-dammed basins (Lakes Zirahuén and Pátzcuaro, Fig. 1d). Table 1 summarizes the main known physical and hydrological characteristics of each studied lake.

These lakes formed during the Pleistocene between 0.33 Myr ago for Lake Atexcac (Carrasco-Núñez et al., 2007) and 23-20 kyr ago for Lake Alberca de Guadalupe (Siebe et al., 2014). The lakes located in the Cuenca de Oriental Basin are underlain by a Mesozoic limestone basement and by Pleistocene volcanic sequences, mostly basaltic rocks (Armienta et al., 2008). In addition, Lake Atexcac lays on a large andesitic basement (Carrasco-Núñez et al., 2007). The local basement of the lakes located in the Michoacán-Guanajuato volcanic field comprises basalts (Lake Zirahuén) and andesites (Lakes La Alberca de Los Espinos, Alberca de Guadalupe and Pátzcuaro). Investigated lakes are located at an elevation comprised between 1985 m (Lake La Alberca de Los Espinos) and 2380 m (Lake Tecuitlapa). Their maximum depth varies between 2.5 m for the shallowest (Lake Tecuitlapa) and ~62 m for Lake Alchichica.

All studied lakes are "closed lakes" located within endorheic basins (Alcocer and Bernal-Brooks, 2002; Davies et al., 2004; Armienta et al., 2008). The term "closed lake" refers to a lacustrine water body with a limited drainage basin that normally retains water and allows no surface outflow to external aquatic systems (*e.g.*, Almendinger, 1990). Accordingly, no surface outflow was observed for the closed lakes during our field campaigns whatever the season. Although we do not know their chemical composition, groundwater inflows/outflows very likely exist as suggested by Armienta et al. (2008) for all maar lakes and mentioned by Siebe et al. (2014) for Lake La Alberca de Guadalupe. Groundwater inflow was also inferred for Lake Alchichica (Kaźmierczak et al., 2011; Zeyen et al., 2019). Hydrological studies of Lake Pátzcuaro (Bischoff et al., 2004) and Lake Alchichica (García Martínez, 2010) also required underground water inflow and outflow to balance the water deficit between evaporation and rainfall.

2. Sample collection

Field campaigns were conducted in June 2007, January 2012 and May 2014. Here, we consider as microbialites all carbonate deposits varying from thin encrustations around basaltic pebbles (oncoliths) to well-developed, meter-scale and massive microbialites (mostly thrombolites). Microbialites from Lake Alchichica can be found down to at least 15 m in depth as reported by Saghaï et al. (2016). However, diving was not systematically performed so that depth distribution remains unknown for the other lakes. Several previous studies have investigated microbialites from Lake Alchichica (Kaźmierczak et al., 2011; Couradeau et al., 2011; Couradeau et al., 2013; Gérard et al., 2013; Saghaï et al., 2015; Valdespino-Castillo et al., 2018; Zeyen et al., 2019). Additionally, we previously described microbialites from Lakes La Preciosa, Quechulac, Atexcac, La Alberca de Los Espinos and Pátzcuaro (Zeyen et al., 2015; Zeyen et al., 2019). To complete the analyses previously performed on these 6 lakes, we sampled microbialites at several additional locations on the shores of these lakes. Moreover, we sampled three other lakes populated by microbialites, which to our knowledge, were undescribed to date: Lake Alberca de Guadalupe, Lake Tecuitlapa and Lake Aljojuca. “Living” microbialites (*i.e.*, microbialites covered and populated by a biofilm) were systematically sampled beneath the water level. In Lake Alchichica, samples were collected by scuba diving at different depths: 1, 5, 10 and 15 m depth in January 2012 (Saghaï et al., 2015) and 4 m depth (sample AL66) in June 2007. In addition, “non-living” microbialites (*i.e.*, dry and not covered by a biofilm, sometimes called “fossil” microbialites; *e.g.*, Casanova and Hillaire-Marcel, 1992; Bouton et al., 2016; Zeyen et al., 2019) were systematically sampled above the water level.

A summary of the location of aqueous samples and performed analyses is reported in Table SI-1. Surface water samples were collected from the shore of the lakes. Some were also collected at the center of Lake Atexcac (Atx-M) and its north shore (Atx-N) as well as at the center of Lake Alchichica (AL-M) and its west shore (AL-W). In addition, water was sampled with a Niskin bottle in May 2014 in the center of Lake Atexcac at 3, 10, 20 and 30 m depth and in January 2012 and May 2014 in the center of Lake Alchichica at 3, 10, 25, 40 and 55 m depth. Temperature, pH and specific conductance (conductivity normalized at 25°C) of lake surface waters were measured *in situ*. Two hundred milliliters of solution were systematically collected from each lake. Solutions were filtered on the same day using 0.22 µm GF/F filters and kept in sterile tubes. For major cation and $^{87}Sr/^{86}Sr$ analyses, 30 and 40 ml, respectively, of filtered solutions were acidified with nitric acid (2%). The remaining 130 ml were used for

measurements of alkalinity, anion and orthosilicic acid (H_4SiO_4) concentrations, without pre-acidification.

3. Chemical analyses of solutions

Orthosilicic acid (H_4SiO_4) concentrations were determined by continuous flow colorimetric analyses. For these analyses, water samples from Lake La Preciosa, Quechulac, Tecuitlpa, Aljojuca and Páztcuaro were diluted 10 times. Water samples from Lakes Atexcac, La Alberca de los Espinos and Alberca de Guadalupe were diluted 20, 50 and 100 times, respectively. Concentrations of nitrogen compounds (nitrites NO_2^-, nitrates NO_3^-, ammonium NH_4^+) and phosphates were measured on non-diluted water samples by continuous flow colorimetric analyses. Anion concentrations (fluorides F^-, chlorides Cl^-, bromines Br^-, and sulfates SO_4^{2-}) were measured by ion chromatography. Concentrations of major (Ca^{2+}, Na^+, Mg^{2+}, K^+) and minor (Al^{3+}, B_T ($B(OH)_3$ and $B(OH)_4^-$), Ba^{2+}, Cu^{2+}, Fe^{2+}, Mn^{2+}, Ni^{2+}, Sr^{2+}, Ti^{4+}, Zn^{2+}) cations were determined by inductively coupled plasma atomic emission spectrometry (ICP-AES). The uncertainty on the concentration measurements of orthosilicic acid, anions and cations was lower than 5%. Salinities were calculated from specific conductance and temperature data, after the method described by Aminot and Kérouel (2004) (Table SI-2).

Activities of anions, cations and orthosilicic acid as well as saturation indices of the surface water solutions of the lakes were calculated using the Visual MINTEQ software (Gustafsson, 2011). Table SI-3 summarizes precipitation reactions and solubility constants of the mineral phases included in our calculations and/or used to plot the solubility lines, *e.g.*, Ca- and/or Mg-carbonates (aragonite, calcite, Mg-calcite ($Mg_{0.1}Ca_{0.9}CO_3$), MHC, vaterite, dolomite, hydromagnesite, amorphous Ca-carbonate (ACC) and amorphous Mg-carbonate), silicates (sepiolite, "amorphous sepiolite", kerolite, talc, stevensite and amorphous silica) and hydroxyapatite. The temperatures of the lakes measured during sampling (Table SI-2) were systematically considered in the calculation of the saturation indices. Calculations were performed using the Davies method (Davies and Morgan, 1989) without allowing any mineral phase precipitation. The saturation index (*SI*) is defined as the decadic logarithm of the ratio of the ion activity product (*IAP*) over the solubility constant (*Ks*):

$$SI = \log (IAP/Ks) \qquad (1)$$

A solution is supersaturated with respect to a mineral phase when *SI* is positive.

Total alkalinities were determined by titration (Gran, 1952) using hydrochloric acid. Commercial mineral water (Evian) was used as a control. The uncertainty on alkalinity

measurements was lower than 1%. Alkalinity (*Alk*) is defined by Dickson (1981) as "the number of moles of hydrogen ion equivalent to the excess of proton acceptors (bases formed from weak acids with a dissociation constant $K \leq 10^{-4.5}$, at 25°C and zero ionic strength) over proton donors (acids with $K > 10^{-4.5}$) in one kilogram of sample", hence:

$$Alk = [HCO_3^-]+2[CO_3^{2-}]+[NH_3]+[H_2BO_3^-]+[H_3SiO_4^-]+[HPO_4^{2-}]+2[PO_4^{3-}]+[OH^-] -[HF]-[H_3PO_4]-[H^+] \quad (2)$$

with brackets indicating concentrations in $mol.kg_{sln}^{-1}$. Given the relatively low contributions of N, P, B, and Si species to alkalinity for the lakes considered in the present study (Tables SI-4 and SI-5), alkalinity was simplified as:

$$Alk = [HCO_3^-]+2[CO_3^{2-}] \quad (3)$$

Concentrations in HCO_3^- and CO_3^{2-} could thus be deduced from pH, alkalinity and the pKa of HCO_3^-/CO_3^{2-} (pKa =10.32 at 25°C).

In order to assess the fractionation of REE+Y between solutions and microbialites, REE + Y concentrations (of the lake solutions) were measured on five lake water samples collected in May 2014 (Alchichica, Atexcac, Quechulac, La Preciosa, La Alberca de Los Espinos) by ICP-MS at the *Service d'Analyse des Roches et Minéraux* (SARM, Centre de Recherches Pétrographiques et Géochimiques, Nancy, France).

Finally, strontium isotope ratios ($^{87}Sr/^{86}Sr$) of the surface water from 5 lakes sampled in May 2014 were measured: Alchichica (center of the lake), La Preciosa (north-east shore of the lake), Atexcac (center of the lake), La Alberca de Los Espinos (north shore of the lake) and Zirahuén (center of the lake). The automated purification of Sr from lake water samples was performed by high performance ion chromatography (HPLC-Dionex 300) according to the procedure described by Meynadier et al. (2006). Strontium isotope ratios ($^{87}Sr/^{86}Sr$) were measured using a Neptune multicollector ICP-MS (Thermo Scientific) at the High-Resolution Analytical Platform (PARI) of the Institut de physique du globe de Paris (IPGP). The strontium isotope ratios were measured three times for each sample, and the reported uncertainty corresponds to the 95% confidence interval calculated using the standard deviation obtained over these three replicates and Student's law.

4. Bulk mineralogical analyses of microbialites

A quantity of about 10 g for each microbialite sample was finely ground and homogenized in an agate mortar and aliquots of the same powdered sample were used for the

different bulk analyses. The surface of microbialite sample (including the dry biofilm) was included in each aliquot except for:

1) the non-living microbialite collected in Lake Quechulac. This sample was divided into three samples: the external surface part (Quechulac-4A-2012), the intermediary part (Quechulac-4B-2012) and the internal part (Quechulac-4C-2012).

2) the non-living microbialite encrusting a basalt collected in Lake Tecuitlapa. This sample was divided into two samples: the external part (Tec2014-05a) and the intermediate part (Tec2014-05b).

These five samples were finely ground separately in an agate mortar and aliquots of each powder sample were used for the different bulk analyses.

4.1. X-ray diffraction

The bulk mineralogical composition of microbialites was determined by x-ray diffraction (XRD). About 1 g of each microbialite sample was deposited on an aluminum sample holder. XRD measurements were performed using a Panalytical X'Pert diffractometer equipped with a cobalt anode (Co-Kα). Data were recorded at 40 kV and 40 mA in the continuous-scan mode between 5 and 90° (2θ) with a step of 0.016° and a total counting time of around 4 h. Diffractograms were analyzed using the PANalytical X'Pert Highscore software for background subtraction, peak finding, and matching with XRD patterns of reference compounds. Reference patterns were obtained from the international crystal structure database (ICSD, Fachinformationszentrum Karlsruhe, Germany; US Institute of Standards and Technology, USA).

4.2. Fourier transform infrared spectroscopy analyses

For Fourier transform infrared (FTIR) spectroscopy analyses, 2.5 mg of microbialite powder and 300 mg of potassium bromide (KBr) were mixed and ground in an agate mortar. A KBr pellet was prepared for each microbialite sample using a vacuum press under 8 tons of pressure for 1 minute. Pellets were placed overnight in a drying oven (95°C) to remove the adsorbed water vapor and were pressed a second time. Transmission spectra were recorded between 400 and 4000 cm^{-1}, using a Nicolet 6700 FTIR spectrometer.

5. Microscopy and spectroscopy analyses of microbialites

5.1. Raman microspectroscopy and mapping

Raman spectromicroscopy was performed on a polished petrographic thin section of a microbialite from Lake Ajojuca (Aljo2014-02), which was composed of three different Ca-carbonate phases (Mg-calcite, MHC and aragonite) as determined by XRD. For this sample, fluorescence induced by the incident laser was low enough so that it did not prevent Raman analyses. Raman spectra were recorded using a Renishaw InVia spectrometer equipped with a 785 nm Renishaw diode laser. The laser was focused on the sample using a DM2500 Leica microscope with a 50× objective (NA= 0.55) to obtain a planar resolution of ~ 5 μm^2. The laser power at the sample surface was set at around 1 mW using neutral density filters to avoid damages due to laser-induced heating. The signal was filtered by edge filters and dispersed by a diffraction grating with 1200 grooves/mm and the signal was analyzed with a RENCAM CCD (charge-coupled device) detector. Before each session, the spectrometer was calibrated using a silicon standard. Spectra were collected using the software WIRE 4.1 provided by Renishaw. The streamline technology provided by Renishaw was used to perform dynamic line-scanning Raman mapping on the petrographic section (Bernard et al., 2008). Mosaics were compiled from 40 112 Raman spectra over a 1240 × 1300 μm^2 with a stepsize of 6 µm in the x-direction and 6.2 µm in the y-direction. The laser power at the sample surface was set at around 0.5 $mW/\mu m^2$ when using the line-scanning mode.

5.2. Scanning electron microscopy analyses

Some microbialite samples (ATX-2C1-2012, ATX-2014-13, ATX2014-02; Preciosa05-2012, Pr2014-09, Quechulac1A-2012, AlbEsp2014-01, AL2012-10m, AL2012-12, AL2012-15, Alb2014-02) were sawed to obtain ~5 mm thick sections. They were polished with diamond polishing paste with a grain size down to a ¼ of a micrometer. Thin-sections were rinsed with two consecutive ultrasonic cleaning baths with 100% ethanol, then milliQ water. Finally, polished sections were dried overnight in an evacuated desiccator. Samples were mounted on 2.5 cm wide aluminum stubs using double-sided carbon tape. Some microbialite samples were embedded in resin (AL13, AL66, AL2014-13, AL2014-15, AlbEsp2014-01, Patz2014-02, Aljo2014-02). For this purpose, microbialite fragments were fixed in a 2.5% formaldehyde solution (methanol free, ultra pure; Polysciences, Inc.) for 4 h at 6°C, then washed 3 times in a phosphate-buffered saline (PBS) solution and finally stored in (1/1) ethanol/PBS at 20°C. Samples were then dehydrated through a graded series of ethanol solutions, each during 30 min (ethanol/milliQ water volume ratios at 15, 30, 50, 70, 90, and 99%), and during 12 h in an ethanol/water volume ratio of 99%. Samples were progressively embedded in a hard grade LR-white resin (Polysciences, Inc.) by incubating the samples at 6°C for 18 h in (1) a 1:2 mixture

of LR-white:ethanol, then (2) a 2:1 mixture of LR-white:ethanol and (3) pure LR-white resin. After 1 h at room temperature, samples were embedded in pure LR-white resin for 1 h at 40°C and for 24 h at 60°C. After polymerization, transverse sections were cut with a diamond wire to obtain ~2 mm thick sections and polished with diamond paste down to a ¼ of a micrometer. After rinsing, thin sections were dried overnight in an evacuated desiccator. Samples were mounted on 1.25 cm wide aluminum stubs using double-sided carbon tape before carbon coating.

Scanning electron microscopy (SEM) analyses were performed using a Zeiss Ultra 55 field emission gun SEM. Backscattered electron (BSE) images were acquired using an angle selective backscattered (AsB) detector at an accelerating voltage of 15 kV, a working distance of ~7.5 mm and a 60 µm aperture at high current. The elemental composition of mineral phases was determined by energy dispersive X-ray spectrometry (EDXS) using an EDS QUANTAX detector. EDXS data were analyzed using the ESPRIT software package (Bruker).

6. Bulk chemical analyses of microbialites

Concentrations of major elements, total organic carbon, total sulfur and trace elements were measured on 32 microbialite samples at the *Service d'Analyse des Roches et Minéraux* (SARM, Centre de Recherches Pétrographiques et Géochimiques, Nancy, France). About two grams of ground powder were used for these analyses. The uncertainties for each analytical method were deduced from relative standard deviations calculated on a miminum of 30 measurements of reference geochemical standards. Major element analyses were performed using an ICP-AES ICap 6500 (Thermo Fischer) after alkali fusion of rock samples with $LiBO_2$ followed by dissolution in HNO_3. The uncertainties on the major element measurements were between 1% and 25% depending on their concentrations. Organic carbon and total sulfur contents were determined using a Horiba EMIA320V2 carbon/sulfur analyzer. The uncertainties on organic carbon measurements were lower than 5% for the highest concentrations (2.55 at.%), lower than 10 % TOC values between 0.7 and 1.47 at.% and lower than 15% for TOC lower than 0.69 at.%. The uncertainty on total sulfur measurements were lower than 10 % for S contents > 0.37 at.%, lower than 15% for S contents between 0.07 to 0.18 at.% and lower than 20 at.% for the lowest values.

A normative abundance (in wt.%) of the mineral phases in microbialites the least affected by detrital contamination (*i.e.,* authigenic-dominated microbialites) was assessed based on their bulk chemical compositions (mainly Mg, Ca and Si concentrations). For this purpose, we considered the following stoichiometries for the main phases detected by XRD, FTIR and

optical and scanning electron microscopy: $CaCO_3$ for aragonite, $Mg_{0.1}Ca_{0.9}CO_3$ for Mg-calcite, $CaCO_3 \cdot H_2O$ for MHC, $Mg_5(CO_3)_4(OH)_2 \cdot 4H_2O$ for hydromagnesite, $Mg_3Si_4O_{10}(OH)_2 \cdot H_2O$ for kerolite and $FeMg_2Si_4O_{10}(OH)_2 \cdot H_2O$ for Fe-rich kerolite. For these estimations, the stoichiometry of Mg-calcite and dehydrated Fe-rich kerolite were chosen arbitrarily. We assumed that all silicon was associated with kerolite since amorphous silica was not observed by microscopy. While some of these assumptions might not be totally accurate, this approach provides an approximate assessment of the bulk mineralogical composition of the microbialites. For samples having an Al content higher than 0.49 wt% (*i.e.,* microbialites from Lakes Aljojuca, Pátzcuaro, Alberca de Guadalupe and Tecuitlapa, as well as some of the microbialites from Lakes La Preciosa, Atexcac and Alchichica), the normative abundance of the mineral phases was not possible to assess.

Trace element analyses, including REE+Y, were performed using an ICP-MS Thermo Elemental X7 following the same procedure as in Carignan et al. (2001) after rock decomposition using alkali fusion. REE+Y data were normalized against the Post-Archean Australian Shale (PAAS) REE+Y pattern (Pourmand et al., 2012). Y was inserted in the pattern between Dy and Ho because of its intermediate ionic radius (Bau and Dulski 1996). In order to characterize the REE+Y patterns of microbialites, the following shale normalized anomalies were calculated: Ce/Ce*, La/La*, Eu/Eu*, Gd/Gd*and Pr/Pr*. The shale-normalized Yb/Nd ratio was used to describe the heavy rare earth elements (HREE) enrichment of microbialites. More details about the calculations are available in Text SI-1 in Supplementary Information.

7. Statistical analyses

Statistical analyses of the chemical composition of lake solutions and microbialites were performed using the R software (R Core Team, 2015).

Twenty-five variables were considered for the aqueous chemistry: temperature, pH, conductivity (noticed as C_{25}), salinity, alkalinity, Mg/Ca, concentrations (expressed in $mmol.l^{-1}$) of Al, B, Ba, Ca, K, Mg, Na, Sr, Zn, H_4SiO_4, PO_4, NH_4, NO_3, F, Cl, SO_4, Br, CO_3 and HCO_3. First, strength and direction of the pairwise monotonic relationships between the 25 aqueous variables on 31 aqueous samples were evaluated by the Spearman's correlation coefficient (values ranging from -1 to +1). The statistical significance of each correlation was assessed and indicated by a *p*-value: correlations were considered as significant when the Spearman's correlation coefficient (r_S) followed the relationship: $|r_S| \geq 0.6$ and/or when the p-value (p) was lower than 1.67×10^{-4} (Bonferroni correction corresponding to a false positive error rate lower

than 5% per test). Pairwise relationships of the variables were drawn using the R package Performance Analytics (Peterson and Carl, 2014).

Sixty-three variables were considered to describe the bulk chemical composition of microbialites: (i) concentrations of the 10 major elements (expressed in wt.%): Si, Al, Fe, Mn, Mg, Ca, Na, K, Ti, P; (ii) concentrations of 33 trace elements (expressed in ppm): As, Ba, Ce, Co, Cs, Dy, Er, Eu, Ga, Gd, Ge, Hf, Ho, La, Lu, Nb, Nd, Pb, Pr, Rb, Sm, Sr, Ta, Tb, Th, Tm, U, V, Y, Yb, Zr and C_{org}, S_{tot} (expressed in at.%); and finally (iii) a total of 20 parameters characterizing the REE+Y patterns of microbialites: three La/La* anomalies, three Ce/Ce* anomalies, two Gd/Gd* anomalies, two Eu/Eu* anomalies, one Pr/Pr* anomaly, Y/Ho ratio, the sum of rare earth elements including Y (noted as ΣREE), $(Yb/Nd)_{SN}$, $(La/Yb)_{SN}$, $(Pr/Yb)_{SN}$, $(Nd/Yb)_{SN}$, non-normalized Nd/Yb, $(Sm/Yb)_{SN}$ and $(Pr/Sm)_{SN}$ (Text SI-1 in Supplementary Information).

In order to identify microbialites significantly affected by detrital contamination *versus* authigenic-dominated microbialites, we performed a clustering on latent (directional) variables using the R package ClustVarLV (Vigneau et al. 2015). We identified a group of elements linearly correlated with Al, an element classicaly considered as the main conservative proxy of detrital silicates (Sageman and Lyons, 2003). We performed a standardized principal component analyses (PCA) on the entire group of 32 microbialites samples described by these variables (potentially indicative of detrital contamination) using the R package FactoMineR (Lê et al., 2008). Then, considering the group of authigenic-dominated microbialites, we evaluated the pairwise monotonic relationships between the 63 solid variables by the Spearman's correlation coefficient (values ranging from -1 to +1) and performed two PCA using (i) the 63 variables and (ii) the 20 variables describing the REE+Y patterns of microbialites. Pairwise correlations were considered as significant when $|r_s| \geq 0.6$ and/or $p \leq 2.56 \times 10^{-5}$ (Bonferroni correction corresponding to a false positive error rate lower than 5% per test). We performed pairwise comparisons of variance of REE+Y patterns of microbialites between groups of samples according to their detrital contamination.

Finally, we tested correlations between microbialite bulk chemical composition and lake water geochemistry. For this purpose, the strength and direction of the pairwise monotonic relationships were evaluated between 24 aqueous variables (listed above without Zn because it was not measured in microbialites) and 63 solid variables on 28 microbialite samples with their corresponding waters by the Spearman's correlation coefficient (values ranging from -1 to +1). Correlations were considered as significant when $|r_s| \geq 0.6$ and/or $p \leq 3.31 \times 10^{-5}$ (Bonferroni correction corresponding to a false positive error rate lower than 5% per test). For this analysis,

we considered only microbialite samples for which a corresponding water sample was available. We excluded microbialites sampled in June 2007 (AL13, AL69-2m, AL60-6m and AL54-11m), as water samples were not analyzed with the same methods during this field campaign (Kaźmierczak et al., 2011).

RESULTS

1. Geochemical diversity of the studied Mexican lakes

The complete set of aqueous geochemical data for the 10 lakes is reported in Table SI-4. Ionic balances were always lower than 10% supporting the consistency of the ICP-AES, continuous flow colorimetry, ion chromatography and alkalinity measurements. All the lakes had an alkaline pH between 8.4 and 9.6. Water temperatures measured in May 2014 ranged between 19°C (Lake La Preciosa) and 29°C (Lake Pátzcuaro). The salinities varied among the lakes: Lakes Zirahuén and Alberca de Guadalupe showed salinities of 0.1 and 0.2 psu, respectively, and were considered as freshwater lakes following Hammer (1986). Lakes Quechulac, Pátzcuáro, La Alberca de Los Espinos, Aljojuca, La Preciosa, and Tecuitlapa were subsaline with salinities comprised between 0.5 and 2.7 psu. Lake Atexcac and Lake Alchichica were hyposaline with salinities of 7.4 and 8.3 psu, respectively. Sodium concentrations were positively correlated with salinities (r_S=0.90) (Fig. SI-1). Therefore, sodium concentrations were also diverse in these lacustrine systems varying between 0.35 mM in Lake Zirahuén and 102.88 mM in the surface water of Lake Alchichica as measured in May 2014. Overall, studied lakes showed a large range of alkalinity: from 1.23 mM for Lake Zirahuén to 49.40 mM for Lake Tecuitlapa. The Mg/Ca ratio of the lakes varied between 1 (Lake Zirahuén) and 90 (Lake Alchichica in May 2014). The concentration of orthosilicic acid (H_4SiO_4) in May 2014 was significantly higher in Lake Alberca de Guadalupe (1.8 mM) and Lake Atexcac (1.1 mM) than in the other lakes (Table SI-4). While pH, magnesium and orthosilicic acid activities were relatively constant through time in Lakes Quechulac, Atexcac and La Preciosa, the H_4SiO_4 activity varied in Lake Alchichica between January 2012 (0.0046 mM in the center and 0.2863 mM on the western shore) and May 2014 (0.0013 mM in the center and 0.0254 mM on the western shore) (Table SI-4).

Several earlier studies monitored the chemical composition of surface water in some of these lakes at different periods during the year (Vilaclara et al., 1993; Armienta et al., 2008; Kaźmierczak et al., 2011; Sigala et al., 2017). A comparison with the present data suggests that the solution chemistry of these lakes have remained relatively constant with the notable

exception of calcium concentrations. For example, the calcium concentration in the center of Lake Alchichica differed by more than a factor of 2 between May 2014 (~0.19 mM) and January 2012 (~0.46 mM) (Table SI-4). Similarly, the calcium concentration in Lake La Preciosa was 2.4 times higher in January 2012 (~0.61 mM) than in May 2014 (~0.25 mM). Moreover, spatial variations were also detected in Lake Alchichica, where the Ca concentration on the western shore (~0.90 mM in January 2012) was significantly higher than in the center of the Lake (~0.46 mM in January 2012). These temporal and spatial variations of calcium concentrations in Lake Alchichica may be due to (i) the seasonal mixing of the lake in December/January bringing deep Ca to shallower depth; (ii) groundwater inflow; (iii) photosynthetic activity and associated carbonate precipitation, which may locally reduce Ca concentration. No strong evidence allows to decipher between these three non-exclusive hypotheses.

Two groups of lakes could be distinguished based on their Sr isotope ratios (Table 2): Lakes Alchichica, La Preciosa and Atexcac had higher $^{87}Sr/^{86}Sr$ values (0.706888 ± 0.000004, 0.706962 ± 0.000021 and 0.706998 ± 0.000040, respectively), than Lakes La Alberca de Los Espinos and Zirahuén (0.703914 ± 0.000020 and 0.704514 ± 0.000024, respectively).

Correlations between aqueous geochemistry parameters of Mexican lakes were systematically assessed (Fig. SI-1). Here, we only considered the strongest and statistically significant correlations with a Spearman's correlation coefficient $|r_s|>0.6$ and a corrected p-value lower than 5% per test (owing to Bonferroni correction for multiple testing). Alkalinity, $[Na^+]$, salinity, conductivity (C_{25}), $[HCO_3^-]$, $[CO_3^{2-}]$, $[K^+]$ and $[SO_4^{2-}]$ were all positively correlated ($r_s \geq 0.74$). In particular, a strong positive correlation between alkalinity and sodium concentration (r_s=0.79) was observed. Since Na^+ and HCO_3^- are among the major cations and anions in the studied lakes, this warrants charge balance. The positive correlation between alkalinity, $[HCO_3^-]$ and $[CO_3^{2-}]$ was an obvious result from (1) the equilibrium between $[HCO_3^-]$ and $[CO_3^{2-}]$ and (2) the relationship between $[HCO_3^-]$, $[CO_3^{2-}]$ and alkalinity (*i.e.*, $Alk=[HCO_3^-]+2[CO_3^{2-}]$) (Table SI-5). The $(Mg/Ca)_{aq}$ ratio was positively correlated with alkalinity (r_s=0.67), $[HCO_3^-]$ (r_s=0.78), SO_4^{2-} (r_s= 0.78) and $[Br^-]$ (r_s=0.66). Alkali metal (potassium and sodium) concentrations were positively correlated with each other (r_s=0.92). High positive correlations were observed between $[Mg^{2+}]$, $[Cl^-]$, $[Br^-]$ and $[B]_T$ (*i.e.,* $B(OH)_3$ and $B(OH)_4^-$) ($r_s \geq 0.89$). Strontium concentration was positively correlated with $[Ca^{2+}]$ (r_s=0.86) and negatively correlated with the $(Mg/Ca)_{aq}$ ratio (r_s =–0.78).

Saturations of the surface solutions of all lakes with respect to several carbonate phases were best visualized in a solubility diagram, where the logarithms of $a(Mg^{2+})$ or $a(Ca^{2+})$ were plotted against the log of $a(CO_3^{2-})$ (Fig. 2). Values of these saturation indices were also reported

in Table SI-6. All lakes, but Lake Zirahuén, were saturated or supersaturated with respect to MHC. Lake Quechulac and Lake La Preciosa samples collected in 2014 lied exactly on the solubility line of MHC as defined by Fukushi and Matsumiya (2018), while other solutions were at a higher saturation. Lake Zirahuén was significantly lower, close to saturation with aragonite (Fig. 2). Considering $a(Mg^{2+})$, Lake Alchichica surface solutions were all supersaturated with an amorphous pure Mg-carbonate phase. Atexcac water sample collected in 2012 was at saturation with amorphous Mg-carbonate, whereas the water sample collected in 2014 as well as all other lake waters were undersaturated with amorphous Mg-carbonate (Fig.2). Moreover, all the other lakes were also undersaturated with respect to hydromagnesite (Table SI-6).

Saturations of the solutions with respect to authigenic silicate phases were best grasped in a solubility diagram, where the logarithm of the $a(Mg^{2+})/a(H^{+})^2$ activity ratio was plotted against the log of $a(H_4SiO_4)$ of the solutions (Fig. 3). Lake Zirahuén was undersaturated with respect to all reported low-temperature Mg-silicates such as sepiolite, kerolite, talc and stevensite. One sample of Lake Alchichica was saturated with talc, while other samples from this lake were saturated or supersaturated with kerolite and stevensite, and only one sample collected in 2012 on the west shore of the lake was supersaturated with "amorphous sepiolite", as defined by Wollast et al. (1968). One sample from Quechulac collected in the center of the lake in 2012 was understurated with respect to amorphous sepiolite. All other lakes were saturated or supersaturated with amorphous sepiolite. Lake Alberca de Guadalupe and one sample of Lake Atexcac collected in 2012 lied above the critical supersaturation line for homogenous nucleation of Mg-silicates as defined by Tosca et al. (2011) and Tosca and Masterson (2014). All lakes lied below the solubility line of amorphous silica.

2. Microbialite occurrence in modern Mexican lakes

No microbialite was found around the shores of Lake Zirahuén, while some microbialites were observed in the other nine lakes (Fig. SI-2). Living microbialites had varying sizes and extents depending on the lakes. For example, microbialites appeared as calcified crusts around volcanic rocks, measuring several hundreds of micrometers in thickness in Lake Alberca de Guadalupe (Fig. SI-2r-s) and few centimeters in thickness in Lake Aljojuca (Fig. SI-2 k-l), Lake Tecuitlapa (Fig. SI-2m-n-o) and Lake Pátzcuaro (Fig. SI-2 t). In contrast, they appeared as meter-sized mounds with various morphologies in Lake Quechulac (Fig. SI-2i-j), Lake La Preciosa (Fig. SI-2f-g-h), Lake Atexcac (Fig. SI-2d-e) and Lake Alchichica (Fig. SI-

2a-b-c). Microbialites from Lake Quechulac were observed on a small island at the center of the lake but were absent from the shores of the lake. Microbialites from Lake Pátzcuaro were stromatolitic, *i.e.*, showing macroscopic laminations (Fig. SI-2t). Microbialites from the other lakes showed a clotted thrombolitic fabric. Microbialites in Lake Alchichica formed a massive continuous reef along the shoreline.

3. Mineralogical diversity of Mexican lacustrine microbialites

The bulk mineralogical composition of the microbialites was assessed by XRD and FTIR (Figs. SI-3 and SI-4). The distribution and texture of mineral phases were characterized by optical microscopy and/or Raman microspectroscopy and/or scanning electron microscopy. Microbialites showed various mineralogical compositions as summarized in Tables 3 and SI-7.

3.1. Carbonate phases: identity, texture and textural relationships

Diverse carbonates were detected in the microbialites: (Mg-)calcite, MHC ($CaCO_3 \cdot H_2O$), aragonite, dolomite and hydromagnesite [$Mg_5(CO_3)_4(OH)_2 \cdot 4H_2O$]. No ACC phase was detected by these bulk methods. Massive occurences of hydromagnesite were observed in Lake Alchichica microbialites, appearing in a rosette-like texture, whereas this was more occasional in Lake Atexcac (Fig. SI-3a and Table SI-7). Dolomite was observed as a minor phase in one living microbialite from Lake Atexcac (ATX2014-13). It appeared as fine-grained crystals located close to some feldspar and aragonite grains. Based on the relative intensity of the XRD peaks and as supported by bulk chemical analyses (Table SI-8), we inferred that microbialites from Lakes Alchichica, Atexcac, La Preciosa and Quechulac all contained abundant aragonite (Fig. SI-3a-b), while microbialites from Lakes Aljojuca, Tecuitlapa and Pátzcuaro contained mostly (Mg-)calcite and/or MHC with minor amounts of aragonite only (Fig. SI-3c). Last, microbialites from Lake La Alberca de Los Espinos and Lake Alberca de Guadalupe contained MHC and/or (Mg-)calcite only, with no aragonite (Fig. SI-3c). Microbialites from Lake Pátzcuaro (Patz2014-02) showed macroscopic laminations. These laminations corresponded to alternations of Mg-calcite, aragonite and Mg-silicates as observed by SEM and optical microscopy (Fig. 4a-b). Although MHC was detected by XRD in microbialites from Lake Pátzcuaro based on a small peak at 23.9° (2θ) (Fig. SI-3c), it was not observed by SEM. Aragonite was mainly distributed as large nodules measuring several hundreds of micrometers (Fig. 4c-d-e-f) particularly in microbialites with high amounts of

603 authigenic Mg-silicates or hydromagnesite such as in Lakes La Preciosa, Atexcac and
604 Alchichica. In these nodules, aragonite mostly showed a micritic texture but was sometimes
605 acicular as observed in microbialites from Lakes La Preciosa, Atexcac, Alchichica and
606 Quechulac.
607 The co-existence of (Mg-)calcite and MHC in microbialites from Lake Aljojuca
608 (Aljo2014-02), as revealed by XRD (Fig. SI-3c), was further investigated by SEM and Raman
609 microspectroscopy to assess their textural relationship (Fig. 5). MHC was identified by Raman
610 microspectroscopy based on a main band at 1068 cm^{-1} (Fig. 5a-b) corresponding to the ν_1
611 internal symmetric stretching of the C-O bonds in the carbonate group (Zhang et al., 2013).
612 This stretching mode in Mg-calcite was shifted to higher wavenumbers. Its exact position
613 depends on the Mg content (Bischoff et al., 1985; Perrin et al., 2016). In the present case, it
614 appeared at a varying energy position between 1087.3 and 1090.1 cm^{-1} (Fig. 5a-b). Following
615 Perrin et al. (2016), the Mg content of Mg-calcite therefore varied between ~5 and 19 mol% of
616 $MgCO_3$. In Lake Aljojuca microbialites, Mg-calcite was distributed as nodules possibly
617 growing at the expense of a matrix composed of MHC (Fig. 5 a-c-d). SEM observations (in the
618 backscattered electron mode) of microbialites from Lake Tecuitlapa and Aljojuca showed that
619 Mg-calcite appeared brighter than MHC (Fig. 5e-f-g).
620 Interestingly, biomorphs possibly resulting from the encrustation of diverse bacterial or
621 eukaryotic cells were repeatedly observed as entombed within the carbonate phases, especially
622 aragonite, MHC and Mg-calcite. Microfossils were mainly associated with aragonite in
623 microbialites from Lake Alchichica (Fig. 6a-b-c-d), Lake Atexcac (Fig. 6e-f), Lake La Preciosa
624 (Fig. 6g) and Lake Quechulac (Fig. 6h). MHC locally contained dense clusters of encrusted
625 cells measuring ~8 μm in width as observed in Aljojuca microbialites (Fig. 6i). Sometimes,
626 MHC also contained particularly well-preserved diatom fossils as observed in the microbialites
627 from Lake Tecuitlapa (Fig. 5f). Dense clusters of filamentous microfossils entombed in Mg-
628 calcite and MHC were observed in the microbialites from Lake La Alberca de Los Espinos
629 (Fig. 6j). To a lesser extent, some microfossils of diatoms and coccoid-shaped cells were
630 observed in association with Mg-calcite in a living microbialite from Lake Alberca de
631 Guadalupe (Fig. 6l). Microbial communities associated with these microbialites are very
632 diverse (Iniesto et al., 2021) and no taxonomical affiliation of the observed fossils could be
633 straightforwardly achieved.
634
635 ***3.2. Identity and micro-texture of authigenic Mg-silicates***
636

Poorly-crystalline Mg-silicates were detected by XRD based on broad peaks at 4.58-4.55 Å (22.8° 2Θ), 2.60-2.58 Å (42.3° 2Θ) and 1.54 Å (72.1° 2Θ) (Fig. SI-3b and c) in microbialites from Lakes Pátzcuaro, Atexcac, La Preciosa, Tecuitlapa and La Alberca de Los Espinos. These peaks correspond to two dimentional *hk* diffraction bands (02,11), (13,20) and (06,33), respectively, characteristic of poorly ordered layer silicates such as kerolite (an hydrated talc), with the general formula ($Mg_3Si_4O_{10}(OH)_2 \cdot nH_2O$), and/or trioctahedral smectite, such as stevensite: $(Ca_{0.5},Na)_{0.33}(Mg,Fe^{2+})_3Si_4O_{10}(OH)_2 \cdot n(H_2O)$ (Brindley et al., 1955; Brindley et al., 1977). Based on the Si-O-Si stretching at 1024 cm^{-1} and the Mg_3-OH stretching around 3680 cm^{-1}, FTIR analyses were more sensitive than XRD to the presence of these phases and allowed detecting them in additional microbialites such as Lake Quechulac (Zeyen et al., 2015) and Lake Alberca de Guadalupe. In contrast, these phases were not detected at all by XRD and FTIR in microbialites from Lake Aljojuca and Lake Alchichica (*i.e.*, AL2012-12) (Figs. SI-3 and SI-4). Consistently, kerolite and/or stevensite was observed by optical and scanning electron microscopies in most of the studied microbialites except those from Lake Aljojuca and most of the samples from Lake Alchichica (Figs. 4 and 7). Kerolite and/or stevensite were only observed in minor amount in one sample from the North-West shore of Lake Alchichica (AL2014-13). In microbialites from the other lakes, kerolite/stevensite was mainly distributed as large homogeneous fractured (indicative of its hydrated nature) patches measuring up to several hundreds of micrometers (Figs. 4c-e and 7). Moreover, we observed in all microbialites containing kerolite/stevensite, an intimate association between kerolite/stevensite and biomorphs (Fig. 7). This supported the previous conclusion that these phases are authigenic (Zeyen et al., 2015 and 2019). Interestingly, some of the Mg-silicate seemed to be partly replaced by carbonates (Fig. 7e-g-h-i).

3.3. Additional mineral phases

In addition to carbonate and silicate phases, several microbialites from Lake Alchichica contained Fe-bearing layered double hydroxides (LDH), belonging to the iowaite ($Mg_6Fe^{3+}_2(OH)_{16}Cl_2 \cdot 4H_2O$) – pyroaurite ($Mg_6Fe^{3+}_2(OH)_{16}CO_3 \cdot 4H_2O$) group. This phase was evidenced by peaks at 7.65 Å (13.4° 2Θ) and 3.76 Å (27.6° 2Θ) in the XRD patterns, consistent with the (003) and (006) Bragg reflections of LDHs, respectively (Fig. SI-3a) (Turvey et al., 2018; Zeyen et al., 2019). In addition, non-authigenic phases were detected by XRD and observed by SEM as well. Na-feldspar (albite) appeared as a major phase in the Alberca de Guadalupe microbialite. Albite also appeared as an abundant phase in Tec2014-06 and Pr2014-03 (Fig. SI-3d). Finally, this mineral phase was detected as a minor phase in Aljo2014-01,

Aljo2014-02 and Tec2014-05b. Anorthite (Ca-feldspar) was detected as a minor phase in AL60-6m, Preciosa05-2012, Preciosa06-2012, ATX2014-13. Last, illite (with the general formula $(K,H_3O)(Al,Mg,Fe)_2(Si,Al)_4O_{10}[(OH)_2,(H_2O)]$) was detected in the AL2012-10m microbialite sample only (Fig. SI-3a). Assuming that all K was in orthose, all Na in albite and that all Al was in the feldspar phases (albite $NaAlSi_3O_8$, anorthite $CaAl_2Si_2O_8$ and orthose $KAlSi_3O_8$), we could estimate that these detrital phases represented 21-22% of the total mass of the microbialites *versus* 78-79% for authigenic phases (carbonate $CaCO_3$ and Mg-silicates) in the three microbialites samples highly affected by detrital contamination (Pr2014-03, Tec2014-05b and LaAlb2014-02, see below). This number was an underestimation of the proportion of the detrital phases in these microbialites since it did not take into account quartz, which was detected in LaAlb2014-02 and Pr2014-03 by XRD, as well as other potential non-Al-bearing detrital phases (Fig. SI-3d).

3.4. Variations of the mineralogical composition of the microbialites within a single lake

Some variations of the mineralogical abundance were detected among microbialites from the same lake. For example, living microbialites located on the north shore of Lake Atexcac were mainly composed of Mg-silicates and aragonite (ATX-2C1-2012, ATX2014-02, ATX2014-07), while one living microbialite from the south shore was mainly composed of aragonite and contained minor amounts of Mg-silicates only (ATX2014-13). Similarly, living microbialites located on the north shore of Lake Alchichica (AL13, AL66, AL69-2m, AL60-6m, AL2012-1m, AL2012-5m, AL2012-10m, AL2012-15m) were composed of 56 to 88% of hydromagnesite with lesser amounts of aragonite, whereas, some living and non living microbialites located on the west shore of the lake (AL2012-17, AL2014-13, AL2014-15), were composed of 74 to 98% of aragonite with minor amounts of hydromagnesite (Table SI-8). Only two living microbialites located on the west shore of Lake Alchichica (AL2012-12 and AL2014-12) contained mainly hydromagnesite (77% for AL2014-12) and to a lesser extent, aragonite.

Moreover, several non-living microbialites had mineralogical compositions differing from living microbialites. For instance, a non-living microbialite sampled on the northeastern shore of Lake Pátzcuaro (Patz2014-01) was composed of Mg-calcite only, while the living microbialite collected in the same area (Patz2014-02) contained Mg-calcite as well as aragonite, MHC and Mg-silicates (Table SI-7). Similarly, a non-living microbialite from the west shore of Lake Alchichica (AL2012-15) was composed of aragonite and some Mg-poor calcite,

whereas living microbialites from this area (AL2014-15) were mainly composed of aragonite and hydromagnesite (Tables SI-7 and SI-8).

4. Bulk chemical composition of microbialites

4.1. Identification of an authigenic-dominated microbialites group

Bulk chemical analyses of major and trace elements were performed on 32 microbialite samples (Tables SI-9, SI-10 and SI-11). The clustering on latent variables (Fig. 8a) revealed the existence of a group of 8 strongly positively correlated chemical elements ($r_s \geq 0.72$), including the alkali metals K and Rb (large ion lithophile elements), high field strength elements (HFSE; Nb, Ta, Hf and Zr), Al and Ga. Na and Th were correlated to a lesser extent to these 8 variables ($r_s \geq 0.85$). Enrichment in those 8 elements is typical of detrital minerals such as feldspars or pyroxenes. A principal component analysis (PCA) was performed using these 8 variables on the 32 microbialite samples (Fig. 8b). From this analysis, it was possible to distinguish 3 groups of samples: a group of samples highly affected by detrital contamination, an intermediate group of microbialites moderately affected by detrital contamination and a third group containing authigenic-dominated microbialites (summary in Table SI-7 and Text SI-2 in Supplementary Information). This classification was supported by XRD and SEM analyses. The three microbialite samples Pr2014-03, Tec2014-05b and LaAlb2014-02 clustered together and were particularly enriched compared to the other samples in the 8 above-mentionned chemical elements (Fig. 8b), with Al concentrations of 3.73 ± 0.19, 3.57 ± 0.18 and 3.46 ± 0.17 wt.%, respectively (Table SI-9). There were some variations between these three samples: microbialite sample LaAlb2014-02 was particularly enriched in Ta and Nb (Table SI-10; Fig. 8b). Pr2014-03 sample was specifically enriched in Rb and Ga (Table SI-10; Fig. 8b). Tec2014-05b sample was distincly enriched in Zr and Hf (Table SI-10; Fig. 8b).

Eleven other microbialites, defined as "intermediately affected by detrital contamination" (Preciosa-05-2012, Preciosa-06-2012, Tec2014-05a, Aljo2014-02, Patz-2014-02, AL54-11m, AL60-6m, AL2012-10m, AL2012-15, ATX-2C1-2012 and ATX2014-13) grouped together in the PCA analysis and were also enriched in these 8 elements, but to a lesser extent. These samples contained relatively high amounts of Al ranging from 0.49 ± 0.07 wt.% for Preciosa-06-2012 to 1.15 ± 0.06 wt.% for Aljo2014-02.

Last, on the PCA biplot, we identified a group of 18 microbialites characterized by low concentrations of K, Rb, Nb, Ta, Hf, Zr, Al and Ga: AL13, AL69-2m, AL2012-1m, AL2012-

5m, AL2012-15m, AL2012-12, AL2012-17, AL2014-13, AL2014-15, ATX2014-07, Pr2014-01, Pr2014-02, Pr2014-09, AlbEsp2014-01, Quechulac1A-2012, Quechulac4A-2012, Quechulac4B-2012 and Quechulac4C-2012 (Fig. 8b). This group contained Al concentration lower than 0.27 ± 0.03 wt.% (Table SI-9) and these samples were considered here as authigenic-dominated.

4.2. Mg-Ca-Si contents of microbialites

Calcium (Ca mass content ranged between 13.9 and 94.9 %, average 57.2 %), magnesium (between 1.3 and 80.8 %, average 26.0 %), and silicon (between 0.7 and 38.5 %, average 12.2 %), were the most abundant chemical elements in all microbialites, followed by aluminum, iron and sodium, depending on samples. Except for the 3 microbialite samples the most affected by detrital contaminations, the 29 others microbialites were plotted in a ternary Ca-Mg-Si diagram (Fig. 9). They were distributed along two main trends: 1) most of the microbialites from Lake Alchichica were distributed along the Ca-Mg line, consistent with the observations that they mostly contained aragonite and hydromagnesite in varying proportions. AL54-11m, AL60-6m, AL2012-10 and AL2012-15 samples, which all appear as "intermediately" contaminated, departed from this trend because of their relatively higher Si content (2.46 ± 0.07, 2.56 ± 0.08, 3.83 ± 0.08 and 1.86 ± 0.09 wt.%, respectively). 2) Microbialites from Lakes Quechulac, La Alberca de Los Espinos, La Preciosa, Atexcac, Tecuitlapa and Pátzcuaro scattered along a second trend between the Ca pole and a pole consisting of a Mg:Si mixture of about 41:59 (in wt.%/wt.%), very close to the 3:4 Mg:Si stoichiometry of kerolite and stevensite. As supported by XRD and FTIR, this second trend corresponded to a mixture of varying proportions of Ca-carbonates (aragonite, calcite and MHC) and an authigenic Mg-silicate (kerolite and/or stevensite). ATX-2C1-2012 departed from this second trend and was closer to the Mg end member, consistent with the fact that it also contained hydromagnesite as shown by XRD analyses (Fig.SI-3b). Preciosa05-2012, Aljo2014-02 and ATX2014-13 samples, which were "intermediately" contaminated, slightly departed from this trend and contained more Si mainly due to the presence of detrital phases (Ca-containing feldspar). The Si *versus* Mg contents of these microbialites (except ATX-2C1-2012) were plotted and a strong positive correlation was observed (R^2=0.93) (Fig. SI-5). The correlation slope was equal to 0.70 ± 0.07 (wt.%/wt.%) corresponding to 0.81 ± 0.07 (at.%/at.%), very close to the theoretically expected atom Mg/Si stoichiometry (0.75) of kerolite and stevensite (Fig. SI-5).

4.3. Statistical analyses of the chemical compositions of the microbialites

A statistical analysis of the dataset was performed on the group of 18 authigenic-dominated microbialites to assess potential correlations between the variables describing the chemical composition of the studied microbialites. Several monotonic associations were detected between major and trace elements composing these microbialites considering $|r_S| \geq 0.6$ and a corrected p-value lower than 5% per test (Fig. SI-6). The diagram of pairwise correlations revealed an expected positive correlation between the alkaline earth elements Ca and Sr (r_S=0.84), all strongly anti-correlated with Mg. Out of the 18 samples, a group of nine samples (Pr2014-09, Pr2014-01, Pr2014-02, Preciosa06-2012, Preciosa05-2012, Al2014-15, AL13, Quechulac1A-2012 and Quechulac4C-2012), showed a linear positive correlation between S_{tot} and C_{org} content (R^2 of 0.99). The S_{tot}/C_{org} atomic ratio was 0.188 ± 0.009 (Fig. SI-7).

A principal component analysis was performed on the complete dataset of 63 variables describing the group of 18 authigenic-dominated microbialites (Fig. 10). The AlbEsp2014-01 and ATX2014-07 microbialite samples significantly contributed to the first axis (explaining 34.5% of the total variability), while the Pr2014-01, Pr2014-02 and AL2012-17 microbialite samples significantly contributed to the second axis (explaining 21.8% of the total variability). On the first axis, the AlbEsp2014-01 microbialite sample was particularly enriched in REE+Y with the sum of the REE+Y reaching 12.22 ppm (Table SI-11). In addition, this microbialite sample was particularly concentrated in Mn (0.464 ± 0.03 wt.%) and P (0.27 ± 0.02 wt.%) (Table SI-9). Last, this sample was one of the most enriched in organic carbon (1.04 ± 0.1 at.%) in the group of authigenic-dominated microbialites (Table SI-9). On the second axis, the AL2012-17 microbialite showed a particularly high Y/Ho ratio, reaching a value of 58 and also departed from the other samples based on its high Eu positive anomaly reaching ~9 as well as a high positive Gd anomaly (expressed as Gd/(2Tb-Dy)) reaching 1.81 (Text SI-1). Moreover, sample AL2012-17 had the highest Fe content (2.49 ± 0.5 wt.%) and a high Sr concentration (equal to 3,441 ppm) in the group of authigenic-dominated microbialites. Last but not least, Pr2014-09 and AL2012-17 microbialites were marked by a pronounced $(Yb/Nd)_{SN}$ anomaly reaching 4.73 and 4.13, respectively, highlighting their HREE enrichment (Fig. 10 and Texts SI-1 and SI-3). Additional interesting but less robust correlations were observed: for example, a positive correlation was observed between the Eu and Ca contents (r_S=0.75) in authigenic-dominated microbialites (Fig. SI-6 and Text SI-4).

4.4. REE+Y patterns of microbialites

Mexican microbialites exhibited a wide range of REE contents, with the sum of REEs+Y (noted ΣREE) content varying from 1.18 ppm up to 65 ppm (Table SI-11). The ΣREE content of microbialites was positively correlated with their Al content (r_s=0.81) (Text SI-3).

A PCA was performed on the group of authigenic-dominated microbialites considering the set of 20 variables describing REE+Y patterns of microbialites (Text SI-3). This allowed to discriminate four main types of REE patterns. (i) Patterns such as the ones of AL2012-17 and Pr2014-09 microbialites showed high positive Eu/Eu* anomalies, Gd/Gd* positive anomalies, a high enrichment in HREE as well as a very high Y/Ho ratio (Fig. 11a). (ii) Patterns such as the ones of samples Pr2014-01 and Pr2014-02 were flat, i.e., showed $(Nd/Yb)_{SN}$, $(Pr/Yb)_{SN}$, $(Pr/Sm)_{SN}$ and $(Sm/Yb)_{SN}$ ratios close to 1 (Fig. 11b). (iii) Patterns of AL2012-5m showed a positive Ce/Ce* anomaly (Fig. 11c). (iv) Patterns of AlbEsp2014-01, Quechulac-4A-2012 and AL2012-15m had a high ΣREE as well as a strong negative Ce/Ce* anomaly and a strong positive Pr/Pr* anomaly (Fig. 11d). Importantly, the lower the Al concentrations in microbialites, the higher the anomalies in Eu, Ce, Pr, La and/or Gd and the HREE to LREE enrichment (Text SI-3). Finally, the Y/Ho ratio of microbialites also depended on the Al content of microbialites. Al-rich microbialites showed a chondritic Y/Ho ratio (26-28), while Al-poor microbialites had a more variable Y/Ho up to 58.0 for AL2012-17 (Text SI-3).

5. Relationships between microbialite composition/occurence and aqueous geochemistry

Relationships between the microbialite composition and aqueous geochemistry are shown on a Spearman pairwise correlations diagram (Fig. SI-8). A strong positive correlation was observed between $[Sr^{2+}]_{aq}$ and the P content of microbialites (r_s=0.9) (Fig. 12). Moreover, fractionations of REEs were detected between solutions and microbialites (Text SI-4). In general, microbialites incorporated more LREE compared to the ambient solutions within which they formed. Microbialites from Lake Quechulac, Lake La Preciosa, Lake Atexcac, and the north shore of Lake Alchichica showed relatively similar solid/solution fractionation patterns with a strong >1 fractionation for Ce and a weaker >1 fractionation for Pr and Nd (*i.e.,* microbialites incorporated more Ce, Pr and Nd compared to the ambient solutions) (Fig. SI-4-1). Last, microbialite from Lake La Alberca de Los Espinos showed high solid/solution fractionations for Nd (Text SI-4).

As mentioned earlier, the alkalinity of the lakes was positively correlated with their Na content (r_S=0.79) and by extension their salinity (r_S=0.71) (Fig. 13) as well as the $(Mg/Ca)_{aq}$ ratio (Fig. 14a) (r_S=0.67 between alkalinity and $[Mg/Ca]_{aq}$ and r_S= 0.63 between salinity and $[Mg/Ca]_{aq}$). Salinity was positively correlated with $[Mg]_{aq}$ (r_S=0.59) (Fig. 14b). Alkalinity-salinity-$(Mg/Ca)_{aq}$ were also qualitatively correlated with the occurrence (abundance and size) of microbialites (Fig. 13). Indeed, no microbialite was observed in Lake Zirahuén, where alkalinity was the lowest (~1.2 mM). At a higher alkalinity of ~4.3 mM such as in Lake Alberca de Guadalupe, very small microbialites consisted in thin crusts measuring around several hundreds of micrometers in thickness around basaltic blocks. At alkalinities higher than ~7.6 mM such as in Lakes La Alberca de Los Espinos, Pátzcuaro, Aljojuca, La Preciosa and Tecuitlapa, living microbialites were well developed along the shore of the lakes. Last, microbialites formed massive and almost continuous reefs at an alkalinity higher than 31 mM such as in Lake Atexcac and Lake Alchichica.

DISCUSSION

1. Origins of the chemical variability of the lakes

Alkalinity was positively correlated with the salinity of the lakes (Fig. 13). Such a correlation can be viewed as the direct effect of electroneutrality and the fact that Na^+ and HCO_3^- are major ionic species. Several of the continental (Lake Van, Pavilion Lake, Fayetteville Green Lake, Bacalar, Cuatro Cienegas) and/or volcanic (Salda, Vai Si'I and Vai Lahi) lakes studied by Chagas et al. (2016) also plotted on the same positive correlation. In contrast, coastal lakes (*i.e.*, Big Pond, Laguna Pirata, Clifton, Lagoa Vermelha, Kirimati-Lake 21, Walyungup and Fellmongery), with a higher salinity, did not plot on this positive correlation. This can be explained by the fact that coastal lakes have an important seawater input increasing their $[Na^+]$ and $[Cl^-]$ relatively to their $[HCO_3^-]$.

One question relates to the origin of the broad variations of salinity (0.35 mM-102.88 mM) and alkalinity (1.3 mM-43.0 mM) among the Mexican lakes studied here. Lakes and ponds in the Pantanal wetland in Brazil show similar correlated variations of alkalinity and salinity over an even broader range (Furian et al., 2013). They were explained as the result of varying concentration stages of the same initial dilute water. Following the concept of chemical divide, when dilute waters feeding lakes have a dissolved inorganic carbon (DIC) concentration higher than the concentrations of alkaline earth metals (Ca^{2+} and Mg^{2+}), they evolve upon evaporation into increasingly alkaline brines with decreasing relative concentrations of Ca^{2+} then Mg^{2+}

874 (Pecoraino et al., 2015). This also explains why alkalinity increases correlatively with $[Na^+]_{aq}$
875 and $(Mg/Ca)_{aq}$ upon evaporation (Gac et al., 1977; Al-droubi et al., 1980; Darragi and Tardy,
876 1987). Dilute waters feeding Mexican lakes most often comprise rainfall and groundwater only.
877 The composition of groundwaters is controlled by the weathering of surrounding bedrocks and
878 in particular their DIC/($[Ca^{2+}]+[Mg^{2+}]$) ratios will depend on the petrological composition of
879 the bedrock (*e.g.,* basaltic/andesitic rocks *versus* carbonates; Gaillardet et al., 1999). Some
880 variations were observed in the nature of the bedrock sourcing Mexican lakes. Indeed, Lake La
881 Alberca de los Espinos and Lake Zirahuén showed low $^{87}Sr/^{86}Sr$ values close to 0.7040. This
882 was within the 0.7037-0.7047 range for $^{87}Sr/^{86}Sr$ values measured by Verma (1999) on basaltic
883 andesites, andesites and dacites from the Sierra de Chichinautzin, located south of Mexico City
884 in the TMVB. This suggested that both lakes were mostly fed by the weathering of
885 basaltic/andesitic rocks, consistently with the rocks outcropping around these lakes (Davies et
886 al., 2004; Siebe et al., 2014). This kind of petrology typically generates high
887 DIC/($[Ca^{2+}]+[Mg^{2+}]$) dilute waters (Pecoraino et al., 2015). In contrast, Lakes Alchichica, La
888 Preciosa and Atexcac had significantly more radiogenic dissolved Sr (*i.e.,* $^{87}Sr/^{86}Sr$ values close
889 to 0.7070) suggesting that they were fed by the dissolution of both basalts and carbonate rocks
890 (Verma, 2000; Gómez-Tuena et al., 2007). Again, this is consistent with the presence of a
891 limestone bedrock outcroping within the Cretaceous Cuenca de Oriental basin (Reyes Cortés,
892 1979; Caballero et al., 2003; Carrasco-Núñez et al., 2007; Armienta et al., 2008). In that case
893 the DIC/($[Ca^{2+}]+[Mg^{2+}]$) of the dilute waters might be lower. However, in both cases, volcanic
894 CO_2 outflows may be an additional parameter increasing the DIC/($[Ca^{2+}]+[Mg^{2+}]$) ratio of
895 groundwater, hence favoring an alkaline-type evolution of the lakes as shown by Milesi et al.
896 (2020) for Lake Dziani Dzaha. Although we did not measure the isotopic composition of DIC,
897 which may offer a definitive answer to this question, we observed that most Mexican lake
898 solutions, except Lakes Zirahuén, Alberca de Guadalupe and Tecuitlapa, were equilibrated with
899 a pCO_2 higher than the atmospheric pCO_2 (Table SI-12). This suggests that volcanic CO_2 may
900 play an additional role in maintaining a high DIC in these lakes (Pecoraino et al. 2015). In any
901 case, all studied Mexican lakes plotted in the alkaline domain of a Ca^{2+}, SO_4^{2-}, $HCO_3^- + CO_3^{2-}$
902 (all expressed in equivalent/L) ternary diagram ("Spencer diagram", Fig. SI-9), supporting the
903 idea that they indeed evolve toward more alkaline conditions over increasing evaporative
904 concentration.
905 Mercedes-Martin et al. (2019) developed a hydrochemical model shedding light on
906 the hydrological parameters that may control varying concentration factors, hence explaining
907 why some Mexican lakes may eventually have higher alkalinities/salinities/$(Mg/Ca)_{aq}$ than

908 others. One of their model focused on closed lakes and allowed a stationary water level for the
909 lake by balancing groundwater input with outputs by evaporation and leakage to the lake bottom
910 aquifer. Therefore, in this case, varying concentration factors cannot be assessed in the field
911 based on an apparent water level decrease. They showed that in this model the major parameters
912 controlling the concentration factor were the rate of solute input to the lake and the rate of
913 leakage to groundwater systems. Similarly, Furian et al. (2013) proposed that the varying
914 concentration stages of Pantanal ponds depended on their hydrological functioning, itself
915 controlled by the presence/absence of low permeability soils as barriers to input/outpur water
916 movements. In conclusion, the hydrology of the lakes controls their concentration stage.
917 Because feeding dilute waters are relatively alkaline, they become even more alkaline, more
918 saline and show an increasing $(Mg/Ca)_{aq}$ upon concentration. Unfortunately, we do not
919 presently have all hydrochemical parameters allowing to model the varying concentration
920 stages of all studied Mexican lakes, but at least, assuming a similar initial Cl^- concentration for
921 all the lakes, we can infer that the concentration factor is more than 500 times higher in Lake
922 Alchichica than in Lake Zirahuén.
923 As an exception, Lake Tecuitlapa departed from the correlation between salinity and
924 (i) $(Mg/Ca)_{aq}$ and (ii) $[Mg^{2+}]_{aq}$, with a marked relative Mg depletion (Fig. 14). This lake showed
925 the highest pH (9.6) and the highest alkalinity (49.40 mM) among the studied lakes. The
926 particular high pH and alkalinity of Lake Tecuitlapa might be of biological origin since this
927 lake is characterized as hypertrophic (Sigala et al., 2017) with high $[PO_4^{3-}]_{aq}$ and total dissolved
928 N species concentrations (Table SI-4) and high photosynthetic biomass was observed (Fig. SI-
929 2). Other studies similarly suggested that high primary production levels can contribute to a
930 high pH and alkalinity (López-Archilla et al., 2004; Milesi et al., 2019; Milesi et al., 2020).
931 Chagas et al. (2016) also reported a positive correlation between salinity and $[Mg^{2+}]_{aq}$ in twenty-
932 one lakes with the departure of one lake (Lake Van located in Turkey) showing a marked Mg
933 depletion relative to its high salinity, similarly to Lake Tecuitlapa in the present study. Lake
934 Van showed the highest alkalinity (~150 mM) and the highest pH (9.9) among the lakes studied
935 by Chagas et al. (2016). They suggested that Lake Van's depletion in Mg was the consequence
936 of its high alkalinity and the availability of CO_3^{2-} ions to react with cations. However, although
937 diverse carbonate phases were observed in Tecuitlapa microbialites, these did not contain
938 particularly insoluble Mg-rich phases that might drag the concentration of Mg downward
939 compared to other lakes. Alternatively, Reimer et al. (2009) explained the Mg^{2+} depletion in
940 Lake Van by abundant Mg-silicate precipitation. Here, Mg-silicates were detected in Lake
941 Tecuitlapa microbialites but also in microbialites from other lakes without any relative

depletion in $[Mg^{2+}]_{aq}$ relative to their salinity. Another possibility could be that some saline, Ca-rich and Mg-poor water may feed Lake Tecuitlapa, relatively decreasing its Mg concentration. Lastly, since Lake Tecuitlapa contains a high biomass and Mg^{2+} is an important cofactor in many enzymes, cells might be an important sink of Mg, decreasing its concentration in solution. Only future studies addressing the hydrology of this lake will be able to test those different hypotheses.

2. Relationships between microbialites and lake aqueous geochemistry

The chemical compositions of lake solutions were measured on samples collected at a specific time. By contrast, microbialites form over a certain time and therefore integrate potential solution chemistry variations that we may not see. Accordingly, we evidenced some, yet limited chemical variations over time in lake solutions as further discuss below. Chemical conditions may also vary spatially within a lake, with depth and possibly locally where a microbialite forms and again, this cannot be tracked by reporting the bulk chemistry of the lakes. Several sampling at different places in one lake consistently showed some chemical variations, which, again, were limited. Therefore, we assumed that these variations were most of the times small in comparison with the large chemical variations between the lakes. This is supported by clear first order relationships evidenced between lake aqueous geochemistries and microbialites that we discuss in this section.

2.1. Geochemical conditions for the formation of microbialites and carbonate precipitation pathways

We observed a correlation between the alkalinity/salinity and the occurrence, abundance, and size of microbialites in Mexican lakes (Fig. 13): no microbialite at the lowest alkalinity and lowest salinity (Lake Zirahuén); thin carbonates crusts at intermediate alkalinities/salinities (Lake Alberca de Guadulupe); larger microbialites at higher alkalinities/salinities (Lakes La Preciosa and Aljojuca); finally, massive microbialitic reefs at the highest alkalinities/salinities (*e.g.*, Lakes Atexcac and Alchichica). A minimum alkalinity between 1.23 and 4.28 mM and a minimum salinity between 0.08 and 0.21 g/L seem required for the formation of microbialites. This corresponded to lakes with a $SI_{Mg\text{-}calcite}$ higher than 1.11. This value is in accordance with the threshold of 1.0 required for cyanobacterial calcification by calcite, as established by Arp et al. (2001). Therefore, based on the hypothesis that alkalinity increases with concentration factor, the onset of microbialite formation may appear as a

976 milestone in the hydrochemical history of a lake, starting only after the achievement of a
977 minimum alkalinity and/or salinity value.
978 The analysis of a solubility diagram, where the logarithms of $a(Mg^{2+})$ or $a(Ca^{2+})$ were
979 plotted against the log of $a(CO_3^{2-})$ offered deeper insight into what may control carbonate
980 precipitation in Mexican lakes (Fig. 2). Similarly to what Fukushi and Matsumiya (2018)
981 evidenced in other alkaline lakes, we observed that several Mexican lakes (Quechulac, La
982 Preciosa and Atexcac) plot along/close to the solubility line of MHC, supporting the idea that
983 the $a(Ca^{2+})/a(CO_3^{2-})$ ratio in these lakes is controlled by the precipitation of this phase. All other
984 lakes but Zirahuén plot above the solubility line of MHC by about 0.5 log unit. Interestingly,
985 Fukushi and Matsumiya (2018) also observed that several alkaline lakes were similarly
986 supersaturated with MHC. This may suggest that additional precursor phases more soluble than
987 MHC control the $a(Ca^{2+})/a(CO_3^{2-})$ ratio in these lakes. Chaka et al. (2018) mentioned that MHC
988 is unlikely to precipitate primarily from a solution but results from the transformation of ACC
989 precursor. Rodriguez-Blanco et al. (2014) and Blue et al. (2017) also concurred that MHC is a
990 metastable intermediate between ACC and anhydrous Ca-carbonate phases such as calcite and
991 aragonite. While all Mexican lakes plot below the solubity line of ACC as determined by
992 Brecevic and Nielsen (1989), Mergelsberg et al. (2020) noticed that ACC with a lower
993 solubility exists. Overall, it is therefore possible that Mexican lakes plot close to the solubility
994 line of such a less soluble ACC phase. Alternatively, heterogenous nucleation of ACC, *e.g.*, on
995 cell surfaces or exopolymeric substances may as well occur at a lower $(Ca^{2+})(CO_3^{2-})$ product
996 than the ACC solubility line by Brecevic and Nielsen (1989). Following an Ostwald step rule,
997 when conditions are thermodynamically favored, the most soluble phases precipitate first since
998 they are kinetically favored (Chaka, 2018). Then they transform to less soluble, more
999 thermodynamically stable phases, either by dissolution-precipitation or solid-state
1000 transformation. Considering all these facts, we therefore suggest the following precipitation
1001 sequence for Ca-carbonates in Mexican lakes: (i) first, there is a homogeneous and/or
1002 heterogenous nucleation of ACC, which may control the $a(Ca^{2+})/a(CO_3^{2-})$ of many of the lakes.
1003 No ACC was detected in Mexican microbialites by bulk XRD and FTIR measurements.
1004 Benzerara et al. (2006) reported ACC in Lake Van microbialites, but this was achieved by
1005 precise TEM analyses and ACC clearly remain difficult to detect in association with other
1006 abundant, crystalline phases. Moreover, ACC might be so reactive that it transforms instantly,
1007 which adds to the difficulty to detect it. (ii) Then, ACC transforms to MHC. (iii) Third, MHC
1008 transforms to calcite or aragonite depending on the aqueous Mg/Ca ratio prevailing in the lake

1009 solution (Figs. 14 and 15). This latter transformation is not complete in some lakes as we detect
1010 MHC in some microbialites (see below).
1011 Only Lake Zirahuén lied much below the MHC solubility line, close to the aragonite
1012 and calcite solubility lines (Fig. 2). We did not observe any microbialite in this lake. This
1013 suggests that saturation with anhydrous carbonate (*i.e.*, aragonite, calcite) is insufficient for the
1014 detectable formation of microbialites and that (super)saturation with MHC might be necessary
1015 for this to happen.
1016 Fukushi and Matsumiya (2018) also observed a correlation between $a(Mg^{2+})$ and
1017 $a(CO_3^{2-})$ in several alkaline lakes, corresponding to the solubility of amorphous magnesium
1018 carbonates and therefore suggested that this phase controls the $a(Mg^{2+})/a(CO_3^{2-})$ in these lakes.
1019 This appears to be valid for Lake Alchichica (and to a lesser extent Lake Atexcac), in which
1020 solution waters are supersaturated with respect to hydromagnesite (Table SI-6) and
1021 microbialites contain hydromagnesite (Fig. 2). Chaka (2018) mentioned that hydromagnesite is
1022 unlikely to precipitate primarily from water and that this goes through transient more hydrated
1023 and more soluble precursor phases such as nesquehonite and dypingite. Overall, we can propose
1024 the following mineral precipitation sequence in Lake Alchichica: (i) there is precipitation of an
1025 amorphous magnesium carbonate, which then (ii) transforms to nesquehonite and which (iii)
1026 ultimately transforms to hydromagnesite. All the other lakes, except Atexcac, lie much lower
1027 than the amorphous Mg-carbonate solubility line (named AMC2 as determined by Fukushi and
1028 Matsumiya (2018)). Therefore, in these lakes, the $a(Mg^{2+})/a(CO_3^{2-})$ ratio is likely impacted by
1029 other mineral phases, possibly the authigenic Mg-silicates that were found pervasively, and/or
1030 Ca-carbonates. All these other lakes are moreover undersaturated with hydromagnesite and
1031 therefore, the formation of this phase is eventually not expected in these lakes. Last, in Lake
1032 Atexcac, waters were sometimes on, sometimes below the solubility line of amorphous Mg-
1033 carbonate (AMC2, Fig. 2). These variations of the chemical composition of the lake, possibly
1034 due to some hydrological variations (*e.g.*, higher concentration stages) may explain the limited
1035 amounts of hydromagnesite and abundant authigenic Mg-silicates in Lake Atexcac
1036 microbialites.
1037
1038 **2.1.1. Relationship between the aqueous Mg/Ca ratio and the carbonate**
1039 **mineralogy of microbialites**
1040
1041 The identity of the carbonate phases (Mg-calcite, MHC, aragonite, hydromagnesite)
1042 composing living Mexican microbialites was clearly correlated with the $(Mg/Ca)_{aq}$ ratio of the

lakes (Figs. 14 and 15). Müller et al. (1972) observed a similar empirical relationship based on the study of authigenic (non microbialitic) sediments collected from twenty-five lakes. The thresholds they inferred were about the same as in our study, except for the onset of hydromagnesite precipitation that they did not observe in the field but simulated by laboratory experiments. Based on these experiments, they suggested that hydromagnesite precipitated at $(Mg/Ca)_{aq}$>500. Chagas et al. (2016) also reported a similar relationship between the identity of the carbonate phases composing microbialites and the $(Mg/Ca)_{aq}$ ratio of the lakes based on a compilation of data from twenty-one lakes. These authors also noted departures from this relationship for lakes where local groundwater discharges influenced the mineralogy of the microbialites, such as in Lake Van (Kempe et al., 1991). Chagas et al. (2016) suggested that $[Mg^{2+}]_{aq}$ was a good predictor for the presence of high Mg-calcite and MHC in microbialites.

As explained above, the formation of hydromagnesite may require Mg^{2+} and CO_3^{2-} activities high enough so that solution activity products are above the solubility line of amorphous magnesium carbonate. The $(Mg/Ca)_{aq}$ ratio would thus appear as an indirect predictor of hydromagnesite formation, because it is generally correlated with DIC, hence CO_3^{2-} activity, and Mg^{2+} concentration. The control of the identity of the anhydrous Ca-carbonate phases composing microbialites appears different. Since ACC and/or MHC might be the same precursors for all lakes, we propose that the control by $(Mg/Ca)_{aq}$ operates on the transformation of the precursor phases into the most stable phases. At a $(Mg/Ca)_{aq}$ ratio higher than 10, MHC transforms completely to aragonite (Fig. 15). At a lower $(Mg/Ca)_{aq}$, MHC transforms partially to Mg-calcite or aragonite. Overall, this scenario is consistent with the claim that MHC might be a widespread metastable intermediate in the formation of anhydrous calcium carbonates and that it has been observed as an intermediate between ACC and aragonite or (Mg-)calcite (Chaka, 2018). Interestingly, it has also been argued that because of its unique structure, MHC is relatively more stable than other hydrated Ca or Mg carbonate phases, and its transformation to anhydrous carbonates occurs through dissolution-precipitation only. By contrast, other hydrated phases may undergo solid state transformations upon dehydration (Chaka, 2018). This may explain why some MHC may be preserved when they are kept away from dissolution, and how $(Mg/Ca)_{aq}$ may direct the transformation of MHC to (Mg-)calcite or aragonite through dissolution-precipitation. Indeed, since $[Mg^{2+}]_{aq}$ inhibits calcite precipitation (Berner, 1975; Deleuze and Brantley, 1997; Pokrovsky, 1998; Bots et al., 2011), the kinetics of aragonite precipitation becomes relatively faster than that of calcite when the Mg content of Mg-calcite exceeds ~18 mol% (Davis et al., 2000).

Several parameters can modify the $(Mg/Ca)_{aq}$ thresholds between the domains of dominance of the different carbonate phases. For instance, $[SO_4^{2-}]_{aq}$ may decrease calcite precipitation rate relative to aragonite (Walter, 1986; Bots et al., 2011) so that high $[SO_4^{2-}]_{aq}$ may favor the dominance of aragonite. Here, deconvoluting the impact of $(Mg/Ca)_{aq}$ *versus* $[SO_4^{2-}]_{aq}$ was difficult since both parameters were positively correlated (r_S=0.78). As an exception, Lake Tecuitlapa had a lower $(Mg/Ca)_{aq}$ ratio (3 *versus* 5.3 to 10.4) but a higher $[SO_4^{2-}]_{aq}$ (1.6 *versus* 0.2 mM) than Lake Quechulac. Lake Tecuitlapa microbialites were mainly composed of Mg-calcite and MHC, while Lake Quechulac microbialites were composed of aragonite only. In that case, the $(Mg/Ca)_{aq}$ ratio was therefore the dominant controlling parameter, consistently with what was reported by Bischoff and Fyfe (1968).

Finally, we observed deviations from this global relationship between the identity of the carbonate phases and the $(Mg/Ca)_{aq}$ ratio in non-living microbialites. Some of these deviations may indicate the impact of diagenesis as suggested by the detection of Mg-poor calcite in fossil microbialites of Lake Alchichica (*e.g.*, AL2012-15). Calcite may result from meteoric alteration of aragonite by dissolution/reprecipitation (*e.g.,* De Boever et al., 2017). In this case, hydromagnesite seems to be leached out. How Mg-silicates are affected by meteoric alteration remains to be understood. In other cases, the deviations may be due to past variations of the $(Mg/Ca)_{aq}$ ratio of the lakes. In this scenario, the carbonate mineralogy of non-living microbialites recorded in most cases lower $(Mg/Ca)_{aq}$ past values: *e.g.,* the non-living microbialite of Lake Pátzcuaro was composed of Mg-calcite only, while the living microbialite contained Mg-calcite, MHC and aragonite; non-living microbialites in Lake Alchichica contained aragonite and calcite, while living ones contained aragonite and hydromagnesite. Overall, one may infer an increasing net concentration factor over time, which increases the alkalinity as well as the $(Mg/Ca)_{aq}$ ratio of the lakes, as discussed above. After the onset of microbialite formation, this would result in the successive formation of living microbialites, which are first composed of Mg-calcite, then aragonite and finally hydromagnesite along with the alkalinity, salinity and aqueous Mg/Ca gradients (Figs. 13-16).

2.1.2. Occurrence of monohydrocalcite and its environmental significance

Based on the (super)saturation of all Mexican microbialites-harbouring lakes with respect to MHC and consistently with several recent theoretical, field and experimental studies (*e.g.,* Chaka, 2018; Fukushi and Matsumiya, 2018; Fukushi et al., 2020), MHC is interpreted as a precursor phase in Mexican lakes. It is sometimes transient, transforming into aragonite

and/or Mg-calcite. Sometimes, it is preserved in several microbialites. Microbialites from Lakes Tecuitlapa and Aljojuca offer some textural examples of MHC replacement by Mg-calcite (Fig. 5). MHC was observed in the living microbialites from Lake La Alberca de Los Espinos ($(Mg/Ca)_{aq}$=2.8), Lake Pátzcuaro ($(Mg/Ca)_{aq}$=3.0) and Lake Tecuitlapa ($(Mg/Ca)_{aq}$=3.0) as the second most abundant carbonate phase after (Mg-)calcite. MHC was the main mineral phase in living microbialites from Lake Aljojuca ($(Mg/Ca)_{aq}$ =6.8) but was absent from microbialites in Lake Quechulac ($(Mg/Ca)_{aq}$=10.4) (Fig. 15; Table 3).

MHC has been frequently found in lacustrine deposits (Domagalski et al., 1989), including microbialites (Kharaka et al., 1984; Rosen et al., 2004; Last et al., 2010), sometimes partially replaced by Mg-calcite (Spencer, 1977). This mineral phase has also been shown to be preserved in ancient (> 1000 years) lacustrine sediments (Stoffers and Fischbeck, 1974). Chagas et al. (2016) proposed that MHC formed in lakes with Mg concentration higher than 37.5 mM. Taylor (1975) argued that a pH higher than 8.6 and a Mg/Ca ratio higher than 10 favored the precipitation of MHC, whereas Fukushi et al. (2011) reported that a pH higher than 8 and a $(Mg/Ca)_{aq}$ ratio higher than 4 could favor this process. Loste et al. (2003) experimentally showed the precipitation of MHC at Mg/Ca ratios higher than 3, but in association with other carbonate phases. Here, we suggest that the precipitation of MHC is determined by (Ca^{2+}) and (CO_3^{2-}) activities being above the solubility line of MHC. Then, MHC secondarily transforms partly or completely to more stable anhydrous Ca-phases by dissolution-precipitation. Therefore, in Mexican microbialites, the control on MHC presence/absence may relate to the efficiency/kinetics/inhibition of its transformation to (Mg-)calcite or aragonite.

Rodriguez-Blanco et al. (2014) consistently proposed that some (Mg-)calcite and aragonite found in the geological record may be of secondary origin, resulting from the transformation of a primary metastable MHC phase. Finding past traces of MHC in ancient microbialites might therefore be challenging. Whether preservation of MHC, observed in non-living microbialites from Lake Aljojuca and Lake Tecuitlapa, may be favored by high concentrations of orthosilicic acid as suggested by Zhang et al. (2013) and/or phosphates (Fukushi et al., 2011) will require further investigations. An additional preservation pathway may involve microorganisms. We observed microcrystalline MHC associated with dense clusters of filamentous microfossils in microbialites from Lakes Tecuitlapa and Aljojuca. Similarly, MHC was observed as the organomineralization by-product of anoxygenic phototrophic bacteria (Bundeleva et al., 2012). These authors suggested that organic matter such as exopolymeric substances (EPS) may preserve MHC from recrystallisation into more

stable carbonates. Future experimental studies exploring the chemical and biological pathways favoring the preservation of MHC will be crucial.

2.1.3. Sr enrichment within microbialites and its relationships with carbonate mineralogy

There was a positive linear correlation between the Sr and Ca microbialite contents (r_S=0.84). Only AlbEsp2014-01 outlied this relationship. Authigenic-dominated microbialites showed a Sr/Ca ratio of 0.009 ± 0.002. We calculated the solid/liquid partition coefficient of Sr normalized to Ca (for the samples collected in 2014 and authigenic-dominated): $(Sr/Ca)_{mic}/(Sr/Ca)_{aq}$=2.4 ± 0.7, indicating an enrichment of Sr in the microbialites compared to the solutions relatively to Ca. Tesoriero and Pankow (1996) measured a partition coefficient of 0.021 between Sr/Ca in calcite *versus* Sr/Ca in the solution at 25°C. Dietzel et al. (2004) measured a partition coefficient of 1.19 at 25°C in aragonite. Here, we therefore observed a relative enrichment of Sr over Ca between the solid and the solution that is not explained by the precipitation of calcite and/or aragonite alone. Some hypotheses can be explored to explain this enrichment but they will need to be investigated in the future. On the one hand, other mineral phases, such as sulfates, may contribute, although they are at low concentration in the studied microbialites and the S content does not correlate with that of Sr (r_S=0.2). Alternatively, some biological processes may play a role in such a fractionation. Extracellular bioprecipitation of carbonates has been reported to induce fractionation but they appear lower than the one measured here. For example, the bacterium *Sporosarcina pasteurii* induces extracellular precipitation of $(Ca,Sr)CO_3$ via ureolysis (Lauchnor et al., 2013), with a solid/liquid partition coefficient of 0.38-1.00. In a similar study, Mitchell and Ferris (2005) found a Sr partition coefficient to be 0.46 at 20 °C in carbonates formed by the ureolytic *Bacillus pasteurii*. Alternatively, Cam et al., (2016) and Blondeau et al. (2018) showed a very high Sr over Ca enrichment in intracellular carbonates formed by *Gloeomargarita lithophora*, a cyanobacterium isolated from Lake Alchichica (Couradeau et al., 2013) and found in other lakes as well (Ragon et al., 2014). Whether ACC formed by these bacteria may eventually feed at least some of the extracellular carbonate phases forming Mexican microbialites in trace elements such as Sr will have to be explored.

2.2. Geochemical conditions allowing authigenic Mg-silicates precipitation and proxies for $[H_4SiO_4]_{aq}$ of ancient lakes

All lakes harboring microbialites were supersaturated with respect to hydrated Mg-silicates such as kerolite, sepiolite or stevensite except at the center of Lake Alchichica (AL-M) (Fig. 3 and Table SI-6). However, hydrated Mg-silicates were systematically observed as authigenic phases, except in microbialites from Lake Aljojuca and in most of the samples from Lake Alchichica (Table SI-7). More soluble phases, such as the "amorphous sepiolite" as defined by Wollast et al. (1968), thus appear as better predictors of authigenic silicate formation since it better accounts for the absence of Mg-silicates in Alchichica samples (Fig. 3). Two lakes (Lakes Alberca de Guadalupe and Atexcac) were located above the critical supersaturation line for homogenous nucleation as defined by Tosca et al. (2011) and Tosca and Masterson (2014). It is therefore thermodynamically and kinetically possible that authigenic silicate phases precipitate spontaneously, without any biological mediation in these lakes. All other lakes harbouring authigenic-silicate-containing microbialites lie below this line and on or above the solubility line of "amorphous sepiolite" (Fig. 3). Two hypotheses can be formulated: (i) The phase forming in Mexican microbialites is closer in solubility to the "amorphous sepiolite" phase formed in Wollast et al. (1968)'s experiments and this phase is different and less soluble than the phase formed in Tosca et al. (2011)'s experiments. Such a difference between the phases formed in both studies was discussed by Tosca et al. (2011) and may relate to the source of Si that was used in these experiments (*i.e.,* sodium metasilicate nonahydrate *versus* tetraethyl orthosilicate). (ii) Authigenic silicates in Mexican microbialites are similar to the ones forming in Tosca et al. (2011)'s experiments but they nucleate heterogeneously, hence at a lower ionic activity product than the critical supersaturation line for homogeneous nucleation. Microscopy observations of biofilms entombed within Mg-silicates in Mexican microbialites support the possibility of such an extensive heterogenous nucleation (Zeyen et al., 2015). Only a better understanding of the structural controls over the solubility of these phases will help to decipher between these two hypotheses. Surprisingly, the saturation index with respect to kerolite in Lake Aljojuca ($SI_{kerolite}$=4.82; $[H_4SiO_4]_{aq}$=0.16 mM) was higher than *e.g.*, in Lake Pátzcuaro ($SI_{kerolite}$=4.17; $[H_4SiO_4]_{aq}$=0.37 mM), although authigenic Mg-silicates were detected and observed in Lake Pátzcuaro microbialites but not in Lake Aljojuca microbialites. The origin of this discrepancy remains to be understood.

Lakes do not plot along a single line in the solubility diagram for authigenic Mg-silicates, meaning that the solubilities of these phases may not control the activities of the dissolved chemical species, at least not in all lakes. Then, what controls H_4SiO_4 activity in the lakes remains an open question. The nature of the weathered protolith and variations of silicate

weathering intensity may be prime parameters. The biomineralization activity of diatoms in the lakes may also play an important role. Indeed, diatoms actively take up H_4SiO_4 from the water (Milligan and Morel, 2002) and precipitate opaline silica even in those Mexican lakes that are undersaturated with respect to amorphous silica. Here, similarly to what has been shown in the oceans (Conley et al., 2017), it is possible that diatom populations decrease $[H_4SiO_4]_{aq}$ to different extents between lakes and/or at different time of the year in a given lake, explaining the observed temporal variations of $[H_4SiO_4]_{aq}$. Upon diatom death, especially in lakes where solutions are undersaturated with respect to amorphous silica, H_4SiO_4 is expected to be "recycled" back to the solution. The maintenance of an out-of-equilibrium state regarding the precipitation of Mg-silicates suggests that either the input of H_4SiO_4 to the lakes by diatom dissolution and/or weathering processes may be constantly higher than the removal of Si by the kerolite/stevensite precipitation. However, at least in some cases, H_4SiO_4 appears to be retained in microbialites rather than released back to solution. Indeed, we observed that diatoms may serve as loci for Mg-silicate precipitation, producing diatoms fossilized by Mg-silicates (kerolite/stevensite) in the microbialites from Lakes Atexcac and Alberca de Guadalupe. This process called "reverse weathering" was also observed by Badaut and Risacher (1983) and Bentz and Peterson (2020) in Andean saline lakes.

We observed Al-poor Mg-silicates as a predominant authigenic phase in Mexican lakes. Gérard et al. (2018) also detected Al-poor Mg-silicates as a predominant phase in microbialites from Lake Dziani. In contrast, Milesi et al. (2019) and Milesi et al. (2020) observed a Mg-rich aluminosilicate as a predominant phase in the sediments of Lake Dziani. Milesi et al. (2019) proposed that the dissolution of detrital silicates and hydromagnesite in sediments provided Al, Si and Mg, and favored the precipitation of a Mg-rich aluminosilicate phase. Unfortunately, we did not analyze the mineralogical composition of the sediments in Mexican lakes to assess how systematic the dichotomy observed in Lake Dziani might be. This will be important to assess since Millot (1970) proposed that Al-rich clay minerals preferably form at basin margins by heterogenous nucleation on detrital Al-silicates, whereas homogenous nucleation of Al-poor Mg-silicates (such as stevensite) occurs preferentially towards the basin center where detrital materials are at a lower amount. The paleoenvironmental significance of this relationship may however not be attested in small-scale basins. In any case, we underline that the presence of Al-poor Mg-silicates in Dziani and Mexican microbialites *vs*. Mg-aluminosilicates in Dziani sediments is supported by the phase equilibria mentioned above. Indeed, Mg-aluminosilicates (such as saponite or montmorillonite) are less soluble than amorphous sepiolite and can therefore precipitate at a lower ionic activity product (Tosca, 2015). Pore waters in Dziani

sediments have an ionic activity product lower than the solubility line of amorphous sepiolite but equal/higher than that of Mg aluminosilicates. In contrast, Dziani and most Mexican lake waters are saturated or supersaturated with amorphous sepiolite, thus allowing precipitation of Al-poor Mg silicates. One major parameter explaining this difference is that Dziani sediment pore waters have a lower H_4SiO_4 activity than Dziani and Mexican lake waters. As mentioned above, the determinism of H_4SiO_4 activity remains to be explored.

Last, similarly to MHC, the long-term preservation of authigenic Mg-silicates in the fossil record can be discussed. Early secondary replacement of Mg-silicates by (Mg-)calcite and/or aragonite was observed by SEM in Lake Alberca de Guadalupe, Lake Atexcac, Lake Quechulac and Lake La Preciosa (Fig. 7). This suggests that a carbonation reaction transforms the silicates, which might be very fast due to their poor crystallinity. Tosca and Wright (2015) adressed in detail several additional processes susceptible to destabilize authigenic Mg-silicates upon diagenesis. They showed that Mg-silicates may dissolve due to organic carbon degradation by *e.g.*, methanogenesis, which decreases pore solution pH and drives solutions out of Mg-silicate stability zone. Moreover, cation migration to octaedral vacancies in these silicates generate protons, which in turn may result in their dissolution (Komadel et al., 2005; Tosca and Wright, 2015). In addition, potential magmatic CO_2 degassing could increase the pH of the pore water of the sediments (Milesi et al., 2020) which could eventually lead to the Mg-silicate destabilization upon diagenesis. Yet, Mg-silicates are sometimes preserved in the geological record (Tettenhorst and Moore 1978; Tosca et al., 2011), urging their systematic search in ancient microbialites.

2.3. Local processes: evidence for microbial influence

The above discussion identifies large-scale chemical and hydrological parameters controlling the formation of microbialites and their mineralogical composition. However, this should not be considered as a negation of the role of biology, which may catalyze precipitation and/or "mold" mineral textures. We discuss several aspects of this below.

Carbonates

Arp et al. (2001) suggested that DIC controls biologically-mediated carbonate precipitation pathways: at high DIC and pH (*e.g.*, soda lakes), carbon removal by cyanobacterial photosynthesis induces only a minor rise in calcite supersaturation in the entire lake, because of the large buffering of pH by DIC. If local pH increase is the biological driver of nucleation, $CaCO_3$ may therefore not precipitate preferentially on cells in these lakes but instead

homogenous $CaCO_3$ nucleation may occur everywhere. In contrast, in low-DIC water, photosynthesis results in a strong rise in calcite supersaturation ($\Delta SI_{calcite} = 0.3 – 0.5$), and Ca-carbonate precipitation occurs prefentially around the cells, thereby inducing the formation of calcimicrobes in the rock record. As mentioned previously, this model should be reconsidered by focusing on local saturations with precursor phases (*e.g.*, ACC and/or MHC) instead of calcite. For example, microorganisms may impact not only the nucleation of the precursor phases but also the different transformation steps to the final most stable phases found in microbialites. Moreover, we observed fossilized bacteria (calcimicrobes) in association with (Mg-)calcite, MHC, or aragonite in microbialites from all the studied lakes including those with high DIC. As already mentioned by Gérard et al. (2013) and Couradeau et al. (2013), this contradicts the idea that calcimicrobes cannot form in high-DIC environment. However, these observations might be reconciliated with Arp et al (2001)'s model by considering that while the alkalinity engine driven by cyanobacterial photosynthesis plays a minor role in high-DIC environments, heterogeneous nucleation of carbonate phases on *e.g.*, cyanobacterial sheaths may play an important role, hence partly localizing precipitation around cells (Giuffre et al., 2013).

Moreover, it has been reported that some microorganisms may orient mineral precipitation towards one carbonate phase at the expense of another, such as the cells of the cyanobacterial *Pleurocapsales* and *Chroococcales* orders, which were shown to induce the precipitation of aragonite in a hydromagnesite-dominated environment (Gérard et al., 2013; Couradeau et al., 2013; Saghaï et al., 2015). Future studies should be directed to determining whether such microorganisms may be present in all the studied lakes and may systematically favor aragonite over hydromagnesite nucleation or if this biological influence is only a parameter of lower importance.

Mg-silicates

The microbial mediation of authigenic Mg-silicate precipitation has been increasingly suggested in various environments based on the observation of close spatial associations between cells and these phases (Léveillée et al., 2002; Arp et al., 2003; Souza Egypsy et al., 2005; Burne et al., 2014; Zeyen et al., 2015; Pace et al., 2016; Gérard et al., 2018). Léveillé et al. (2002) argued that the precipitation of authigenic Mg-silicates, at least in part, results from the binding effect of the EPS concentrating ions (Mg and silica) from solution and serving as nucleation sites for kerolite precipitation. This mechanism was also favored by Pace et al., (2016). Zeyen et al (2015) observed an intimate and pervasive association of EPS with Mg-

silicates, down to the nm-scale, also supporting the importance of these polymers in mineral precipitation. An additional question relates on how EPS could fractionate Mg, Si and Al. Burne et al. (2014) proposed that Mg-silicate formation is promoted by high local silica activity from dissolving diatoms. As described above, spontaneous homogeneous nucleation is possible in two Mexican lakes. In other lakes, it remains to understand if the spontaneous nucleation of a phase with a solubility close to that of amorphous sepiolite is possible. In this case, the involvement of microbes may not be strictly necessary for the precipitation of this phase in Mexican microbialites. Otherwise, we observe in the solubility diagram of Mg-silicates evidence of heterogeneous nucleation of a phase with a solubility similar to that measured by Tosca et al. (2011) and this might be catalyzed, at least in part, by microorganisms.

P-rich phases

The present study highlighted a positive linear correlation between the P content of the studied microbialites and the $[Sr]_{aq}$ of the corresponding lakes (Figs. 12 and SI-8). $[Sr]_{aq}$ was also positively correlated with $[Ca]_{aq}$, which can be explained by the similar chemical behavior of both elements. The correlation between the P content of the studied microbialites and $[Sr]_{aq}$ may suggest that (i) some of the phosphorus in the microbialites is in the form of Ca-phosphate mineral phases and (ii) this phosphate mineral reservoir is relatively bigger at lower $(Mg/Ca)_{aq}$ ratio and lower alkalinity, *i.e.*, where the precipitation of Ca-phosphate may be favored relatively to that of carbonate phases. Consistently, it can be noted that the saturation index with respect to hydroxyapatite was the highest under these conditions (Table SI-6). Recently, Toner and Catling (2019) highlighted a positive correlation between $[PO_4^{3-}]_{aq}$ and dissolved inorganic carbon (DIC) in different North American and African lakes. These authors explained that this positive correlation resulted from the precipitation of Ca-carbonates in highly alkaline lakes, which acted as a sink for Ca^{2+}, which therefore did not precipitate with P, resulting in its accumulation in the water column. In this present study, we did not observe such a correlation, possibly because $[PO_4^{3-}]_{aq}$ measurements were not precise enough. Alternatively, the removal of phosphorus via biotic mechanisms may have a strong impact on the PO_4^{3-} concentration in these lacustrine systems. Interestingly, statistical analyses highlighted the fact that there is a positive correlation between P and Mn contents of microbialites. These elements are also correlated with the C_{org} content of microbialites. Especially, the living microbialite sample from Lake La Alberca de Los Espinos showed the highest concentrations in P, Mn and C_{org}. It is not clear if Mn and P are part of the same phase within this microbialite, but the incorporation of

these two nutrients could be mediated by the activity of microorganisms. The speciation of P in these microbialites will need further investigations using, *e.g.*, spectro(micro)scopy tools.

S-rich organic molecules

We observed a positive correlation between the organic carbon and total sulphur contents for 9 microbialite samples, with a S_{tot}/C_{org} atomic ratio equal to 0.188 ± 0.009 (Fig. SI-7). This correlation may be consistent with S being associated with organic carbon in microbialites. However, the measured S/C ratio is significantly higher than the mean S/C ratio of 0.012 (at./at.) with a range of 0.006 – 0.032 (at./at.) measured on 8 types of natural and cultured bacteria by Fagerbakke et al. (1996). Heldal et al. (2003) measured even lower ratios between 0.003 and 0.009 (at./at.) for marine *Synecchococcus* and *Prochlorococcus* strains. One possibility is that organic matter entombed within microbialites becomes sulfurized, a process, which would increase the S/C ratio as this has been observed in 2.72 Ga old microbialites (Lepot et al., 2009). Atomic S/C ratio of organic matter globules from these ancient microbialites reach up to 0.042 (Lepot et al., 2019). The presence of sulfurized organic compounds (thiopenes) was also observed in modern freshwater microbialites from Cuatro Ciénegas (Mexico) (Nitti et al., 2012). Alternatively, some S may be in the form of sulfates within carbonate phases or sulfide phases explaining the departure of some samples towards compositions richer in S. A major obstacle to address these questions deals with the speciation of S in these samples, which would need to be assessed in the future to discriminate between these different possibilities.

3. REE+Y patterns of authigenic-dominated microbialites

REE+Y patterns of ancient chemical sediments have often been used as proxies to identify their depositional environments (Van Kranendonk et al., 2003; Bolhar and Van Kranendonk, 2007; Awramik and Buchheim, 2009; Zhao and Zheng, 2017; Eltom et al., 2017) and reconstruct the geochemistry of ancient seawater (Kamber and Webb, 2001; Kamber et al., 2004; Bolhar et al., 2004; Bolhar and Van Kranendonk, 2007; Frimmel, 2009; Riding et al., 2014; Kamber et al., 2014). However, as also reported before, we observe that detrital contaminations strongly affects microbialite REE+Y patterns and blurs this message. As a result, REE+Y patterns of Mexican microbialites highly affected by detritism hold no information on their formation environments (Text SI-3). These microbialites showed: (i) a high total REE+Y contents, above 12.2 ppm; (ii) a flat REE pattern and less marked REE anomalies, and finally (iii) a low Y/Ho ratio (close to that of chondrites). By contrast, although authigenic-dominated microbialites also showed some hints of contamination (Text SI-3), some

variations were observed in their REE+Y patterns, which may be indicative of the conditions under which they form. REE+Y patterns of Mexican authigenic-dominated microbialites showed (i) a relatively higher proportion of HREE, (ii) relatively high (positive or negative) anomalies in Eu, Ce, La, Gd and Pr and (iii) a high Y/Ho ratio. The possible origins of these signatures are discussed in Supplementary Data. However, whatever their origins, it is particularly interesting to observe that these signatures have been classically attributed to microbialites formed in seawater. The REE+Y pattern of marine microbialites from the Heron Reef, Great Barrier Reef has been used as a modern reference for marine microbialites (Webb and Kamber, 2000). Similarly to modern seawater, they showed HREE enrichment with $(Nd/Yb)_{SN}$= 0.236 ± 0.026, negative Ce and positive La and Gd anomalies, and a uniformly superchondritic Y/Ho ratio (56.17 ± 2.66). Similar features were observed in Messinian carbonates from Calcare di Base (Sicily) by Guido et al. (2011): a HREE enrichment with $(Nd/Yb)_{SN}$ of 0.5; positive La, Gd, Eu and Y anomalies, a negative Ce anomaly and a superchondritic Y/Ho ratio of 57.1. This led the authors to conclude about a marine origin of these carbonates. However, here we demonstrate that some of the modern Mexican lacustrine microbialites also show similar REE+Y patterns, despite their freshwater origin: a HREE enrichment (mean value Nd/Yb_{SN} = 0.56, SD= 0.19), La, Gd, Eu positive anomalies, Ce negative anomalies and a superchondritic Y/Ho value (reaching up to 58). Many continental waters exhibit REE+Y patterns that closely resemble those of modern seawater (Johannesson et al., 2006). Overall, this calls for a careful reassessment of the criteria discriminating between marine and freshwater environments and a better understanding of the diversity of the processes, including the role of microbes, involved in the fractionation of REE+Y in these systems.

CONCLUSION

Ten alkaline Mexican lakes showed correlated salinities, alkalinities and $(Mg/Ca)_{aq}$ ratios varying over a broad range. These environmental parameters controlled the presence/absence and size/amount of microbialites in the lakes, as well as their mineralogical composition as illustrated by Figure 16. A minimum alkalinity between 1.23 and 4.28 mM and a salinity between 0.08 and 0.21 g/L appeared necessary for the formation of microbialites. This may more accurately relate to the achievement of saturation levels of the solutions close or above the solubility of MHC. A precipitation pathway for Ca-carbonate phases is inferred: ACC may precipitate first before transforming to MHC, which itself transforms partly or completely

to Mg-calcite or aragonite, depending on the $(Mg/Ca)_{aq}$ of the solution. Moreover, when (Mg^{2+}) and (CO_3^{2-}) activites are higher than the solubility of amorphous magnesium carbonate, Mg-carbonates precipitate and transform ultimately to hydromagnesite. The occurrence of authigenic Mg-silicates was decoupled from this global trend. Such phases were detected in microbialites from lakes saturated or supersaturated with a phase reported in the litterature as "amorphous sepiolite" and with a concentration of orthosilicic acid higher than 0.2 mM. Overall, by identifying the primary mineralogy of a microbialite, one may obtain information on several chemical conditions prevailing in the lake where these microbialites formed. Moreover, since higher salinity-alkalinity-$(Mg/Ca)_{aq}$ result from an increasing concentration of alkaline lakes, we can propose an integrated evolutionnary scenario in which microbialite formation evolves with the changing lake hydrochemistry, which itself depends on the hydrological functioning of the lake. As the concentration stage of an alkaline lake increases, salinity/alkalinity increases and, at some point, microbialites start to form. Upon further concentration, the $(Mg/Ca)_{aq}$ ratio increases and the mineralogy of the microbialites shifts from Mg-calcite to aragonite and eventually hydromagnesite appears as well. In parallel, microbialite formation populating the lakes become more massive (Fig. 16).

The trace element composition of microbialites also offers additional information. High concentrations in Al, Ga, Nb, Ta, K, Rb, Hf and Zr were diagnostic of microbialite contamination by detrital particles. This resulted in high REE+Y contents of these microbialites together with a flat REE+Y pattern. In contrast, lacustrine authigenic-dominated microbialites showed an HREE enrichment, and marked REE anomalies with, in particular, a positive Eu anomaly, a negative Ce anomaly and a high Y/Ho ratio. Therefore, these characteristics, used in past studies as diagnostic of a marine origin, can also be found in some lacustrine microbialites, questioning their diagnostic value for marine settings.

This study suggests that the abundance and the mineralogical and chemical composition of lacustrine microbialites can be predicted at a first order based on the global physico-chemical and hydrological conditions prevailing in the lake. However, these physicochemical conditions, while being necessary, might not always be sufficient and other processes may explain some of the observed variability across microbialites within a single lake. This is the case of groundwater vents, and/or the presence of certain microorganisms influencing local conditions and precipitation of specific mineral phases. Moreover, since the global physico-chemical conditions prevailing in a lake may influence the taxonomic and functional diversity of microbial communities and vice-versa, this relationship between environmental parameters and the composition of microbialites does not preclude the importance of biology. Future integrative

(meta-)analyses of taxonomic and functional diversity of microbial populations in addition to solution geochemistry, microbialite mineralogical and chemical composition in different lakes may reveal some of these connections. The general rules exposed here offer a new framework for a better interpretation of the paleo-environmental conditions under which ancient lacustrine microbialites formed. Last, for this purpose, the diversity of transformations occurring upon diagenesis and/or metamorphism of the phases composing modern microbialites, including monohydrocalcite and Mg-silicates, will be crucial to assess.

ACKNOWLEDGMENTS

The research leading to these results has received funding from the European Research Council under the European Union's Seven Framework Program: ERC grants Calcyan (PI: K. Benzerara, Grant Agreement no. 307110) and ProtistWorld (PI: P. López-García, Grant Agreement no. 322669). Part of the work was supported by the ANR Microbialites (ANR-18-CE02-0013-02). Some of the analytical measurements were supported by the IPGP multidisciplinary program PARI and by Region île-de-France SESAME Grant no. 12015908. We thank Aurélien Saghaï, Marie Ragon, Paola Bertolino, Eleonor Cortés, Angela Delgado Buscalioni and Ana Isabel López-Archilla for their help during the field trip in May 2014. We thank Ludovic Delbes and Benoit Baptiste who managed the XRD platform at IMPMC where analyses were performed. We thank Keevin Beneut and Maxime Guillaumet who managed the FTIR platform at IMPMC where analyses were performed. We thank Imene Esteve, Béatrice Doisneau and Stéphanie Delbrel who managed the SEM platform at IMPMC where analyses were performed. The SEM facility at IMPMC was purchased owing to a support by Region Ile de France grant SESAME 2006 I-07-593/R. We thank Laure Cordier (ICP-AES and ion chromatography analyses) and Emmanuelle Raimbault (continuous flow colorimetric analyses and alkalinity measurements) for technical support at IPGP. We thank Julien Bouchez for performing strontium isotopic analysis at IPGP and for his valuable feedbacks on the manuscript. We thank the three anonymous reviewers and Nicholas Tosca for their constructive reviews.

REFERENCES

Alcocer J. and Bernal-Brooks F. W. (2002) Spatial and temporal heterogeneity of physical and chemical variables for an endorheic, shallow water body: lake Pátzcuaro, Mexico. *Arch Hydrobiol*, **155-2**, 239-253.

1483 Alcocer J. and Bernal-Brooks F. W. (2010) Limnology in Mexico. *Hydrobiologia* **644**, 15–68.

1484 Al-droubi A., Fritz B., Gac J. and Tardy Y. (1980) Generalized Residual Alkalinity Concept - Application to
1485 Prediction of the Chemical Evolution of Natural-Waters by Evaporation. *Am. J. Sci.* **280**, 560–572.

1486 Allwood A. C., Walter M. R., Kamber B. S., Marshall C. P. and Burch I. W. (2006) Stromatolite reef from the
1487 Early Archaean era of Australia. *Nature* **441**, 714–718.

1488 Almendinger J. E. (1990) Groundwater control of closed-basin lake levels under steady-state conditions. *Journal*
1489 *of Hydrology* **112**, 293–318.

1490 Aminot A. and Kérouel R. (2004) Hydrologie des écosystèmes marins. Paramètres et analyses. 74–78.
1491
1492 Armienta M. A., Vilaclara G., De la Cruz-Reyna S., Ramos S., Ceniceros N., Cruz O., Aguayo A. and Arcega-
1493 Cabrera F. (2008) Water chemistry of lakes related to active and inactive Mexican volcanoes. *Journal of*
1494 *Volcanology and Geothermal Research* **178**, 249–258.

1495 Arp G., Hofmann J. and Reitner J. (1998) Microbial fabric formation in spring mounds ("Microbialites") of
1496 alkaline salt lakes in the Badain Jaran Sand Sea, PR China. *Palaios* **13**, 581–592.

1497 Arp G., Thiel V., Reimer A., Michaelis W. and Reitner J. (1999a) Biofilm exopolymers control microbialite
1498 formation at thermal springs discharging into the alkaline Pyramid Lake, Nevada, USA. *Sedimentary*
1499 *Geology* **126**, 159–176.

1500 Arp G., Reimer A. and Reitner J. (2001) Photosynthesis-induced biofilm calcification and calcium concentrations
1501 in Phanerozoic oceans. *Science* **292**, 1701–1704.

1502 Arp G., Reimer A. and Reitner J. (2003) Microbialite formation in seawater of increased alkalinity, Satonda Crater
1503 Lake, Indonesia. *Journal of Sedimentary Research* **73**, 105–127.

1504 Awramik S. M. and Buchheim H. P. (2009) A giant, Late Archean lake system: The Meentheena Member
1505 (Tumbiana Formation; Fortescue Group), Western Australia. *Precambrian Research* **174**, 215–240.

1506 Badaut D. and Risacher F. (1983) Authigenic Smectite on Diatom Frustules in Bolivian Saline Lakes. *Geochim.*
1507 *Cosmochim. Acta* **47**, 363–375.

1508 Bahniuk A., McKenzie J. A., Perri E., Bontognali T. R. R., Vogeli N., Rezende C. E., Rangel T. P. and Vasconcelos
1509 C. (2015) Characterization of environmental conditions during microbial Mg-carbonate precipitation and
1510 early diagenetic dolomite crust formation: Brejo do Espinho, Rio de Janeiro, Brazil. *Geological Society,*
1511 *London, Special Publications* **418**, 243–259.

1512 Bau M. and Dulski P. (1996) Distribution of yttrium and rare-earth elements in the Penge and Kuruman iron-
1513 formations, Transvaal Supergroup, South Africa. *Precamb. Res.* **79**, 37–55.
1514
1515 Bentz J. L. and Peterson R. C. (2020) The formation of clay minerals in the mudflats of Bolivian Salars. *Clays*
1516 *Clay Miner.* **68**, 115–134.

1517 Benzerara K., Menguy N., López-García P., Yoon T.-H., Kazmierczak J., Tyliszczak T., Guyot F. and Brown G.
1518 E. (2006) Nanoscale detection of organic signatures in carbonate microbialites. *Proceedings of the*
1519 *National Academy of Sciences* **103**, 9440–9445.

1520 Benzerara K., Meibom A., Gautier Q., Kaźmierczak J., Stolarski J., Menguy N. and Brown G. E. (2010)
1521 Nanotextures of aragonite in stromatolites from the quasi-marine Satonda crater lake, Indonesia.
1522 *Geological Society, London, Special Publications* **336**, 211–224.

1523 Bernard S., Beyssac O. and Benzerara K. (2008) Raman mapping using advanced line-scanning systems:
1524 geological applications. *Applied spectroscopy* **62**, 1180–1188.

1525 Berner R. A. (1975) The role of magnesium in the crystal growth of calcite and aragonite from sea water.
1526 *Geochimica et Cosmochimica Acta* **39**, 489–504.

1527 Bischoff J. L. and Fyfe W. S. (1968) Catalysis, inhibition, and the calcite-aragonite problem; [Part] 1, The
1528 aragonite-calcite transformation. *Am J Sci* **266**, 65–79.

1529 Bischoff J. L., Israde-Alcántara I., Garduño-Monroy V. H. and Shanks III W. C. (2004) The springs of Lake
1530 Pátzcuaro: chemistry, salt-balance, and implications for the water balance of the lake. *Applied*
1531 *Geochemistry* **19**, 1827–1835.

1532 Bischoff W. D., Sharma S. K. and MacKenzie F. T. (1985) Carbonate ion disorder in synthetic and biogenic
1533 magnesian calcites; a Raman spectral study. *American Mineralogist* **70**, 581–589.

1534 Blondeau M., Benzerara K., Ferard C., Guigner J.-M., Poinsot M., Coutaud M., Tharaud M., Cordier L. and
1535 Skouri-Panet F. (2018) Impact of the cyanobacterium Gloeomargarita lithophora on the geochemical
1536 cycles of Sr and Ba. *Chemical Geology* **483**, 88–97.

1537 Blue C. R., Giuffre A., Mergelsberg S., Han N., De Yoreo J. J. and Dove P. M. (2017) Chemical and physical
1538 controls on the transformation of amorphous calcium carbonate into crystalline CaCO3 polymorphs.
1539 *Geochimica et Cosmochimica Acta* **196**, 179–196.

1540 Bolhar R., Kamber B. S., Moorbath S., Fedo C. M. and Whitehouse M. J. (2004) Characterisation of early
1541 Archaean chemical sediments by trace element signatures. *Earth and Planetary Science Letters* **222**, 43–
1542 60.

1543 Bolhar R. and Van Kranendonk M. (2007) A non-marine depositional setting for the northern Fortescue Group,
1544 Pilbara Craton, inferred from trace element geochemistry of stromatolitic carbonates. *Precambrian*
1545 *Research* **155**, 229–250.

1546 Bontognali T. R. R., Sessions A. L., Allwood A. C., Fischer W. W., Grotzinger J. P., Summons R. E. and Eiler J.
1547 M. (2012) Sulfur isotopes of organic matter preserved in 3.45-billion-year-old stromatolites reveal
1548 microbial metabolism. *PNAS* **109**, 15146–15151.

1549 Bots P., Benning L. G., Rickaby R. E. M. and Shaw S. (2011) The role of SO4 in the switch from calcite to
1550 aragonite seas. *Geology* **39**, 331–334.

1551 Bouton A., Vennin E., Boulle J., Pace A., Bourillot R., Thomazo C., Brayard A., Désaubliaux G., Goslar T.,
1552 Yokoyama Y., Dupraz C. and Visscher P. T. (2016) Linking the distribution of microbial deposits from
1553 the Great Salt Lake (Utah, USA) to tectonic and climatic processes. *Biogeosciences* **13**, 5511–5526.

1554 Braithwaite C. J. R. and Zedef V. (1994) Living hydromagnesite stromatolites from Turkey. *Sedimentary Geology*
1555 **92**, 1–5.

1556 Brecevic L. and Nielsen A.E. (1989) Solubility of amorphous calcium carbonate. *J. Cryst. Growth* **98(3)**, 504-510.

1557 Brindley G. (1955) Stevensite, a Montmorillonite-Type Mineral Showing Mixed-Layer Characteristics. *Am.*
1558 *Miner.* **40**, 239–247.

1559 Brindley G. W. (1977) The Nature of Kerolite, Its Relation to Talc and Stevensite. *Mineralogical Magazine* **41**,
1560 443–452.

1561 Buick R. (1992) The Antiquity of Oxygenic Photosynthesis - Evidence from Stromatolites. *Science* **255**, 74–77.

1562 Bundeleva I. A., Shirokova L. S., Bénézeth P., Pokrovsky O. S., Kompantseva E. I. and Balor S. (2012) Calcium
1563 carbonate precipitation by anoxygenic phototrophic bacteria. *Chemical Geology* **291**, 116–131.

1564 Burne R. V. and Moore L. S. (1987) Microbialites: Organosedimentary Deposits of Benthic Microbial
1565 Communities. *PALAIOS* **2**, 241.

1566 Burne R. V., Moore L. S., Christy A. G., Troitzsch U., King P. L., Carnerup A. M. and Hamilton P. J. (2014)
1567 Stevensite in the modern thrombolites of Lake Clifton, Western Australia: A missing link in microbialite
1568 mineralization? *Geology* **42**, 575–578.

1569 Caballero M., Vilaclara G., Rodríguez A. and Juárez D. (2003) Short-term climatic change in lake sediments from
1570 lake Alchichica, Oriental, Mexico. *Geofísica Internacional*. Available at:
1571 http://www.redalyc.org/resumen.oa?id=56842325

1572 Cam N., Benzerara K., Georgelin T., Jaber M., Lambert J.-F., Poinsot M., Skouri-Panet F. and Cordier L. (2016)
1573 Selective Uptake of Alkaline Earth Metals by Cyanobacteria Forming Intracellular Carbonates. *Environ.*
1574 *Sci. Technol.* **50**, 11654–11662.

1575 Carignan J., Hild P., Mevelle G., Morel J. and Yeghicheyan D. (2001) Routine analyses of trace elements in
1576 geological samples using flow injection and low pressure on-line liquid chromatography coupled to ICP-
1577 MS: a study of geochemical reference materials BR, DR-N, UB-N, AN-G and GH. *Geostandards and*
1578 *Geoanalytical Research* **25**, 187–198.

1579 Carrasco-Núñez G., Ort M. H. and Romero C. (2007) Evolution and hydrological conditions of a maar volcano
1580 (Atexcac crater, Eastern Mexico). *Journal of Volcanology and Geothermal Research* **159**, 179–197.

1581 Casanova J. and Hillaire-Marcel C. (1992) Late holocene hydrological history of Lake Tanganyika, East Africa,
1582 from isotopic data on fossil stromatolites. *Palaeogeography, Palaeoclimatology, Palaeoecology* **91**, 35–
1583 48.

1584 Centeno C. M., Legendre P., Beltrán Y., Alcántara-Hernández R. J., Lidström U. E., Ashby M. N. and Falcón L.
1585 I. (2012) Microbialite genetic diversity and composition relate to environmental variables. *FEMS*
1586 *Microbiology Ecology* **82**, 724–735.

1587 Chagas A. A. P., Webb G. E., Burne R. V. and Southam G. (2016) Modern lacustrine microbialites: Towards a
1588 synthesis of aqueous and carbonate geochemistry and mineralogy. *Earth-Science Reviews* **162**, 338–363.

1589 Chaka A. M. (2018) Ab Initio Thermodynamics of Hydrated Calcium Carbonates and Calcium Analogues of
1590 Magnesium Carbonates: Implications for Carbonate Crystallization Pathways. *ACS Earth Space Chem.*
1591 **2**, 210–224.

1592 Cohen A. S., Talbot M. R., Awramik S. M., Dettman D. L. and Abell P. (1997) Lake level and paleoenvironmental
1593 history of Lake Tanganyika, Africa, as inferred from late Holocene and modern stromatolites. *Geological*
1594 *Society of America Bulletin* **109**, 444–460.

1595 Conley D. J., Frings P. J., Fontorbe G., Clymans W., Stadmark J., Hendry K. R., Marron A. O. and De La Rocha
1596 C. L. (2017) Biosilicification Drives a Decline of Dissolved Si in the Oceans through Geologic Time.
1597 *Front. Mar. Sci.* **4,** 397. doi: 10.3389/fmars.2017.00397
1598
1599 Coshell L., Rosen M. R. and Mcnamara K. J. (1998) Hydromagnesite replacement of biomineralized aragonite in
1600 a new location of Holocene stromatolites, Lake Walyungup, Western Australia. *Sedimentology* **45**, 1005–
1601 1018.

1602 Couradeau E., Benzerara K., Moreira D., Gérard E., Kaźmierczak J., Tavera R. and López-García P. (2011)
1603 Prokaryotic and Eukaryotic Community Structure in Field and Cultured Microbialites from the Alkaline
1604 Lake Alchichica (Mexico) ed. J. A. Gilbert. *PLoS ONE* **6**, e28767.

1605 Couradeau E., Benzerara K., Gérard E., Estève I., Moreira D., Tavera R. and López-García P. (2013)
1606 Cyanobacterial calcification in modern microbialites at the submicrometer scale. *Biogeosciences* **10**,
1607 5255–5266.

1608 Darragi F. and Tardy Y. (1987) Authigenic trioctahedral smectites controlling pH, alkalinity, silica and magnesium
1609 concentrations in alkaline lakes. *Chemical geology* **63**, 59–72.

1610 Davies S.H.R. and Morgan J.J., (1989) Manganese(II) oxidation-kinetics on metal-oxide surfaces. *J. Colloid*
1611 *Interface Sci*. **129**, 63–77.
1612
1613 Davies S. J., Metcalfe S. E., MacKenzie A. B., Newton A. J., Endfield G. H. and Farmer J. G. (2004)
1614 Environmental changes in the Zirahuén Basin, Michoacán, Mexico, during the last 1000 years. *Journal*
1615 *of Paleolimnology* **31**, 77–98.

Davis K.J., Dove P.M., and De Yoreo J.J. (2000) The role of Mg^{2+} as an impurity in calcite growth. *Science* **290**, 1134–1137.

De Boever E., Brasier A. T., Foubert A. and Kele S. (2017) What do we really know about early diagenesis of non-marine carbonates? *Sedimentary Geology* **361**, 25–51.

Decarreau A. (1983) Etude expérimentale de la crystallogenèse des smectite. Mesures des coefficients de partage smectite trioctahédrique/solution aqueuse pour les métaux M^{2+} de la première série de transition. Sciences géologiques. Mémoire, **74**, 185p.

Deleuze M. and Brantley S. L. (1997) Inhibition of calcite crystal growth by Mg2+ at 100°C and 100 bars: Influence of growth regime. *Geochimica et Cosmochimica Acta* **61**, 1475–1485.

Dickson A. G. (1981) An exact definition of total alkalinity and a procedure for the estimation of alkalinity and total inorganic carbon from titration data. *Deep Sea Research Part A. Oceanographic Research Papers* **28**, 609–623.

Dietzel M., Gussone N. and Eisenhauer A. (2004) Co-precipitation of Sr2+ and Ba2+ with aragonite by membrane diffusion of CO2 between 10 and 50 °C. *Chemical Geology* **203**, 139–151.

Domagalski J. L., Orem W. H. and Eugster H. P. (1989) Organic geochemistry and brine composition in Great Salt, Mono, and Walker Lakes. *Geochimica et Cosmochimica Acta* **53**, 2857–2872.

Eltom H. A., Abdullatif O. M., Makkawi M. H. and Eltoum I.-E. A. (2017) Rare earth element geochemistry of shallow carbonate outcropping strata in Saudi Arabia: Application for depositional environments prediction. *Sedimentary Geology* **348**, 51–68.

Fagerbakke K., Heldal M. and Norland S. (1996) Content of carbon, nitrogen, oxygen, sulfur and phosphorus in native aquatic and cultured bacteria. *Aquat. Microb. Ecol.* **10**, 15–27.

Ferrari L., Orozco-Esquivel T., Manea V. and Manea M. (2012) The dynamic history of the Trans-Mexican Volcanic Belt and the Mexico subduction zone. *Tectonophysics* **522–523**, 122–149.

Frimmel H. E. (2009) Trace element distribution in Neoproterozoic carbonates as palaeoenvironmental indicator. *Chemical Geology* **258**, 338–353.

Fukushi K., Munemoto T., Sakai M. and Yagi S. (2011) Monohydrocalcite: a promising remediation material for hazardous anions. *Science and Technology of Advanced Materials* **12**, 064702.

Fukushi K. and Matsumiya H. (2018) Control of Water Chemistry in Alkaline Lakes: Solubility of Monohydrocalcite and Amorphous Magnesium Carbonate in $CaCl_2$–$MgCl_2$–Na_2CO_3 Solutions. *ACS Earth Space Chem.* **2**, 735–744.

Fukushi K., Imai E., Sekine Y., Kitajima T., Gankhurel B., Davaasuren D. and Hasebe N. (2020) In Situ Formation of Monohydrocalcite in Alkaline Saline Lakes of the Valley of Gobi Lakes: Prediction for Mg, Ca, and Total Dissolved Carbonate Concentrations in Enceladus' Ocean and Alkaline-Carbonate Ocean Worlds. *Minerals* **10**, 669.

Furian S., Martins E. R. C., Parizotto T. M., Rezende-Filho A. T., Victoria R. L. and Barbiero L. (2013) Chemical diversity and spatial variability in myriad lakes in Nhecolândia in the Pantanal wetlands of Brazil. *Limnol. Oceanogr.* **58**, 2249–2261.

Gac J. Y., Droubi A., Fritz B. and Tardy Y. (1977) Geochemical behaviour of silica and magnesium during the evaporation of waters in Chad. *Chemical Geology* **19**, 215–228.

Gaillardet J., Dupré B., Louvat P. and Allegre C. J. (1999) Global silicate weathering and CO2 consumption rates deduced from the chemistry of large rivers. *Chemical geology* **159**, 3–30.

García Martínez J. (2010) Efectos climáticos sobre el agua subterránea y el lago Alchichica Puebla, México/ (Thesis). Universidad Nacional Autónoma de México, México.

https://repositorio.unam.mx/contenidos/64601

Gérard E., Ménez B., Couradeau E., Moreira D., Benzerara K., Tavera R. and López-García P. (2013) Specific carbonate–microbe interactions in the modern microbialites of Lake Alchichica (Mexico). *The ISME journal* **7**, 1997–2009.

Gérard E., De Goeyse S., Hugoni M., Agogué H., Richard L., Milesi V., Guyot F., Lecourt L., Borensztajn S., Joseph M.-B., Leclerc T., Sarazin G., Jézéquel D., Leboulanger C. and Ader M. (2018) Key Role of Alphaproteobacteria and Cyanobacteria in the Formation of Stromatolites of Lake Dziani Dzaha (Mayotte, Western Indian Ocean). *Frontiers in Microbiology* **9,** 796.

Glunk C., Dupraz C., Braissant O., Gallagher K. L., Verrecchia E. P. and Visscher P. T. (2011) Microbially mediated carbonate precipitation in a hypersaline lake, Big Pond (Eleuthera, Bahamas): Microbially mediated carbonate precipitation. *Sedimentology* **58**, 720–736.

Gómez-Tuena A., LaGatta A. B., Langmuir C. H., Goldstein S. L., Ortega-Gutiérrez F. and Carrasco-Núñez G. (2003) Temporal control of subduction magmatism in the eastern Trans-Mexican Volcanic Belt: Mantle sources, slab contributions, and crustal contamination. *Geochemistry, Geophysics, Geosystems* **4** (8), 8912, doi:10.1029/2003GC000524, 2003.

Gómez-Tuena A., Orozco-Esquivel Ma. T. and Ferrari L. (2007) Igneous petrogenesis of the Trans-Mexican Volcanic Belt. In *Special Paper 422: Geology of México: Celebrating the Centenary of the Geological Society of México* Geological Society of America.129–181.

Gran G. (1952) Determination of the equivalence point in potentiometric titrations. Part II. *Analyst* **77**, 661–671.

Guido A., Mastandrea A., Tosti F. and Russo F. (2011) Importance of Rare Earth Element Patterns in Discrimination Between Biotic and Abiotic Mineralization. In *Advances in Stromatolite Geobiology* Springer Berlin Heidelberg, Berlin, Heidelberg. pp. 453–462.

Giuffre A. J., Hamm L. M., Han N., De Yoreo J. J. and Dove P. M. (2013) Polysaccharide chemistry regulates kinetics of calcite nucleation through competition of interfacial energies. *Proc Natl Acad Sci USA* **110**, 9261–9266.

Guo X. and Chafetz H. S. (2012) Large tufa mounds, Searles Lake, California. *Sedimentology* **59**, 1509–1535.

Gustafsson J.P. (2011) Visual MINTEQ: a free equilibrium speciation model. KTH, Department of Land and Water Resources Engineering.

Hammer U. T. (1986) *Saline Lake Ecosystems of the World Monographiae Biologicae* 59, Dr. W. Junk, Publishers, Dordrecht, The Netherlands

Harris P. M., Ellis J. and Purkis S. J. (2013) Assessing the extent of carbonate deposition in early rift settings. *AAPG Bulletin* **97**, 27–60.

Heldal M., Scanlan D. J., Norland S., Thingstad F. and Mann N. H. (2003) Elemental composition of single cells of various strains of marine *Prochlorococcus* and *Synechococcus* using X-ray microanalysis. *Limnol. Oceanogr.* **48**, 1732–1743.

Iniesto M., Moreira D., Reboul G., Deschamps P., Benzerara K., Bertolino P., Saghaï A., Tavera R. and López-García P. (2021) Core microbial communities of lacustrine microbialites sampled along an alkalinity gradient. *Environmental Microbiology* **23**, 51–68.

Israde-Alcántara I., Garduño-Monroy V. H., Fisher C. T., Pollard H. P. and Rodríguez-Pascua M. A. (2005) Lake level change, climate, and the impact of natural events: the role of seismic and volcanic events in the formation of the Lake Patzcuaro Basin, Michoacan, Mexico. *Quaternary International* **135**, 35–46.

Johannesson K. H., Hawkins D. L. and Cortés A. (2006) Do Archean chemical sediments record ancient seawater rare earth element patterns? *Geochimica et Cosmochimica Acta* **70**, 871–890.

Jones B. F. and Galan E. (1988) Sepiolite and palygorskite. *Reviews in Mineralogy and Geochemistry* **19**, 631–674.

Kamber B. S. and Webb G. E. (2001) The geochemistry of late Archaean microbial carbonate: implications for ocean chemistry and continental erosion history. *Geochimica et Cosmochimica Acta* **65**, 2509–2525.

Kamber B. S., Bolhar R. and Webb G. E. (2004) Geochemistry of late Archaean stromatolites from Zimbabwe: evidence for microbial life in restricted epicontinental seas. *Precambrian Research* **132**, 379–399.

Kamber B. S., Webb G. E. and Gallagher M. (2014) The rare earth element signal in Archaean microbial carbonate: information on ocean redox and biogenicity. *Journal of the Geological Society* **171**, 745–763.

Kaźmierczak J., Kempe S., Kremer B., López-García P., Moreira D. and Tavera R. (2011) Hydrochemistry and microbialites of the alkaline crater lake Alchichica, Mexico. *Facies* **57**, 543–570.

Kempe S., Kaźmierczak J., Landmann G., Konuk T., Reimer A. and Lipp A. (1991) Largest Known Microbialites Discovered in Lake Van, Turkey. *Nature* **349**, 605–608.

Kharaka Y.K., Robinson S.W., Law L.M. and Carothers W.W. (1984). Hydrogeochemistry of Big Soda Lake, Nevada; an alkaline meromictic desert lake. *Geochimica et Cosmochimica Acta* **48**, 823–835.

Knoll A. H., Wörndle S. and Kah L. C. (2013) Covariance of microfossil assemblages and microbialite textures across an upper mesoproterozoic carbonate platform. *PALAIOS* **28**, 453–470.

Komadel P., Madejová J. and Bujdák J. (2005) Preparation and properties of reduced-charge smectites – a review. *Clays Clay Miner.* **53**, 313–334.

Last F. M., Last W. M. and Halden N. M. (2010) Carbonate microbialites and hardgrounds from Manito Lake, an alkaline, hypersaline lake in the northern Great Plains of Canada. *Sedimentary Geology* **225**, 34–49.

Last F. M., Last W. M. and Halden N. M. (2012) Modern and late Holocene dolomite formation: Manito Lake, Saskatchewan, Canada. *Sedimentary Geology* **281**, 222–237.

Lauchnor E. G., Schultz L. N., Bugni S., Mitchell A. C., Cunningham A. B. and Gerlach R. (2013) Bacterially Induced Calcium Carbonate Precipitation and Strontium Coprecipitation in a Porous Media Flow System. *Environ. Sci. Technol.* **47**, 1557–1564.

Lê S., Josse J. and Husson F. (2008). FactoMineR: An R Package for Multivariate Analysis. *Journal of Statistical Software* **25(1)**, 1–18.

Lepot K., Benzerara K., Rividi N., Cotte M., Brown G. E. and Philippot P. (2009) Organic matter heterogeneities in 2.72Ga stromatolites: Alteration versus preservation by sulfur incorporation. *Geochimica et Cosmochimica Acta* **73**, 6579–6599.

Lepot K., Williford K. H., Philippot P., Thomazo C., Ushikubo T., Kitajima K., Mostefaoui S. and Valley J. W. (2019) Extreme 13C-depletions and organic sulfur content argue for S-fueled anaerobic methane oxidation in 2.72 Ga old stromatolites. *Geochimica et Cosmochimica Acta* **244**, 522–547.

Léveillé R. J., Longstaffe F. J. and Fyfe W. S. (2002) Kerolite in carbonate-rich speleothems and microbial deposits from basaltic caves, Kauai, Hawaii. *Clays and clay minerals* **50**, 514–524.

Lim D. S. S., Laval B. E., Slater G., Antoniades D., Forrest A. L., Pike W., Pieters R., Saffari M., Reid D., Schulze-Makuch D., Andersen D. and McKay C. P. (2009) Limnology of Pavilion Lake, B. C., Canada – Characterization of a microbialite forming environment. *Fundamental and Applied Limnology / Archiv für Hydrobiologie* **173**, 329–351.

López-Archilla A. I., Moreira D., López-García P. and Guerrero C. (2004) Phytoplankton diversity and cyanobacterial dominance in a hypereutrophic shallow lake with biologically produced alkaline pH. *Extremophiles* **8**, 109–115

López-García P., Kaźmierczak J., Benzerara K., Kempe S., Guyot F. and Moreira D. (2005) Bacterial diversity and carbonate precipitation in the giant microbialites from the highly alkaline Lake Van, Turkey. *Extremophiles* **9**, 263–274.

Loste E., Wilson R. M., Seshadri R. and Meldrum F. C. (2003) The role of magnesium in stabilising amorphous calcium carbonate and controlling calcite morphologies. *Journal of Crystal Growth* **254**, 206–218.

Mercedes-Martín R., Ayora C., Tritlla J. and Sánchez-Román M. (2019) The hydrochemical evolution of alkaline volcanic lakes: a model to understand the South Atlantic Pre-salt mineral assemblages. *Earth-Science Reviews* **198**, 102938.

Mergelsberg S. T., De Yoreo J. J., Miller Q. R. S., Marc Michel F., Ulrich R. N. and Dove P. M. (2020) Metastable solubility and local structure of amorphous calcium carbonate (ACC). *Geochimica et Cosmochimica Acta* **289**, 196–206.

Meynadier L., Gorge C., Birck J. L., and Allègre C. J. (2006) Automated separation of Sr from natural water samples or carbonate rocks by high performance ion chromatography. *Chemical geology* **227(1)**, 26–36.

Milesi V. P., Jézéquel D., Debure M., Cadeau P., Guyot F., Sarazin G., Claret F., Vennin E., Chaduteau C., Virgone A., Gaucher E. C. and Ader M. (2019) Formation of magnesium-smectite during lacustrine carbonates early diagenesis: Study case of the volcanic crater lake Dziani Dzaha (Mayotte – Indian Ocean). *Sedimentology* **66**, 983–1001.

Milesi V. P., Debure M., Marty N. C. M., Capano M., Jézéquel D., Steefel C., Rouchon V., Albéric P., Bard E., Sarazin G., Guyot F., Virgone A., Gaucher É. C. and Ader M. (2020) Early Diagenesis of Lacustrine Carbonates in Volcanic Settings: The Role of Magmatic CO_2 (Lake Dziani Dzaha, Mayotte, Indian Ocean). *ACS Earth Space Chem.* **4**, 363–378.

Milligan A. J. and Morel F. M. M. (2002) A Proton Buffering Role for Silica in Diatoms. *Science* **297**, 1848–1850.

Millot G. (1970) *Geology of Clays*. Springer-Verlag, Berlin, Heidelberg, pp 430

Mitchell A. C. and Ferris F. G. (2005) The coprecipitation of Sr into calcite precipitates induced by bacterial ureolysis in artificial groundwater: Temperature and kinetic dependence. *Geochimica et Cosmochimica Acta* **69**, 4199–4210.

Müller G., Irion G. and Förstner U. (1972) Formation and diagenesis of inorganic Ca- Mg carbonates in the lacustrine environment. *Naturwissenschaften* **59**, 158–164.

Nitti A., Daniels C. A., Siefert J., Souza V., Hollander D. and Breitbart M. (2012) Spatially Resolved Genomic, Stable Isotopic, and Lipid Analyses of a Modern Freshwater Microbialite from Cuatro Ciénegas, Mexico. *Astrobiology* **12**, 685–698.

Nutman A. P., Bennett V. C., Friend C. R. L., Van Kranendonk M. J. and Chivas A. R. (2016) Rapid emergence of life shown by discovery of 3,700-million-year-old microbial structures. *Nature* **537**, 535–538.

Pace A., Bourillot R., Bouton A., Vennin E., Galaup S., Bundeleva I., Patrier P., Dupraz C., Thomazo C., Sansjofre P., Yokoyama Y., Franceschi M., Anguy Y., Pigot L., Virgone A. and Visscher P. T. (2016) Microbial and diagenetic steps leading to the mineralisation of Great Salt Lake microbialites. *Scientific Reports* **6**, 31495.

Pecoraino G., D'Alessandro W. and Inguaggiato S. (2015) The Other Side of the Coin: Geochemistry of Alkaline Lakes in Volcanic Areas. In *Volcanic Lakes* (eds. D. Rouwet, B. Christenson, F. Tassi, and J. Vandemeulebrouck). Springer Berlin Heidelberg. pp. 219–237.

Perrin J., Vielzeuf D., Laporte D., Ricolleau A., Rossman G. R. and Floquet N. (2016) Raman characterization of synthetic magnesian calcites. *The American Mineralogist* **101**, 2525–2538.

Peterson B.G. and Carl P. (2014) Performance Analytics: Econometric tools for performance and risk analysis. R package version 1.4.3541.

Plummer L. N. and Busenberg E. (1982) The solubilities of calcite, aragonite and vaterite in CO2-H2O solutions between 0 and 90°C, and an evaluation of the aqueous model for the system CaCO3-CO2-H2O. *Geochimica et Cosmochimica Acta* **46**, 1011–1040.

Pokrovsky O. S. (1998) Precipitation of calcium and magnesium carbonates from homogeneous supersaturated solutions. *Journal of Crystal Growth* **186**, 233–239.

Pola A., Macías J. L., Osorio-Ocampo S., Sosa-Ceballos G., Garduño-Monroy V. H. and Martínez-Martínez J. (2015) El Estribo Volcanic Complex: Evolution from a shield volcano to a cinder cone, Pátzcuaro Lake, Michoacán, México. *Journal of Volcanology and Geothermal Research* **303**, 130–145.

Pourmand A., Dauphas N. and Ireland T. J. (2012) A novel extraction chromatography and MC-ICP-MS technique for rapid analysis of REE, Sc and Y: Revising CI-chondrite and Post-Archean Australian Shale (PAAS) abundances. *Chemical Geology* **291**, 38–54.

Power I. M., Wilson S. A., Dipple G. M. and Southam G. (2011) Modern carbonate microbialites from an asbestos open pit pond, Yukon, Canada.*Geobiology* **9**, 180-195.

R Core Team (2015) R: A Language and Environment for Statistical computing. R Foundation for Statistical Computing, Vienna, Austria. https://www.R-project.org

Ragon M., Benzerara K., Moreira D., Tavera R. and López-García P. (2014) 16S rDNA-based analysis reveals cosmopolitan occurrence but limited diversity of two cyanobacterial lineages with contrasted patterns of intracellular carbonate mineralization. *Front. Microbiol.* **5**.

Reimer A., Landmann G. and Kempe S. (2009) Lake Van, Eastern Anatolia, Hydrochemistry and History. *Aquatic Geochemistry* **15**, 195–222.

Reyes Cortés M. (1979) *Geología de la Cuenca de Oriental: estados de Puebla, Veracruz, y Tlaxcala*., SEP, Instituto Nacional de Antropología e Historia, México.

Riding R., Fralick P. and Liang L. (2014) Identification of an Archean marine oxygen oasis. *Precambrian Research* **251**, 232–237.

Roche A., Vennin E., Bundeleva I., Bouton A., Payandi-Rolland D., Amiotte-Suchet P., Gaucher E. C., Courvoisier H. and Visscher P. T. (2019) The Role of the Substrate on the Mineralization Potential of Microbial Mats in A Modern Freshwater River (Paris Basin, France). *Minerals* **9**, 359.

Rodriguez-Blanco J. D., Shaw S., Bots P., Roncal-Herrero T. and Benning L. G. (2014) The role of Mg in the crystallization of monohydrocalcite. *Geochimica et Cosmochimica Acta* **127**, 204–220.

Rosen M. R., Arehart G. B. and Lico M. S. (2004) Exceptionally fast growth rate of< 100-yr-old tufa, Big Soda Lake, Nevada: Implications for using tufa as a paleoclimate proxy. *Geology* **32**, 409–412.

Sageman B.B. and Lyons T.W., (2003) Geochemistry of fine-grained sediments and sedimentary rocks. In *Sediments, Diagenesis, and Sedimentary Rocks: Treatise in geochemistry, Volume 7* (eds. F.T. Mackenzie). Elsevier, New York. pp. 115-158.

Saghaï A., Zivanovic Y., Zeyen N., Moreira D., Benzerara K., Deschamps P., Bertolino P., Ragon M., Tavera R., López-Archilla A. I. and López-García P. (2015) Metagenome-based diversity analyses suggest a significant contribution of non-cyanobacterial lineages to carbonate precipitation in modern microbialites. *Frontiers in Microbiology* **6,** 797.

Saghaï A., Zivanovic Y., Moreira D., Benzerara K., Bertolino P., Ragon M., Tavera R., López-Archilla A.I. and López- García P. (2016). Comparative metagenomics unveils functions and genome features of microbialite-associated communities along a depth gradient. *Environmental Microbiology* **18**, 4990-5004.

Sakurai R., Ito M., Ueno Y., Kitajima K., Maruyama S. (2005). Facies architecture and sequence-stratigraphic features of the Tumbiana Formation in the Pilbara Craton, northwestern Australia: implications for depositional environments of oxygenic stromatolites during the Late Archean. *Precambrian Research.* **138**, 255–273

Sarg J. F., Suriamin N., TÌnavsuu-Milkeviciene K. and Humphrey J. D. (2013) Lithofacies, stable isotopic composition, and stratigraphic evolution of microbial and associated carbonates, Green River Formation (Eocene), Piceance Basin, Colorado. *AAPG Bulletin* **97**, 1937–1966.

Siahi M., Hofmann A., Master S., Wilson A. and Mayr C. (2018) Trace element and stable (C, O) and radiogenic (Sr) isotope geochemistry of stromatolitic carbonate rocks of the Mesoarchaean Pongola Supergroup: Implications for seawater composition. *Chemical Geology* **476**, 389–406.

Siebe C. et al., (2014) Monogenetic volcanism of the Michoacán-Guanajuato Volcanic Field: Maar craters of the Zacapu basin and domes, shields, and scoria cones of the Tarascan highlands (Paracho-Paricutin region). Pre-meeting field guide for the 5th international maar conference, Querétaro, México.

Sigala I., Caballero M., Correa-Metrio A., Lozano-García S., Vázquez G., Pérez L. and Zawisza E. (2017) Basic limnology of 30 continental waterbodies of the Transmexican Volcanic Belt across climatic and environmental gradients. *Boletín de la Sociedad Geológica Mexicana* **69**, 313–370.

Souza-Egipsy V., Wierzchos J., Ascaso C. and Nealson K. H. (2005) Mg–silica precipitation in fossilization mechanisms of sand tufa endolithic microbial community, Mono Lake (California). *Chemical Geology* **217**, 77–87.

Souza-Egipsy V., García Del Cura M. A., Ascaso C., De Los Ríos A., Wierzchos J. and González-Martín J. A. (2006) Interaction between Calcite and Phosphorus in Biomineralization Processes in Tufa Carbonates. *International Review of Hydrobiology* **91**, 222–241.

Spencer, R. J., 1977. Silicate and carbonate sediment-water relationships in Walker Lake, Nevada. M.S. thesis, Univ. of Nevada, Reno.

Stoessell R. K. (1988) 25°C and 1 atm dissolution experiments of sepiolite and kerolite. *Geochimica et Cosmochimica Acta* **52**, 365–374.

Stoffers P. and Fischbeck R. (1974) Monohydrocalcite in the sediments of Lake Kivu (East Africa). *Sedimentology* **21**, 163–170.

Stüeken E. E., Buick R. and Schauer A. J. (2015) Nitrogen isotope evidence for alkaline lakes on late Archean continents. *Earth and Planetary Science Letters* **411**, 1–10.

Taylor G. (1975) Occurrence of Monohydrocalcite in 2 Small Lakes in Southeast of South-Australia. *Am. Miner.* **60**, 690–697.

Tesoriero A. J. and Pankow J. F. (1996) Solid solution partitioning of Sr2+, Ba2+, and Cd2+ to calcite. *Geochimica et Cosmochimica Acta* **60**, 1053–1063.

Tettenhorst R. and Moore Jr G. E. (1978) Stevensite oolites from the Green River Formation of central Utah. *Journal of Sedimentary Research* **48**.

Theisen C. H., Sumner D. Y., Mackey T. J., Lim D. S. S., Brady A. L. and Slater G. F. (2015) Carbonate fabrics in the modern microbialites of Pavilion Lake: two suites of microfabrics that reflect variation in microbial community morphology, growth habit, and lithification. *Geobiology* **13**, 357–372.

Thomazo C., Ader M. and Philippot P. (2011) Extreme 15N-enrichments in 2.72-Gyr-old sediments: evidence for a turning point in the nitrogen cycle. *Geobiology* **9**, 107–120.

Thorne A. M. and Trendall A. F., (2001) Geology of the Fortescue Group, Pilbara Craton, Western Australia. Western Aust. Geol. Surv. Bull. **144**, 249.

1893 Toner J. D. and Catling D. C. (2019) Alkaline lake settings for concentrated prebiotic cyanide and the origin of
1894 life. *Geochimica et Cosmochimica Acta* **260**, 124–132.

1895 Tosca N. J., Macdonald F. A., Strauss J. V., Johnston D. T. and Knoll A. H. (2011) Sedimentary talc in
1896 Neoproterozoic carbonate successions. *Earth and Planetary Science Letters* **306**, 11–22.

1897 Tosca N. J. and Masterson A. L. (2014) Chemical controls on incipient Mg-silicate crystallization at 25°C:
1898 Implications for early and late diagenesis. *Clay Minerals* **49**, 165–194.

1899 Tosca, N.J. (2015) Geochemical pathways to Mg-clay formation. In: Magnesian Clays: Characterization, Origins
1900 and Applications (Eds M. Pozo and E. Galán). AIPEA Special Publications, **2**, 283–329.

1901 Tosca N. J. and Wright V. P. (2015) Diagenetic pathways linked to labile Mg-clays in lacustrine carbonate
1902 reservoirs: a model for the origin of secondary porosity in the Cretaceous pre-salt Barra Velha Formation,
1903 offshore Brazil. *Geological Society, London, Special Publications* **435**

1904 Truesdell A. H. and Jones B. F. (1974) WATEQ, a computer program for calculating chemical equilibria of natural
1905 waters. US department of the interior, Geological survey

1906 Turvey C. C., Hamilton J. L. and Wilson S. A. (2018) Comparison of Rietveld-compatible structureless fitting
1907 analysis methods for accurate quantification of carbon dioxide fixation in ultramafic mine tailings.
1908 *American Mineralogist* **103**, 1649–1662.

1909 Valdespino-Castillo P. M., Hu P., Merino-Ibarra M., López-Gómez L. M., Cerqueda-García D., González-De
1910 Zayas R., Pi-Puig T., Lestayo J. A., Holman H.-Y. and Falcón L. I. (2018) Exploring Biogeochemistry
1911 and Microbial Diversity of Extant Microbialites in Mexico and Cuba. *Frontiers in Microbiology* **9,** 510.

1912 Van Kranendonk M. J., Webb G. E. and Kamber B. S. (2003) Geological and trace element evidence for a marine
1913 sedimentary environment of deposition and biogenicity of 3.45 Ga stromatolitic carbonates in the Pilbara
1914 Craton, and support for a reducing Archaean ocean. *Geobiology* **1**, 91–108.

1915 Van Kranendonk M., Philippot P., Lepot K., Bodorkos S. and Pirajno F. (2008) Geological setting of Earth's oldest
1916 fossils in the ca. 3.5Ga Dresser Formation, Pilbara Craton, Western Australia. *Precambrian Research*
1917 **167**, 93–124.

1918 Verma S. P. (1999) Geochemistry of evolved magmas and their relationship to subduction-unrelated mafic
1919 volcanism at the volcanic front of the central Mexican Volcanic Belt. *Journal of Volcanology and*
1920 *Geothermal Research* **93**, 151–171.

1921 Verma S. P. (2000) Geochemistry of the subducting Cocos plate and the origin of subduction-unrelated mafic
1922 volcanism at the volcanic front of the central Mexican Volcanic Belt. In *Special Paper 334: Cenozoic*
1923 *tectonics and volcanism of Mexico* Geological Society of America. pp. 195–222.

1924 Vigneau E., Chen M. and Qannari E.M. (2015) ClustVarLV : an R package for the clustering of variables around
1925 latent variables. *The R Journal* **7(2)**, 134-148.

1926 Vilaclara G., Chávez M., Lugo A., González H., Gaytán M. (1993) Comparative description of crater-lakes basic
1927 chemistry in Puebla State, Mexico. Verhandlungen Internationale Vereinigung für Theoretische und
1928 Angewandte Limnologie **25**, 435–440.
1929
1930 Walter L.M. (1986) Relative efficiency of carbonate dissolution and precipitation during diagenesis: A progress
1931 report on the role of solution chemistry, in Gautier, D.L., ed., Roles of Organic Matter in Sediment
1932 Diagenesis: Society of Economic Paleontologists and Mineralogists Special Publication **38**, 1–11.
1933 Weaver C. E. and Beck K. C. (1977) Miocene of the S.E. United States: A model for chemical sedimentation in a
1934 peri-marine environment. *Sedimentary Geology* **17**, 1–234.

1935 Webb G. E. and Kamber B. S. (2000) Rare earth elements in Holocene reefal microbialites: a new shallow seawater
1936 proxy. *Geochimica et Cosmochimica Acta* **64**, 1557–1565.

1937 Wollast R., Mackenzie F. T. and Bricker O. P. (1968) Experimental Precipitation and Genesis of Sepiolite at Earth-

Surface Conditions. *Am. Miner.* **53**, 1645–1661.

Zeyen N., Benzerara K., Li J., Groleau A., Balan E., Robert J.-L., Estève I., Tavera R., Moreira D. and López-García P. (2015) Formation of low-T hydrated silicates in modern microbialites from Mexico and implications for microbial fossilization. *Front. Earth Sci*. **3,** 64.

Zeyen N., Benzerara K., Menguy N., Brest J., Templeton A. S., Webb S. M., Gérard E., Moreira D., López-García P., Tavera R. and Morin G. (2019) Fe-bearing phases in modern lacustrine microbialites from Mexico. *Geochimica et Cosmochimica Acta* **253**, 201–230.

Zhang G., Delgado-López J. M., Choquesillo-Lazarte D. and García-Ruiz J. M. (2013) Crystallization of monohydrocalcite in a silica-rich alkaline solution. *CrystEngComm* **15**, 6526.

Zhao M.-Y. and Zheng Y.-F. (2017) A geochemical framework for retrieving the linked depositional and diagenetic histories of marine carbonates. *Earth and Planetary Science Letters* **460**, 213–221.

FIGURE CAPTIONS

Figure 1. Geographic location of the ten studied lakes. (**a**) Geological map representing the location of the trans-Mexican volcanic belt (TMVB, green area) from Ferrari et al. (2012) and the location of studied lakes marked by red squares. (**b-f**) Google Earth images of the lakes. Blue, yellow and red circle symbols correspond to microbialite sampling areas in June 2007, January 2012 and May 2014, respectively. No dot for Lake Zirahuén because this lake was not populated by microbialites; solutions have been sampled in the center of the lake. AH: Anegada high; LTVF: Los Tuxtlas volcanic field.

Figure 2. Solubility diagram in the $\log[a(CO_3^{2-})] - \log[a(Ca^{2+})]$ (in red) or $-\log[a(Mg^{2+})]$ (in black) space determined at 25°C. All surface waters are plotted after correction of their temperature variations. The solubilities of calcite and aragonite were defined by Plummer and Busenberg (1982); the solubility of amorphous Ca-carbonate (ACC) was measured by Brecevic and Nielsen (1989). The solubilities of monohydrocalcite (MHC) and amorphous Mg-carbonate (AMC2) were determined by Fukushi and Matsumiya (2018). AMC2 corresponds to a phase precipitating during the late-stage of the precipitation of AMC (Fukushi and Matsumiya, 2018) Diamond symbols stand for water solutions sampled in Lakes Quechulac (Q), La Preciosa (LP), Atexcac (Atx-N) and Alchichica (AL-M and AL-W) in January 2012. Circle symbols correspond to solutions sampled in Lakes Alberca de Guadalupe (Alb), Pátzcuaro (P), Tecuitlapa (T), La Alberca de Los Espinos (AE), Aljojuca (Alj), Zirahuén (Z), Alchichica (AL-M), Quechulac (Q), Atexcac (Atx-M) and La Preciosa (LP) in May 2014.

Figure 3. Solubility diagram in the $\log[a(Mg^{2+})/a(H^+)^2] - \log[a(H_4SiO_4)]$ space determined at 25°C. All surface waters are plotted after correction of their temperature variations. The equilibrium solubilities of talc (Jones and Galan, 1988), amorphous sepiolite (Wollast et al.,

1968), stevensite (Decarreau, 1983), kerolite and sepiolite (Stoessell, 1988), are indicated as oblique lines. Vertical dashed lines indicate the equilibrium solubility of quartz and amorphous silica (Truesdell and Jones, 1974). The Mg-saponite-montmorillonite equilibrium was estimated by Tosca (2015) using thermodynamic data estimated from Weaver and Beck (1977). The "critical saturation" line results from experiments conducted by Tosca et al., (2011) and Tosca and Masterson (2014) and relates to homogeneous nucleation of Mg-silicate phases from solution. Diamond symbols stand for water solutions sampled in Lakes Quechulac (Q), La Preciosa (LP), Atexcac (Atx-N) and Alchichica (AL-M and AL-W) on January 2012. Circle symbols correspond to water solutions sampled in Lakes Alberca de Guadalupe (Alb), Pátzcuaro (P), Tecuitlapa (T), La Alberca de Los Espinos (AE), Aljojuca (Alj), Zirahuén (Z), Alchichica (AL-M and AL-W), Quechulac (Q), Atexcac (Atx-M and ATX-N) and La Preciosa (LP) on May 2014. Red symbols stand for lakes where kerolite/stevensite were not observed nor detected within microbialites, whereas green symbols stand for lakes where microbialites contained kerolite/stevensite. The 'Mg-silicates' vertical solid line corresponds to the [H_4SiO_4] threshold over which kerolite/stevensite precipitation was observed for the studied microbialites.

Figure 4. Textures of mineral phases observed in Mexican microbialites by light microscopy. (**a**) Plane-polarized light photomicrograph of Pátzcuaro microbialite sample (Patz2014-01) showing a stromatolite-type texture with laminations. (**b**) Cross-polarized light photomicrograph of the same area showing the presence of a poorly crystalline phase, interpreted here as kerolite and/or stevensite (K/S) and a layer of Mg-calcite (MgC). (**c**) Plane-polarized light photomicrograph of La Preciosa microbialite sample (LP2014-08) showing aragonite dark nodules (A) surrounded by a brighter brown kerolite and/or stevensite matrix (K/S). (**d**) Cross-polarized light photomicrograph of the same area revealing the poor

2001 crystallinity of kerolite and/or stevensite and the acicular texture of aragonite apparent on the
2002 edges. (**e-f**) Plane-polarized and cross-polarized light photomicrographs of Atexcac
2003 microbialite sample (ATX-2C1-2012) showing a matrix of kerolite (K/S) and/or stevensite and
2004 the aragonite nodules (A).
2005
2006 **Figure 5.** Distribution and texture of Mg-calcite and monohydrocalcite in microbialites from
2007 Lakes Aljojuca and Tecuitlapa (Aljo214-02 and Tec2014-06). (**a**) Plane polarized light
2008 photomicrograph of the Aljojuca microbialite sample showing alternations between 2 phases:
2009 a dark phase (Mg-calcite) distributed as a large nodule possibly growing within a bright matrix
2010 (monohydrocalcite). (**b**) Raman spectra of (1) Mg-calcite showing a ν_1 band at 1090.1 cm^{-1}, (2)
2011 Mg-calcite showing a ν_1 band at 1087.3 cm^{-1}, (3) monohydrocalcite (MHC) with a ν_1 band at
2012 1068.6 cm^{-1} corresponding to the bright matrix. In these spectra, the bands below 400 cm^{-1}
2013 correspond to lattice mode vibrations and the band around 750 cm^{-1} to the in-plane bend (ν_4) of
2014 C-O bonds. (**c**) Plane polarized light photomicrograph overview of the studied area with a
2015 predominance of MHC in the Aljojuca microbialite. (**d**) Dynamic line-scanning Raman
2016 mapping of the area marked by a rectangle on (c) showing the correlation index for each
2017 spectrum with the reference spectra of MHC (green) and Mg-calcite (red). Bright colors
2018 indicate a greater correlation between the sampled spot and the references. Black pixels
2019 correspond to the glue used for sample preparation and/or organic matter (**e**) SEM image of the
2020 Aljojuca microbialite in the backscattered electron mode with MHC (dark phase) and Mg-
2021 calcite (white nodules). (**f)** SEM image of the Tecuitlapa microbialite in the backscattered
2022 electron mode showing a chemical contrast between MHC (darker phase), which embeds a
2023 diatom microfossil on the left (arrow), and the brighter Mg-calcite phase. (**g**) EDXS spectra of
2024 (1) Mg-calcite and (2) MHC in Aljojuca microbialite (outlined in (e)), and (3) Mg-calcite and
2025 (4) MHC in Tecuitlapa microbialite (outlined in (f)).

Figure 6. Biomorphs entombed within carbonates in Mexican microbialites. (**a-l**) SEM images in the backscattered electron mode of microbialites from Lakes Alchichica (AL), Atexcac (ATX), La Preciosa, Quechulac, Aljojuca (Aljo), La Alberca de Los Espinos (AlbEsp), Tecuitlapa (Tec), Alberca de Guadalupe (LaAlb). Abbreviations for the mineral phases are: A: aragonite; C: calcite, Mg-C: magnesian calcite, MHC: monohydrocalcite, H: hydromagnesite, K/S: kerolite/stevensite.

Figure 7. Frequent associations between Mg-silicates (kerolite and/or stevensite) and biomorphs (indicated by dashed red arrows). SEM images taken in the backscattered electron mode of microbialites from Lakes (**a**) La Preciosa (Preciosa05-2012), (**b**) La Preciosa (Pr2014-09), (**c**) Quechulac (Quechulac-1A-2012), (**d**) Atexcac (ATX-2C1-2012) and (**e**) (ATX2014-13) (**f**) La Alberca de los Espinos (AlbEsp2014-01), (**g**) Alberca de Guadalupe (LaAlb2014-02), (**h**) Pátzcuaro (Patz2014-02) and (**i**) Tecuitlapa (Tec2014-06). Abbreviations for the mineral phases are: A: aragonite; Mg-C: magnesian calcite, MHC: monohydrocalcite, H: hydromagnesite, K/S: kerolite/stevensite.

Figure 8. Classification of three groups of samples according to their detrital contamination. (**a**) Dendrogram of the hierarchical relationships between 43 variables representing major and trace elements (represented as tree leaves) describing the 32 microbialite samples. The order by which the leaves are connected in the dendrogram is directlty related to the strength of the linear correlation between the variables: the smaller the vertical distance between two leaves and the node connecting them, the stronger the correlation beteen the two corresponding variables. Optimal grouping of correlated variables was inferred. The group composed by Al and seven variables linearly correlated to Al is highlighted. (**b**) PCA analyses with biplot of variables

(vectors represented by arrows) and samples (dots). Each axis (or principal component) is a linear combination of variables defined in order to maximize the spatial discrimination of samples; coordinates of vectors on each axis indicate the coefficient of the variables in the linear combination. Longer the orthogonal projection of an arrow on a given axis, stronger the contribution of the variable to this axis. Smaller the angle between arrows, stronger the positive linear correlation between corresponding variable. Orthogonal arrows indicate no correlation, while arrows pointing in opposite directions indicate a negative correlation. The samples are plotted in two dimensions using their projections onto the first two principal components. The part of the total sample variability explained by each axis is indicated in the axis titles.
Three major groups of samples are highlighted: -HDC: three samples highly affected by detrital contamination (red squares); -IDC: eleven samples intermediately affected by detrital contamination (green diamonds) and -LDC: eighteen samples the least affected by detrital contamination (=authigenic-dominated) microbialites (blue dots).

Figure 9. Ternary Mg-Ca-Si diagram reporting bulk chemical composition (wt.%) of studied microbialites except the 3 microbialite samples affected by strong detrital contamination (Pr2014-03, LaAlb2014-02 and Tec2014-05b). Arrows correspond to: (1) the hydromagnesite-aragonite trend followed by Alchichica microbialites and (2) a trend between an aragonite and/or (low Mg-)calcite and/or monohydrocalcite, and a Mg-silicate endmember (noted 2 on the Mg-Si axis) corresponding to microbialites from the other lakes. The sample ATX-2C1-2012 departs from this trend because in addition to aragonite and Mg-silicate, it is composed of hydromagnesite.

Figure 10. PCA performed on the group of 18 authigenic-dominated microbialites, (**a**) PCA variables factor map representing the complete dataset of 63 variables describing the

microbialite bulk chemistry. (**b**) PCA plot with samples plotted in two dimensions using their projections onto the first two principal components. More guidance can be found in the caption of Figure 8.

Figure 11. REE+Y patterns of some of the authigenic-dominated microbialites. Four main signatures are observed as highlighted by PCA (Figure SI-9). (**a**) REE+Y patterns showing high positive Eu/Eu* anomalies, Gd/Gd* positive anomalies, high Yb/Nd_{SN} ratio revealing an enrichment in HREE and a very high Y/Ho ratio; (**b**) REE+Y pattern showing the absence of Ce anomaly and a particular low (ΣREE+Y) content; (**c**) REE+Y patterns showing high ΣREE+Y and marked negative Ce/Ce* anomalies; (**d**) relatively flat REE+Y patterns.

Figure 12. Scatter plot of aqueous Sr content of the lakes *versus* P content of microbialites showing a positive correlation (r_s=0.9). Samples with high detrital contamination (red squares); intermediately contaminated samples (green diamonds); authigenic-dominated samples (blue dots).

Figure 13. Scatter plot (log-log) of the alkalinity *versus* the salinity of the lakes normalized to the Lake Zirahuen's salinity. The degree of microbialite occurrence is documented in red. These alkalinity and salinity data correspond to samples collected in May 2014. The dashed blue line indicates the positive correlation. The regression coefficient (R^2) of the plot is equal to 0.89.

Figure 14. Scatter plot (log-log) of the salinity *versus* (**a**) $(Mg/Ca)_{aq}$ and (**b**) $[Mg]_{aq}$. Positive correlation are observed between salinity *versus* aqueous Mg/Ca and aqueous Mg concentrations. Lake Tecuitlapa (T) is below the two trends. Abbreviations for the carbonate phases are: Mg-calcite (MgC); monohydrocalcite (MHC); aragonite (A); hydromagnesite (H).

Figure 15. Scatter plot of $(Mg/Ca)_{aq}$ and $[Mg]_{aq}$. The carbonate microbialite mineralogy for each lake is reported in square brackets. Lakes: Zirahuén (Z), Alberca de Guadalupe (Alb), La Alberca de Los Espinos (AE), Pátzcuaro (P), Tecuitlapa (T), Aljojuca (Alj), Quechulac (Q), La Preciosa (LP), center (Atx-M) and north side (Atx-N) of Lake Atexcac, west side (AL-W) and center (AL-M) of Lake Alchichica. Abbreviations for the carbonate phases are: Mg-calcite (MgC); monohydrocalcite (MHC); aragonite (A); hydromagnesite (H).

Figure 16. Model of lake evolution over time. Microbialites start emerging at a certain stage of evaporation and/or weathering of the lake (when $[Na^+]_{aq}$ and alkalinity become higher than certain treshold values). Then microbialite mineralogy changes according to key parameters such as the aqueous (Mg/Ca), which controls carbonate mineralogy, and aqueous $[H_4SiO_4]$ controlling the precipitation of authigenic Mg-silicate.

TABLES

Lake	General location	Sampling location (January 2012 / May 2014)	Elevation (masl)	Lake type	Lake basement
La Preciosa	Los Llanos de San Juan region, eastern TMVB	19° 22' 32.70"N; 97° 23' 12.14"W / 19° 22' 09.80"N; 97° 23' 00.26"W	2330	Triple phreatic explosion maar	limestone, basalts
Quechulac	Los Llanos de San Juan region, eastern TMVB	19° 22' 31.56"N; 97° 21' 18.29"W / Ø	2330	Phreatic explosion maar	limestone, basalts
Atexcac	Los Llanos de San Juan region, eastern TMVB	19° 20' 08.27"N; 97° 27' 10.24"W / 19° 20' 08.27"N; 97° 27' 10.24"W	2360	Phreato-magmatic explosion maar	limestones, andesites, basalts
Alchichica	Los Llanos de San Juan region, eastern TMVB	19° 25' 12.32''N; 97° 24' 11.79''W / 19° 25' 00.76''N; 97° 24' 41.64''W	2320	Phreatic explosion maar	limestone, basalts
Aljojuca	Los Llanos de San Andrés, eastern TMVB	Ø / 19° 05' 36.27"N; 97° 31' 50.91"W	2379	Phreatic explosion maar	limestone, basalts
Tecuitlapa	Los Llanos de San Andrés, eastern TMVB	Ø / 19° 07' 29.35"N; 97° 32' 35.30"W	2380	Phreato-magmatic explosion maar	limestone, basalts
La Alberca de Los Espinos	Zacapu Basin, MGVF, central TMVB	Ø / 19° 54' 29.20"N; 101° 46' 02.90"W	1985	Phreato-magmatic explosion maar	andesite xenoliths
Alberca de Guadalupe	Zacapu Basin, MGVF, central TMVB	Ø / 19° 48' 21.11"N; 101° 27' 10.91"W	2066	Phreato-magmatic explosion maar	andesites, ignimbrite clasts
Pátzcuaro	El Estribo volcanic complex, MGVF, central TMVB	Ø / 19°40' 08.30"N; 101° 33' 44.40"W	2044	Lava-dammed basin associated with fractures	andesites
Zirahuén	Highland Michoacán, MGVF, central TMVB	Ø / 19° 26' 18.21"N; 101° 44' 40.03"W	2082	Lava-dammed endorheic basin	basalts

Lake	Water type	Mixing Type	Max depth (m)	Inflow/ outflow	Age	Microbialite Description	References
La Preciosa	Bic-Mg	Warm monomictic	46	ND	Pleistocene	Living and non-living microbialites	Armienta et al., 2008; Sigala et al., 2017
Quechulac	Bic-Mg	Warm monomictic	40	ND	Pleistocene	Living and non-living microbialites	Armienta et al., 2008; Sigala et al., 2017
Atexcac	Cl(+HCO_3)-Na	Warm monomictic	39	ND	~ 0.33 Myr	Living and non-living microbialites	Carrasco-Núñez et al., 2007; Armienta et al., 2008
Alchichica	Cl(+HCO_3)-Na	Warm monomictic	62	Groundwater inflow on the W shore	Pleistocene	Living and non-living microbialites	Armienta et al., 2008; Sigala et al., 2017 ; Zeyen et al., 2019
Aljojuca	Na-Bic	Warm monomictic	51	ND	Pleistocene	Basalts encrusted by living and non-living microbialites	Armienta et al., 2008; Sigala et al., 2017
Tecuitlapa	Na-Bic	Warm polymictic	2.5	ND	Pleistocene	Basalts encrusted by living and non-living microbialites	Armienta et al., 2008; Sigala et al., 2017
La Alberca de Los Espinos	Bic(+Cl)-Na	Warm monomictic	30	ND	~ 25 kyr	Living and non-living microbialites	Siebe et al., 2014
Alberca de Guadalupe	Bic-Mixed(Na-Mg)	Warm polymictic	9	Groundwater inflow on the E shore	~23 -20 kyr	Andesites finely encrusted by living and non-living microbialites	Siebe et al., 2014
Pátzcuaro	Na-Bic	Warm polymictic	9	Groundwater inflows along the S shore and the N shore	> ~30 kyr	Andesites encrusted by living and non-living microbialites	Bischoff et al., 2004 ; Israde-Alcántara et al., 2005; Pola et al., 2015 ; Sigala et al., 2017
Zirahuén	Bic-Mixed(Na-Ca-Mg)	Warm monomictic	40	Inflows from rivers Rio de la Palma and Arroyo Zirahuen	Late Pleistocene (100-11 Kyr)	No microbialites	Davies et al., 2004; Armienta et al., 2008. Sigala et al., 2017

Table 1.

Location, elevation, type of lake, geology, water type, mixing type, maximum depth, documented inflow and outflow, age and microbialite type of the studied lakes. Meaning of the abbreviations: TMVB: trans-Mexican volcanic belt; MGVF: Michoaćan-Guanajuato volcanic field. masl: meters above sea level. Ø: no sample was collected during this field campaign.

Lake surface water	$^{87}Sr/^{86}Sr$	95% confidence interval
Alchichica – AL2014_0m_M	0.706888	0.000004
La Preciosa – Preciosa2014-0m	0.706962	0.000021
Atexcac – ATX2014_0m_M	0.706998	0.000040
La Alberca de Los Espinos – AlbEsp2014_0m	0.703914	0.000020
Zirahuén –Zirahuen2014_0m	0.704514	0.000024

Table 2.
Strontium isotopic compositions of five lake surface waters sampled in May 2014.

Lake	Main phases
La Preciosa	A – K/S
Quechulac	A – K/S
Atexcac	A – K/S and K/S –A
Alchichica	H – A and A – H
Aljojuca	MHC – (Mg-)C – A
Tecuitlapa	(Mg-)C – MHC – A – K/S
La Alberca de Los Espinos	(Mg-)C – MHC – K/S
Alberca de Guadalupe	(Mg-)C – K/S
Pátzcuaro	(Mg-)C – MHC – A – K/S
Zirahuén	Ø

Table 3.
List of the main mineral phases of the microbialites in decreasing order of abundance, as detected by XRD and FTIR and/or observed by optical and scanning electron microscopy. This table was derived from results obtained on living microbialites. Lake Zirahuén has no living or non-living microbialites (Ø). ((Mg-)C: (Mg-)calcite; MHC: Monohydrocalcite; A: Aragonite; H: Hydromagnesite; K/S: Kerolite and/or Stevensite).

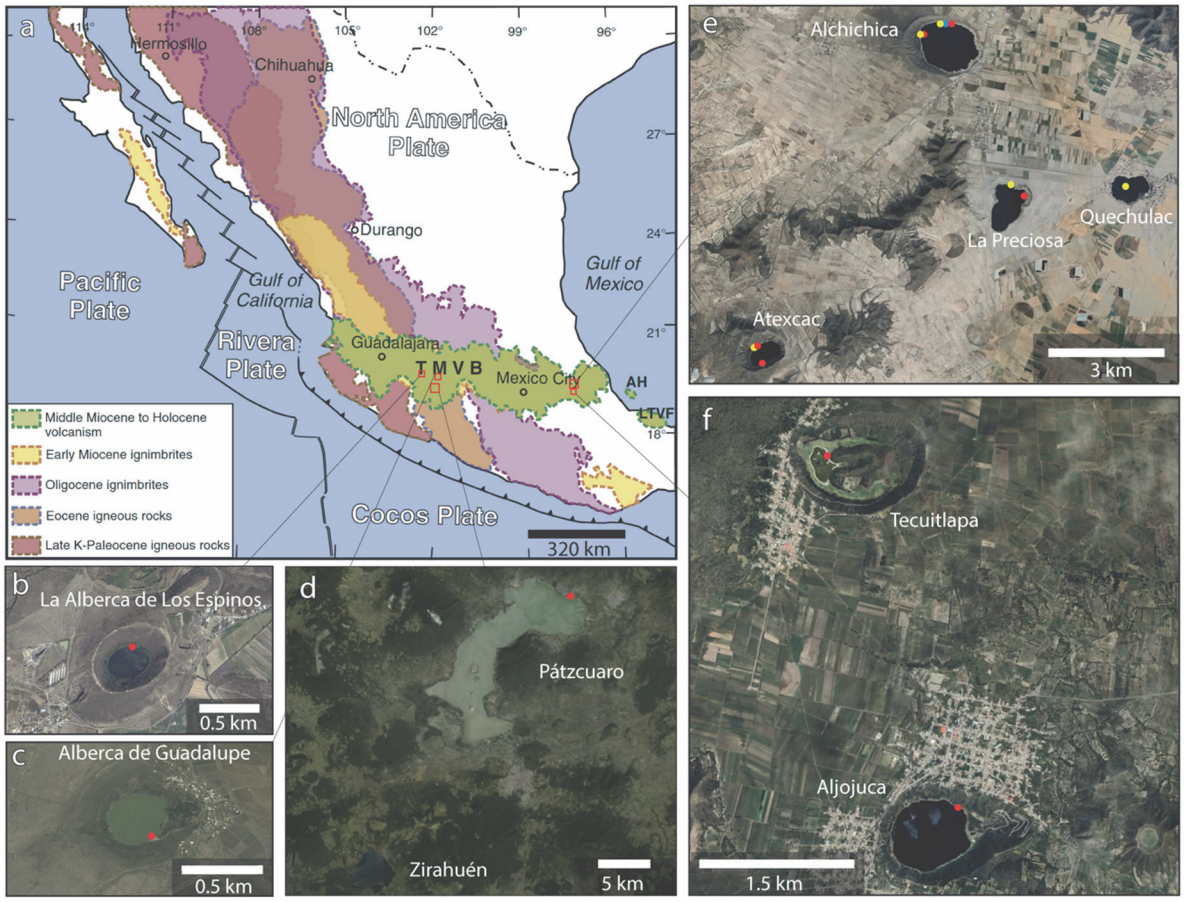
a
Hermosillo
Chihuahua
Durango
Guadalajara
Mexico City
TMVB
AH
LTVF
North America Plate
Pacific Plate
Rivera Plate
Cocos Plate
Gulf of California
Gulf of Mexico
320 km
Middle Miocene to Holocene volcanism
Early Miocene ignimbrites
Oligocene ignimbrites
Eocene igneous rocks
Late K-Paleocene igneous rocks
b
La Alberca de Los Espinos
0.5 km
c
Alberca de Guadalupe
0.5 km
d
Pátzcuaro
Zirahuén
5 km
e
Alchichica
La Preciosa
Quechulac
Atexcac
3 km
f
Tecuitlapa
Aljojuca
1.5 km

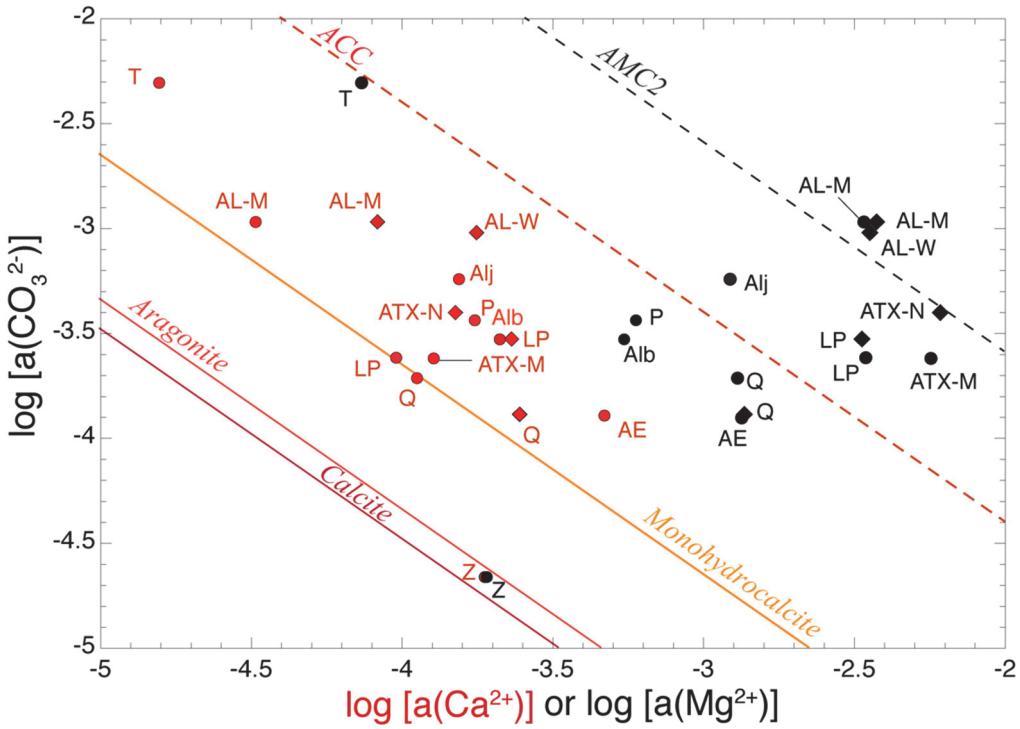
ACC
AMC2
Aragonite
Calcite
Monohydrocalcite
T
AL-M
AL-W
Alj
ATX-N
P
Alb
LP
ATX-M
Q
AE
Z
log [a(CO3 2-)]
log [a(Ca2+)] or log [a(Mg2+)]
-2
-2.5
-3
-3.5
-4
-4.5
-5

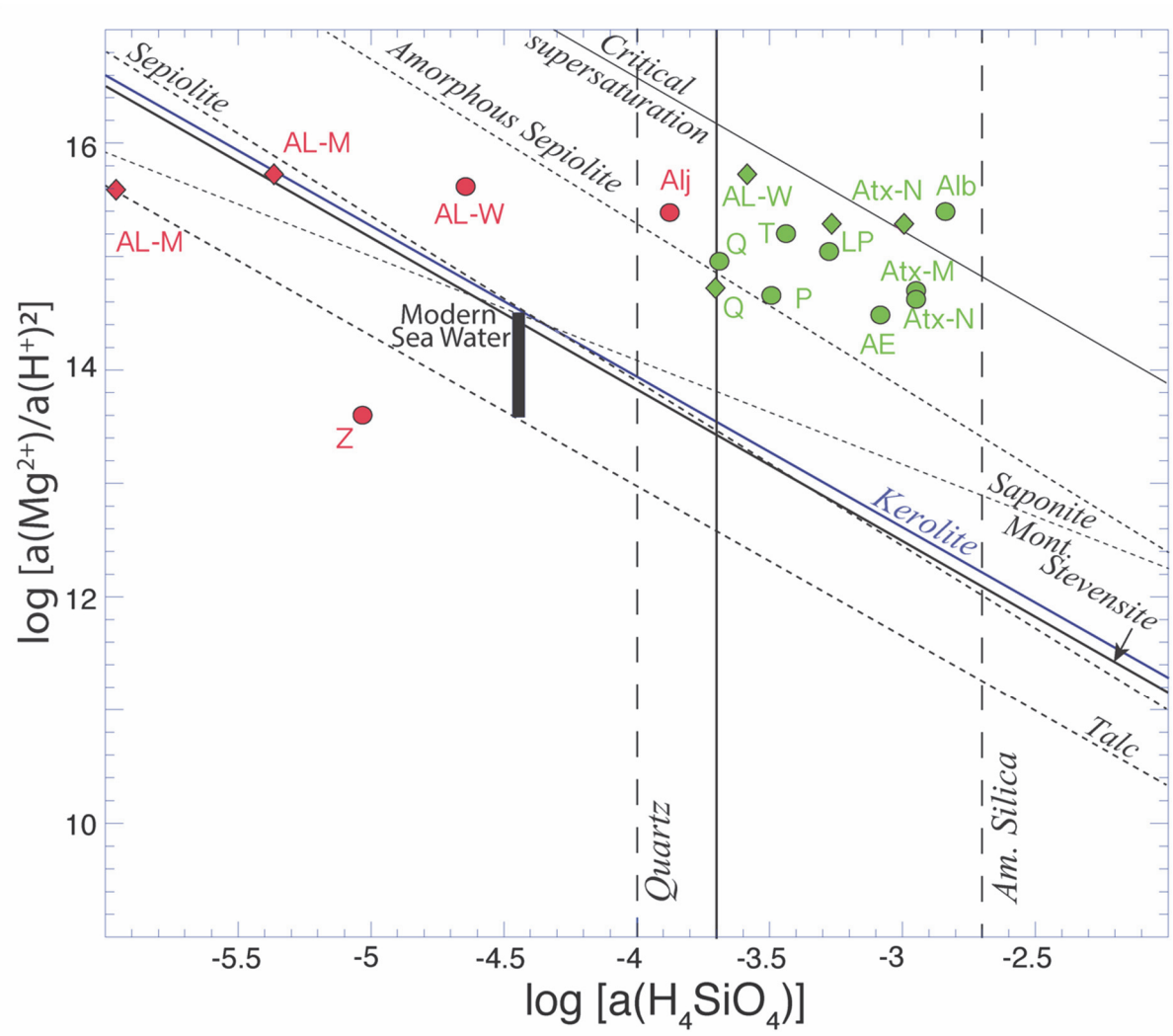
Sepiolite
Amorphous Sepiolite
Critical supersaturation
AL-M
AL-W
Alj
AL-M
Modern Sea Water
Z
Q
T
LP
Atx-N
Alb
AL-W
Atx-M
Q
P
Atx-N
AE
Saponite
Mont.
Stevensite
Kerolite
Talc
Quartz
Am. Silica
16
14
12
10
-5.5
-5
-4.5
-4
-3.5
-3
-2.5
log [a(Mg2+)/a(H+)2]
log [a(H4SiO4)]

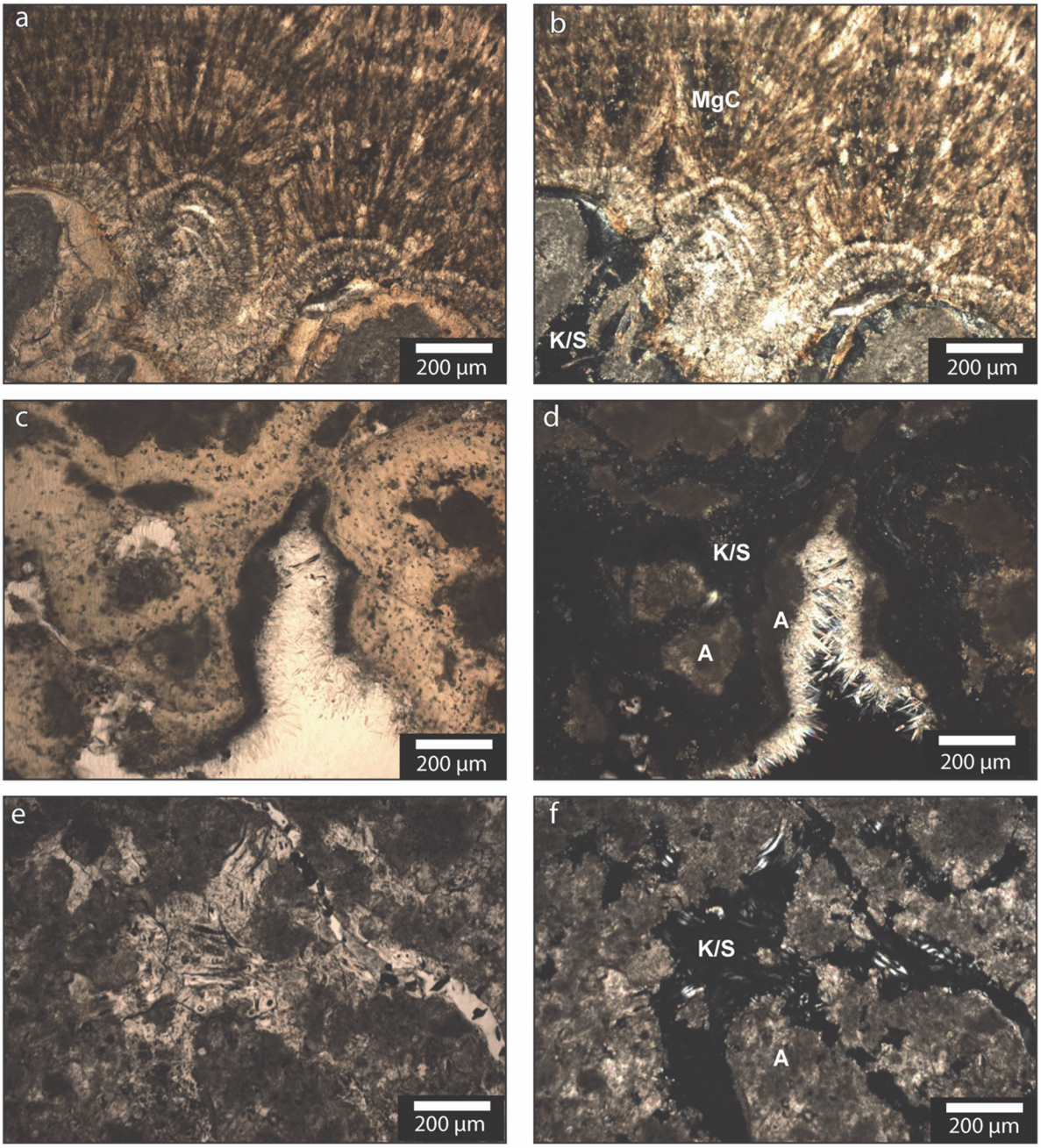
a
200 µm
b
MgC
K/S
200 µm
c
200 µm
d
K/S
A
A
200 µm
e
200 µm
f
K/S
A
200 µm

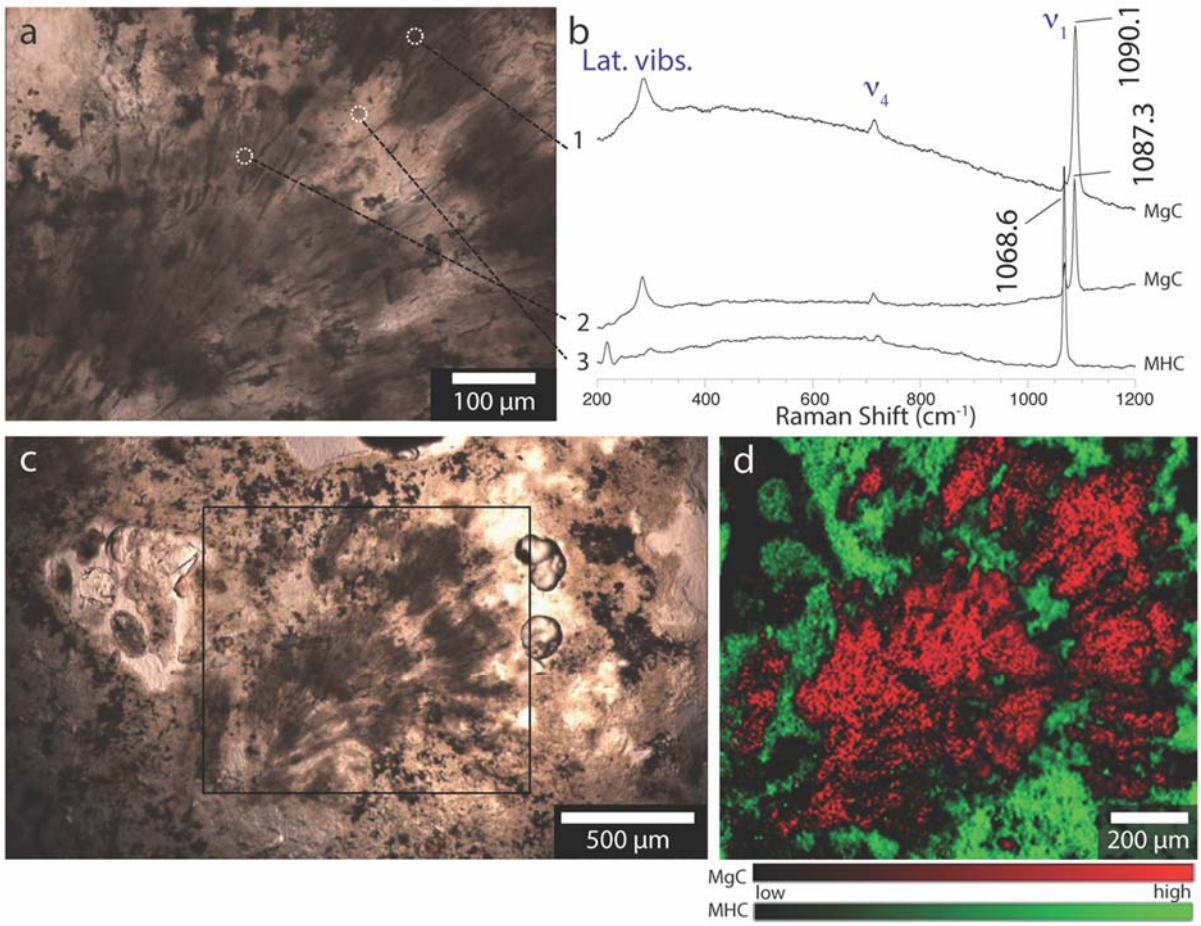
a
100 µm
b
Lat. vibs.
ν_4
ν_1
1090.1
1087.3
1068.6
1
2
3
MgC
MgC
MHC
200
400
600
800
1000
1200
Raman Shift (cm^{-1})
c
500 µm
d
200 µm
MgC
low
high
MHC

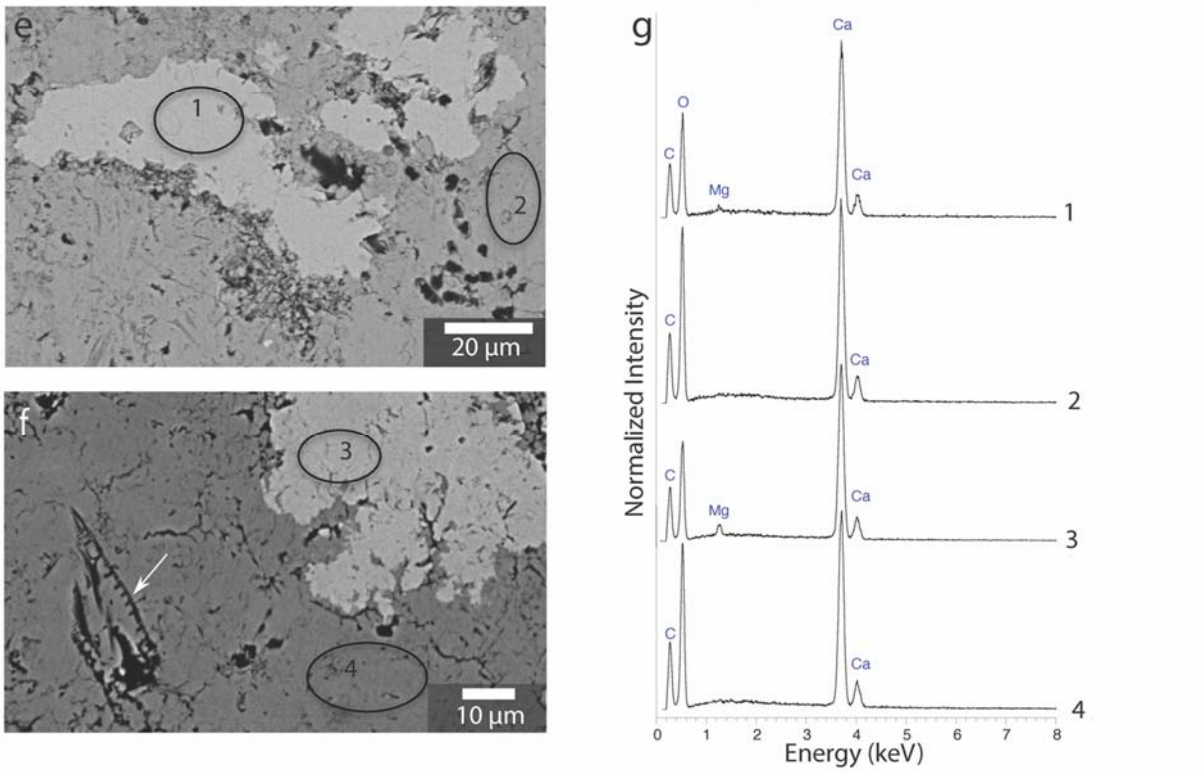
e
1
2
20 µm
f
3
4
10 µm
g
Ca
O
C
Mg
Ca
1
C
Ca
2
C
Mg
Ca
3
C
Ca
4
Normalized Intensity
0
1
2
3
4
5
6
7
8
Energy (keV)

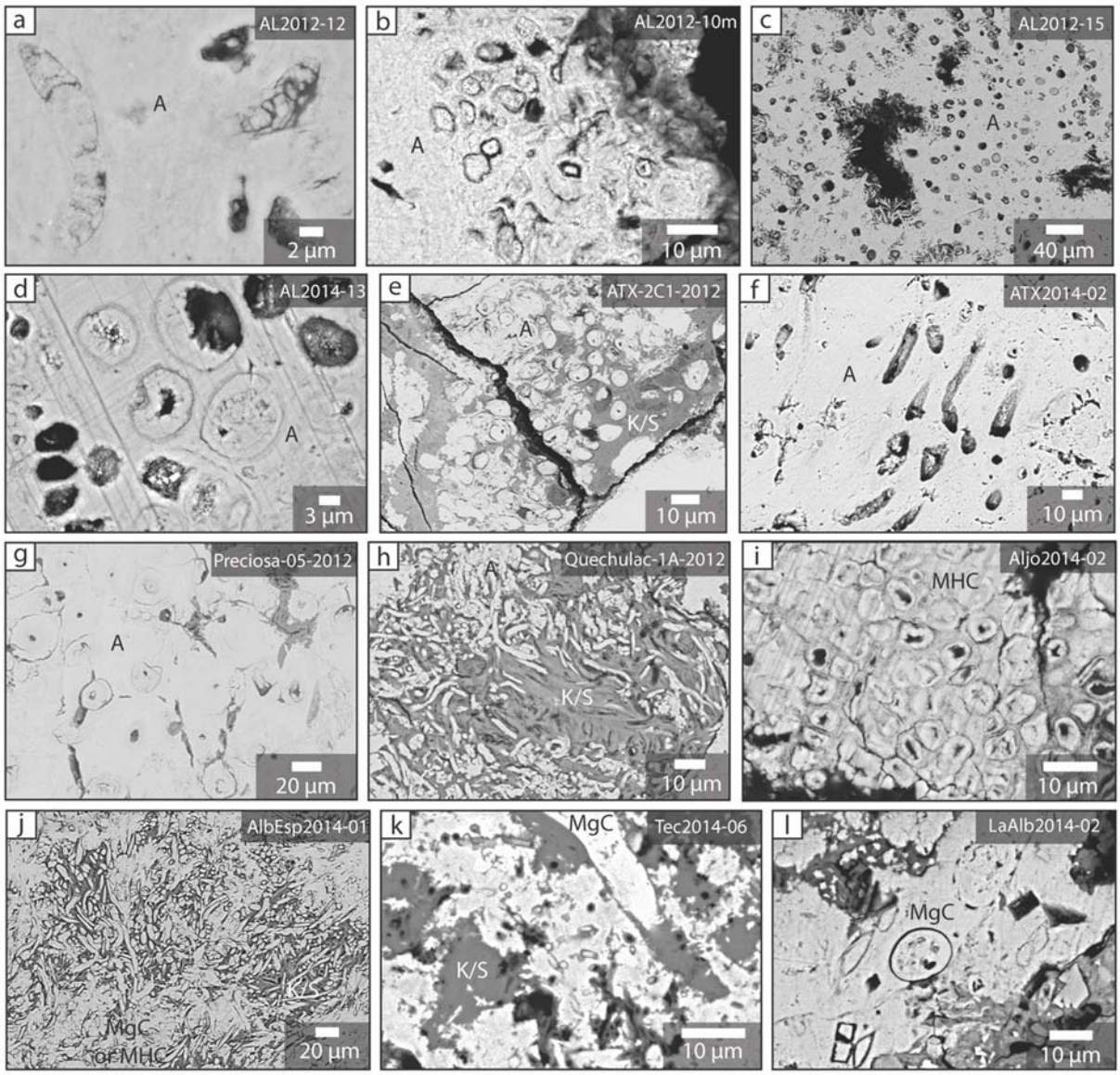
a
AL2012-12
A
2 µm
b
AL2012-10m
A
10 µm
c
AL2012-15
A
40 µm
d
AL2014-13
A
3 µm
e
ATX-2C1-2012
A
K/S
10 µm
f
ATX2014-02
A
10 µm
g
Preciosa-05-2012
A
20 µm
h
Quechulac-1A-2012
A
K/S
10 µm
i
Aljo2014-02
MHC
10 µm
j
AlbEsp2014-01
K/S
MgC
or MHC
20 µm
k
MgC
Tec2014-06
K/S
10 µm
l
LaAlb2014-02
MgC
10 µm

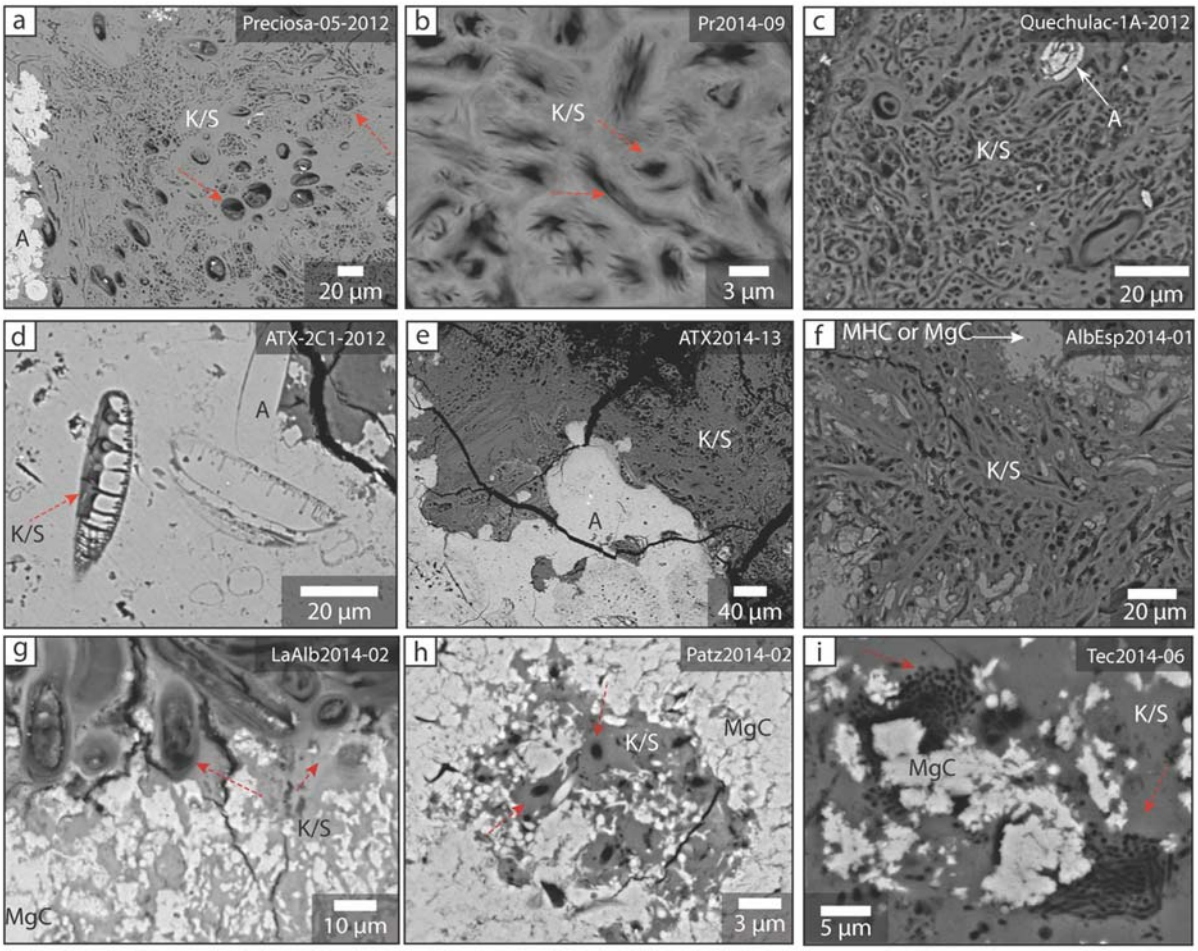
a
Preciosa-05-2012
K/S
A
20 µm
b
Pr2014-09
K/S
3 µm
c
Quechulac-1A-2012
A
K/S
20 µm
d
ATX-2C1-2012
A
K/S
20 µm
e
ATX2014-13
K/S
A
40 µm
f
MHC or MgC
AlbEsp2014-01
K/S
20 µm
g
LaAlb2014-02
K/S
MgC
10 µm
h
Patz2014-02
MgC
K/S
3 µm
i
Tec2014-06
K/S
MgC
5 µm

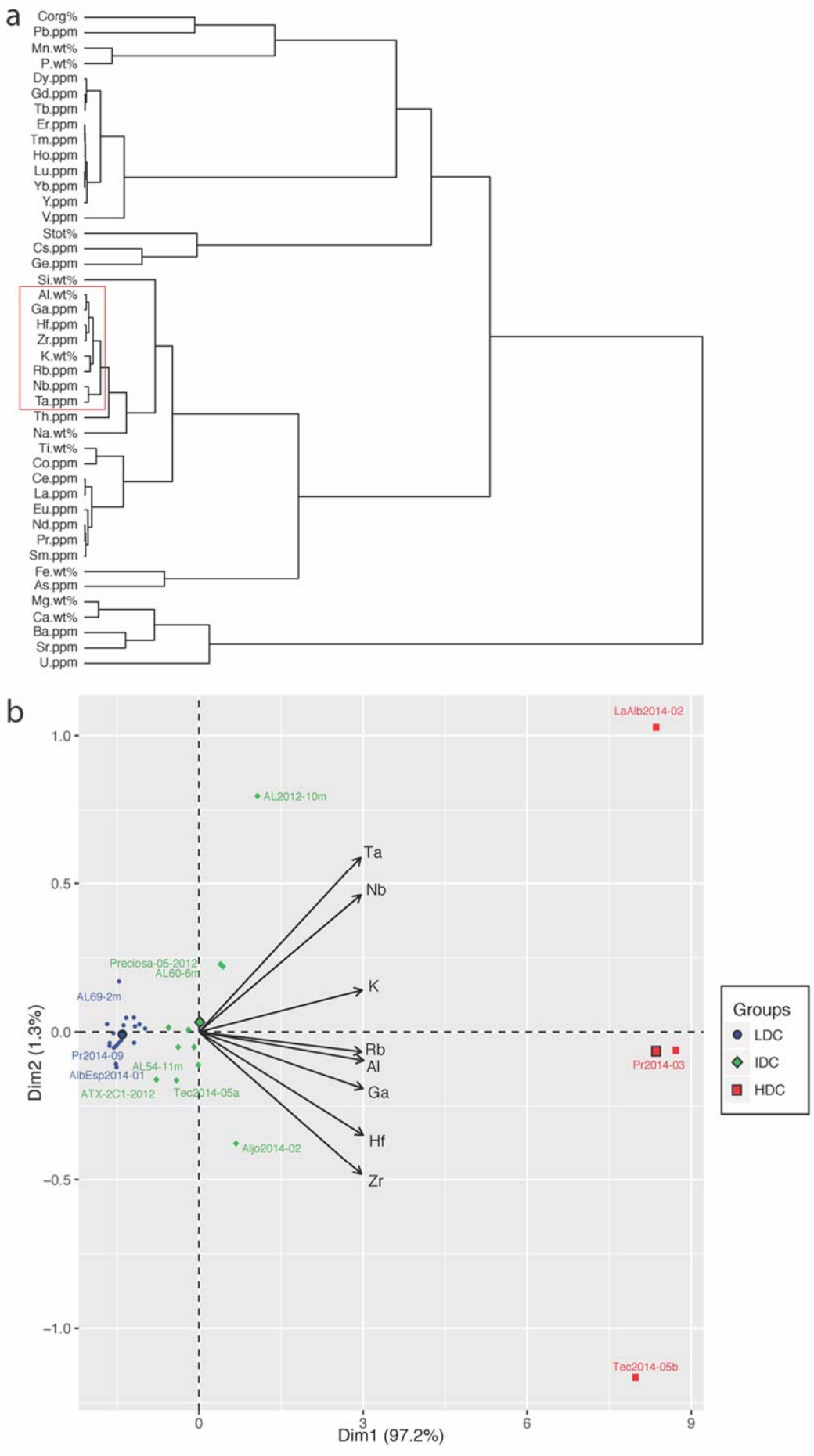
a
Corg%
Pb.ppm
Mn.wt%
P.wt%
Dy.ppm
Gd.ppm
Tb.ppm
Er.ppm
Tm.ppm
Ho.ppm
Lu.ppm
Yb.ppm
Y.ppm
V.ppm
Stot%
Cs.ppm
Ge.ppm
Si.wt%
Al.wt%
Ga.ppm
Hf.ppm
Zr.ppm
K.wt%
Rb.ppm
Nb.ppm
Ta.ppm
Th.ppm
Na.wt%
Ti.wt%
Co.ppm
Ce.ppm
La.ppm
Eu.ppm
Nd.ppm
Pr.ppm
Sm.ppm
Fe.wt%
As.ppm
Mg.wt%
Ca.wt%
Ba.ppm
Sr.ppm
U.ppm
b
LaAlb2014-02
AL2012-10m
Ta
Nb
K
Rb
Al
Ga
Hf
Zr
Preciosa-05-2012
AL60-6m
AL69-2m
Pr2014-09
AlbEsp2014-01
AL54-11m
ATX-2C1-2012
Tec2014-05a
Aljo2014-02
Pr2014-03
Tec2014-05b
Groups
LDC
IDC
HDC
Dim2 (1.3%)
Dim1 (97.2%)
1.0
0.5
0.0
−0.5
−1.0
0
3
6
9

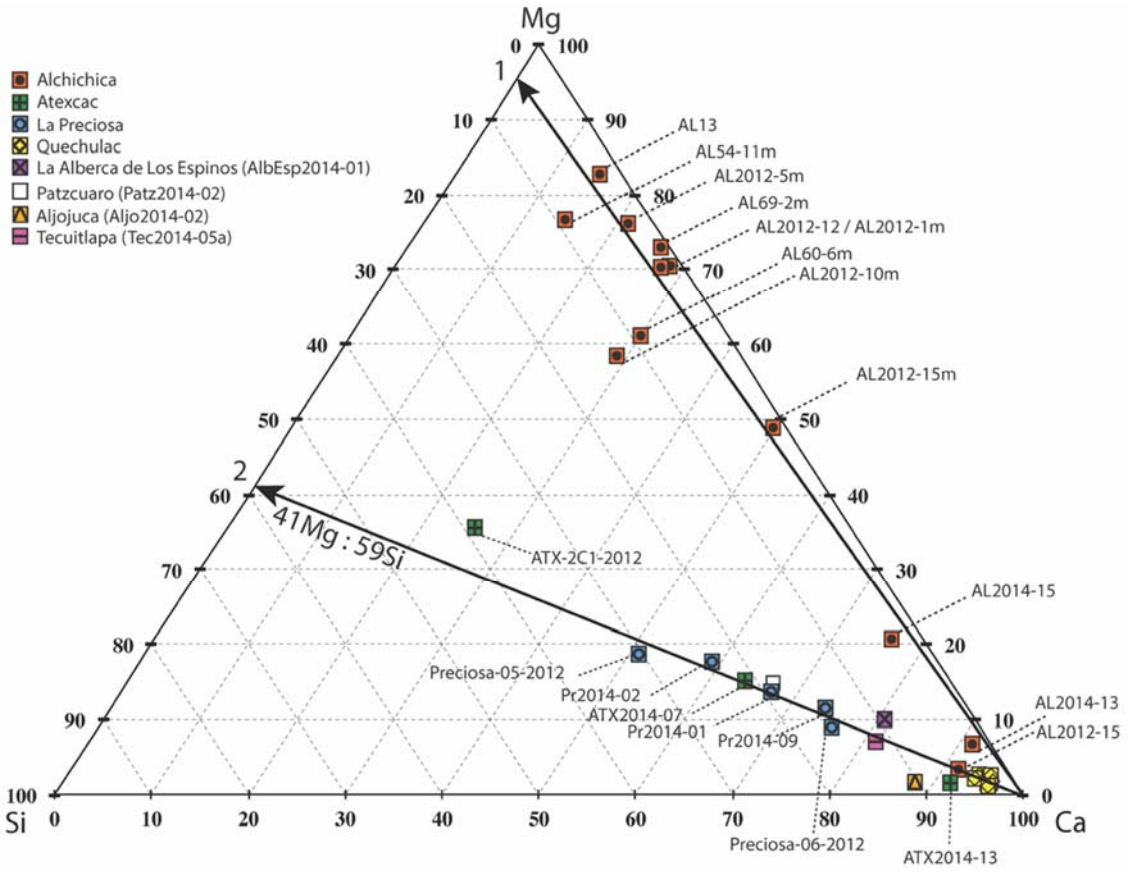
Mg
Si
Ca
Alchichica
Atexcac
La Preciosa
Quechulac
La Alberca de Los Espinos (AlbEsp2014-01)
Patzcuaro (Patz2014-02)
Aljojuca (Aljo2014-02)
Tecuitlapa (Tec2014-05a)
1
2
41Mg : 59Si
AL13
AL54-11m
AL2012-5m
AL69-2m
AL2012-12 / AL2012-1m
AL60-6m
AL2012-10m
AL2012-15m
AL2014-15
AL2014-13
AL2012-15
ATX-2C1-2012
Preciosa-05-2012
Pr2014-02
ATX2014-07
Pr2014-01
Pr2014-09
Preciosa-06-2012
ATX2014-13

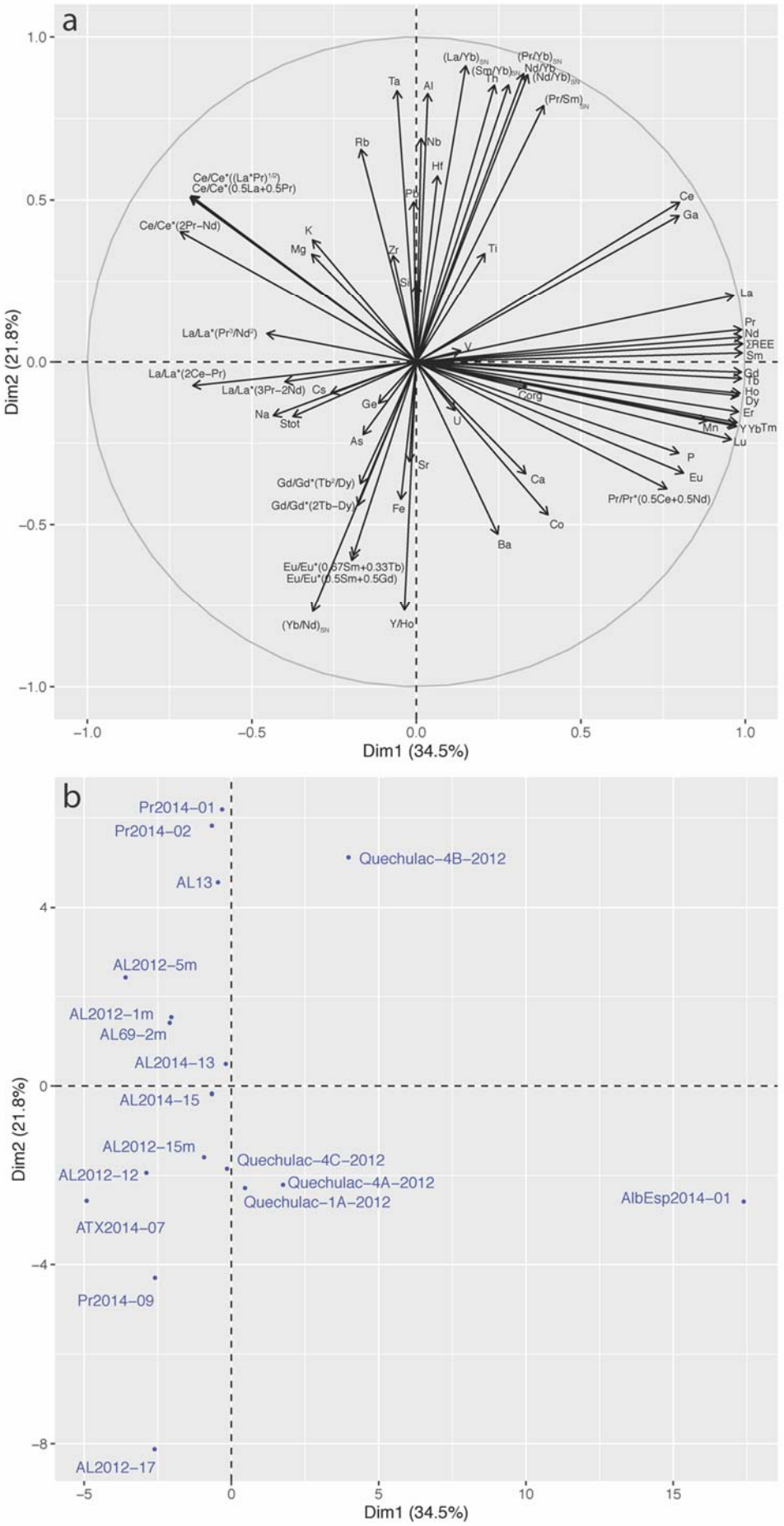
a
Dim1 (34.5%)
Dim2 (21.8%)
1.0
0.5
0.0
−0.5
−1.0
Ta
Al
Rb
Nb
Hf
Ti
Zr
Si
K
Mg
Ce
Ga
La
Pr
Nd
ΣREE
Sm
Gd
Tb
Ho
Dy
Er
Y
Yb
Tm
Lu
Mn
P
Eu
Corg
U
Ca
Co
Ba
Sr
Fe
Ge
As
Na
Stot
Cs
(La/Yb)SN
(Sm/Yb)SN
Th
(Pr/Yb)SN
Nd/Yb
(Nd/Yb)SR
(Pr/Sm)SN
Ce/Ce*((La*Pr)1/2)
Ce/Ce*(0.5La+0.5Pr)
Ce/Ce*(2Pr−Nd)
La/La*(Pr3/Nd2)
La/La*(2Ce−Pr)
La/La*(3Pr−2Nd)
Gd/Gd*(Tb2/Dy)
Gd/Gd*(2Tb−Dy)
Eu/Eu*(0.67Sm+0.33Tb)
Eu/Eu*(0.5Sm+0.5Gd)
(Yb/Nd)SN
Y/Ho
Pr/Pr*(0.5Ce+0.5Nd)
b
Dim1 (34.5%)
Dim2 (21.8%)
Pr2014−01
Pr2014−02
AL13
Quechulac−4B−2012
AL2012−5m
AL2012−1m
AL69−2m
AL2014−13
AL2014−15
AL2012−15m
Quechulac−4C−2012
AL2012−12
Quechulac−4A−2012
Quechulac−1A−2012
AlbEsp2014−01
ATX2014−07
Pr2014−09
AL2012−17
4
0
−4
−8
−5
0
5
10
15

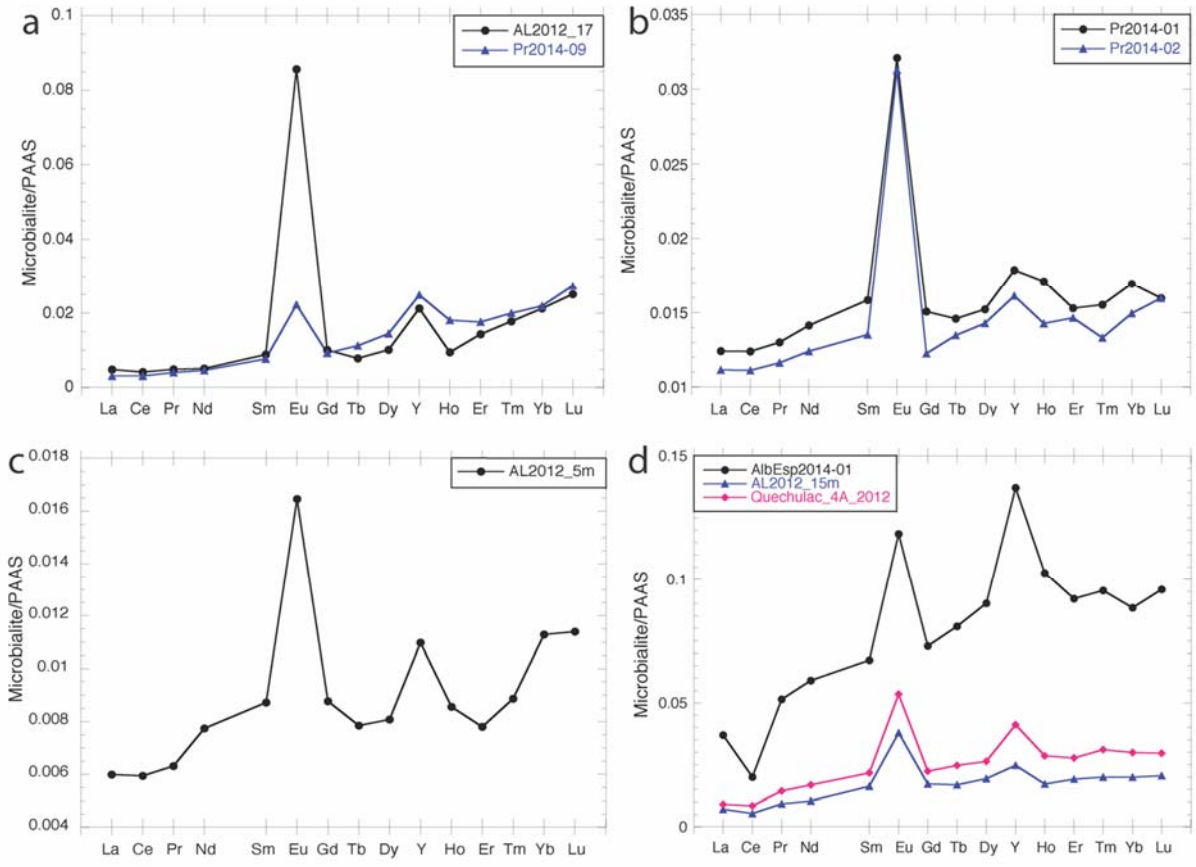
a
AL2012_17
Pr2014-09
Microbialite/PAAS
0.1
0.08
0.06
0.04
0.02
0
La Ce Pr Nd Sm Eu Gd Tb Dy Y Ho Er Tm Yb Lu
b
Pr2014-01
Pr2014-02
Microbialite/PAAS
0.035
0.03
0.025
0.02
0.015
0.01
La Ce Pr Nd Sm Eu Gd Tb Dy Y Ho Er Tm Yb Lu
c
AL2012_5m
Microbialite/PAAS
0.018
0.016
0.014
0.012
0.01
0.008
0.006
0.004
La Ce Pr Nd Sm Eu Gd Tb Dy Y Ho Er Tm Yb Lu
d
AlbEsp2014-01
AL2012_15m
Quechulac_4A_2012
Microbialite/PAAS
0.15
0.1
0.05
0
La Ce Pr Nd Sm Eu Gd Tb Dy Y Ho Er Tm Yb Lu

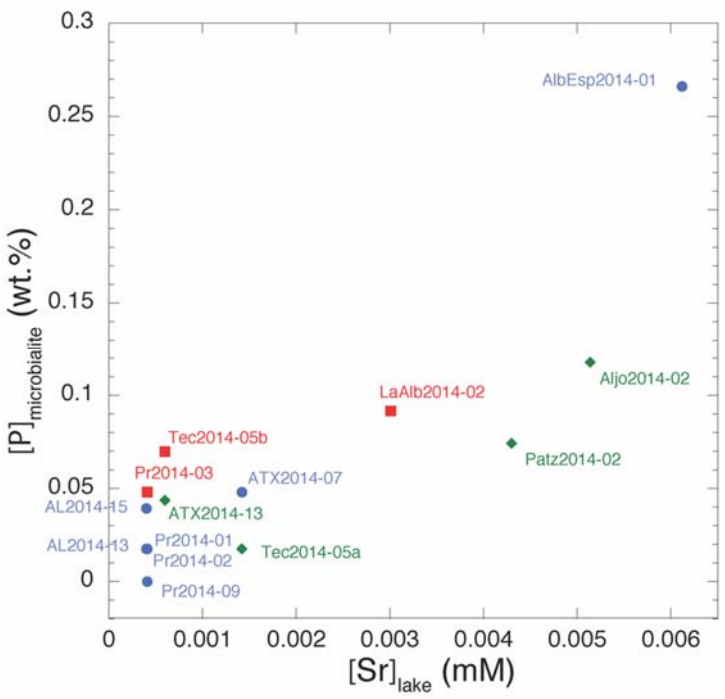
0.3
0.25
0.2
0.15
0.1
0.05
0
[P]microbialite (wt.%)
0
0.001
0.002
0.003
0.004
0.005
0.006
[Sr]lake (mM)
AlbEsp2014-01
Aljo2014-02
LaAlb2014-02
Patz2014-02
Tec2014-05b
Pr2014-03
ATX2014-07
AL2014-15
ATX2014-13
AL2014-13
Pr2014-01
Pr2014-02
Tec2014-05a
Pr2014-09

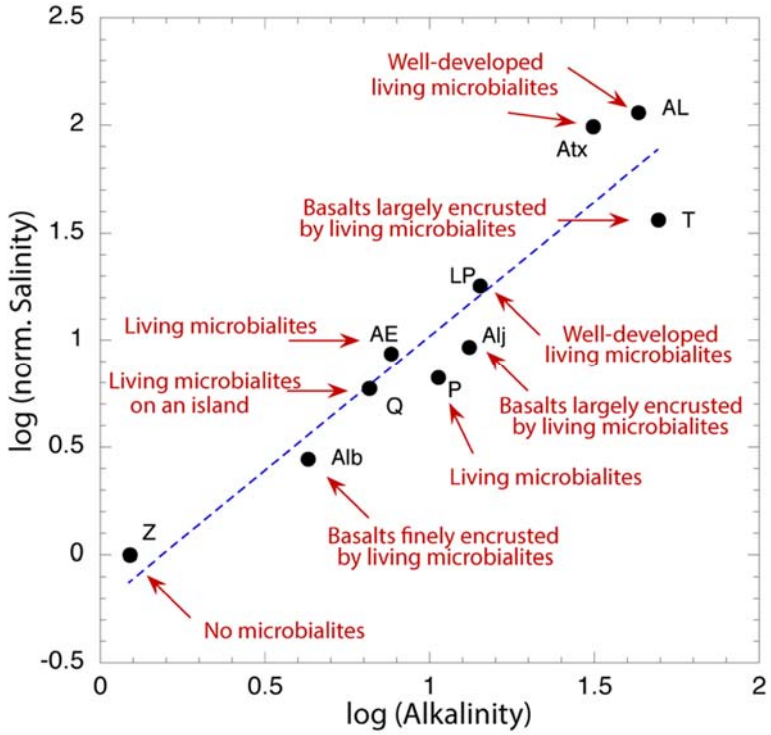
Well-developed
living microbialites
AL
Atx
Basalts largely encrusted
by living microbialites
T
LP
Living microbialites
AE
Alj
Well-developed
living microbialites
Living microbialites
on an island
Q
P
Basalts largely encrusted
by living microbialites
Alb
Living microbialites
Basalts finely encrusted
by living microbialites
Z
No microbialites
log (norm. Salinity)
log (Alkalinity)
2.5
2
1.5
1
0.5
0
-0.5
0
0.5
1
1.5
2

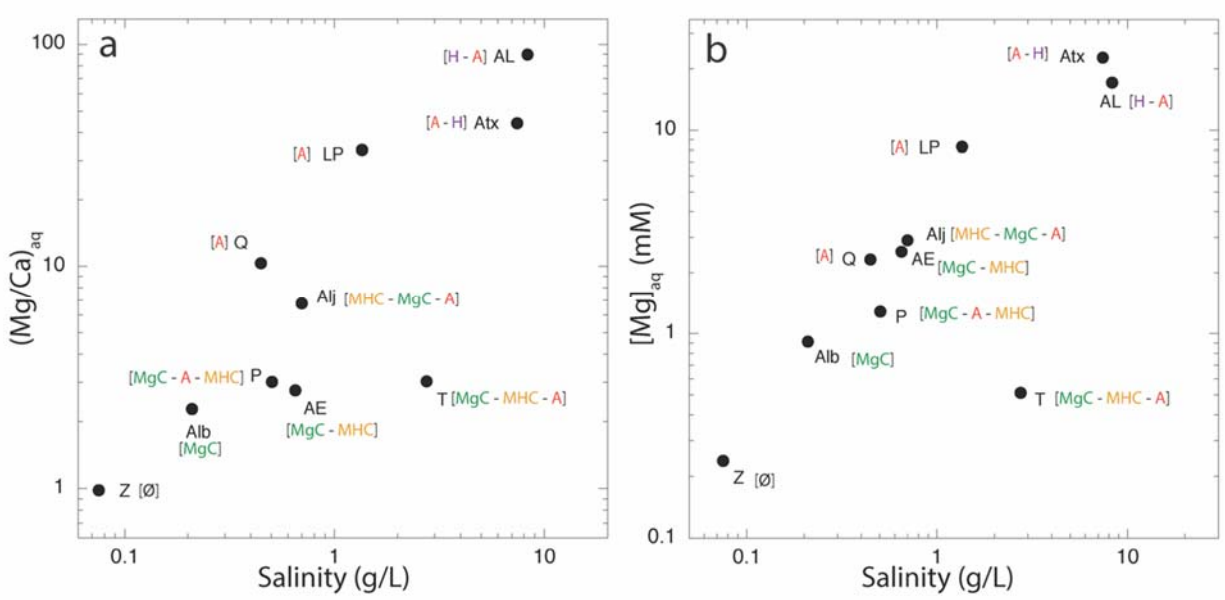
a
100
10
1
$(Mg/Ca)_{aq}$
[H - A] AL
[A - H] Atx
[A] LP
[A] Q
Alj [MHC - MgC - A]
[MgC - A - MHC] P
AE
[MgC - MHC]
T [MgC - MHC - A]
Alb
[MgC]
Z [Ø]
0.1
1
10
Salinity (g/L)
b
10
1
0.1
$[Mg]_{aq}$ (mM)
[A - H] Atx
AL [H - A]
[A] LP
Alj [MHC - MgC - A]
[A] Q
AE
[MgC - MHC]
P [MgC - A - MHC]
Alb [MgC]
T [MgC - MHC - A]
Z [Ø]
0.1
1
10
Salinity (g/L)

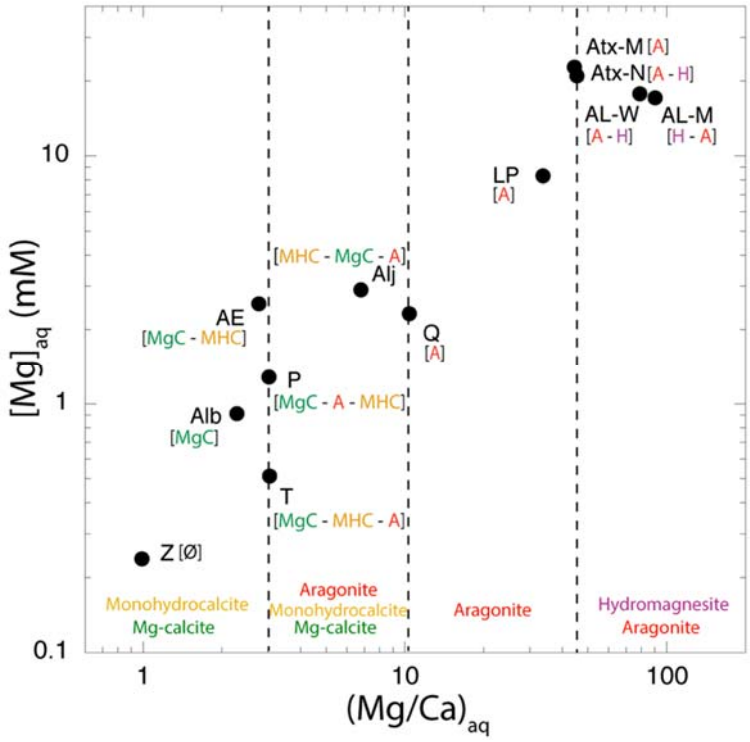
Atx-M [A]
Atx-N [A - H]
AL-W
[A - H]
AL-M
[H - A]
LP
[A]
[MHC - MgC - A]
Alj
AE
[MgC - MHC]
Q
[A]
P
[MgC - A - MHC]
Alb
[MgC]
T
[MgC - MHC - A]
Z [Ø]
Monohydrocalcite
Mg-calcite
Aragonite
Monohydrocalcite
Mg-calcite
Aragonite
Hydromagnesite
Aragonite
10
1
0.1
1
10
100
[Mg]aq (mM)
(Mg/Ca)aq

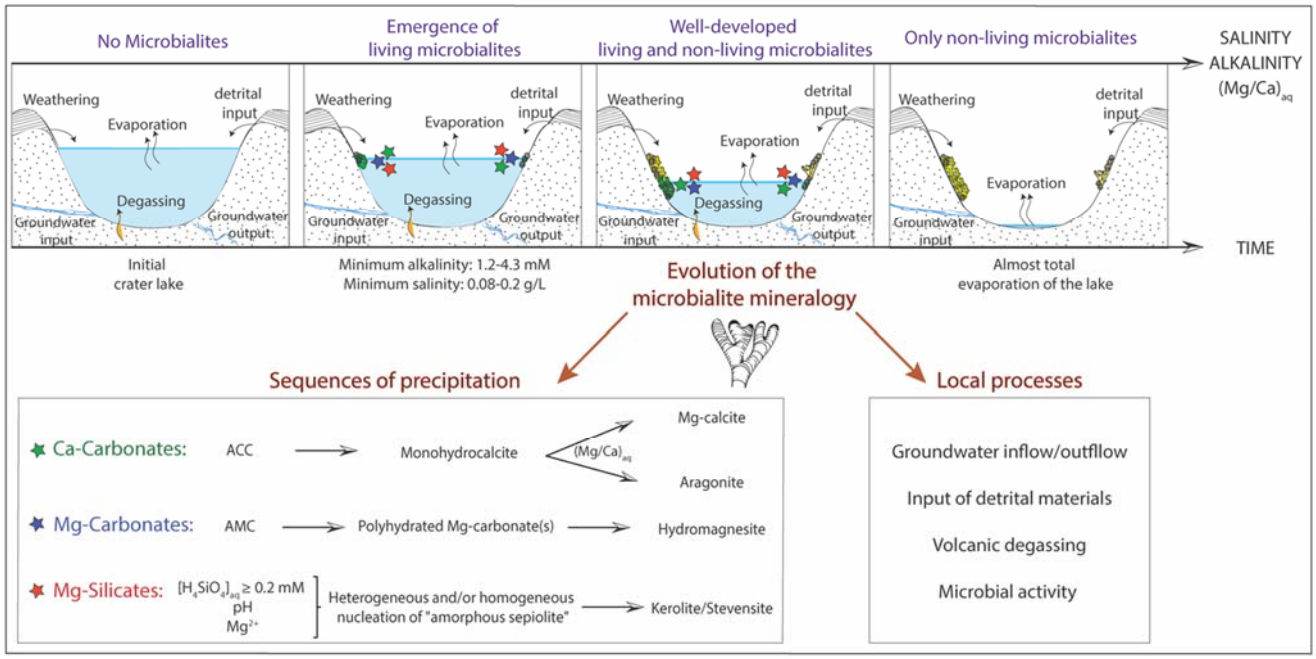
No Microbialites
Emergence of living microbialites
Well-developed living and non-living microbialites
Only non-living microbialites
SALINITY
ALKALINITY
(Mg/Ca)aq
TIME
Weathering
detrital input
Evaporation
Degassing
Groundwater input
Groundwater output
Initial crater lake
Minimum alkalinity: 1.2-4.3 mM
Minimum salinity: 0.08-0.2 g/L
Almost total evaporation of the lake
Evolution of the microbialite mineralogy
Sequences of precipitation
Local processes
Ca-Carbonates:
ACC
Monohydrocalcite
(Mg/Ca)aq
Mg-calcite
Aragonite
Mg-Carbonates:
AMC
Polyhydrated Mg-carbonate(s)
Hydromagnesite
Mg-Silicates:
[H4SiO4]aq ≥ 0.2 mM
pH
Mg2+
Heterogeneous and/or homogeneous nucleation of "amorphous sepiolite"
Kerolite/Stevensite
Groundwater inflow/outfllow
Input of detrital materials
Volcanic degassing
Microbial activity

Supporting Information in:

Integrative analysis of the mineralogical and chemical composition of modern microbialites from ten Mexican lakes: what do we learn about their formation?

Nina Zeyen[a+], Karim Benzerara*[a], Olivier Beyssac[a], Damien Daval[b], Elodie Muller[a], Christophe Thomazo[c,d], Rosaluz Tavera[e], Purificación López-García[f], David Moreira[f] and Elodie Duprat[a]

[a] *Sorbonne Université, Muséum National d'Histoire Naturelle, UMR CNRS 7590, IRD, Institut de Minéralogie, de Physique des Matériaux et de Cosmochimie, IMPMC, Paris 75005, France*

[b] *Laboratoire d'Hydrologie et de Géochimie de Strasbourg, EOST-ENGEES, Univ Strasbourg, EOST CNRS UMR 7517, 67084 Strasbourg, France*

[c] *UMR CNRS/uB6282 Biogéosciences, Université de Bourgogne Franche-Comté, 6 Bd Gabriel, 21000, Dijon, France*

[d] *Institut Universitaire de France*

[e] *Departamento de Ecología y Recursos Naturales, Universidad Nacional Autónoma de México, DF México, México*

[f] *Ecologie, Systématique et Evolution, CNRS, Université Paris-Saclay, AgroParisTech, Orsay, France*

* Corresponding author

Tel.: +33(0)144277542

E-mail address: karim.benzerara@upmc.fr

[+]*Now at Department of Earth and Atmospheric Sciences, University of Alberta, Edmonton, AB T6G 2E3, Canada*

Keywords: microbialites; crater lake; alkalinity; monohydrocalcite; (Mg-)calcite; aragonite; hydromagnesite; kerolite; REE+Y

CONTENTS

I. FIGURES ~~33~~ 33

FIGURE SI-1. CORRELATION MATRIX OF THE CHEMICAL VARIABLES DESCRIBING LAKE SOLUTIONS ~~33~~ 33
FIGURE SI-2. OVERVIEWS OF THE STUDIED LAKES AND PHOTOGRAPHS OF THE MICROBIALITES ~~44~~ 44
FIGURE SI-3. POWDER X-RAY DIFFRACTION PATTERNS OF SOME OF THE STUDIED MICROBIALITES ~~77~~ 77
FIGURE SI-4. FTIR SPECTRA OF SOME OF THE STUDIED MICROBIALITES ~~1212~~ 1212
FIGURE SI-5. SILICON *VS.* MAGNESIUM CONTENTS OF THE MICROBIALITES ~~1313~~ 1313
FIGURE SI-6. CORRELATION MATRIX OF THE CHEMICAL VARIABLES DESCRIBING THE AUTHIGENIC-DOMINATED MICROBIALITES ~~1414~~ 1414
FIGURE SI-7. ORGANIC CARBON *VS.* TOTAL SULPHUR OF ALL THE STUDIED MICROBIALITE SAMPLES ~~1515~~ 1515
FIGURE SI-8. CORRELATION MATRIX OF THE MICROBIALITE CHEMICAL VARIABLES AND THE AQUEOUS VARIABLES ~~1616~~ 1616
FIGURE SI-9. DISTRIBUTION OF MEXICAN LAKES IN THE SPENCER (ALK-SO_4-CA) TERNARY DIAGRAM ~~1717~~ 1717

II. TABLES ~~1818~~ 1818

TABLE SI-1. LIST OF THE AQUEOUS SAMPLES, THEIR LOCATION AND PERFORMED ANALYSES ~~1818~~ 1818
TABLE SI-2. DETERMINATION OF SALINITY ~~1919~~ 1919
TABLE SI-3. PRECIPITATION REACTIONS OF DIVERSE PHASES AND THEIR ASSOCIATED SOLUBILITY CONSTANTS ~~2121~~ 2121
TABLE SI-4. PHYSICAL AND CHEMICAL PARAMETERS OF THE STUDIED LAKES ~~2222~~ 2222
TABLE SI-5. CALCULATIONS OF [HCO_3^-] AND [CO_3^{2-}] BY TWO DIFFERENT METHODS ~~2626~~ 2626
TABLE SI-6. SATURATION INDICES OF THE 2012 AND 2014 SURFACE WATER SOLUTIONS ~~2727~~ 2727
TABLE SI-7. MINERALOGICAL COMPOSITION OF THE STUDIED MICROBIALITES ~~2828~~ 2828
TABLE SI-8. PROPORTIONS OF THE MINERAL PHASES IN THE AUTHIGENIC-DOMINATED MICROBIALITES ~~3030~~ 3030
TABLE SI-9. BULK CHEMICAL COMPOSITIONS OF THE STUDIED MICROBIALITES (MAJOR ELEMENTS) ~~3131~~ 3131
TABLE SI-10. BULK CHEMICAL COMPOSITIONS OF THE STUDIED MICROBIALITES (MINOR AND TRACE ELEMENTS EXCLUDING REE+Y) ~~3232~~ 3232
TABLE SI-11. BULK CHEMICAL COMPOSITION OF THE STUDIED MICROBIALITES: REE (+Y) ~~3434~~ 3434
TABLE SI-12. DETERMINATION OF THE $pCO_{2(G)}$/pCO_{2ATM} RATIO OF THE 2014 SURFACE WATER LAKES ~~3535~~ 3535

III. TEXTS ~~3636~~ 3636

TEXT SI-1. REE+Y CALCULATIONS AND CORRELATIONS BETWEEN VARIABLES ~~3636~~ 3636
TEXT SI-2. GEOCHEMICAL SIGNATURES OF DETRITAL CONTAMINATION IN MICROBIALITES ~~3939~~ 3939
TEXT SI-3. REE+Y PATTERNS OF MICROBIALITES DEPENDING ON THEIR LEVEL OF CONTAMINATION BY DETRITAL PARTICLES ~~4141~~ 4141
TEXT SI-4. DISCUSSION ABOUT THE POTENTIAL ORIGINS OF REE SIGNATURES OF MEXICAN AUTHIGENIC-DOMINATED MICROBIALITES ~~5252~~ 5252

IV. REFERENCES ~~5656~~ 5656

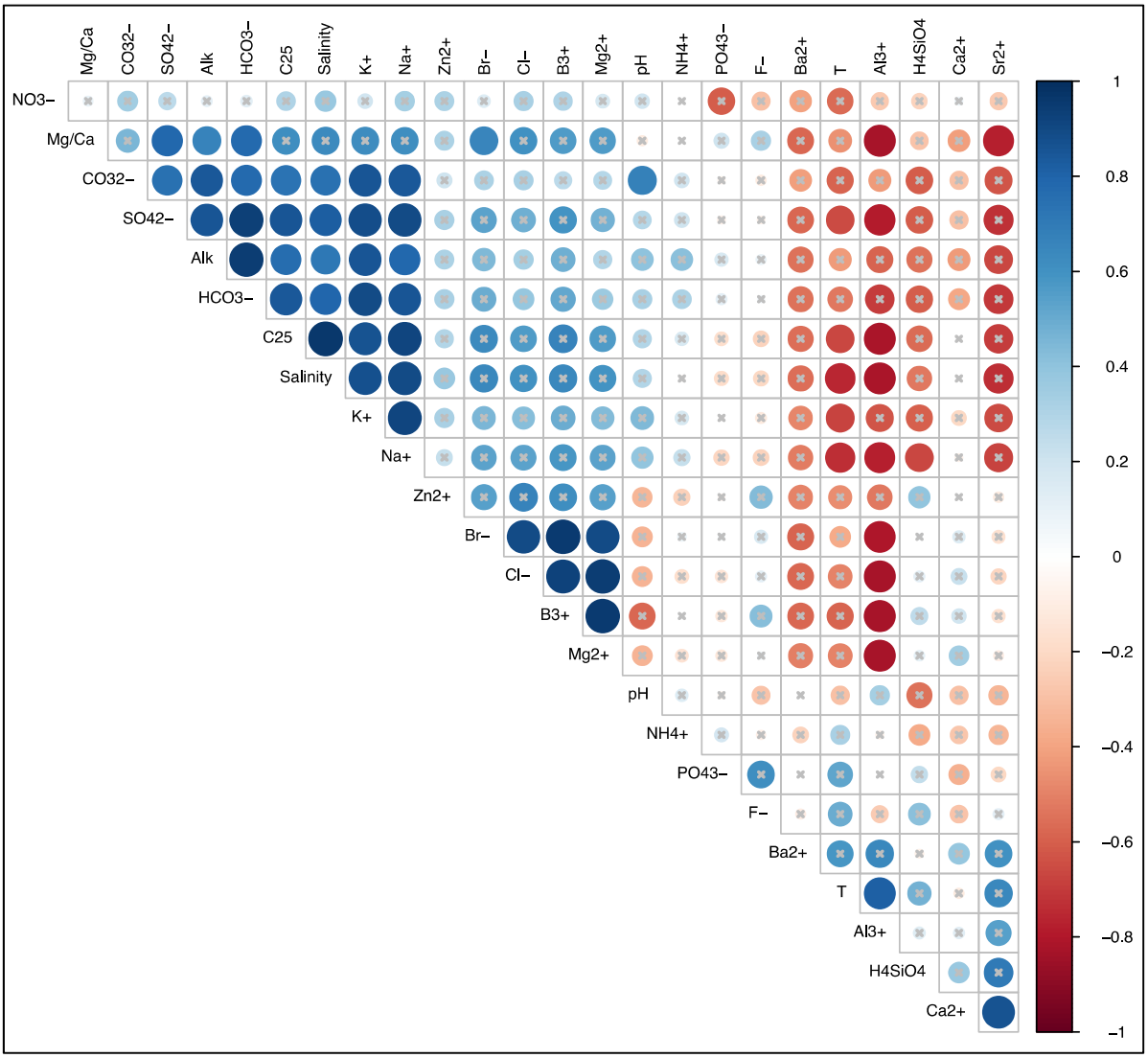
Mg/Ca
CO32−
SO42−
Alk
HCO3−
C25
Salinity
K+
Na+
Zn2+
Br−
Cl−
B3+
Mg2+
pH
NH4+
PO43−
F−
Ba2+
T
Al3+
H4SiO4
Ca2+
Sr2+
NO3−
1
0.8
0.6
0.4
0.2
0
−0.2
−0.4
−0.6
−0.8
−1

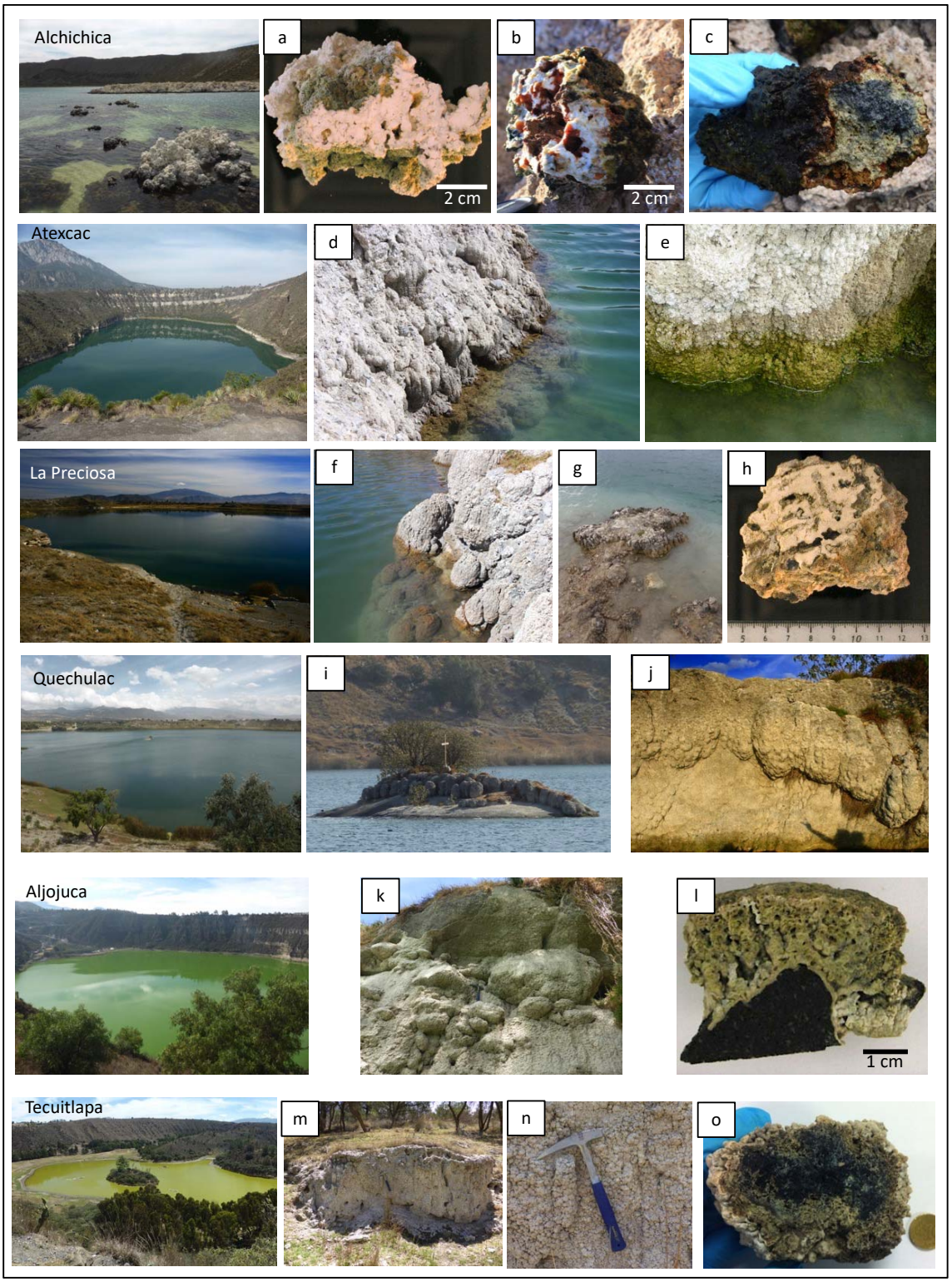

Figure SI-2. Overviews of the studied lakes and photographs of the microbialites

Lakes Alchichica **(a, b, c)**, Atexcac **(d, e)**, La Preciosa (**f, g, h**), Quechulac **(i, j)**, Aljojuca (**k,l**), Tecuitlapa (**m, n, o**), La Alberca de los Espinos (**p, q**), Alberca de Guadalupe (**r, s**), Pátzcuaro (**t**), and Zirahuén.

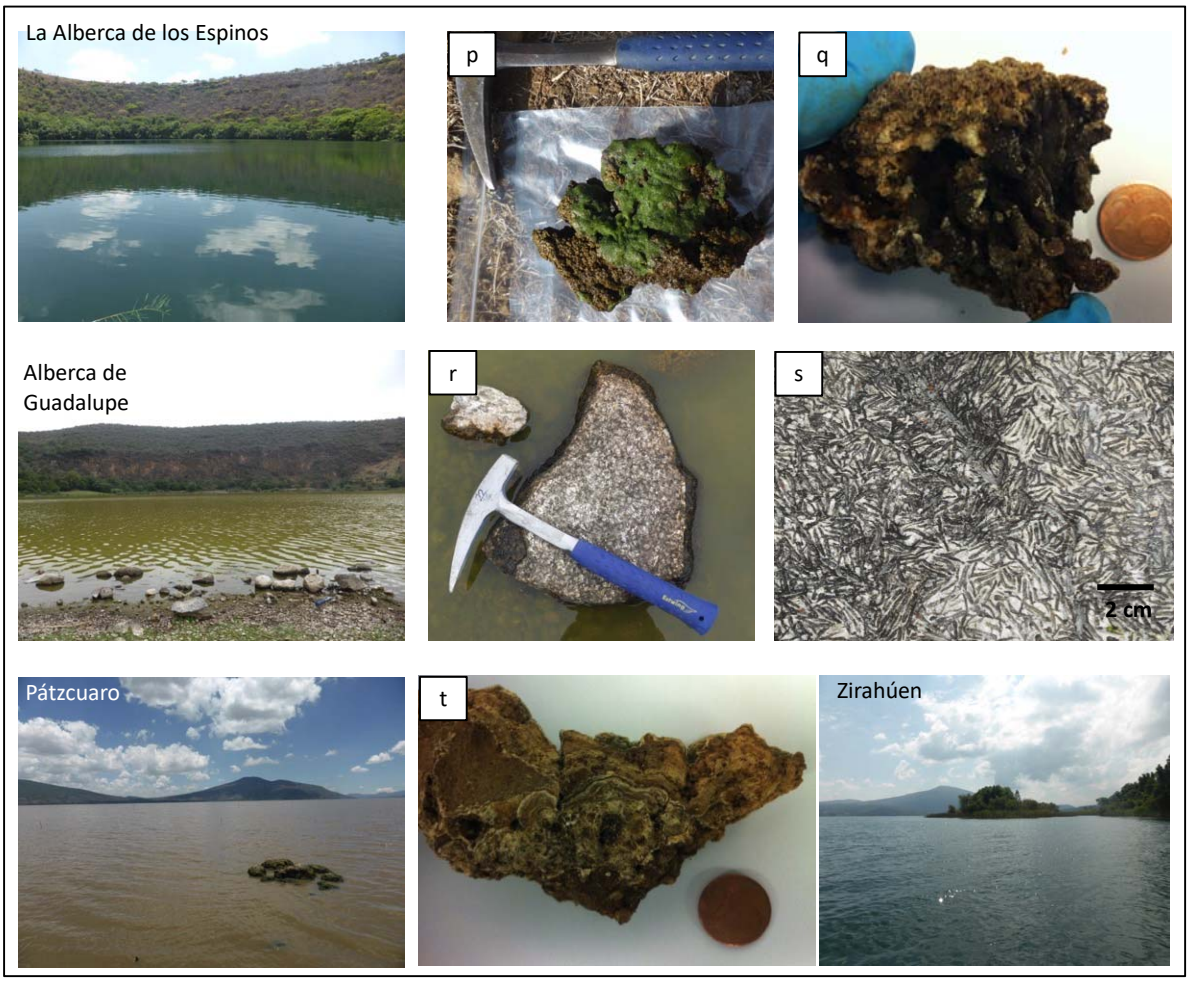

Figure SI-2. Continued

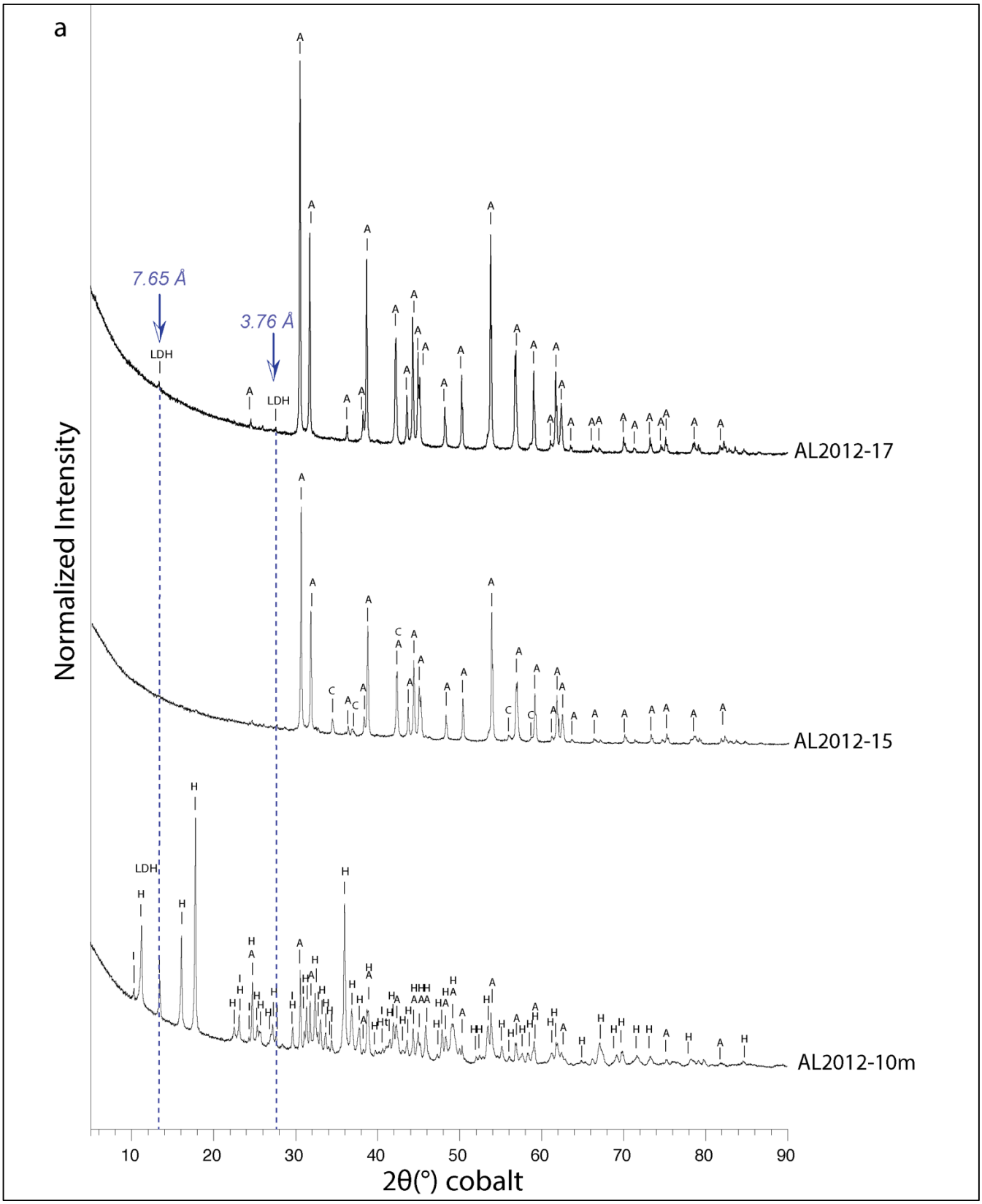
a
7.65 Å
3.76 Å
LDH
LDH
AL2012-17
AL2012-15
AL2012-10m
Normalized Intensity
10
20
30
40
50
60
70
80
90
2θ(°) cobalt

Figure SI-3. Powder x-ray diffraction patterns of some of the studied microbialites
(**a**) Microbialites mainly composed of aragonite and/or hydromagnesite, (**b**) microbialites mainly composed of aragonite and Mg-silicates, (**c**) microbialites mainly composed of Mg-calcite and/or monohydrocalcite, (**d**) microbialites affected by high detrital contamination. Abbreviations for the phases are: H: hydromagnesite; A: aragonite; C: calcite; MC: monohydrocalcite; D: dolomite; K/S: kerolite and/or stevensite; LDH: layered double hydroxide; I: illite; An: anorthite; Ab: albite; Q: quartz; Px: pyroxene.

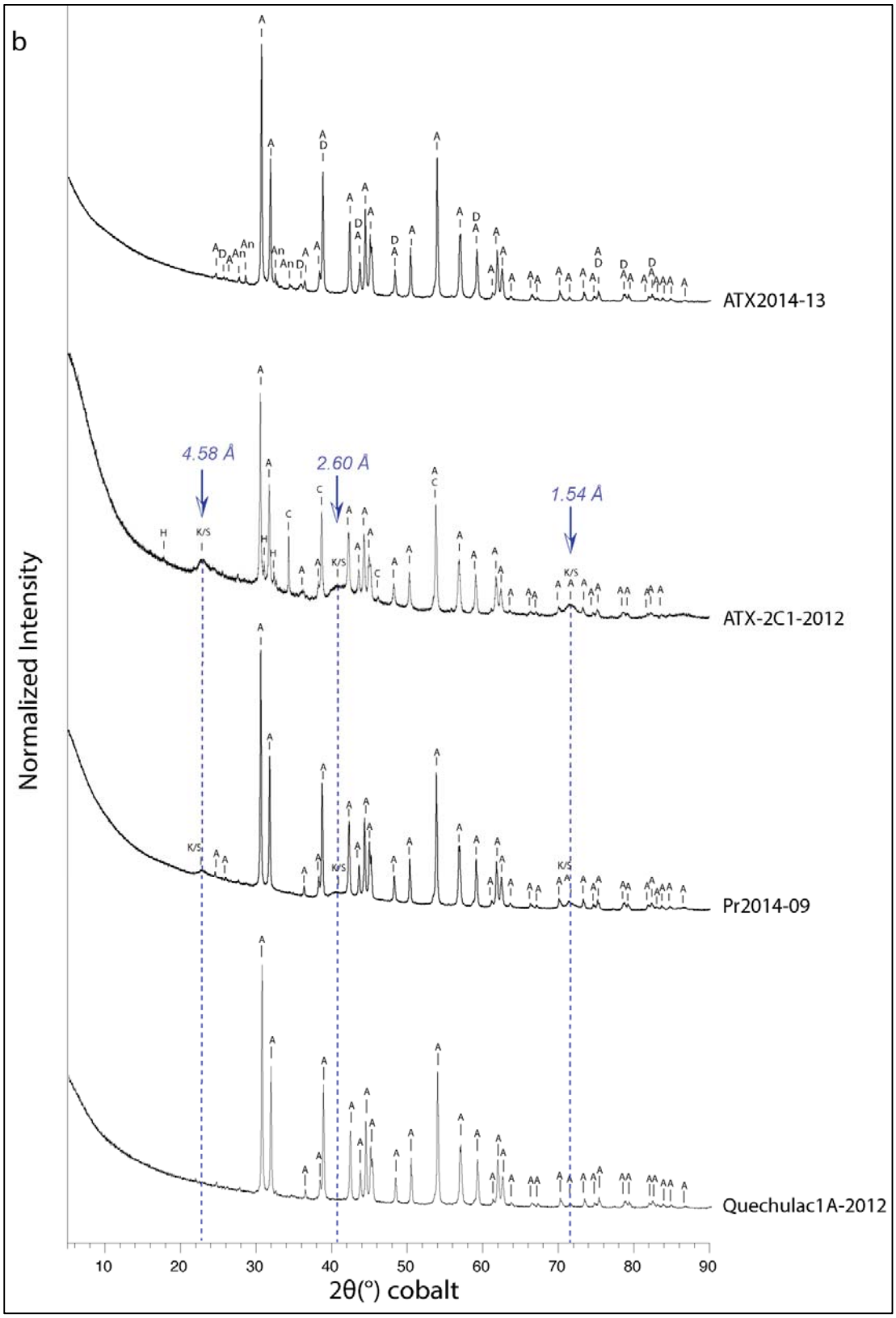

Figure SI-3. Continued

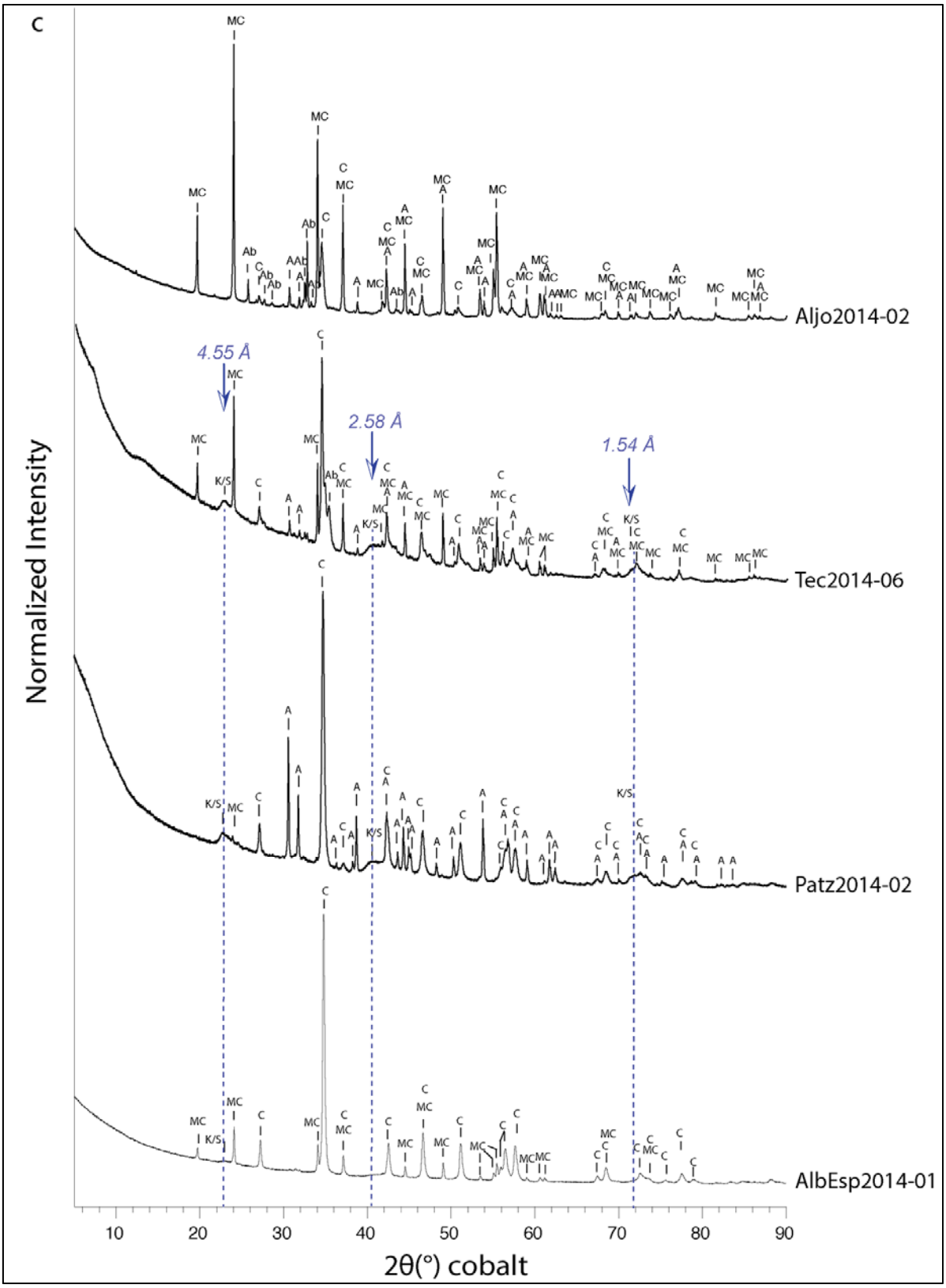

Figure SI-3. Continued

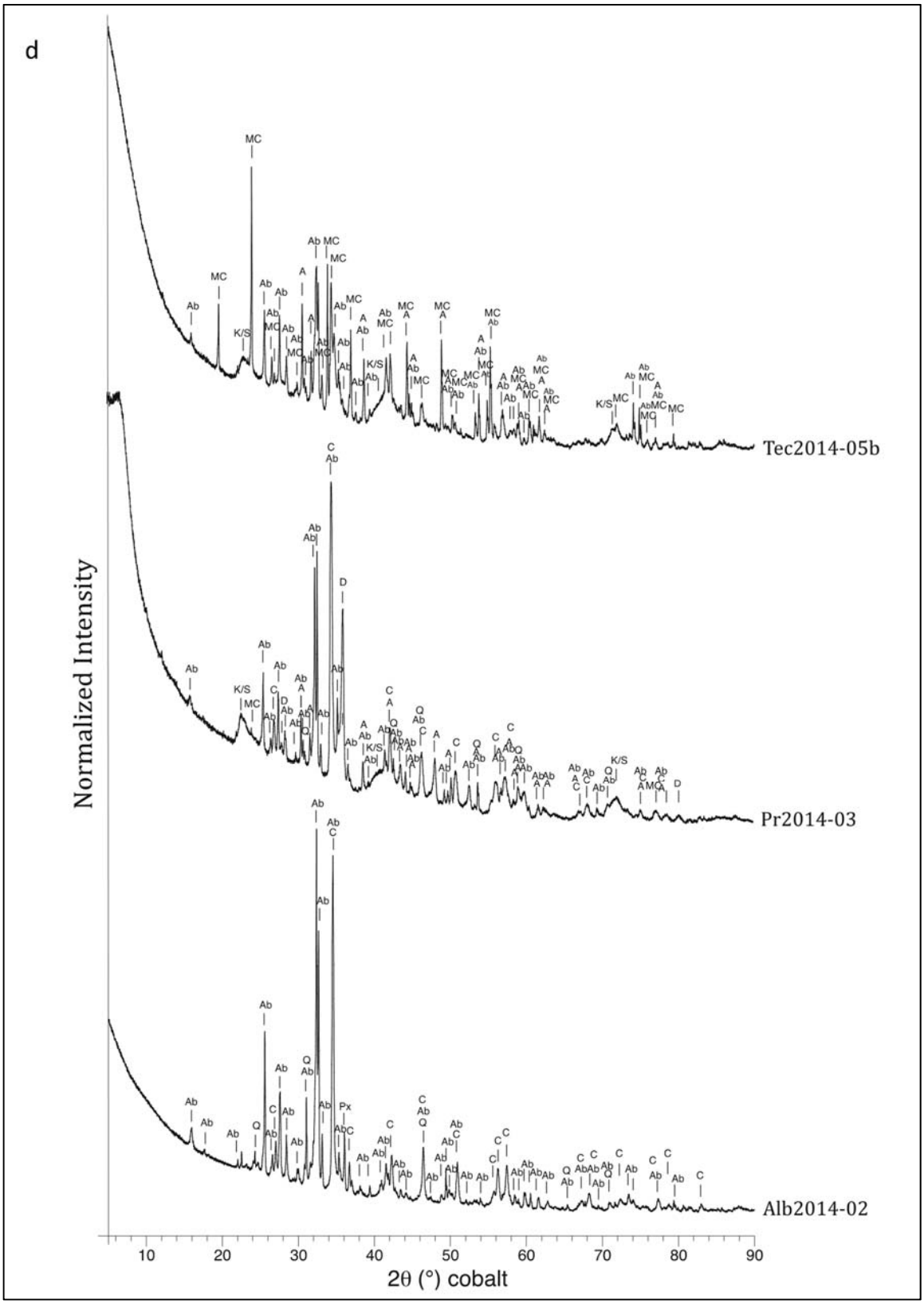

Figure SI-3. Continued

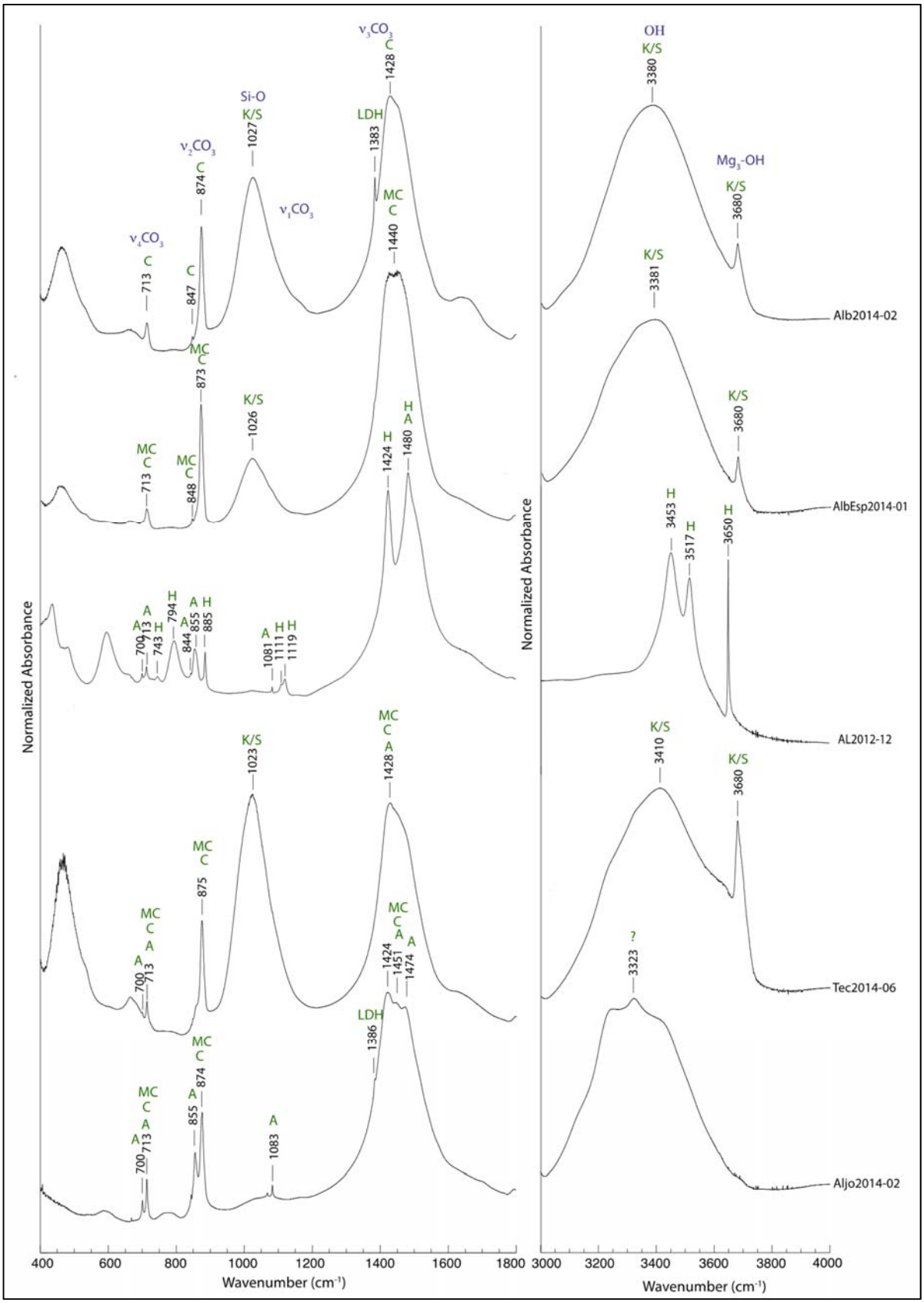
Normalized Absorbance
Wavenumber (cm-1)
Normalized Absorbance
Wavenumber (cm-1)
Alb2014-02
AlbEsp2014-01
AL2012-12
Tec2014-06
Aljo2014-02

Figure SI-4. FTIR spectra of some of the studied microbialites

Microbialites from Lakes Alberca de Guadalupe (Alb), La Alberca de Los Espinos (AlbEsp), Alchichica (AL), Tecuitlapa (Tec) and Aljojuca (Aljo). Phase indexations are in green; FTIR band indexation are in purple. Abbreviations for the phases are: H: hydromagnesite; A: aragonite; C: calcite; MC: monohydrocalcite; K/S: kerolite and/or stevensite; LDH: layered double hydroxide.

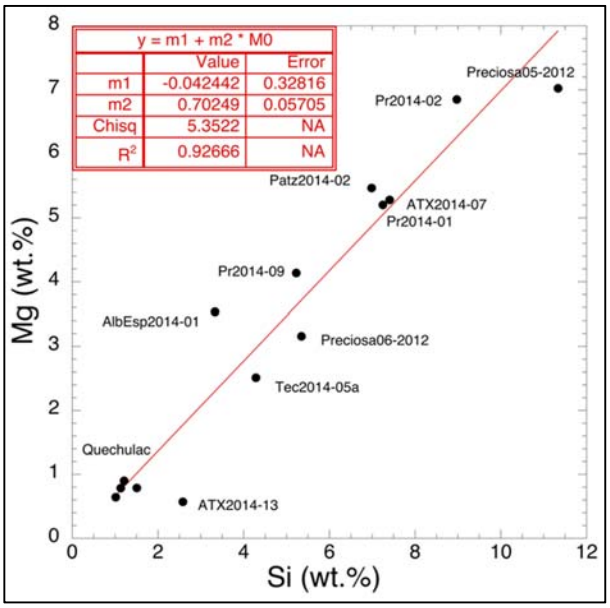

Figure SI-5. Silicon *vs.* magnesium contents of the microbialites

Silicon *versus* magnesium contents (wt.%) of the microbialites the least (authigenic-dominated) and intermediately affected by detrital contamination and containing kerolite and/or stevensite (excluding ATX-2C1-2012 which also contained hydromagnesite). The regression coefficient (R^2) of this plot is equal to 0.93. The slope of the regression line is 0.70 ± 0.06 in wt.%/wt.% (corresponding to 0.81 ± 0.07 at.%/at.%), close to the stoichiometry of kerolite and stevensite (*i.e.*, 0.75 in atomic ratio).

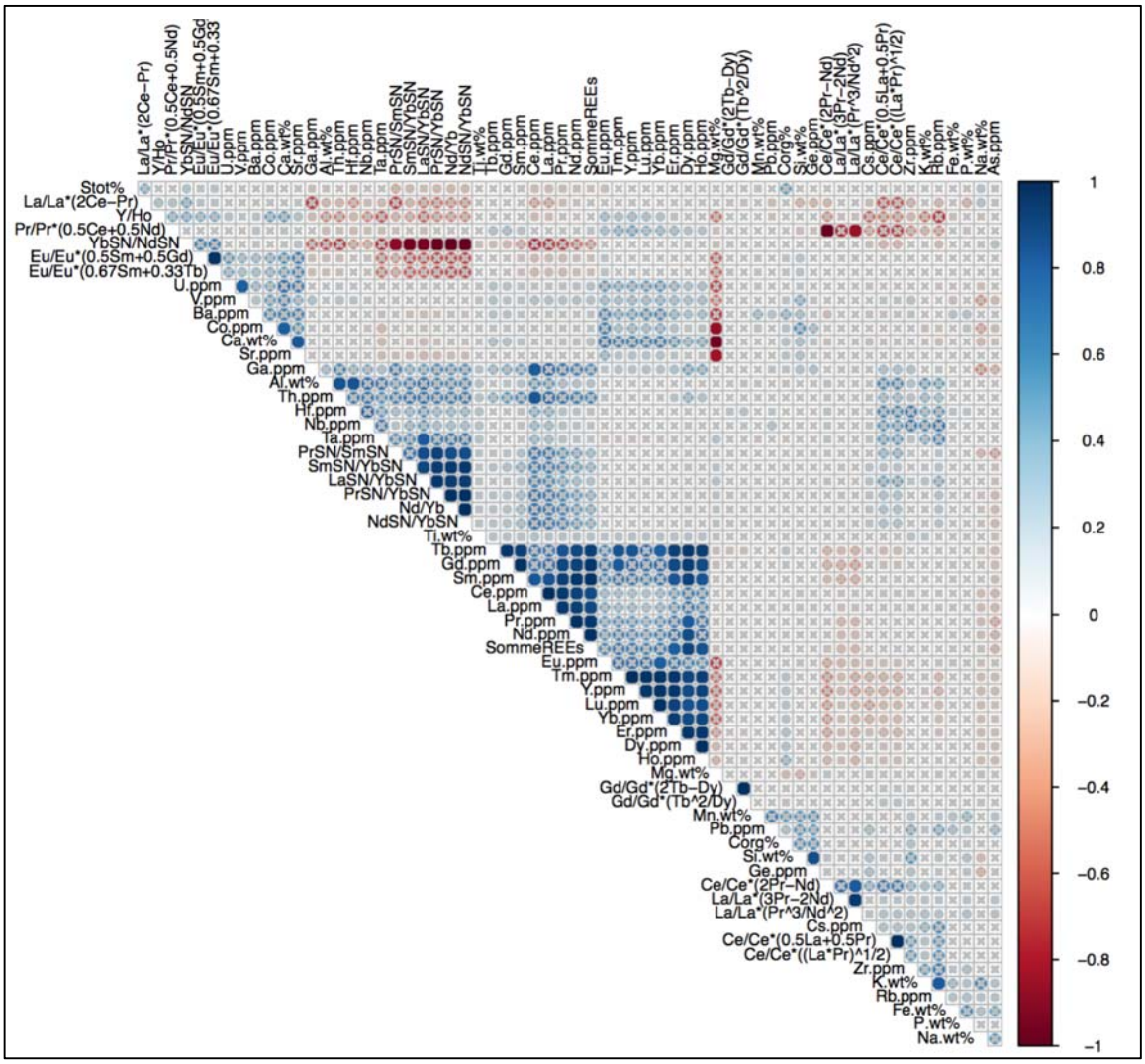

Figure SI-6. Correlation matrix of the chemical variables describing the authigenic-dominated microbialites

Spearman pairwise correlations of the 63 chemical variables (major, trace elements, REEs anomalies) describing the group of 18 authigenic-dominated microbialite samples. The Spearman's correlation coefficients (*i.e.*, r_s values) are ranging from -1 to +1 and are represented by both the circle color (see the color scale bar on the right side of the diagram) and the circle size in the diagram. The statistical significance of each correlation was assessed and indicated by a *p*-value: correlations were considered as significant when the Spearman's correlation coefficient (r_s) followed the relationship: $|r_s| \geq 0.6$ and/or when the p-value (p) was lower than 2.56×10^{-5} (corresponding to an error lower than 5% per test). Non-significant correlations were marked by grey crosses in the Spearman diagram.

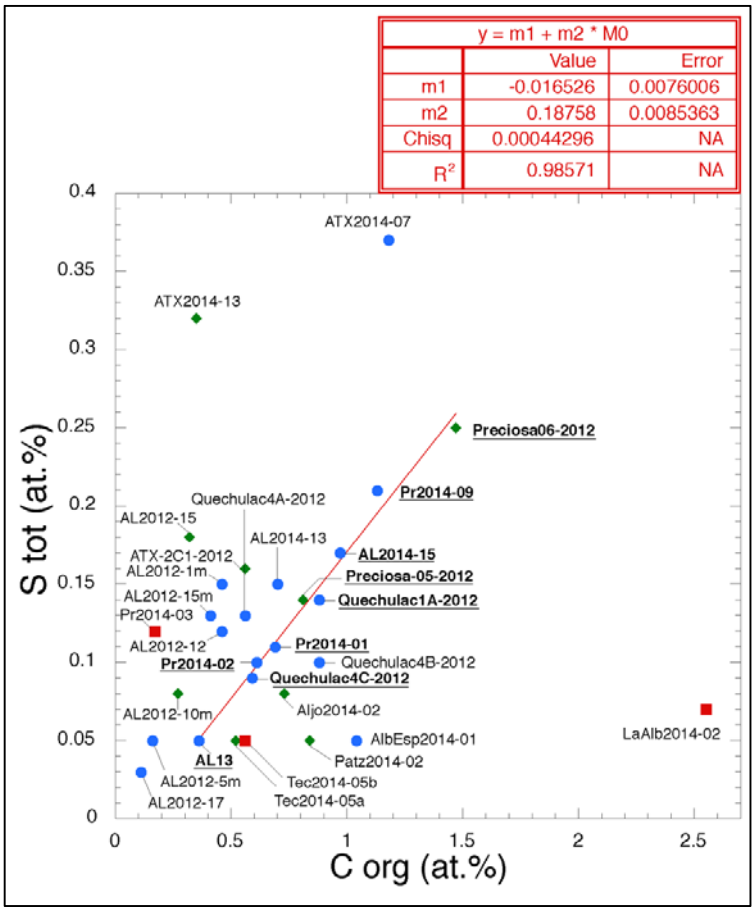

Figure SI-7. Organic carbon *vs.* total sulphur of all the studied microbialite samples (except 3 microbialite samples collected in 2007 for which total S was not measured). A strong positive correlation was observed for 9 samples (in bold and underlined). The regression coefficient (R^2) of the plot is 0.99. The correlation slope is 0.188 ± 0.009. Blue dots stand for 18 microbialites poorly concentrated in Al (authigenic-dominated); red squares correspond to microbialites highly affected by detrital contamination; green diamonds stand for intermediately contaminated microbialites considered in this study as moderately affected by detrital input.

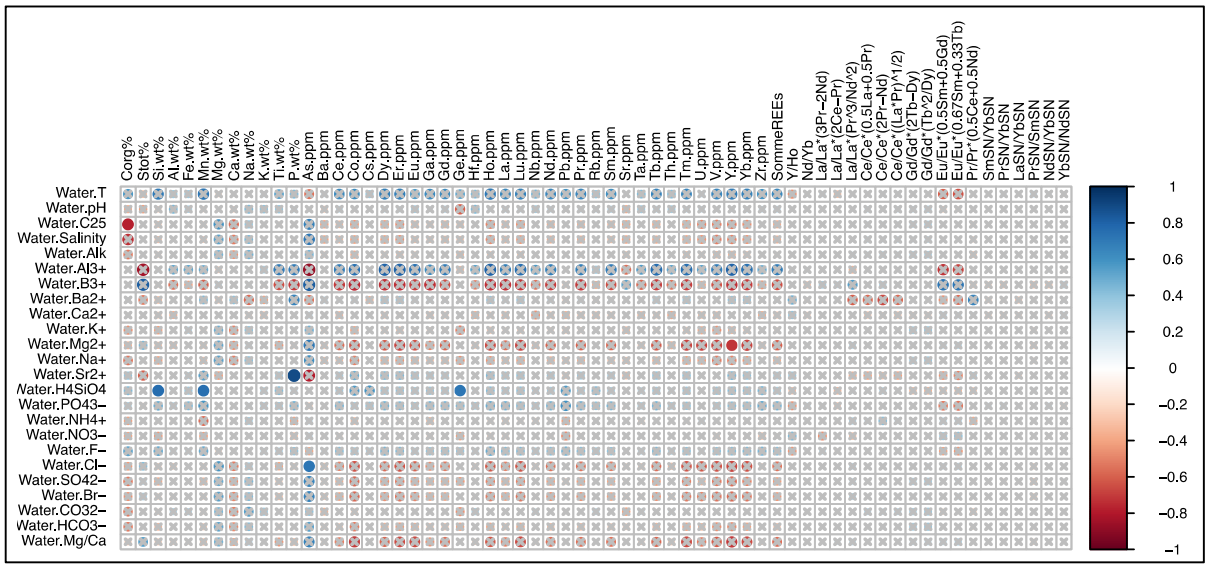
Corg%
Stot%
Si.wt%
Al.wt%
Fe.wt%
Mn.wt%
Mg.wt%
Ca.wt%
Na.wt%
K.wt%
Ti.wt%
P.wt%
As.ppm
Ba.ppm
Ce.ppm
Co.ppm
Cs.ppm
Dy.ppm
Er.ppm
Eu.ppm
Ga.ppm
Gd.ppm
Ge.ppm
Hf.ppm
Ho.ppm
La.ppm
Lu.ppm
Nb.ppm
Nd.ppm
Pb.ppm
Pr.ppm
Rb.ppm
Sm.ppm
Sr.ppm
Ta.ppm
Tb.ppm
Th.ppm
Tm.ppm
U.ppm
V.ppm
Y.ppm
Yb.ppm
Zr.ppm
SommeREEs
Y/Ho
Nd/Yb
La/La*(3Pr−2Nd)
La/La*(2Ce−Pr)
La/La*(Pr^3/Nd^2)
Ce/Ce*(0.5La+0.5Pr)
Ce/Ce*(2Pr−Nd)
Ce/Ce*((La*Pr)^1/2)
Gd/Gd*(2Tb−Dy)
Gd/Gd*(Tb^2/Dy)
Eu/Eu*(0.5Sm+0.5Gd)
Eu/Eu*(0.67Sm+0.33Tb)
Pr/Pr*(0.5Ce+0.5Nd)
SmSN/YbSN
PrSN/YbSN
LaSN/YbSN
PrSN/SmSN
NdSN/YbSN
YbSN/NdSN
Water.T
Water.pH
Water.C25
Water.Salinity
Water.Alk
Water.Al3+
Water.B3+
Water.Ba2+
Water.Ca2+
Water.K+
Water.Mg2+
Water.Na+
Water.Sr2+
Water.H4SiO4
Water.PO43−
Water.NH4+
Water.NO3−
Water.F−
Water.Cl−
Water.SO42−
Water.Br−
Water.CO32−
Water.HCO3−
Water.Mg/Ca
1
0.8
0.6
0.4
0.2
0
−0.2
−0.4
−0.6
−0.8
−1

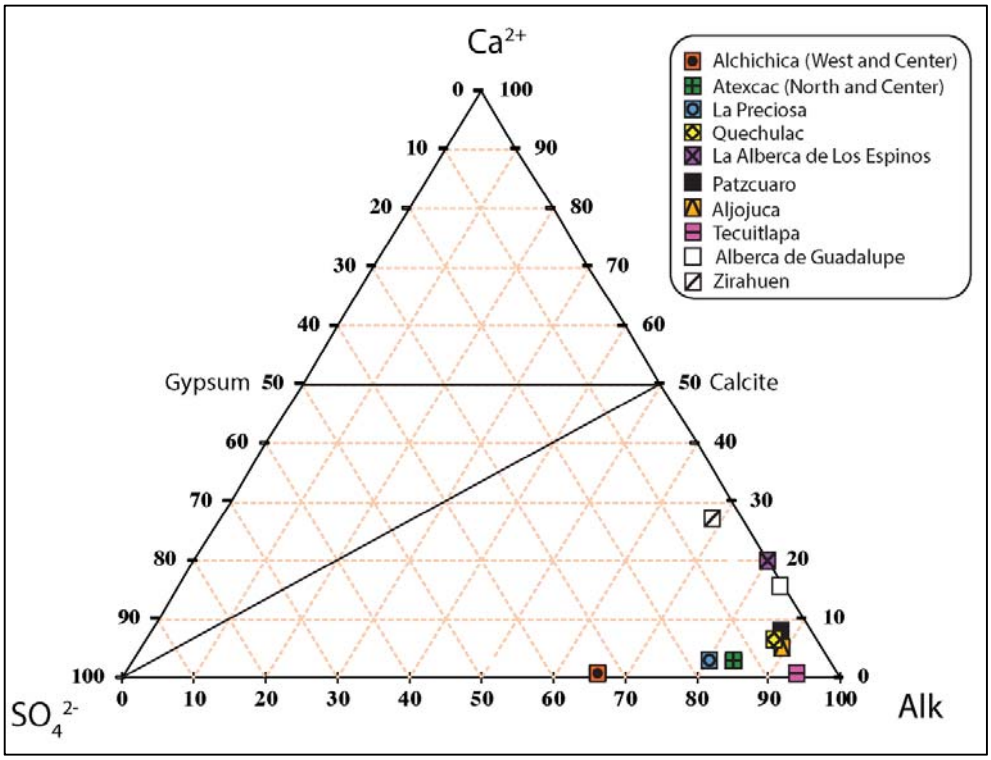

Figure SI-9. Distribution of Mexican lakes in the Spencer (Alk-SO_4-Ca) ternary diagram
The aqueous concentrations are reported in meq.

II. TABLES

Aqueous sample	Location in the lake	Analyses
Preciosa2014_0m	North-East (close to the collected microbialites)	cations; Si-P-N ; anions ; alk; $^{87}Sr/^{86}Sr$; REE+Y
Preciosa2012_0m	North (close to the collected microbialites)	cations; Si; anions ; alk
Quechulac2014_0m_N	North	cations; Si-P-N ; anions ; alk; REE+Y
Quechulac2012_0m_M	Center (close to the collected microbialites forming the island)	cations; Si; anions ; alk
ATX2014_0m_M	Center (Niskin bottle)	cations; Si-P-N ; anions ; alk; $^{87}Sr/^{86}Sr$; REE+Y
ATX2014_3m	Center (Niskin bottle)	cations; Si-P-N ; anions ; alk
ATX2014_10m	Center (Niskin bottle)	cations; Si-P-N ; anions ; alk
ATX2014_20m	Center (Niskin bottle)	cations; Si-P-N ; anions ; alk
ATX2014_30m	Center (Niskin bottle)	cations; Si-P-N ; anions ; alk
ATX2014_0m_N	North (close to the collected microbialites)	cations; Si-P-N ; anions
ATX2012_0m_N	North West (close to the collected microbialites)	cations; Si; anions ; alk
AL2014_0m_M	Center (Niskin bottle)	cations; Si-P-N ; anions ; alk; $^{87}Sr/^{86}Sr$
AL2014_3m	Center (Niskin bottle)	cations; Si-P-N ; anions ; alk REE+Y
AL2014_10m	Center (Niskin bottle)	cations; Si-P-N ; anions ; alk
AL2014_25m	Center (Niskin bottle)	cations; Si-P-N ; anions ; alk
AL2014_40m	Center (Niskin bottle)	cations; Si-P-N ; anions ; alk
AL2014_55m	Center (Niskin bottle)	cations; Si-P-N ; anions ; alk
AL2014_0m_W	West (close to the collected microbialites)	cations; Si-P-N ; anions
AL2012_0m_M	Center (Niskin bottle)	cations; Si; anions ; alk
AL2012_3m	Center (Niskin bottle)	cations; Si; anions ; alk
AL2012_10m	Center (Niskin bottle)	cations; Si ; anions ; alk
AL2012_25m	Center (Niskin bottle)	cations; Si; anions ; alk
AL2012_40m	Center (Niskin bottle)	cations; Si; anions ; alk
AL2012_55m	Center (Niskin bottle)	cations; Si; anions ; alk
AL2012_0m_W	North West (close to the microbialites)	cations; Si; anions ; alk
Aljojuca2014_0m	North East (close to the microbialites)	cations; Si-P-N ; anions ; alk
Tecuitlapa2014_0m	North-East (close to the microbialites)	cations; Si-P-N ; anions ; alk
AlbEsp2014_0m	North (close to the microbialites)	cations; Si-P-N ; anions ; alk; $^{87}Sr/^{86}Sr$; REE+Y
Alb2014_0m	South (close to the microbialites)	cations; Si-P-N ; anions ; alk
Patz2014_0m	North East (close to the microbialites)	cations; Si-P-N ; anions ; alk
Zirahuen2014_0m	Center	cations; Si-P-N ; anions ; alk; $^{87}Sr/^{86}Sr$

Table SI-1. List of the aqueous samples, their location and performed analyses

Cation concentrations were determined by ICP-AES; H_4SiO_4 (noted Si), nitrogen compounds (noted N) and phosphate (noted P) concentrations were determined by continuous flow colorimetry; other anion concentrations were determined by ion chromatography; alkalinity (alk) was determined by titration; strontium isotope ratios ($^{87}Sr/^{86}Sr$) were measured using high performance ion chromatography and ICP-MS; trace element concentrations (REE+Y) were determined by ICP-MS. See the main text for more details about these analyses. The sampling location using a Niskin bottle at the center of Lake Alchichica was different in January 2012 and May 2014.

Aqueous sample	Temperature (°C)	C_{25} (mS/cm)	Salinity (g/l)
Preciosa2014_0m	19.0	2.30	1.35
Preciosa2012_0m	16.2	2.24	1.40
Quechulac2014_0m_N	22.5	0.86	0.45
Quechulac2012_0m_M	15.4	0.84	0.51
ATX2014_0m_M	20.2	11.65	7.39
ATX2014_3m	19.6	11.51	7.40
ATX2014_10m	19.4	11.55	7.46
ATX2014_20m	16.8	11.41	7.84
ATX2014_30m	15.7	11.37	8.03
ATX2014_0m_N	NM	NM	-
ATX2012_0m_N	15.8	12.31	8.73
AL2014_0m_M	19.5	12.76	8.29
AL2014_3m	19.2	12.48	8.15
AL2014_10m	18.1	12.61	8.46
AL2014_25m	15.9	12.38	8.76
AL2014_40m	15.3	12.56	9.03
AL2014_55m	15.1	12.51	9.04
AL2014_0m_W	NM	NM	-
AL2012_0m_M	15.1	13.45	9.78
AL2012_3m	15.1	13.46	9.78
AL2012_10m	15.0	13.47	9.82
AL2012_25m	14.9	NM	-
AL2012_40m	14.8	13.40	9.81
AL2012_55m	15.2	NM	-
AL2012_0m_W	15.1	13.45	9.78
Aljojuca2014_0m	20.6	1.27	0.70
Tecuitlapa2014_0m	23.4	4.94	2.74
AlbEsp2014_0m	23.0	1.25	0.65
Alb2014_0m	21.0	0.40	0.21
Patz2014_0m	28.5	1.09	0.50
Zirahuen2014_0m	22.2	0.14	0.08

Table SI-2. Determination of salinity

Salinity (S) determined using the equation described by Aminot and Kérouel (2004) and using temperature (t) and specific conductance C_{25}:

$S = a_0 + a_1.R_t^{0.5} + a_2.R_t + a_3.R_t^{1.5} + a_4.R_t^2 + a_5.R_t^{2.5} + \{(t - 15)/[1 + k(t-15)]\} \times (b_0 + b_1.R_t^{0.5} + b_2.R_t + b_3.R_t^{1.5} + b_4.R_t^2 + b_5.R_t^{2.5})$

With k=0.0162; a_0= 0.0080; a_1=-0.1692; a_2=25.3851; a_3=14.0941; a_4=-7.0261; a_5=2.7081; b_0= 0.0005; b_1=-0.0056; b_2=-0.0066; b_3=-0.0375; b_4=0.0636; b_5=-0.0144;

$R_t = C_{25} / (42.914.r_t)$

$r_t = c_0 + c_1 t + c_2 t^2 + c_3 t^3 + c_4 t^4$, with c_0= 0.6766097; c_1=0.0200564; c_2=0.00011043; c_3=-6.9698E-07; c_4=1.0031E-09

(NM): not measured. (-): calculation not possible.

Mineral Phase	Reaction	*Log Ks*	Reference(s)
Aragonite	$CaCO_3 \leftrightarrows Ca^{2+} + CO_3^{2-}$	-8.34	Plummer and Busenberg, 1982
Calcite	$CaCO_3 \leftrightarrows Ca^{2+} + CO_3^{2-}$	-8.48	Plummer and Busenberg, 1982
Mg-calcite	$Mg_{0.1}Ca_{0.9}CO_3 \leftrightarrows 0.9Ca^{2+} + 0.1Mg^{2+} + CO_3^{2-}$	-8.30	obtained from Testemale et al., 2009
Monohydrocalcite (MHC)	$CaCO_3{\cdot}nH_2O \leftrightarrows Ca^{2+} + CO_3^{2-} + nH_2O$	-7.65	Fukushi and Matsumiya, 2018
Vaterite	$CaCO_3 \leftrightarrows Ca^{2+} + CO_3^{2-}$	-7.91	Plummer and Busenberg, 1982
Dolomite	$CaMg(CO_3)_2 \leftrightarrows Ca^{2+} + Mg^{2+} + 2CO_3^{2-}$	-17.09	Ball and Nordstrom, 1991
Hydromagnesite	$Mg_5(CO_3)_4(OH)_2{\cdot}4H_2O + 2H^{+} \leftrightarrows 5Mg^{2+} + 4CO_3^{2-} + 4H_2O$	-8.77	Robie and Hemingway, 1973
Amorphous Ca-carbonate (ACC)	$CaCO_3{\cdot}nH_2O \leftrightarrows Ca^{2+} + CO_3^{2-} + nH_2O$	-6.40	Brecevic and Nielsen, 1989
Amorphous Mg-carbonate (AMC2)	$MgCO_3{\cdot}nH_2O \leftrightarrows Mg^{2+} + CO_3^{2-} + nH_2O$	-5.59	Fukushi and Matsumiya, 2018
Sepiolite (crystalline)	$Mg_2Si_3O_{7.5}(OH){\cdot}3H_2O + 4H^{+} + 1/2H_2O \leftrightarrows 2Mg^{2+} + 3H_4SiO_4(aq)$	15.76	Stoessell, 1988
Sepiolite (amorphous)	$Mg_2Si_3O_{7.5}(OH){\cdot}3H_2O + 4H^{+} + 1/2H_2O \leftrightarrows 2Mg^{2+} + 3H_4SiO_4(aq)$	18.78	Wollast et al., 1968
Kerolite	$Mg_3Si_4O_{10}(OH)_2{\cdot}H_2O + 6H^{+} + 3H_2O \leftrightarrows 3Mg^{2+} + 4H_4SiO_4(aq)$	25.79	Stoessell, 1988
Stevensite	$Mg_{2.9}Ca_{0.1}Si_4O_{10}(OH)_2{\cdot}H_2O + 6H^{+} + 3H_2O \leftrightarrows 2.9Mg^{2+} + 4H_4SiO_4\ (aq) + 0.1Ca^{2+}$	25.45	Chahi et al., 1997
Talc	$Mg_3Si_4O_{10}(OH)_2 + 6H^{+} + 4H_2O \leftrightarrows 3Mg^{2+} + 4H_4SiO_4(aq)$	23.02	Jones and Galan, 1988
Amorphous silica	$SiO_2 + 2H_2O \leftrightarrows H_4SiO_4(aq)$	-2.71	Ball and Nordstrom, 1991
Hydroxyapatite	$Ca_5(PO_4)_3(OH) + 4H^{+} \leftrightarrows 5Ca^{2+} + 3HPO_4^{2-} + H_2O$	-44.33	NIST 46.7 (Shen et al.)

Table SI-3. Precipitation reactions of diverse phases and their associated solubility constants

Equations of precipitation for the main phases (Ca- and/or Mg-carbonates, silicates and hydroxyapatite) susceptible to form in Mexican lakes and thermodynamic solubility constants (*log Ks*) at 25 °C (see references) used in Visual MINTEQ for the calculations of saturation index (*SI*) and/or used to plot the solubility lines in the figs. 2 and 3 (main text).

Sites	Sampling Period	Aqueous sample	pH	Alk mM	Al^{3+} mM	B^{3+} mM	Ba^{2+} mM
La Preciosa	May 2014	**Preciosa2014_0m**	8.75	14.22	< 0.0002	0.2439	0.0001
La Preciosa	Jan. 2012	**Preciosa2012_0m**	8.88	14.13	NM	NM	NM
Quechulac	May 2014	**Quechulac2014_0m _N**	8.92	6.55	0.0002	0.0463	0.0001
Quechulac	Jan. 2012	**Quechulac2012_0m _M**	8.80	6.68	NM	NM	NM
Atexcac	May 2014	**ATX2014_0m_M**	8.45	31.37	< 0.0002	5.8564	0.0001
Atexcac	May 2014	**ATX2014_3m**	8.55	31.80	< 0.0002	5.7283	0.0001
Atexcac	May 2014	**ATX2014_10m**	8.64	31.16	< 0.0002	5.7009	0.0001
Atexcac	May 2014	**ATX2014_20m**	8.62	30.98	< 0.0002	5.6845	0.0001
Atexcac	May 2014	**ATX2014_30m**	8.61	30.90	< 0.0002	5.6993	0.0001
Atexcac	May 2014	**ATX2014_0m_N**	8.45	31.37*	< 0.0002	5.7947	0.0001
Atexcac	Jan. 2012	**ATX2012_0m_N**	8.75	30.53	NM	NM	NM
Alchichica	May 2014	**AL2014_0m_M**	9.02	43.01	< 0.0002	3.6142	0.0001
Alchichica	May 2014	**AL2014_3m**	9.07	43.10	< 0.0002	3.6755	0.0001
Alchichica	May 2014	**AL2014_10m**	9.06	43.16	< 0.0002	3.6962	0.0001
Alchichica	May 2014	**AL2014_25m**	9.05	42.77	< 0.0002	3.6322	0.0001
Alchichica	May 2014	**AL2014_40m**	9.07	42.97	< 0.0002	3.6440	0.0001
Alchichica	May 2014	**AL2014_55m**	9.02	43.05	< 0.0002	3.6937	0.0001
Alchichica	May 2014	**AL2014_0m_W**	9.02	43.01**	< 0.0002	3.6571	0.0001
Alchichica	Jan. 2012	**AL2012_0m_M**	9.08	42.66	NM	NM	NM
Alchichica	Jan. 2012	**AL2012_3m**	9.10	42.99	NM	NM	NM
Alchichica	Jan. 2012	**AL2012_10m**	9.11	42.86	NM	NM	NM
Alchichica	Jan. 2012	**AL2012_25m**	9.11	42.88	NM	NM	NM
Alchichica	Jan. 2012	**AL2012_40m**	9.12	42.81	NM	NM	NM
Alchichica	Jan. 2012	**AL2012_55m**	9.06	42.94	NM	NM	NM
Alchichica	Jan. 2012	**AL2012_0m_W**	9.08	36.81	NM	NM	NM
Aljojuca	May 2014	**Aljojuca2014_0m**	9.14	13.17	0.0002	0.0379	0.0004
Tecuitlapa	May 2014	**Tecuitlapa2014_0m**	9.63	49.40	0.0003	0.0548	0.0001
La Alberca de los Espinos	May 2014	**AlbEsp2014_0m**	8.67	7.64	0.0002	0.0470	0.0007
Alberca de Guadalupe	May 2014	**Alb2014_0m**	9.32	4.28	0.0255	0.0131	0.0001
Pátzcuaro	May 2014	**Patz2014_0m**	8.94	10.62	0.0045	0.0275	0.0008
Zirahuén	May 2014	**Zirahuen2014_0m**	8.65	1.23	0.0007	0.0136	0.0002

Table SI-4. Physical and chemical parameters of the studied lakes

Concentrations of main cations and anions, dissolved silica (H_4SiO_4) and alkalinity (Alk) are in mmol/L. C_{25} stands for specific conductance of water (conductivity normalized at 25°C). Asterisks (*) and (**) stand for alkalinity values measured from the middle of the corresponding lakes (ATX2014_0m_M and AL2014_0m_M, respectively) at the time of the sampling. NM stands for "not measured" and concerns some minor/trace elements in the 2012 samples. Detection limits are given for Al^{3+}, Cu^{2+}, Fe^{2+}, Mn^{2+}, Ni^{2+}, Ti^{2+}, Zn^{2+}, H_4SiO_4, NH_4^+, NO_3^-, F^-. Charge balances (Bal), calculated as 100*(Σcations - Σanions)/((Σcations +Σanions)/2), are in %. "_xm" refers to the depth at which samples were collected; "_M" means: sampled at the center of the lake; "_W" means: sampled on the western shore of the lake; "_N means": sampled on the northern shore of the lake.

Aqueous Sample	Ca^{2+} mM	Cu^{2+} mM	Fe^{2+} mM	K^{+} mM	Mg^{2+} mM	Mn^{2+} mM	Na^{+} mM	Ni^{2+} mM	Sr^{2+} mM
Preciosa2014_0m	0.25	< 0.00002	< 0.00002	0.38	8.33	< 0.0000004	7.72	< 0.0001	0.0004
Preciosa2012_0m	0.61	NM	NM	0.40	8.12	NM	9.00	NM	NM
Quechulac2014_0m _N	0.22	< 0.00002	< 0.00002	0.18	2.33	< 0.0000004	3.32	< 0.0001	0.0004
Quechulac2012_0m _M	0.45	NM	NM	0.20	2.37	NM	3.40	NM	NM
ATX2014_0m_M	0.52	< 0.00002	0.0006	2.32	22.82	< 0.0000004	79.31	< 0.0001	0.0014
ATX2014_3m	0.50	< 0.00002	0.0006	2.25	22.19	< 0.0000004	77.86	< 0.0001	0.0014
ATX2014_10m	0.47	< 0.00002	0.0005	2.35	22.01	< 0.0000004	77.74	< 0.0001	0.0014
ATX2014_20m	0.35	< 0.00002	< 0.00002	2.15	21.95	< 0.0000004	77.02	< 0.0001	0.0009
ATX2014_30m	0.28	< 0.00002	< 0.00002	2.35	21.96	0.0001	77.21	< 0.0001	0.0007
ATX2014_0m_N	0.47	< 0.00002	< 0.00002	2.36	21.04	< 0.0000004	82.17	< 0.0001	0.0014
ATX2012_0m_N	0.62	NM	NM	2.93	24.39	NM	80.67	NM	NM
AL2014_0m_M	0.19	< 0.00002	< 0.00002	5.47	17.18	< 0.0000004	102.88	< 0.0001	0.0003
AL2014_3m	0.19	< 0.00002	< 0.00002	5.70	17.45	< 0.0000004	101.97	< 0.0001	0.0003
AL2014_10m	0.19	< 0.00002	< 0.00002	5.67	17.84	< 0.0000004	103.17	< 0.0001	0.0003
AL2014_25m	0.19	< 0.00002	< 0.00002	5.52	17.41	< 0.0000004	102.25	< 0.0001	0.0003
AL2014_40m	0.18	< 0.00002	< 0.00002	5.69	17.37	< 0.0000004	102.48	< 0.0001	0.0003
AL2014_55m	0.18	< 0.00002	< 0.00002	5.91	18.07	0.0001	101.15	< 0.0001	0.0003
AL2014_0m_W	0.23	< 0.00002	< 0.00002	5.82	17.83	< 0.0000004	100.66	< 0.0001	0.0004
AL2012_0m_M	0.46	NM	NM	5.94	18.34	NM	105.73	NM	NM
AL2012_3m	0.47	NM	NM	5.83	18.51	NM	106.76	NM	NM
AL2012_10m	0.41	NM	NM	5.63	18.34	NM	105.21	NM	NM
AL2012_25m	0.43	NM	NM	5.66	18.46	NM	104.46	NM	NM
AL2012_40m	0.42	NM	NM	5.89	18.61	NM	106.31	NM	NM
AL2012_55m	0.46	NM	NM	5.81	18.68	NM	106.25	NM	NM
AL2012_0m_W	0.90	NM	NM	4.73	15.97	NM	85.89	NM	NM
Aljojuca2014_0m	0.43	< 0.00002	< 0.00002	0.68	2.90	< 0.0000004	8.13	< 0.0001	0.0051
Tecuitlapa2014_0m	0.17	< 0.00002	< 0.00002	3.06	0.51	< 0.0000004	51.29	< 0.0001	0.0006
AlbEsp2014_0m	0.92	< 0.00002	0.0002	0.68	2.55	< 0.0000004	5.04	< 0.0001	0.0061
Alb2014_0m	0.40	< 0.00002	0.0018	0.38	0.91	< 0.0000004	1.36	< 0.0001	0.0030
Patz2014_0m	0.43	0.0001	0.0011	1.18	1.28	< 0.0000004	7.72	< 0.0001	0.0043
Zirahuen2014_0m	0.24	< 0.00002	0.0001	0.11	0.24	< 0.0000004	0.35	< 0.0001	0.0012

Table SI-4. Continued

Aqueous Sample	Ti^{2+} mM	Zn^{2+} mM	H_4SiO_4 mM	PO_4^{3-} mM	NH_4^+ mM	NO_2^- mM	NO_3^- mM	F^- mM	Cl^- mM
Preciosa2014_0m	< 0.0000006	0.0001	0.5626	0.0007	0.0009	0.0001	< 0.0001	0.1838	9.62
Preciosa2012_0m	NM	NM	0.5750	NM	NM	NM	0.020	0.0454	9.36
Quechulac2014_0m _N	< 0.0000006	< 0.000009	0.2268	0.0005	0.0019	0.0005	0.0048	0.0285	2.48
Quechulac2012_0m _M	NM	NM	0.2080	NM	NM	NM	0.008	0.0262	2.09
ATX2014_0m_M	< 0.0000006	0.0001	1.1233	0.0008	0.0011	0.0002	0.0005	0.6817	109.57
ATX2014_3m	< 0.0000006	0.0001	1.1264	0.0007	0.0008	0.0002	0.0005	0.6970	109.35
ATX2014_10m	< 0.0000006	0.0001	1.1292	0.0007	< 0.0005	0.0002	0.0005	0.6874	110.70
ATX2014_20m	< 0.0000006	0.0001	1.0940	0.0006	< 0.0005	0.0017	0.0027	0.6517	110.42
ATX2014_30m	< 0.0000006	0.0001	1.0795	0.0006	< 0.0005	0.0002	0.0097	0.5703	112.05
ATX2014_0m_N	< 0.0000006	0.0001	1.1222	0.0006	0.0010	0.0002	0.0004	0.7424	110.65
ATX2012_0m_N	NM	NM	1.0368	NM	NM	NM	< 0.0001	0.0068	107.36
AL2014_0m_M	< 0.0000006	< 0.000009	0.0013	0.0012	0.0034	0.0006	0.0008	0.2653	87.48
AL2014_3m	< 0.0000006	< 0.000009	0.0011	0.0011	0.0011	0.0005	0.0003	0.3340	87.05
AL2014_10m	< 0.0000006	< 0.000009	< 0.001	0.0009	0.0014	0.0005	< 0.0001	0.4965	87.24
AL2014_25m	< 0.0000006	< 0.000009	0.0016	0.0009	0.0009	0.0064	0.0024	0.8601	87.56
AL2014_40m	< 0.0000006	0.0002	0.0132	0.0012	< 0.0005	0.0120	0.0029	0.6940	89.11
AL2014_55m	< 0.0000006	0.0001	0.0300	0.0019	< 0.0005	0.0083	0.0002	0.5933	87.83
AL2014_0m_W	< 0.0000006	0.0001	0.0254	0.0008	0.0013	0.0008	< 0.0001	0.6422	85.84
AL2012_0m_M	NM	NM	0.0046	NM	NM	NM	0.045	< 0.0003	94.51
AL2012_3m	NM	NM	< 0.001	NM	NM	NM	0.000	< 0.0003	94.48
AL2012_10m	NM	NM	< 0.001	NM	NM	NM	0.054	< 0.0003	99.44
AL2012_25m	NM	NM	0.0044	NM	NM	NM	0.074	< 0.0003	94.90
AL2012_40m	NM	NM	0.0037	NM	NM	NM	0.060	0.0959	94.72
AL2012_55m	NM	NM	< 0.001	NM	NM	NM	0.068	< 0.0003	100.87
AL2012_0m_W	NM	NM	0.2863	NM	NM	NM	0.043	< 0.0003	74.47
Aljojuca2014_0m	< 0.0000006	< 0.000009	0.1572	0.0012	0.0007	0.0004	0.0003	0.7109	1.49
Tecuitlapa2014_0m	< 0.0000006	0.0001	0.6174	0.0033	0.0448	0.0102	0.0012	0.8568	6.12
AlbEsp2014_0m	< 0.0000006	< 0.000009	0.8770	0.0055	0.0009	0.0003	< 0.0001	0.4838	4.77
Alb2014_0m	< 0.0000006	< 0.000009	1.7737	0.0009	< 0.0005	0.0001	< 0.0001	0.0296	0.17
Patz2014_0m	0.0001	< 0.000009	0.3660	0.0006	< 0.0005	0.0001	< 0.0001	0.6493	1.49
Zirahuen2014_0m	< 0.0000006	< 0.000009	0.0099	0.0004	0.0008	0.0003	0.0003	0.0045	0.17

Table SI-4. Continued

Aqueous Sample	SO_4^{2-} mM	Br^- mM	CO_3^{2-} mM	HCO_3^- mM	Σ Cations mM	Σ Anions mM	Bal %	Mg/Ca
Preciosa2014_0m	1.475	0.0139	0.36	13.50	25.99	27.00	-3.8	33.6
Preciosa2012_0m	1.296	0.013	0.48	13.17	26.86	26.15	2.6	13.3
Quechulac2014_0m _N	0.197	0.0026	0.24	6.07	8.76	9.46	-7.7	10.4
Quechulac2012_0m _M	0.182	0.003	0.19	6.30	9.24	9.17	0.7	5.3
ATX2014_0m_M	2.453	0.1318	0.41	30.54	145.88	146.65	-0.5	44.2
ATX2014_3m	2.423	0.1334	0.52	30.75	142.69	146.83	-2.9	44.4
ATX2014_10m	2.449	0.1308	0.62	29.91	142.15	147.58	-3.7	46.5
ATX2014_20m	2.431	0.1306	0.59	29.79	140.82	147.05	-4.3	63.5
ATX2014_30m	2.440	0.1326	0.58	29.74	141.16	148.54	-5.1	77.1
ATX2014_0m_N	2.547	0.1340	0.41	30.54	144.93	147.99	-2.1	45.2
ATX2012_0m_N	2.063	0.166	0.78	28.98	133.62	142.19	-6.2	39.3
AL2014_0m_M	10.837	0.1148	1.96	39.09	153.93	152.55	0.9	90.0
AL2014_3m	9.661	0.1151	2.18	38.74	153.99	149.92	2.7	90.8
AL2014_10m	12.692	0.1138	2.14	38.89	155.99	156.41	-0.3	93.5
AL2014_25m	10.153	0.1112	2.07	38.62	153.86	151.62	1.5	93.0
AL2014_40m	10.639	0.1101	2.17	38.63	154.21	154.18	0	96.7
AL2014_55m	10.929	0.1131	1.96	39.13	154.64	153.45	0.8	98.3
AL2014_0m_W	10.842	0.1141	1.96	39.09	153.56	151.29	1.5	78.6
AL2012_0m_M	10.178	0.104	2.22	38.23	149.28	157.67	-5.5	40.0
AL2012_3m	10.105	0.111	2.32	38.35	150.55	157.79	-4.7	39.1
AL2012_10m	10.174	0.117	2.33	38.20	148.34	162.81	-9.3	45.0
AL2012_25m	10.212	0.108	2.35	38.18	147.90	158.38	-6.8	42.7
AL2012_40m	10.194	0.114	2.39	38.02	150.27	158.19	-5.1	44.3
AL2012_55m	10.964	0.144	2.13	38.69	150.33	165.96	-9.9	40.5
AL2012_0m_W	8.196	0.092	1.91	32.99	124.35	127.81	-2.7	17.8
Aljojuca2014_0m	0.403	0.0020	0.77	11.64	15.60	16.19	-3.7	6.8
Tecuitlapa2014_0m	1.596	0.0221	7.16	35.08	55.93	59.61	-6.4	3.0
AlbEsp2014_0m	0.003	0.0050	0.16	7.31	12.83	12.92	-0.7	2.8
Alb2014_0m	0.010	0.0004	0.36	3.56	4.50	4.50	0	2.3
Patz2014_0m	0.268	0.0010	0.41	9.80	12.43	13.29	-6.7	3.0
Zirahuen2014_0m	0.038	< 0.0004	0.03	1.18	1.48	1.49	-0.7	1.0

Table SI-4. Continued

Aqueous Sample	pH	Alk	CO_3^{2-} (1)	HCO_3^- (1)	NH_3	$H_2BO_3^-$	H_3SiO_4	H_3PO_4	HPO_4^{2-}	PO_4^{3-}	HF	OH^-	H^+	Σ	CO_3^2 (2)	HCO_3^- (2)
Preciosa2014_0m	8.75	14.22	**0.36**	**13.50**	1.33E-04	0.06	0.04	1.12E-12	3.25E-04	1.56E-07	2.97E-07	0.004	2.10E-06	0.10	**0.36**	**13.40**
Quechulac2014_0m_N	8.92	6.55	**0.24**	**6.07**	5.06E-04	0.02	0.02	6.09E-13	2.97E-04	1.70E-07	4.02E-08	0.008	1.34E-06	0.05	**0.24**	**6.02**
ATX2014_0m-M	8.45	31.37	**0.41**	**30.54**	8.65E-05	0.94	0.05	2.88E-12	3.26E-04	1.37E-07	1.69E-06	0.003	4.66E-06	0.99	**0.40**	**29.58**
ATX2014_0m_N	8.45	31.37*	**0.41**	**30.54**	7.42E-05	0.93	0.05	2.24E-12	2.53E-04	1.06E-07	1.88E-06	0.003	4.65E-06	0.98	**0.40**	**29.58**
AL2014_0m_M	9.02	43.01	**1.96**	**39.09**	7.69E-04	1.41	0.00	3.63E-13	5.75E-04	8.91E-07	1.94E-07	0.009	1.26E-06	1.42	**1.89**	**37.80**
AL2014_0m_W	9.02	43.01**	**1.96**	**39.09**	2.91E-04	1.43	0.00	2.40E-13	3.79E-04	5.87E-07	4.67E-07	0.009	1.26E-06	1.44	**1.89**	**37.78**
Aljojuca2014_0m	9.14	13.17	**0.77**	**11.64**	2.17E-04	0.02	0.02	4.66E-13	6.98E-04	7.15E-07	5.70E-07	0.011	8.26E-07	0.05	**0.77**	**11.59**
Tecuitlapa2014_0m	9.63	49.40	**7.16**	**35.08**	2.83E-02	0.04	0.26	1.25E-13	2.47E-03	1.25E-05	2.26E-07	0.047	2.90E-07	0.37	**7.11**	**34.81**
AlbEsp2014_0m	8.67	7.64	**0.16**	**7.31**	1.52E-04	0.01	0.06	1.78E-11	2.93E-03	1.03E-06	1.19E-06	0.005	2.42E-06	0.08	**0.16**	**7.24**
Alb2014_0m	9.32	4.28	**0.36**	**3.56**	4.52E-14	0.01	0.37	1.86E-13	5.15E-04	6.19E-07	1.76E-08	0.017	5.18E-07	0.40	**0.32**	**3.23**
Patz2014_0m	8.94	10.62	**0.41**	**9.80**	3.59E-14	0.01	0.05	7.87E-13	4.28E-04	3.08E-07	1.00E-06	0.013	1.30E-06	0.08	**0.41**	**9.73**
Zirahuen2014_0m	8.65	1.23	**0.03**	**1.18**	1.32E-04	0.00	0.00	2.81E-12	3.12E-04	7.10E-08	1.36E-08	0.004	2.35E-06	0.01	**0.03**	**1.17**

Table SI-5. Calculations of $[HCO_3^-]$ and $[CO_3^{2-}]$ by two different methods

(1) from alkalinity, pH and (HCO_3^-; CO_3^{2-}) pKa. (2) based on the exact formula of alkalinity (Dickson, 1981) including aqueous species (*i.e.*, NH_3, $H_2BO_3^-$, $H_3SiO_4^-$, H_3PO_4, HPO_4^{2-}, PO_4^{3-}, HF, OH^- and H^+). Overall, both methods provide the same results. Asterisks (*) and (**) indicate that in these cases, alkalinity value was taken from another sample, collected in the center of the corresponding lakes (ATX2014_0m_M and AL2014_0m_M, respectively) at the same date.

Lake	Zirahuén	Alberca de Guadalupe	Quechulac (center)	Quechulac (North)	La Alberca de Los Espinos	La Preciosa (North)	La Preciosa (North-East)	Pátzcuaro	Aljojuca	Tecuitlapa	Atexcac (North)	Atexcac (center)	Alchichica (West)	Alchichica (center)	Alchichica (center)
Sampling Time	May 2014	May 2014	Jan. 2012	May 2014	May 2014	Jan. 2012	May 2014	May 2014	May 2014	May 2014	Jan. 2012	May 2014	Jan. 2012	Jan. 2012	May 2014
Sample Symbol	●Z	●Alb	◆Q	●Q	●AE	◆LP	●LP	●P	●Alj	●T	◆ATX-N	●ATX-M	◆AL-W	◆AL-M	●AL-M
Phase															
Aragonite $CaCO_3$	- 0.06	**1.11**	**0.79**	**0.66**	**1.11**	**1.13**	**0.67**	**1.17**	**1.26**	**1.22**	**1.06**	**0.80**	**1.51**	**1.23**	**0.85**
Calcite $CaCO_3$	**0.09**	**1.26**	**0.94**	**0.81**	**1.25**	**1.28**	**0.82**	**1.31**	**1.41**	**1.36**	**1.21**	**0.95**	**1.66**	**1.38**	**1.00**
Mg-calcite $Mg_{0.1}Ca_{0.9}CO_3$	- 0.04	**1.20**	**1.03**	**0.79**	**1.16**	**1.39**	**0.92**	**1.11**	**1.41**	**1.28**	**1.38**	**1.03**	**1.81**	**1.57**	**1.13**
Monohydrocalcite $CaCO_3{\cdot}nH_2O$	-0.73	**0.45**	**0.16**	- 0.01	**0.44**	**0.49**	**0.02**	**0.46**	**0.60**	**0.54**	**0.43**	**0.14**	**0.88**	**0.60**	**0.20**
Vaterite $CaCO_3$	- 0.49	**0.68**	**0.35**	**0.24**	**0.68**	**0.69**	**0.24**	**0.75**	**0.83**	**0.79**	**0.62**	**0.37**	**1.07**	**0.79**	**0.42**
Dolomite $CaMg(CO_3)_2$	**0.28**	**3.01**	**2.63**	**2.78**	**3.08**	**3.72**	**3.25**	**3.32**	**3.79**	**3.50**	**4.04**	**3.61**	**4.61**	**4.41**	**4.07**
Hydromagnesite $Mg_5(CO_3)_4(OH)_2{\cdot}4H_2O$	- 11.50	- 3.53	-4.75	- 2.99	- 4.03	-1.10	- 1.28	- 2.76	- 1.04	- 2.08	**0.38**	- 0.66	**1.28**	**1.60**	**1.87**
Sepiolite $Mg_4Si_6O_{15}(OH)_2{\cdot}nH_2O$	-3.87	**6.16**	**1.93**	**2.90**	**3.80**	**4.39**	**4.08**	**3.27**	**3.05**	**4.07**	**5.18**	**4.36**	**4.22**	-1.11	- 2.79
Amorph. Sepiolite $Mg_4Si_6O_{15}(OH)_2{\cdot}nH_2O$	- 6.70	**3.41**	-0.43	**0.05**	**0.91**	**1.98**	**1.47**	**0.02**	**0.33**	**1.16**	**2.80**	**1.67**	**1.89**	-3.45	- 5.44
Kerolite $Mg_3Si_4O_{10}(OH)_2{\cdot}nH_2O$	- 5.16	**8.93**	**3.60**	**4.30**	**5.29**	**6.99**	**6.22**	**4.17**	**4.82**	**5.84**	**8.08**	**6.37**	**7.01**	-0.09	- 2.80
Talc $Mg_3Si_4O_{10}(OH)_2$	- 2.35	**11.76**	**6.51**	**7.11**	**8.09**	**9.89**	**9.08**	**6.88**	**7.65**	**8.63**	**11.00**	**9.21**	**9.93**	**2.83**	**0.05**
Stevensite $Ca_{0.1}Mg_{2.9}Si_4O_{10}(OH)_2{\cdot}nH_2O$	- 4.78	**9.29**	**4.01**	**4.57**	**5.62**	**7.34**	**6.49**	**4.40**	**5.13**	**6.14**	**8.41**	**6.62**	**7.37**	**0.23**	- 2.58
Amorph. Silica SiO_2	- 2.26	- 0.08	-0.88	- 0.93	- 0.33	-0.45	- 0.48	- 0.79	- 1.09	- 0.68	-0.17	- 0.17	-0.75	-2.54	- 3.14
Hydroxyapatite $Ca_5(PO_4)_3(OH)$	**3.34**	**6.75**	/	**2.94**	**7.95**	/	**1.63**	**4.41**	**5.46**	**3.70**	/	**0.53**	/	/	**0.59**

Table SI-6. Saturation indices of the 2012 and 2014 surface water solutions

Saturation indices of the surface water solutions of the lakes sampled in May 2014 and January 2012 for various Ca- and/or Mg-carbonates, silicates and hydroxyapatite. Saturation indices were calculated using the Visual MINTEQ software. Positive values (in bold characters) indicate that solutions are supersaturated. Saturation indices with respect to hydroxyapatite were not calculated for the 2012 surface water (/) because [PO_4^{3-}] was not analyzed for those samples.

Lake	Microbialite Sample	Type	Location on the lake	Detrital contamination	Main Mineralogy
Alchichica	**AL13** (*)	Living	North	LDC	H – A – LDH
	AL66 (*)	Living	North	/	H – A – LDH
	AL69-2m	Living	North	LDD	H – A
	AL60-6m	Living	North	IDC	H – A – An
	AL54-11m	Living	North	IDC	H – A
	AL2012-1m	Living	North	LDC	H – A
	AL2012-5m	Living	North	LDC	H – A
	AL2012-10m (*)	Living	North	IDC	H – A – LDH – I
	AL2012-15m	Living	North	LDC	H – A
	AL2012-12 (*)	Living	North-West	LDC	H – A
	AL2012-15 (*)	Non-living	North-West	IDC	A – C
	AL2012-17	Non-living	North-West	LDC	A – LDH
	AL2014-12	Living	North-West	/	H – A
	AL2014-13 (*)	Living	North-West	LDC	A – H – K/S
	AL2014-15 (*)	Living	North-West	LDC	A – H – LDH
	AL2014-26	Living	North-West	/	A – H – LDH
Atexcac	**ATX-2C1-2012** (*)	Living	North	IDC	K/S – A – C – H
	ATX2014-02 (*)	Non-living	North	/	A – K/S
	ATX2014-07	Living	North	LDC	A – K/S – C
	ATX2014-13 (*)	Living	South	IDC	A – K/S – D – C – An
La Preciosa	**Preciosa-05-2012** (*)	Non-living	North	IDC	A – K/S – C – An
	Preciosa-06-2012	Living	North	IDC	A – K/S – C – An
	Pr2014-01	Non-living	East	LDC	A – K/S – C
	Pr2014-02	Non-living	East	LDC	A – K/S – D – C
	Pr2014-03	Non-living	East	HDC	MgC – An – D – A – K/S
	Pr2014-05	Non-living	East	/	A – K/S
	Pr2014-06	Non-living	East	/	A – K/S
	Pr2014-08	Living	East	/	A – K/S
	Pr2014-09 (*)	Living	East	LDC	A – K/S
Quechulac	**Quechulac-1A-2012** (*)	Living	Center	LDC	A – K/S
	Quechulac-4A-2012	Non-living (external part)	Center	LDC	A – C
	Quechulac-4B-2012	Non-living (intermediate part)	Center	LDC	A – C
	Quechulac-4C-2012	Non-living (internal part)	Center	LDC	A – C
Tecuitlapa	**Tec2014-05a**	Non-living (external white part)	East	IDC	MHC – MgC – A – Ab
	Tec2014-05b	Non-living (intermediate green part)	East	HDC	MHC – Ab – A – K/S
	Tec2014-06 (*)	Living	East	/	MgC – MHC – A – K/S
La Alberca de Los Espinos	**AlbEsp2014-01** (*)	Living	West	LDC	MgC – MHC – K/S
Pátzcuaro	Patz2014-01	Non-living	North-East	/	MgC
	Patz2014-02 (*)	Living	North-East	IDC	MgC – A – MHC – K/S
Aljojuca	Aljo2014-01	Non-living	North	/	MgC – MHC – A – Ab
	Aljo2014-02 (*)	Living	North	IDC	MHC – MgC – A – Ab
Alberca de Guadalupe	**Alb2014-02** (*)	Living	South	HDC	Ab – MgC – K/S

Table SI-7. Mineralogical composition of the studied microbialites

Mineralogical composition of living and non-living microbialites hosted by the studied Mexican lakes as determined by XRD and FTIR and/or observed by optical and scanning electron microscopy. Mineralogical differences exist in a given lake between non-living *vs* living microbialites and/or microbialites at different locations in the lake. Mineral phases are listed in order of abundance. (C: calcite; MgC: magnesian calcite; MHC: monohydrocalcite; A: aragonite; D: dolomite; H: hydromagnesite; K/S: kerolite and/or stevensite; LDH: layered double hydroxide; Ab: albite; An: anorthite; Q: quartz; I: illite). Asterisk (*) stands for samples observed by SEM and/or optical microscopy. The bulk chemistry of samples in bold was analyzed (32 samples in total). The extent of detrital contamination was assessed based on bulk chemistry. HDC: samples highly affected by detrital contamination; IDC: samples intermediately affected by detrital contamination and LDC: samples the least affected by detrital contamination (*i.e.*, authigenic-dominated samples).

Microbialite Sample	Aragonite wt.%	Mg-Calcite wt.%	Monohydrocalcite wt.%	Hydromagnesite wt.%	Talc wt.%	Fe-Talc wt.%
AL13	12	/	/	88	/	/
AL69-2m	22	/	/	78	/	/
AL2012-1m	23	/	/	77	/	/
AL2012-5m	18	/	/	82	/	/
AL2012-15m	44	/	/	56	/	/
AL2012-12	23	/	/	77	/	/
AL2012-17	98	/	/	2	/	/
AL2014-13	91	/	/	9	/	/
AL2014-15	74	/	/	26	/	/
ATX2014-07	67	/	/	/	32	1
Pr2014-01	70	/	/	/	29	1
Pr2014-02	62	/	/	/	38	1
Pr2014-09	75	/	/	/	24	1
Quechulac-1A-2012	96	/	/	/	4	/
Quechulac-4A-2012	100	/	/	/	/	/
Quechulac-4B-2012	99	/	/	/	/	1
Quechulac-4C-2012	97	/	/	/	/	3
AlbEsp2014-01	/	61	27	/	12	/

Table SI-8. Proportions of the mineral phases in the authigenic-dominated microbialites
Approximate mass proportions of the mineral phases composing Al-poor microbialite samples, based on bulk chemical composition, XRD and FTIR analyses, and optical and scanning electron microscopies.

Microbialite Sample	Corg (at.%)	S total (at.%)	Si (wt.%)	Al (wt.%)	Fe (wt.%)	Mn (wt.%)	Mg (wt.%)	Ca (wt.%)	Na (wt.%)	K (wt.%)	Ti (wt.%)	P (wt.%)
AL13	0.36 ±0.05	0.05 ±0.01	0.65 ±0.03	0.21 ±0.02	0.12 ±0.01	< 0.0002	22.23 ±0.44	4.0 ±0.1	0.20 ±0.02	0.06 ±0.01	< 0.01	< 0.02
AL69-2m	0.36 ±0.05	NM	0.2 ±0.02	0.08 ±0.01	0.078 ±0.004	0.005 ±0.001	19.71 ±0.39	7.1 ±0.1	0.22 ±0.02	0.04 ±0.01	<0.01	< 0.02
AL60-6m	0.28 ±0.04	NM	2.56 ±0.08	0.83 ±0.08	0.39 ±0.01	0.017 ±0.002	17.33 ±0.35	8.5 ±0.2	0.50 ±0.02	0.18 ±0.02	0.04 ±0.01	0.022 ±0.005
AL54-11m	0.29 ±0.04	NM	2.46 ±0.07	0.29 ±0.03	0.15 ±0.01	0.011 ±0.001	20.85 ±0.42	3.9 ±0.1	0.24 ±0.02	0.07 ±0.01	0.020 ±0.005	0.022 ±0.005
AL2012-1m	0.46 ±0.07	0.15 ±0.02	0.54 ±0.03	0.14 ±0.02	0.090 ±0.004	0.007 ±0.002	19.04 ±0.38	7.5 ±0.1	0.23 ±0.02	0.05 ±0.01	< 0.01	0.017 ±0.004
AL2012-5m	0.16 ±0.02	0.05 ±0.01	0.75 ±0.04	0.11 ±0.02	0.049 ±0.005	0.004 ±0.001	21.02 ±0.42	5.8 ±0.1	0.15 ±0.01	0.03 ±0.01	< 0.01	0.022 ±0.005
AL2012-10m	0.27 ±0.04	0.08 ±0.02	3.83 ±0.08	1.01 ±0.1	0.17 ±0.01	0.014 ±0.001	17.22 ±0.34	8.5 ±0.2	0.48 ±0.02	0.21 ±0.02	0.014 ±0.003	0.017 ±0.004
AL2012-15m	0.41 ±0.06	0.13 ±0.02	0.45 ±0.02	0.09 ±0.01	0.1 ±0.005	0.009 ±0.001	14.59 ±0.29	14.9 ±0.3	0.32 ±0.03	0.04 ±0.01	< 0.01	< 0.02
AL2012-12	0.46 ±0.07	0.12 ±0.02	0.26 ±0.03	0.06 ±0.01	0.2 ±0.01	0.007 ±0.002	18.79 ±0.38	7.5 ±0.2	0.21 ±0.02	0.03 ±0.01	< 0.01	0.017 ±0.004
AL2012-15	0.32 ±0.05	0.18 ±0.02	1.86 ±0.09	0.26 ±0.03	1.68 ±0.03	0.018 ±0.002	1.11 ±0.06	32.6 ±0.7	0.79 ±0.02	0.17 ±0.02	0.018 ±0.004	0.048 ±0.005
AL2012-17	0.11 ±0.02	0.03 ±0.01	1.02 ±0.05	0.09 ±0.01	2.49 ±0.05	0.012 ±0.001	0.52 ±0.03	35.1 ±0.7	0.27 ±0.03	0.05 ±0.01	< 0.01	0.092 ±0.009
AL2014-13	0.70 ±0.07	0.15 ±0.02	0.73 ±0.04	0.15 ±0.02	0.15 ±0.01	0.005 ±0.001	2.38 ±0.07	32.5 ±0.6	0.44 ±0.02	0.06 ±0.01	< 0.01	0.017 ±0.004
AL2014-15	0.97 ±0.1	0.17 ±0.02	1.02 ±0.05	0.12 ±0.02	2.24 ±0.04	0.015 ±0.001	6.34 ±0.13	23.6 ±0.5	0.46 ±0.02	0.07 ±0.01	< 0.01	0.04 ±0.01
ATX-2C1-2012	0.56 ±0.08	0.16 ±0.02	13.87 ±0.14	0.29 ±0.03	0.54 ±0.02	0.036 ±0.004	12.76 ±0.26	9.1 ±0.2	0.33 ±0.03	0.11 ±0.01	0.019 ±0.005	< 0.02
ATX2014-07	1.18 ±0.12	0.37 ±0.02	7.4 ±0.07	0.05 ±0.01	0.12 ±0.01	0.033 ±0.003	5.28 ±0.11	22.3 ±0.4	0.54 ±0.02	0.07 ±0.01	< 0.01	0.048 ±0.005
ATX2014-13	0.35 ±0.05	0.32 ±0.02	2.58 ±0.08	0.58 ±0.06	0.67 ±0.01	0.018 ±0.002	0.57 ±0.03	34.9 ±0.7	0.5 ±0.02	0.13 ±0.01	0.035 ±0.009	0.017 ±0.004
Preciosa-05-2012	0.81 ±0.08	0.14 ±0.02	11.34 ±0.11	0.63 ±0.06	0.31 ±0.01	0.037 ±0.004	7.03 ±0.14	19.0 ±0.4	0.29 ±0.03	0.16 ±0.02	0.031 ±0.008	< 0.02
Preciosa-06-2012	1.47 ±0.15	0.25 ±0.01	5.35 ±0.05	0.49 ±0.07	0.26 ±0.01	0.033 ±0.003	3.16 ±0.06	26.4 ±0.5	0.26 ±0.03	0.12 ±0.01	0.031 ±0.008	< 0.02
Pr2014-01	0.69 ±0.1	0.11 ±0.02	7.25 ±0.07	0.22 ±0.02	0.13 ±0.01	0.032 ±0.003	5.2 ±0.1	25.2 ±0.5	0.12 ±0.01	0.06 ±0.01	< 0.01	0.017 ±0.004
Pr2014-02	0.61 ±0.09	0.1 ±0.02	8.98 ±0.09	0.19 ±0.02	0.088 ±0.004	0.02 ±0.002	6.85 ±0.14	22.9 ±0.5	0.11 ±0.01	0.05 ±0.01	< 0.01	0.017 ±0.004
Pr2014-03	0.17 ±0.03	0.12 ±0.02	15.29 ±0.15	3.73 ±0.19	1.28 ±0.03	0.06 ±0.006	7.2 ±0.1	13.5 ±0.3	1.10 ±0.03	0.55 ±0.03	0.15 ±0.01	0.048 ±0.005
Pr2014-09	1.13 ±0.11	0.21 ±0.02	5.23 ±0.05	0.06 ±0.01	0.082 ±0.004	0.044 ±0.004	4.14 ±0.08	26.6 ±0.5	0.10 ±0.01	0.02 ±0.01	< 0.01	< 0.02
Quechulac-1A-2012	0.88 ±0.09	0.14 ±0.02	1.01 ±0.05	0.08 ±0.01	0.03 ±0.01	0.005 ±0.001	0.65 ±0.01	35.3 ±0.7	0.10 ±0.01	0.02 ±0.01	< 0.01	< 0.02
Quechulac-4A-2012	0.56 ±0.08	0.13 ±0.02	1.21 ±0.06	0.06 ±0.01	0.03 ±0.01	0.005 ±0.001	0.90 ±0.02	35.4 ±0.7	0.13 ±0.01	0.02 ±0.01	< 0.01	< 0.02
Quechulac-4B-2012	0.88 ±0.09	0.1 ±0.02	1.51 ±0.08	0.27 ±0.03	0.12 ±0.01	0.007 ±0.002	0.79 ±0.02	34.4 ±0.7	0.14 ±0.01	0.06 ±0.01	0.015 ±0.004	0.031 ±0.008
Quechulac-4C-2012	0.59 ±0.09	0.09 ±0.01	1.13 ±0.06	0.08 ±0.01	0.02 ±0.01	0.004 ±0.001	0.79 ±0.02	35.9 ±0.7	0.10 ±0.01	0.03 ±0.01	< 0.01	< 0.02
Tec2014-05a	0.52 ±0.08	0.05 ±0.01	4.28 ±0.09	0.59 ±0.06	0.29 ±0.01	0.017 ±0.002	2.51 ±0.08	29.0 ±0.6	0.28 ±0.03	0.13 ±0.01	0.034 ±0.009	0.044 ±0.004
Tec2014-05b	0.56 ±0.08	0.05 ±0.01	16.9 ±0.17	3.57 ±0.18	2.11 ±0.04	0.053 ±0.005	6.8 ±0.1	12.4 ±0.2	1.2 ±0.1	0.56 ±0.03	0.24 ±0.02	0.070 ±0.007
AlbEsp2014-01	1.04 ±0.1	0.05 ±0.01	3.33 ±0.1	0.06 ±0.01	0.38 ±0.01	0.464 ±0.009	3.54 ±0.07	28.7 ±0.6	0.04 ±0.01	0.02 ±0.01	< 0.01	0.27 ±0.02
Patz2014-02	0.84 ±0.08	0.05 ±0.01	6.98 ±0.07	0.35 ±0.04	0.62 ±0.02	0.121 ±0.006	5.5 ±0.1	25.2 ±0.5	0.09 ±0.01	0.04 ±0.01	0.019 ±0.005	0.074 ±0.007
Aljo2014-02	0.73 ±0.07	0.08 ±0.02	3.6 ±0.04	1.15 ±0.06	0.54 ±0.02	0.023 ±0.002	0.60 ±0.03	30.7 ±0.6	0.42 ±0.04	0.20 ±0.02	0.054 ±0.013	0.12 ±0.01
LaAlb2014-02	2.55 ±0.13	0.07 ±0.01	14.53 ±0.15	3.46 ±0.17	2.23 ±0.04	0.218 ±0.011	3.94 ±0.08	12.9 ±0.3	1.06 ±0.11	0.63 ±0.03	0.27 ±0.02	0.092 ±0.008

Table SI-9. Bulk chemical compositions of the studied microbialites (major elements)

Microbialite sample	As	Ba	Be	Bi	Cd	Co	Cr	Cs	Cu	Ga	Ge	Hf	In	Mo	Nb
	ppm	ppm	ppm	ppm	ppm	ppm	ppm	ppm	ppm	ppm	ppm	ppm	ppm	ppm	ppm
AL13	2.40	73.45	< 0.40	< 0.10	< 0.12	0.44	2.96	0.10	< 5.00	0.52	< 0.15	0.11	< 0.07	< 0.50	0.25
AL69-2m	2.88	99.50	< 0.40	< 0.10	< 0.12	0.30	< 2.00	< 0.10	< 5.00	0.23	< 0.15	0.05	< 0.07	< 0.50	0.16
AL60-6m	6.67	167.30	< 0.40	< 0.10	< 0.12	1.32	7.68	0.31	< 5.00	1.78	0.14	0.32	< 0.07	< 0.50	0.82
AL54-11m	3.11	68.67	< 0.40	< 0.10	< 0.12	0.55	< 2.00	0.10	< 5.00	0.85	0.12	0.24	< 0.07	< 0.50	0.38
AL2012-1m	2.37	121.70	< 0.40	< 0.10	< 0.12	0.76	< 2.00	< 0.10	< 5.00	0.35	< 0.15	0.08	< 0.07	< 0.50	0.16
AL2012-5m	1.66	82.41	< 0.40	< 0.10	< 0.12	1.10	< 2.00	< 0.10	< 5.00	0.25	< 0.15	0.10	< 0.07	< 0.50	0.15
AL2012-10m	6.58	236.90	< 0.40	< 0.10	< 0.12	0.62	< 2.00	0.15	< 5.00	2.13	0.18	0.35	< 0.07	< 0.50	1.41
AL2012-15m	5.97	262.70	< 0.40	< 0.10	< 0.12	0.83	< 2.00	< 0.10	< 5.00	< 0.20	< 0.15	0.07	< 0.07	< 0.50	0.17
AL2012-12	7.39	166.20	< 0.40	< 0.10	< 0.12	0.70	< 2.00	< 0.10	< 5.00	< 0.20	< 0.15	0.03	< 0.07	< 0.50	0.10
AL2012-15	27.60	886.60	< 0.40	0.10	< 0.12	3.83	< 2.00	0.14	5.38	0.53	< 0.15	0.20	< 0.07	< 0.50	0.43
AL2012-17	25.39	1120.00	< 0.40	< 0.10	< 0.12	2.80	< 2.00	< 0.10	< 5.00	< 0.20	< 0.15	0.09	< 0.07	< 0.50	0.14
AL2014-13	4.06	612.30	< 0.40	< 0.10	< 0.12	1.06	< 2.00	< 0.10	< 5.00	0.27	< 0.15	0.08	< 0.07	< 0.50	0.19
AL2014-15	56.81	739.40	< 0.40	< 0.10	< 0.12	0.88	< 2.00	< 0.10	< 5.00	0.26	< 0.15	0.13	< 0.07	< 0.50	0.28
ATX-2C1-2012	24.51	191.20	< 0.40	< 0.10	0.17	1.84	< 2.00	3.87	5.55	0.83	4.07	0.21	< 0.07	1.12	0.42
ATX2014-07	4.04	286.90	< 0.40	< 0.10	< 0.12	1.26	< 2.00	1.53	< 5.00	< 0.20	8.20	0.04	< 0.07	< 0.50	0.13
ATX2014-13	5.44	657.00	< 0.40	< 0.10	< 0.12	2.58	5.20	0.56	< 5.00	1.23	1.09	0.30	< 0.07	< 0.50	0.59
Preciosa-05-2012	7.90	268.50	< 0.40	< 0.10	< 0.12	3.01	< 2.00	0.21	7.65	1.61	0.67	0.31	< 0.07	< 0.50	0.85
Preciosa-06-2012	4.42	442.30	< 0.40	< 0.10	< 0.12	2.52	< 2.00	0.15	< 5.00	1.32	0.73	0.24	< 0.07	< 0.50	0.62
Pr2014-01	3.46	359.90	< 0.40	< 0.10	0.17	1.42	< 2.00	0.10	5.07	0.46	1.11	0.13	< 0.07	< 0.50	0.29
Pr2014-02	4.12	366.30	< 0.40	< 0.10	0.18	1.23	< 2.00	0.10	8.12	0.44	0.91	0.10	< 0.07	< 0.50	0.24
Pr2014-03	2.24	316.80	0.92	< 0.10	0.13	5.93	20.71	0.91	12.87	9.02	0.84	1.87	< 0.07	< 0.50	3.57
Pr2014-09	4.26	432.50	< 0.40	< 0.10	< 0.12	1.33	< 2.00	< 0.10	< 5.00	0.31	0.89	0.07	< 0.07	< 0.50	0.19
Quechulac-1A-2012	< 1.50	407.90	< 0.40	< 0.10	< 0.12	1.85	< 2.00	< 0.10	< 5.00	0.24	< 0.15	0.05	< 0.07	< 0.50	0.11
Quechulac-4A-2012	< 1.50	366.30	< 0.40	< 0.10	< 0.12	1.82	< 2.00	< 0.10	< 5.00	0.26	0.17	0.05	< 0.07	< 0.50	0.12
Quechulac-4B-2012	< 1.50	378.60	< 0.40	< 0.10	< 0.12	1.81	< 2.00	< 0.10	< 5.00	0.74	0.24	0.16	< 0.07	< 0.50	0.35
Quechulac-4C-2012	< 1.50	358.90	< 0.40	< 0.10	< 0.12	1.67	< 2.00	< 0.10	10.40	0.37	0.20	0.07	< 0.07	< 0.50	0.15
Tec2014-05a	< 1.50	207.90	< 0.40	< 0.10	< 0.12	2.51	9.28	0.15	6.55	1.42	0.18	0.31	< 0.07	< 0.50	0.65
Tec2014-05b	< 1.50	363.30	0.55	< 0.10	0.13	11.64	76.99	0.58	12.34	8.10	0.64	1.92	< 0.07	< 0.50	3.42
AlbEsp2014-01	< 1.50	620.20	< 0.40	< 0.10	< 0.12	2.14	< 2.00	< 0.10	< 5.00	0.97	1.38	0.06	< 0.07	< 0.50	0.12
Patz2014-02	< 1.50	660.30	< 0.40	< 0.10	< 0.12	4.15	4.89	< 0.10	13.67	1.88	< 0.15	0.25	< 0.07	< 0.50	0.95
Aljo2014-02	< 1.50	231.20	< 0.40	< 0.10	< 0.12	3.09	6.78	0.17	11.12	2.39	0.18	0.46	< 0.07	< 0.50	0.60
LaAlb2014-02	< 1.50	351.80	0.59	< 0.10	< 0.12	10.14	180.30	0.44	10.31	7.41	0.72	1.60	< 0.07	1.68	4.84

Table SI-10. Bulk chemical compositions of the studied microbialites (minor and trace elements excluding REE+Y)

Microbialite sample	Ni	Pb	Rb	Sc	Sb	Sn	Sr	Ta	Th	U	V	W	Zn	Zr
	ppm	ppm	ppm	ppm	ppm	ppm	ppm	ppm	ppm	ppm	ppm	ppm	ppm	ppm
AL13	< 5.00	1.05	1.73	< 1.00	< 0.20	< 0.45	359.05	0.02	0.15	0.11	3.07	< 0.10	7.55	4.18
AL69-2m	< 5.00	0.65	1.00	< 1.00	< 0.20	< 0.45	628.30	0.03	0.06	0.04	1.15	< 0.10	< 7.00	2.05
AL60-6m	< 5.00	1.70	5.80	< 1.00	< 0.20	< 0.45	719.20	0.08	0.46	0.20	7.16	0.12	< 7.00	10.75
AL54-11m	< 5.00	0.72	1.88	< 1.00	< 0.20	< 0.45	311.40	0.03	0.19	0.15	4.36	< 0.10	< 7.00	11.49
AL2012-1m	< 5.00	< 0.60	1.25	< 1.00	< 0.20	< 0.45	694.80	0.01	0.10	0.09	1.75	< 0.10	< 7.00	3.22
AL2012-5m	< 5.00	< 0.60	0.85	< 1.00	< 0.20	< 0.45	538.60	0.01	0.08	0.10	2.39	< 0.10	< 7.00	4.10
AL2012-10m	< 5.00	2.02	5.52	< 1.00	< 0.20	< 0.45	739.60	0.14	0.86	0.60	4.92	< 0.10	14.35	12.02
AL2012-15m	< 5.00	1.14	0.80	< 1.00	< 0.20	< 0.45	1484.00	< 0.01	0.08	0.09	1.59	< 0.10	< 7.00	2.69
AL2012-12	< 5.00	0.78	0.70	< 1.00	< 0.20	< 0.45	735.10	< 0.01	0.07	0.11	1.10	< 0.10	< 7.00	1.28
AL2012-15	< 5.00	1.76	3.71	< 1.00	< 0.20	0.63	3232.00	0.02	0.21	1.48	8.39	< 0.10	11.52	9.47
AL2012-17	< 5.00	1.06	0.93	< 1.00	< 0.20	< 0.45	3441.00	< 0.01	< 0.06	1.25	3.05	< 0.10	< 7.00	3.75
AL2014-13	< 5.00	0.96	1.56	< 1.00	< 0.20	< 0.45	4133.00	0.02	0.13	1.07	2.36	< 0.10	< 7.00	3.59
AL2014-15	< 5.00	2.17	1.87	< 1.00	< 0.20	< 0.45	2448.00	0.01	0.13	0.62	4.84	< 0.10	< 7.00	6.54
ATX-2C1-2012	7.03	2.78	5.48	< 1.00	1.34	< 0.45	837.50	0.03	0.23	0.25	13.67	< 0.10	28.02	13.59
ATX2014-07	< 5.00	1.22	2.12	< 1.00	0.31	< 0.45	2624.00	< 0.01	< 0.06	0.05	2.23	< 0.10	< 7.00	4.70
ATX2014-13	< 5.00	1.61	4.68	< 1.00	0.23	< 0.45	4217.00	0.05	0.35	0.43	9.28	< 0.10	< 7.00	12.68
Preciosa-05-2012	6.61	2.75	6.28	< 1.00	1.99	< 0.45	1470.00	0.08	0.70	0.62	12.18	< 0.10	14.31	12.57
Preciosa-06-2012	7.82	4.71	4.14	< 1.00	0.42	< 0.45	2237.00	0.05	0.42	0.59	11.53	< 0.10	14.17	12.49
Pr2014-01	< 5.00	23.78	2.50	< 1.00	1.55	< 0.45	2162.00	0.02	0.17	0.37	3.73	< 0.10	13.88	5.33
Pr2014-02	< 5.00	28.83	2.70	< 1.00	2.94	< 0.45	2628.00	0.02	0.16	0.54	5.82	< 0.10	< 7.00	4.33
Pr2014-03	< 5.00	6.93	22.68	4.61	0.71	0.76	1153.00	0.37	3.15	0.90	27.85	< 0.10	29.54	68.83
Pr2014-09	< 5.00	8.07	0.91	< 1.00	0.36	< 0.45	2616.00	< 0.01	< 0.06	0.43	4.33	< 0.10	< 7.00	5.54
Quechulac-1A-2012	< 5.00	< 0.60	0.50	< 1.00	< 0.20	< 0.45	2724.00	< 0.01	0.07	2.73	12.13	< 0.10	< 7.00	2.65
Quechulac-4A-2012	< 5.00	< 0.60	0.50	< 1.00	< 0.20	< 0.45	2795.00	< 0.01	0.08	2.77	7.59	< 0.10	< 7.00	2.78
Quechulac-4B-2012	< 5.00	0.89	1.80	< 1.00	< 0.20	< 0.45	2589.00	0.03	0.22	2.55	10.47	< 0.10	11.08	6.54
Quechulac-4C-2012	< 5.00	0.95	0.63	< 1.00	< 0.20	< 0.45	2694.00	< 0.01	0.08	2.88	12.50	< 0.10	13.02	2.97
Tec2014-05a	< 5.00	1.64	4.01	< 1.00	< 0.20	< 0.45	914.00	0.05	0.50	1.84	51.40	< 0.10	< 7.00	15.56
Tec2014-05b	34.34	4.53	17.71	7.03	0.26	0.81	971.30	0.24	1.88	3.27	117.80	< 0.10	33.62	84.99
AlbEsp2014-01	< 5.00	2.99	0.70	< 1.00	< 0.20	< 0.45	1312.00	< 0.01	0.08	0.05	2.24	< 0.10	< 7.00	2.79
Patz2014-02	< 5.00	1.41	2.43	1.47	< 0.20	< 0.45	3297.00	0.03	0.33	1.76	63.08	< 0.10	12.65	13.41
Aljo2014-02	< 5.00	6.07	4.72	1.82	< 0.20	< 0.45	1092.00	0.05	0.53	1.57	18.31	< 0.10	14.55	17.89
LaAlb2014-02	85.65	20.25	16.96	6.11	0.30	0.69	813.30	0.37	1.24	0.57	56.55	0.82	35.32	67.88

Table SI-10. Continued

Microbialite sample	La	Ce	Pr	Nd	Sm	Eu	Gd	Tb	Dy	Y	Ho	Er	Tm	Yb	Lu	∑REE
	ppm	ppm	ppm	ppm	ppm	ppm	ppm	ppm	ppm	ppm	ppm	ppm	ppm	ppm	ppm	ppm
AL13	0.51	1.03	0.14	0.54	0.13	0.04	0.11	0.02	0.10	0.60	0.02	0.06	0.01	0.06	0.01	3.37
AL69-2m	0.26	0.47	0.07	0.29	0.07	0.02	0.06	0.01	0.07	0.44	0.01	0.04	0.01	0.04	0.01	1.87
AL60-6m	1.64	3.15	0.44	1.65	0.36	0.10	0.31	0.04	0.25	1.51	0.05	0.13	0.02	0.14	0.02	9.81
AL54-11m	0.63	1.21	0.17	0.62	0.14	0.04	0.12	0.02	0.10	0.64	0.02	0.06	0.01	0.06	0.01	3.84
AL2012-1m	0.32	0.65	0.09	0.33	0.08	0.03	0.07	0.01	0.07	0.46	0.02	0.04	0.01	0.05	0.01	2.22
AL2012-5m	0.27	0.52	0.06	0.29	0.06	0.02	0.05	0.01	0.04	0.30	0.01	0.02	0.00	0.03	0.01	1.70
AL2012-10m	2.31	4.37	0.48	1.65	0.31	0.11	0.25	0.03	0.17	0.91	0.03	0.08	0.01	0.07	0.01	10.78
AL2012-15m	0.32	0.48	0.09	0.39	0.11	0.05	0.10	0.02	0.10	0.68	0.02	0.06	0.01	0.06	0.01	2.49
AL2012-12	0.21	0.39	0.06	0.30	0.07	0.03	0.07	0.01	0.07	0.53	0.02	0.05	0.01	0.06	0.01	1.89
AL2012-15	0.74	1.39	0.19	0.74	0.18	0.12	0.16	0.03	0.15	1.12	0.03	0.09	0.02	0.11	0.02	5.09
AL2012-17	0.22	0.37	0.05	0.19	0.06	0.10	0.06	0.01	0.05	0.58	0.01	0.04	0.01	0.06	0.01	1.83
AL2014-13	0.44	0.83	0.12	0.50	0.12	0.05	0.12	0.02	0.11	0.78	0.03	0.07	0.01	0.07	0.01	3.28
AL2014-15	0.43	0.76	0.12	0.51	0.12	0.06	0.12	0.02	0.11	0.82	0.03	0.08	0.01	0.09	0.01	3.27
ATX-2C1-2012	0.85	1.58	0.21	0.87	0.21	0.06	0.19	0.03	0.16	1.14	0.03	0.09	0.02	0.10	0.02	5.54
ATX2014-07	0.13	0.24	0.04	0.16	0.04	0.02	0.04	0.01	0.05	0.36	0.01	0.03	0.01	0.03	0.01	1.18
ATX2014-13	1.42	2.86	0.40	1.67	0.37	0.12	0.35	0.05	0.34	2.26	0.07	0.21	0.03	0.21	0.03	10.39
Preciosa-05-2012	1.87	3.70	0.44	1.62	0.33	0.09	0.29	0.04	0.26	1.65	0.05	0.15	0.03	0.17	0.03	10.71
Preciosa-06-2012	1.40	2.81	0.34	1.37	0.29	0.11	0.26	0.04	0.26	1.79	0.06	0.16	0.03	0.18	0.03	9.12
Pr2014-01	0.55	1.09	0.13	0.53	0.11	0.04	0.09	0.01	0.08	0.49	0.02	0.05	0.01	0.05	0.01	3.26
Pr2014-02	0.50	0.98	0.12	0.46	0.09	0.04	0.07	0.01	0.08	0.44	0.02	0.05	0.01	0.05	0.01	2.91
Pr2014-03	9.64	19.17	2.35	9.05	1.89	0.47	1.59	0.23	1.41	7.99	0.29	0.77	0.11	0.80	0.12	55.88
Pr2014-09	0.14	0.28	0.04	0.17	0.05	0.03	0.06	0.01	0.08	0.68	0.02	0.05	0.01	0.07	0.01	1.69
Quechulac-1A-2012	0.35	0.66	0.11	0.44	0.11	0.06	0.10	0.02	0.10	0.96	0.02	0.07	0.01	0.07	0.01	3.09
Quechulac-4A-2012	0.41	0.75	0.15	0.63	0.15	0.07	0.14	0.02	0.14	1.12	0.03	0.09	0.01	0.09	0.01	3.80
Quechulac-4B-2012	0.90	1.79	0.24	0.97	0.21	0.09	0.18	0.03	0.16	1.21	0.04	0.10	0.02	0.11	0.02	6.04
Quechulac-4C-2012	0.37	0.75	0.11	0.49	0.11	0.06	0.10	0.02	0.11	0.95	0.02	0.07	0.01	0.08	0.01	3.24
Tec2014-05-a	2.43	5.66	0.72	3.05	0.68	0.18	0.65	0.11	0.75	6.00	0.17	0.52	0.08	0.57	0.09	21.65
Tec2014-05-b	10.70	21.78	2.72	10.87	2.22	0.65	1.89	0.28	1.65	9.87	0.35	0.94	0.14	0.95	0.15	65.15
AlbEsp2014-01	1.65	1.76	0.52	2.20	0.46	0.14	0.44	0.07	0.48	3.75	0.11	0.28	0.04	0.27	0.04	12.22
Patz2014-02	4.15	7.77	1.33	5.88	1.43	0.39	1.55	0.26	1.80	15.69	0.44	1.26	0.18	1.21	0.19	43.53
Aljo2014-02	2.69	5.39	0.75	3.10	0.67	0.20	0.60	0.09	0.56	3.68	0.12	0.32	0.05	0.33	0.05	18.59
LaAlb2014-02	7.90	15.36	2.01	8.13	1.75	0.52	1.56	0.23	1.41	8.51	0.30	0.79	0.11	0.73	0.12	49.44

Table SI-11. Bulk chemical composition of the studied microbialites: REE (+Y)
∑REE stands for the sum of the REE +Y

Aqueous Sample	Altitude (m)	SI-CO_2(g)	pCO_2(g) /pCO_2atm
Preciosa2014_0m	2330	-2.99	3.4
Quechulac2014_0m_N	2330	-3.44	1.2
ATX2014_0m-M	2360	-2.41	12.8
AL2014_0m_M	2320	-2.95	3.7
Aljojuca2014_0m	2379	-3.42	1.3
Tecuitlapa2014_0m	2380	-3.54	1.0
AlbEsp2014_0m	1985	-3.10	2.5
Alb2014_0m	2066	-4.12	0.2
Patz2014_0m	2044	-3.21	1.9
Zirahuen2014_0m	2082	-3.81	0.5

Table SI-12. Determination of the $pCO_{2(g)}$/pCO_{2atm} ratio of the 2014 surface water lakes
SI-CO_2 (g) corresponds to the saturation index of the lake water solutions with respect to CO_2 gas, SI=log(pCO_2). It was calculated using the software PHREEQC 3 (Parkhurst and Appelo, 2013) and the thermodynamic database "thermoddem.dat" (Blanc et al., 2012). pCO_{2atm} is based on the global atmospheric pCO_2 recorded in May 2014 at 1.01325 bar = 401.78 ppm (from NOAA database) and calculated at the pressure corresponding to the elevation of each sites. Determination of the $pCO_{2(g)}$/$pCO_{2(atm)}$ of the studied lakes

III. TEXTS

Text SI-1. REE+Y calculations and correlations between variables

In order to characterize the REE+Y patterns of microbialites, we calculated different shale normalized (SN) indices (Table SI-1-1 below). Ce anomalies were expressed in 3 different manners: $Ce/Ce^*=(Ce/(0.5La+0.5Pr))_{SN}$ (Bau and Dulski, 1996), $Ce/Ce^*=(Ce/(2Pr-Nd))_{SN}$ (Bolhar and Van Kranendonk, 2007) and $Ce/Ce^*=(Ce/((La\times Pr)^{1/2}))_{SN}$ (Barrat et al., 2000). La/La* anomalies were also defined in 3 different ways: $(La/(3Pr-2Nd))_{SN}$ (Bau and Dulski, 1996), $(La/(2Ce-Pr))_{SN}$ (Bolhar and Van Kranendonk, 2007) and $(La/(Pr^3/Nd^2))_{SN}$ (Bolhar and Van Kranendonk, 2007). Gd/Gd* anomalies were defined in 2 different ways: $(Gd/(2Tb-Dy))_{SN}$ (Bau and Dulski, 1996) and $(Gd/(Tb^2/Dy))_{SN}$ (Bolhar and Van Kranendonk, 2007). Eu/Eu* anomalies were defined as $(Eu/(0.5Sm+0.5Gd))_{SN}$ (Johannesson et al., 2014) and $(Eu/(0.67Sm+0.33Tb))_{SN}$ (Kamber and Webb, 2001). Pr/Pr* anomaly was expressed as $(Pr/(0.5Ce+0.5Nd))_{SN}$,(Bau and Dulski, 1996). Additionally, we calculated $(Pr/Yb)_{SN}$ (Bolhar and Van Kranendonk, 2007; Corkeron et al., 2012), $(La/Yb)_{SN}$ (Barrat et al., 2000), $(Nd/Yb)_{SN}$ (Webb and Kamber, 2000) and $(Pr/Sm)_{SN}$ (Bolhar and Van Kranendonk, 2007) to describe the LREE (light rare earth elements) enrichment of microbialites. We calculated the $(Sm/Yb)_{SN}$ ratio to describe the MREE (middle rare earth elements) enrichment of microbialites (Bolhar and Van Kranendonk, 2007). We calculated the $(Yb/Nd)_{SN}$ ratio to describe the HREE (heavy rare earth elements) enrichment of microbialites. In addition, we calculated the non-normalized Nd/Yb ratio, used by Webb and Kamber (2000) to compare this ratio with that of seawater (between 2.69 and 3.22 in South Pacific) (Zhang and Nozaki, 1996). Finally, the Y/Ho ratio was determined and compared with that of chondrites (*i.e.*, 26-28; Kamber and Webb, 2001).

Several anomalies (*i.e.*, Eu/Eu*, Gd/Gd*, Ce/Ce*, La/La*) used to describe REE+Y patterns have varying expressions in the literature. We observed that most of the varying expressions of a given anomaly were highly correlated between each other (Fig. SI-6). However, one of the expression for the La/La* anomaly $(La/(2Ce-Pr))_{SN}$ was not correlated with the other two (r_S=–0.06 with the expression $(La/(3Pr-2Nd))_{SN}$ and –0.13 with the expression $(La/(Pr^3/Nd^2))_{SN}$). As expected, the four variables describing an enrichment in LREE (light rare earth elements), *i.e.*, $(La/Yb)_{SN}$, $(Pr/Yb)_{SN}$, $(Nd/Yb)_{SN}$ and $(Pr/Sm)_{SN}$ shale normalized ratios, were

positively correlated ($r_s \geq 0.88$). These four variables were correlated with $(Sm/Yb)_{SN}$ ($r_s \geq 0.78$) describing the MREE (middle rare earth elements) enrichment of microbialites and negatively correlated with $(Yb/Nd)_{SN}$ ($r_s \geq -0.89$), which measures the HREE (heavy rare earth elements) enrichment of microbialites. The Ce/Ce* anomaly $(Ce/(2Pr-Nd))_{SN}$ was positively correlated with the La/La* anomaly $(La/((Pr^3/Nd^2))_{SN}$ ($r_s=0.84$) and negatively correlated with the Pr/Pr* anomaly $(Pr/(0.5Ce+0.5Nd))_{SN}$ ($r_s=-1$) (Fig. SI-6).

Microbialite sample	La/La* (3Pr-2Nd)	La/La* (2Ce-Pr)	La/La* (Pr^3/Nd^2)	Ce/Ce* (0.5La+0.5Pr)	Ce/Ce* (2Pr-Nd)	Ce/Ce* $(La*Pr)^{1/2}$	Gd/Gd* (2Tb-Dy)	Gd/Gd* (Tb^2/Dy)	Eu/Eu* (0.5Sm+0.5Gd)	Eu/Eu* (0.67Sm+0.33Tb)	Pr/Pr* (0.5Ce+0.5Nd)
AL13	1.03	1.15	1.01	0.94	0.95	0.94	1.08	1.07	1.55	1.56	1.02
AL69-2m	1.05	1.67	1.02	0.82	0.84	0.82	0.81	0.81	1.47	1.37	1.08
AL60-6m	0.86	1.33	0.86	0.89	0.83	0.89	0.96	0.95	1.61	1.61	1.09
AL54-11m	0.90	1.26	0.90	0.90	0.86	0.91	1.05	1.05	1.50	1.51	1.07
AL2012-1m	0.98	1.14	0.97	0.94	0.94	0.95	1.30	1.26	2.26	2.35	1.03
AL2012-5m	1.75	1.08	1.43	0.97	1.22	0.97	1.15	1.15	1.88	1.95	0.92
AL2012-10m	0.98	1.00	0.97	1.00	0.99	1.00	1.08	1.07	2.06	2.14	1.00
AL2012-15m	1.02	4.51	0.97	0.66	0.67	0.67	1.20	1.18	2.26	2.30	1.17
AL2012-12	1.71	1.84	1.25	0.80	0.98	0.81	0.84	0.84	2.35	2.19	1.01
AL2012-15	1.05	1.26	1.03	0.90	0.92	0.90	0.89	0.89	3.87	3.73	1.04
AL2012-17	1.08	1.38	1.07	0.86	0.90	0.86	1.81	1.66	9.03	10.04	1.05
AL2014-13	1.12	1.43	1.06	0.86	0.91	0.87	1.17	1.17	1.93	2.03	1.04
AL2014-15	1.39	1.61	1.21	0.83	0.95	0.83	0.99	0.99	2.52	2.50	1.02
ATX-2C1-2012	1.19	1.27	1.14	0.90	0.97	0.90	0.96	0.96	1.64	1.66	1.01
ATX2014-07	1.79	1.57	1.37	0.83	1.05	0.83	1.06	1.04	2.68	2.67	0.98
ATX2014-13	1.15	1.24	1.07	0.91	0.97	0.92	1.16	1.14	1.74	1.77	1.01
Preciosa-05-2012	1.01	1.02	1.01	0.99	0.99	0.99	1.00	1.00	1.60	1.60	1.00
Preciosa-06-2012	1.14	1.04	1.11	0.98	1.04	0.98	1.02	1.02	2.18	2.16	0.98
Pr2014-01	1.15	1.05	1.13	0.97	1.04	0.97	1.08	1.08	2.08	2.08	0.98
Pr2014-02	1.11	1.05	1.09	0.98	1.03	0.98	0.97	0.96	2.43	2.32	0.99
Pr2014-03	1.02	1.07	1.02	0.97	0.98	0.97	1.05	1.05	1.45	1.45	1.01
Pr2014-09	1.11	1.41	1.03	0.87	0.91	0.88	1.16	1.06	2.62	2.51	1.04
Quechulac-1A-2012	1.03	1.79	0.97	0.81	0.82	0.82	0.89	0.89	3.19	3.09	1.08
Quechulac-4A-2012	0.96	3.47	0.87	0.72	0.71	0.74	0.97	0.96	2.43	2.36	1.14
Quechulac-4B-2012	1.10	1.17	1.06	0.93	0.97	0.94	0.97	0.97	2.32	2.30	1.01
Quechulac-4C-2012	1.28	1.35	1.10	0.89	0.98	0.90	1.17	1.13	3.02	2.97	1.01
Tec2014-05a	1.13	0.94	1.04	1.03	1.08	1.04	1.13	1.09	1.44	1.42	0.97
Tec2014-05b	1.08	1.07	1.06	0.97	1.01	0.97	1.00	1.00	1.68	1.68	1.00
AlbEsp2014-01	1.02	-3.22	0.95	0.45	0.46	0.46	1.02	1.01	1.69	1.65	1.30
Patz2014-02	1.18	2.08	1.02	0.78	0.84	0.80	1.09	1.05	1.38	1.37	1.07
Aljo2014-02	1.09	1.25	1.04	0.91	0.95	0.91	1.07	1.07	1.64	1.65	1.02
LaAlb2014-02	1.13	1.18	1.09	0.93	0.98	0.93	1.04	1.04	1.66	1.67	1.01

Table SI-1-1.
REE anomalies. The detailed expression of each anomaly is reported. For example, La/La* is defined as La/(3Pr-2Nd). SN stands for the shale-normalized data (normalization against the Post-Archean Australian Shale) after Pourmand et al. (2012).

Microbialite sample	Y/Ho	Nd/Yb	$(Sm/Yb)_{SN}$	$(Pr/Yb)_{SN}$	$(La/Yb)_{SN}$	$(Pr/Sm)_{SN}$	$(Nd/Yb)_{SN}$	$(Yb/Nd)_{SN}$
AL13	28.42	8.60	0.90	0.64	0.55	0.71	0.69	1.44
AL69-2m	34.15	7.30	0.75	0.53	0.45	0.71	0.59	1.70
AL60-6m	31.44	11.61	1.12	0.93	0.78	0.83	0.94	1.07
AL54-11m	30.33	9.66	0.97	0.77	0.66	0.79	0.78	1.28
AL2012-1m	30.40	6.92	0.70	0.53	0.45	0.75	0.56	1.79
AL2012-5m	33.33	8.50	0.77	0.56	0.53	0.72	0.69	1.46
AL2012-10m	36.56	23.21	1.90	1.99	2.20	1.05	1.87	0.53
AL2012-15m	37.56	6.48	0.82	0.46	0.36	0.57	0.52	1.91
AL2012-12	33.31	5.09	0.56	0.32	0.25	0.58	0.41	2.44
AL2012-15	36.10	6.51	0.70	0.49	0.44	0.70	0.53	1.90
AL2012-17	58.00	3.00	0.42	0.23	0.23	0.56	0.24	4.13
AL2014-13	31.08	7.08	0.76	0.51	0.42	0.67	0.57	1.75
AL2014-15	31.54	5.95	0.64	0.40	0.34	0.63	0.48	2.08
ATX-2C1-2012	35.59	8.65	0.90	0.63	0.57	0.70	0.70	1.43
ATX2014-07	32.73	4.76	0.55	0.31	0.26	0.55	0.38	2.60
ATX2014-13	30.93	7.79	0.76	0.55	0.45	0.72	0.63	1.59
Preciosa-05-2012	31.69	9.42	0.83	0.75	0.74	0.90	0.76	1.32
Preciosa-06-2012	31.46	7.76	0.71	0.57	0.54	0.81	0.63	1.60
Pr2014-01	27.11	10.33	0.94	0.77	0.73	0.82	0.83	1.20
Pr2014-02	29.33	10.29	0.90	0.78	0.75	0.86	0.83	1.20
Pr2014-03	27.64	11.32	1.03	0.87	0.82	0.84	0.91	1.09
Pr2014-09	35.74	2.62	0.35	0.18	0.14	0.52	0.21	4.73
Quechulac-1A-2012	39.88	6.23	0.65	0.44	0.34	0.68	0.50	1.99
Quechulac-4A-2012	37.47	6.98	0.72	0.48	0.31	0.66	0.56	1.78
Quechulac-4B-2012	34.60	9.03	0.86	0.66	0.57	0.77	0.73	1.37
Quechulac-4C-2012	39.42	5.94	0.58	0.40	0.30	0.69	0.48	2.09
Tec2014-05a	34.90	5.37	0.53	0.37	0.29	0.71	0.43	2.31
Tec2014-05b	28.52	11.45	1.02	0.85	0.76	0.83	0.92	1.08
AlbEsp2014-01	34.68	8.29	0.76	0.58	0.42	0.76	0.67	1.50
Patz2014-02	36.07	4.86	0.52	0.33	0.23	0.63	0.39	2.55
Aljo2014-02	31.48	9.52	0.89	0.68	0.56	0.76	0.77	1.30
LaAlb2014-02	28.36	11.11	1.05	0.81	0.73	0.78	0.90	1.12

Table SI-1-1. Continued.

Text SI-2. Geochemical signatures of detrital contamination in microbialites

It is of first importance to identify the chemical signatures of detrital contamination and defining thresholds below which such contamination is not affecting the chemical signature of the authigenic fraction of microbialites. This is crucial if one intends to use the mineralogy and chemistry of microbialites as reliable proxies for their formation environments. Modern and past lacustrine microbialites have often been mentioned to be affected by important detrital contamination, which obscures the message conveyed by their REE+Y composition (Solari et al., 2010; Álvaro et al., 2010; Sarg et al., 2013; Gallois et al., 2018). Previous studies have followed different strategies to limit issues due to contamination by terrigenous detritus: 1) analysis of the REE+Y composition of the carbonate fraction only, after its dissolution and/or 2) checking the low bulk content of samples in some specific chemical elements tracing detrital contamination (*e.g.*, Sc, Th, Hf, Zr) (Webb and Kamber, 2000; Frimmel, 2009; Kamber et al., 2014). Here, we followed the second strategy.

Several samples of Mexican microbialites were clearly affected by detrital contamination. This contamination was assessed based on PCA analyses of the bulk chemical composition of the microbialites, especially their content in Al as well as in elements strongly correlated with Al: Ga, Nb, Ta, K, Rb, Hf and Zr (Fig. 8 in the Main text). All these elements have been used before as tracers of the contribution of detrital particles (Weaver, 1967; Gertsch et al., 2011; Bassetti et al., 2016). They are all lithophile, except Ga, which is chalcophile but can replace Al or Fe in amphibole, feldspar, mica and clay minerals (Salminen et al., 2005). Nb, Ta, Hf and Zr are high field strength elements (HFSE), *i.e.*, they have high cationic charges and small ionic radii and are immobile during alteration (Babechuk et al., 2015). K and Rb are large ion lithophile elements (LILE) with a low cationic charge and a large ionic radius, and are considered as mobile during weathering processes because of their high hydration energies.

Three microbialites (LaAlb2014-02, Pr2014-03 and Tec2014-05b) were identified as highly affected by input of detrital particles with a content in Al, Ga, Nb, Ta, K, Rb, Hf and Zr significantly higher than that of all other samples. Eleven microbialites, clustered in an "intermediate" group as moderately affected by detrital contamination. Last, 18 samples clustered as a group of authigenic-dominated microbialites (Fig. 8 in the Main text). Consistently, all three microbialite samples identified as strongly affected by detrital inputs contained plagioclase grains and LaAlb2014-02 also contained quartz and pyroxene as shown by XRD analyses (Fig. SI-3d)

and SEM-EDXS (data not shown). In contrast, no detrital phase was detected by SEM, XRD and FTIR in the group of authigenic-dominated microbialite samples. Microbialites clustering in the authigenic-dominated microbialite group showed concentrations in Al≤0.27 wt.%, Ga≤0.97 ppm, Nb≤0.35 ppm, Ta≤0.027 ppm, K≤0.07 wt.%, Rb≤2.70 ppm, Hf≤0.157 ppm and Zr≤6.54 ppm.

Interestingly, the 3 samples strongly affected by detrital contamination showed different contents in the different elements tracing detritism (Fig. 8b in the Main Text). This suggests that they were affected by different sources of contamination. The LaAlb2014-02 microbialite had relatively higher Nb and Ta contents, while Pr2014-03 had higher K and Rb contents and Tec2014-05b had higher Hf and Zr contents. Nb and Ta are highly incompatible elements and may reach high concentrations in evolved rocks (Dostal and Chatterjee, 2000). As shown by the XRD pattern of LaAlb2014-02, feldspar is one of the main minerals observed in this sample and could be associated with Nb and Ta as also described by Larsen (2002). Since K and Rb are easily lost during weathering processes (Nath et al., 2000), the relatively higher concentration of these elements in Pr2014-03 may indicate that this microbialite was contaminated by detrital particles, which have experienced a low intensity of weathering. Last, Zr and Hf are mostly concentrated in heavy minerals and in the coarse (silt-sand) fraction of fine-grained siliciclastic sediments, while Rb is mainly in the fine-grained fraction (Condie, 1991; Fralick and Kronberg, 1997; Dypvik and Harris, 2001). How different detrital contaminations can be traced by these elements remain however to be further understood.

Text SI-3. REE+Y patterns of microbialites depending on their level of contamination by detrital particles

As mentioned in the main text, the ΣREE content of microbialites was positively correlated with their Al content (Fig. SI-3-1), and there were clear correlations between the Al content of microbialites and several REE anomalies, in particular in Eu, Ce, Pr, La and/or Gd, their Y/Ho ratio and the HREE to LREE enrichment [$(Yb/Nd)_{SN}$]. Three categories of microbialites were discriminated based on their content of detritism-indicative elements: authigenic-dominated microbialites, microbialites intermediately affected by detrital contamination and microbialites highly affected by detrital contamination. Here, we detail their respective REE+Y signatures.

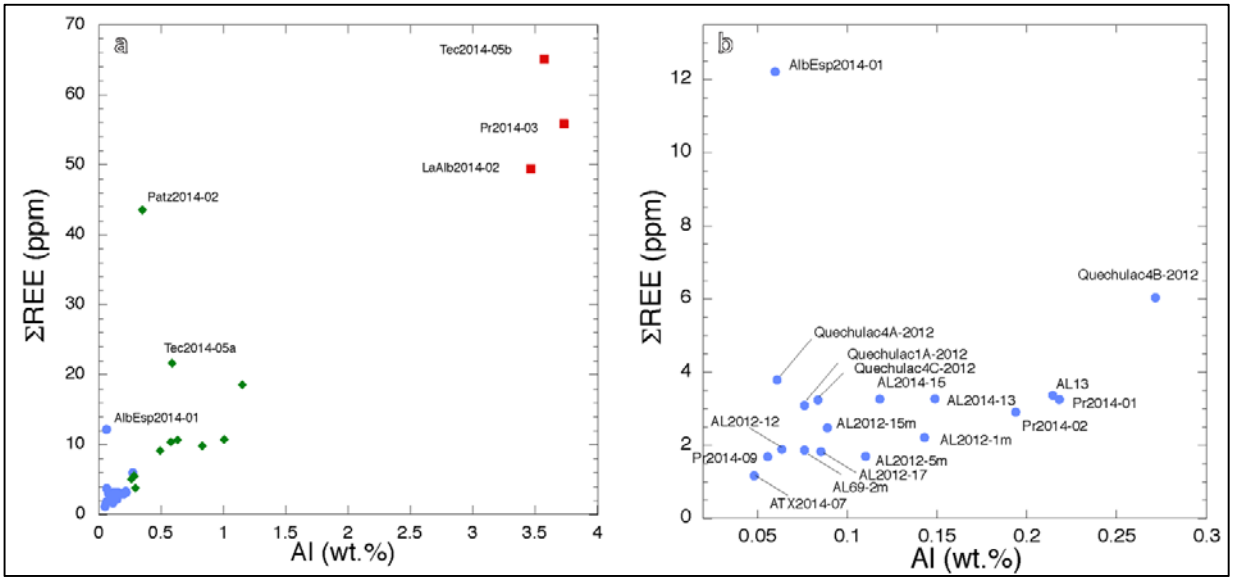

Figure SI-3-1.
Aluminum content versus sum of REEs(+Y) of the studied microbialites. (**a**) All the samples showing a positive correlation (r_S=0.81). (**b**) Only the authigenic-dominated samples are plotted, showing no significant positive correlation (r_S=0.39). Blue dots stand for 18 microbialites poorly concentrated in Al (authigenic-dominated); red squares correspond to microbialites highly affected by detrital contamination; green diamonds stand for intermediately contaminated microbialites considered in this study as moderately affected by detrital input.

A PCA was performed on the group of authigenic-dominated microbialites considering the set of 20 variables describing REE+Y patterns of microbialites (Fig. SI-3-2).

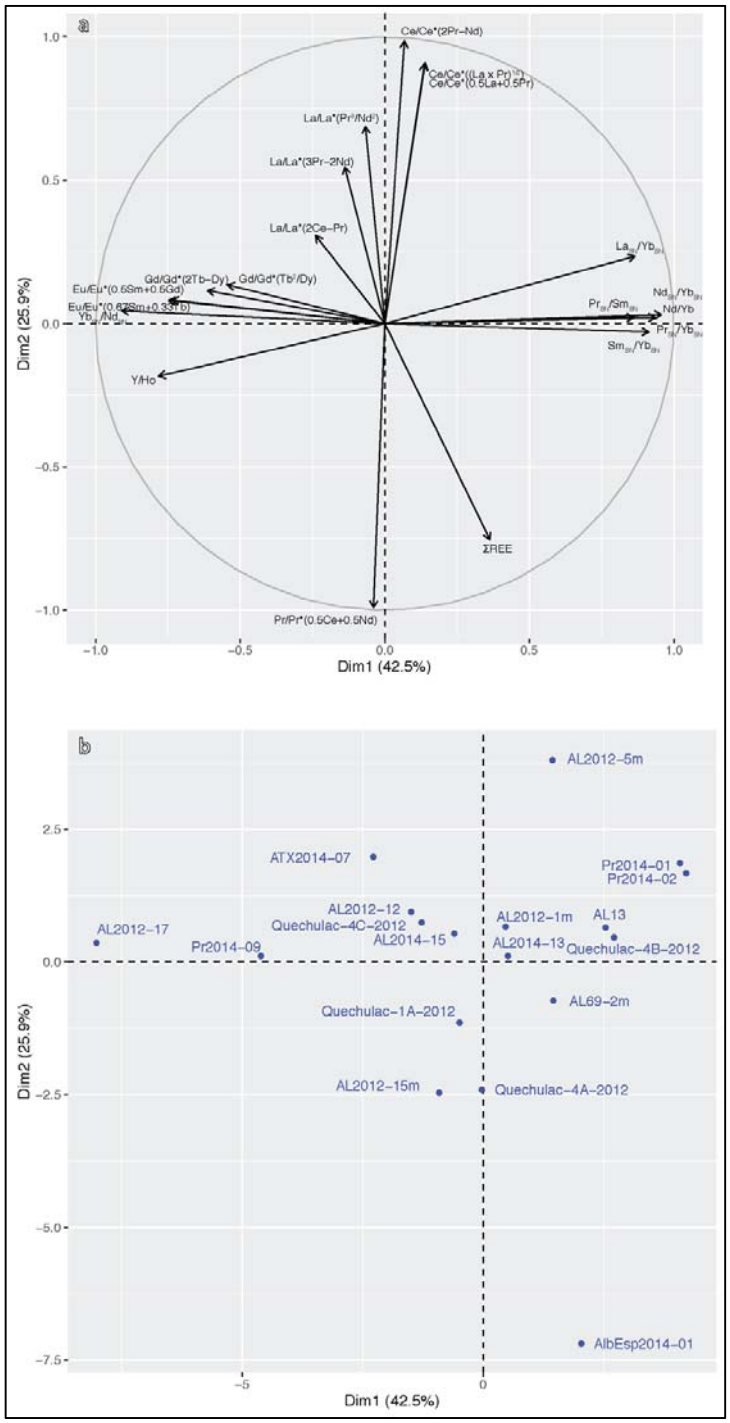

Figure SI-3-2.

PCA performed on the group of the 18 authigenic-dominated microbialite samples. (**a**) PCA variables factor map representing the 20 variables describing the REE+Y patterns of microbialites. Eu/Eu* anomalies, Y/Ho and variables describing the enrichment in LREE ($(La/Yb)_{SN}$, $(Pr/Sm)_{SN}$, $(Pr/Yb)_{SN}$, Nd/Yb), MREE ($(Sm/Yb)_{SN}$) and HREE ($(Yb/Nd)_{SN}$), contributed significantly to axis 1 (explaining 42.5% of the total variability). The Pr/Pr* anomalies, ΣREE, all the Ce/Ce*

anomalies, and the 2 expressions of La/La* anomalies significantly contributed to axis 2 (explaining 25.9% of the total variability). (**b**) PCA plot with samples plotted in two dimensions using their projections onto the first two principal components. The AL2012-17, Pr2014-09, Pr2014-01 and Pr2014-02 microbialite samples contributed significantly to axis 1. The AlbEsp2014-01, Quechulac-4A-2012, AL2012-15m and AL2012-5m microbialite samples contributed significantly to axis 2.

For microbialites highly affected by detrital contamination (Al≥3.46 wt.%, *e.g.*, Tec2014-05b, Pr2014-03 and LaAlb2014-02 samples), there was no HREE to LREE enrichment, as expected (Fig. SI-3-3a). For microbialites intermediately affected by detrital contamination, the AL2012-10m microbialite stood out of the relationship and showed a pronounced LREE enrichment with a $(Yb/Nd)_{SN}$ ratio of 0.53 (Fig. SI-3-3a and Table SI-11). For authigenic-dominated microbialites, HREE to LREE enrichment (*i.e.*, $(Yb/Nd)_{SN}$) ranged between 1.20 for Pr2014-01 and Pr2014-02 up to 4.73 for Pr2014-09 (Fig. SI-3-3b).

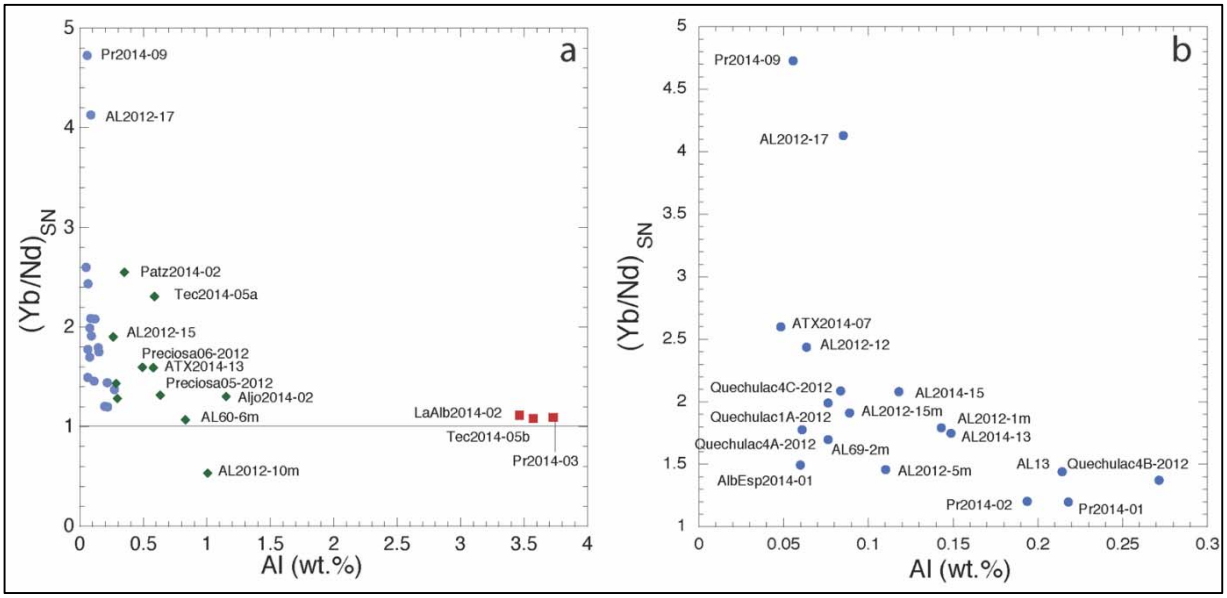

Figure SI-3-3.
Shale-normalized $(Yb/Nd)_{SN}$ ratio of microbialites indicating an enrichment in HREE, *versus* Al content. Samples with high detrital contamination: red squares; "intermediately" contaminated samples: green diamonds; authigenic-dominated samples: blue circles. (**a**) All samples. Microbialites strongly affected by detrital contamination (red squares) show a $(Yb/Nd)_{SN}$ close to 1 and a variability in HREE enrichment significantly lower compared to both intermediately contaminated samples ($p=0.0056$) and samples the least affected by detrital contamination ($p=0.0019$). (**b**) Close-up on the group of authigenic-dominated samples showing a negative correlation of $(Yb/Nd)_{SN}$ with the microbialite Al content (r_s=-0.68).

Microbialites systematically showed positive Eu anomalies. When the microbialites were Al-rich, their Eu anomaly were close to 1.6, while Eu/Eu* were more variable for the other samples, reaching 9.03 for AL2012-17, an authigenic-dominated microbialite (Fig. SI-3-4a). In addition, considering specifically the group of authigenic-dominated microbialites, Eu/Eu* was positively correlated (r_s=0.61) with their Ca content (Fig. SI-3-4b). As a result, microbialites from Lake Quechulac, AL2014-13, AL2014-15, Pr2014-09, Pr2014-01, Pr2014-02, which were composed of aragonite as the main carbonate phase showed the highest Eu/Eu* values. In contrast, Mg-rich microbialites dominated by hydromagnesite (*i.e.,* microbialite samples AL2012-12, AL2012-1m and AL13) showed lower Eu/Eu* values (Fig. SI-3-4b). AL2012-17 sample departed from this trend with a very high Eu/Eu* compared to the other samples rich in aragonite (Fig. SI-3-4b). Moreover, for these microbialites, we observed a particularly clear positive correlation between Eu/Eu* (with Eu*=0.5Sm+0.5Gd) and the HREE enrichment of microbialites (r_s=0.69) (Fig. SI-3-4c).

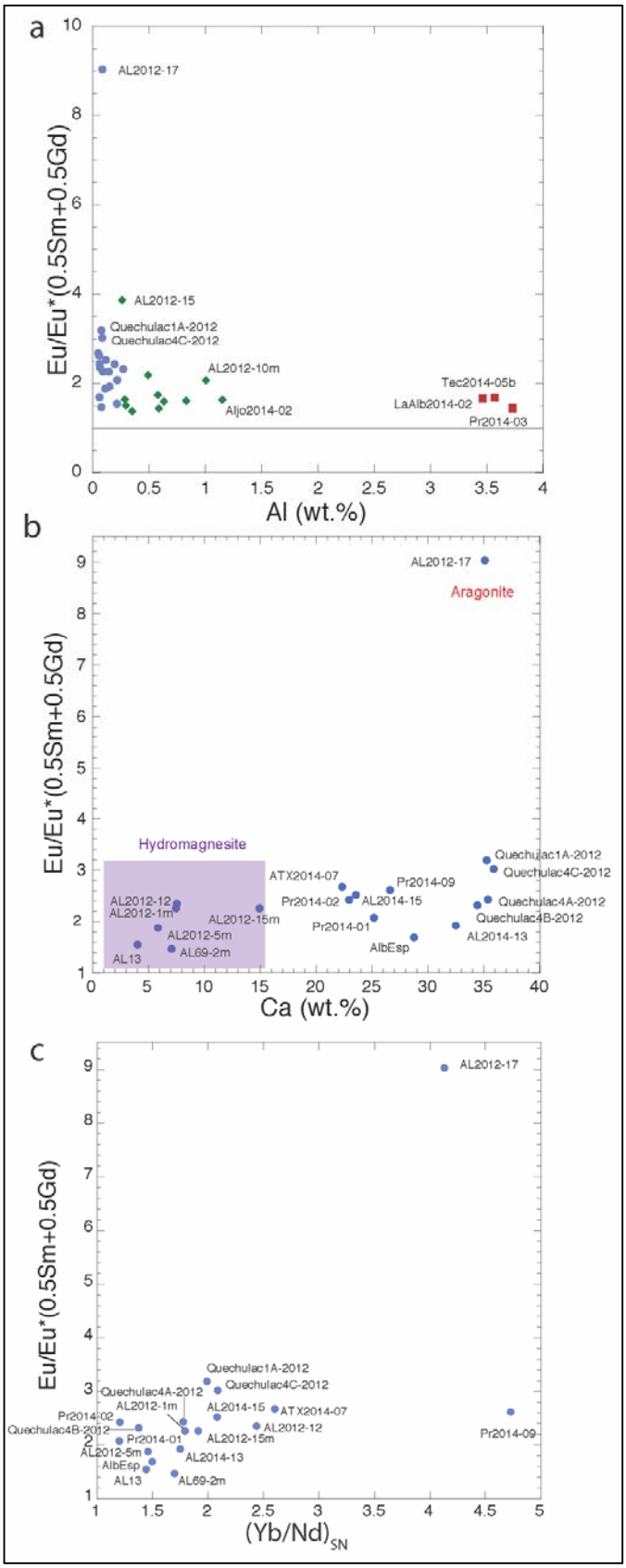
a
Eu/Eu*(0.5Sm+0.5Gd)
Al (wt.%)
AL2012-17
AL2012-15
Quechulac1A-2012
Quechulac4C-2012
AL2012-10m
Aljo2014-02
Tec2014-05b
LaAlb2014-02
Pr2014-03
b
Eu/Eu*(0.5Sm+0.5Gd)
Ca (wt.%)
AL2012-17
Aragonite
Hydromagnesite
Quechulac1A-2012
Quechulac4C-2012
ATX2014-07
Pr2014-09
AL2012-12
AL2012-1m
Pr2014-02
AL2014-15
Quechulac4A-2012
AL2012-15m
Pr2014-01
Quechulac4B-2012
AL2012-5m
AL2014-13
AlbEsp
AL69-2m
AL13
c
Eu/Eu*(0.5Sm+0.5Gd)
(Yb/Nd)SN
AL2012-17
Quechulac1A-2012
Quechulac4C-2012
Quechulac4A-2012
AL2012-1m
AL2014-15
ATX2014-07
Pr2014-02
Quechulac4B-2012
Pr2014-01
AL2012-15m
AL2012-12
Pr2014-09
AL2012-5m
AL2014-13
AlbEsp
AL13
AL69-2m

Figure SI-3-4.
Scatter plots of Europium anomaly *versus* other chemical parameters. Samples with high detrital contamination: red squares; "intermediately" contaminated samples: green diamonds; authigenic-dominated samples: blue circles. (**a**) Eu/Eu* *versus* Al for all microbialites. Microbialites the least affected by detrital contamination exhibited a broader variability of the (positive) Eu anomaly compared to both intermediately contaminated samples (p=0.026) and samples strongly affected by detrital contamination (p=0.037). (**b**) Eu/Eu* *versus* Ca for the authigenic-dominated samples. There is a linear relationship between the Ca content of the microbialites and the Eu anomaly except for AL2012-17. **(c**) Eu/Eu * *versus* $(Yb/Nd)_{SN}$ (HREE enrichment) for the authigenic-dominated samples. Eu anomaly is positively correlated with $(Yb/Nd)_{SN}$ (r_s =0.69).

Microbialites intermediately and strongly affected by detrital contamination showed constant Pr/Pr* values close to 1 except the “intermediate” samples AL60-6m, AL54-11m and Patz2014-02, which showed Pr/Pr* of 1.06-1.09 (Fig. SI-3-5a). By contrast, authigenic-dominated microbialites exhibited variable Pr anomalies (considering Pr/Pr* as $(Pr/(0.5Ce+0.5Nd))_{SN}$), higher than 1 for most of them, up to 1.30 for AlbEsp2014-01 and lower than 1 in several other cases (*e.g.*, 0.92 for AL2012-5m).

Most microbialites exhibited Ce anomalies (expressed as $Ce/Ce^*=(Ce/(0.5La+0.5Pr))_{SN}$) lower than 1 (negative anomalies), except the “intermediate” samples Tec2014-05a and AL2012-10m (1.03 and 1.00 respectively), (Fig. SI-3-5b). As already mentioned, the lower the Al content, the higher the Ce depletion, with Ce/Ce* as low as 0.45 for AlbEsp2014-01 (Table SI-11 and Fig. SI-3-5b). Most of the authigenic-dominated microbialites showed La anomalies (considering La/La* as $(La/(3Pr-2Nd))_{SN}$) higher than 1 (Fig. SI-3-5c). For example, positive La anomalies were remarkably high for the ATX2014-07, AL2012-5m and AL2012-12 microbialites, with values reaching 1.79, 1.75 and 1.71, respectively. Authigenic-dominated microbialites showed variable Gd anomalies (considering the anomaly $Gd/Gd^*=(Gd/(2Tb-Dy))_{SN}$) between 0.81 (AL69-2m) and 1.81 (AL2012-17), while microbialites highly affected by detrital contamination showed Gd/Gd* anomalies close to 1 (Fig. SI-3-5d).

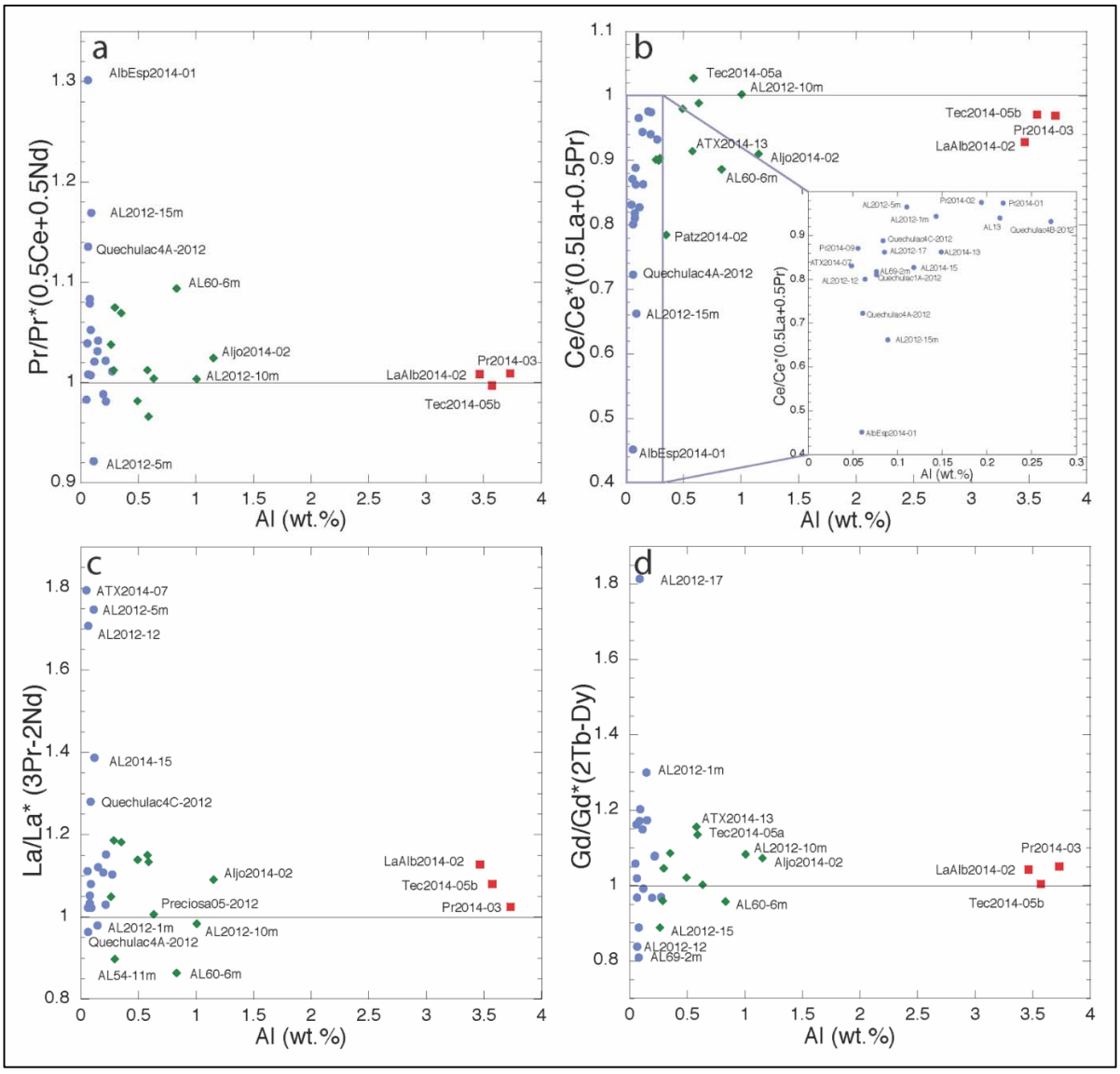

Figure SI-3-5.
Scatter plots of Pr, Ce, La and Gd REE anomalies versus the Al content of microbialites. Authigenic-dominated microbialites (Al-poor) show more variable Pr, Ce, La and Gd anomalies. (**a**) Al *versus* Pr/Pr*: broader variability of the anomaly within authigenic-dominated microbialites compared to samples strongly affected by detrital contamination (p=0.038); (**b**) Al *versus* Ce/Ce* and close-up showing a positive correlation between both parameters for the authigenic-dominated microbialites (r_s= 0.66); (**c**) Al *versus* La/La* (**d**) Al *versus* Gd/Gd*. Samples with strong detrital contamination: red squares; intermediately contaminated samples: green diamonds; Authigenic-dominated samples: blue dots. Authigenic-dominated microbialites exhibited a broader variability of the La and Gd anomalies compared to intermediate samples (p=0.021 and p=0.0073, respectively).

Finally, the Y/Ho ratio of microbialites also depended on the Al content of microbialites. Al-rich microbialites showed a chondritic Y/Ho ratio (26-28), while Al-poor microbialites had a more variable Y/Ho. In the latter case, the Y/Ho ranged from 27.1 (Pr2014-01) up to 58.0 (AL2012-17) (Table SI-11 and Fig. SI-3-6a). Again, considering authigenic-dominated microbialites, there was a negative correlation (r_S=-0.53) between Y/Ho and their Al content (Fig. SI-3-6b). In addition, similarly to the Eu/Eu* anomaly, Y/Ho was positively correlated with the Ca content of the authigenic-dominated microbialites (r_S=0.58) (Fig. SI-3-6c).

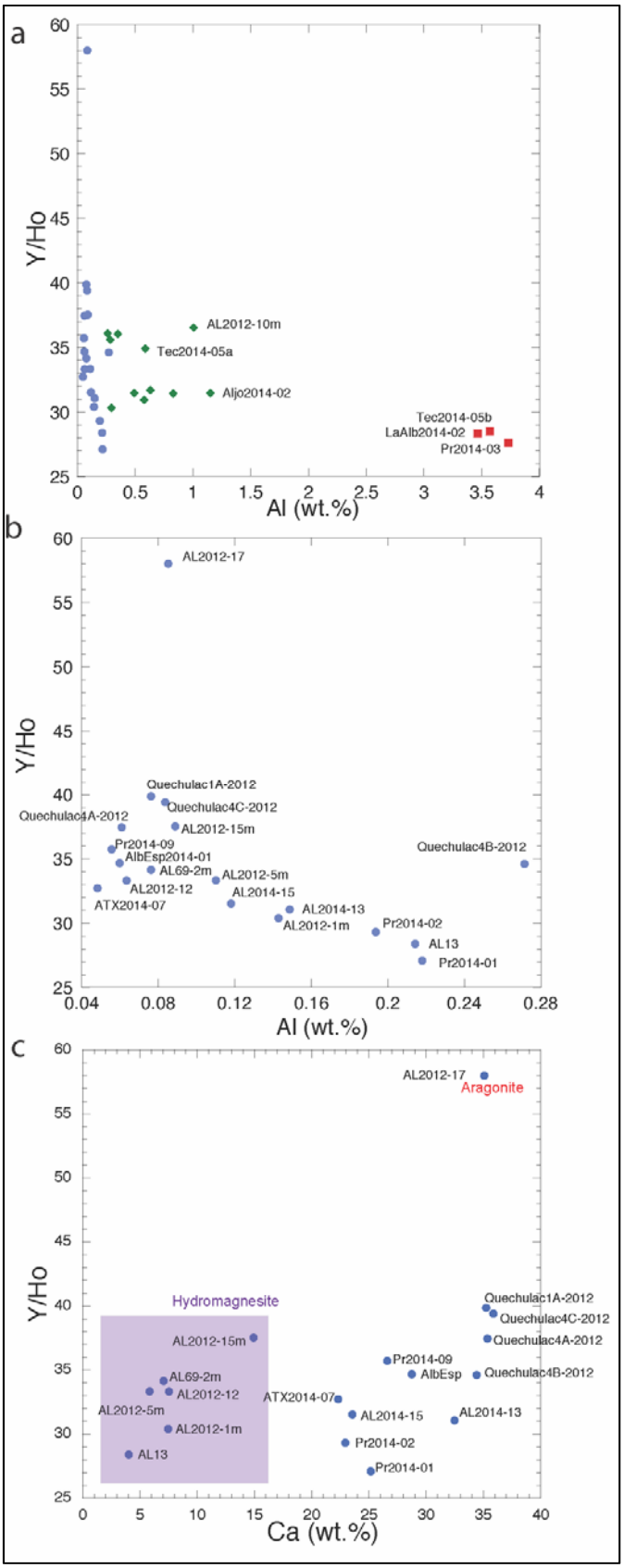
a
Y/Ho
Al (wt.%)
AL2012-10m
Tec2014-05a
Aljo2014-02
Tec2014-05b
LaAlb2014-02
Pr2014-03
b
Y/Ho
Al (wt.%)
AL2012-17
Quechulac1A-2012
Quechulac4C-2012
Quechulac4A-2012
AL2012-15m
Pr2014-09
AlbEsp2014-01
AL69-2m
AL2012-5m
AL2012-12
AL2014-15
ATX2014-07
AL2014-13
AL2012-1m
Pr2014-02
AL13
Pr2014-01
Quechulac4B-2012
c
Y/Ho
Ca (wt.%)
AL2012-17
Aragonite
Hydromagnesite
AL2012-15m
AL69-2m
AL2012-12
AL2012-5m
AL2012-1m
AL13
Quechulac1A-2012
Quechulac4C-2012
Quechulac4A-2012
Pr2014-09
AlbEsp
Quechulac4B-2012
ATX2014-07
AL2014-15
AL2014-13
Pr2014-02
Pr2014-01

Figure SI-3-6.
Scatter plots of the Y/Ho ratio versus the Al and Ca contents of microbialites. (**a**) Al *versus* Y/Ho for all microbialites: authigenic-dominated microbialites exhibited a broader variability of the (positive) Y/Ho anomaly compared to both intermediately contaminated samples (p=0.0076) and samples strongly affected by detrital contamination (p=0.028); (**b**) Close-up on the samples poorly affected by detrital contamination showing a non-significant negative correlation between Al content and Y/Ho ratio (r_S= -0.53). (**c**) Ca *versus* Y/Ho. Samples with high detrital contamination: red squares; Intermediately contaminated samples: green diamonds; Authigenic-dominated samples: blue dots.

Overall, microbialites highly affected by detritism showed a flat REE+Y pattern, grasped by, *e.g.*, a shale normalized Yb/Nd ratio close to 1. This is consistent with the results by Álvaro et al. (2010) who showed that lacustrine stromatolites from the Ediacaran Ouarzazate Supergroup (Anti-atlas, Morroco) had a flat REE+Y pattern with the lack of distinct REE anomalies and mentioned a potentially strong contamination of the stromatolites by andesites and andesitic/rhyolitic tuffs. The flat REE+Y patterns of these Ediacaran lacustrine stromatolites were associated with high REE+Y contents (between 26.0 and 30.6 ppm) and concentrations in Al, Ga, Nb, Ta, K, Rb, Hf and Zr higher than those measured in the Mexican microbialites. A similar flat REE+Y pattern with a lack of pronounced anomalies were described for a mixed carbonate-siliciclastic microbialite sample from the Upper Jurassic Pagny-sur-Meuse formation (France) (Olivier and Boyet, 2006).

One question is whether the authigenic-dominated microbialites are not affected by detrital contamination at all. There are contrasted views in the literature about how to assess whether detrital contamination affects REE signatures. For example, Zhao and Zheng (2017) suggested that marine carbonate samples with a Th content lower than 0.6 ppm had seawater-like REE+Y patterns, indicating a poor contribution by silicate contamination. In contrast, they observed that samples with [Th]>1.0 ppm showed higher REE+Y concentrations and shale-like REE+Y patterns. Consistently, Th correlated in our study with the 8 elements that we used as tracers of detritism and is therefore likely a good indicator of detritism (Fig. 8 in the main text). Mexican authigenic-dominated microbialites showed Th contents systematically lower than 0.22 ppm, *i.e.*, fitting with Zhao and Zheng's definition of poorly affected by contamination. In contrast, Li et al. (2019) suggested that a Zr content above 0.5 ppm in ooids was indicative of siliciclastic contamination as also attested by flat shale-normalized REE+Y patterns. Moreover, Webb and Kamber (2000)

suggested that very low contents in Th (<0.062 ppm), Hf (<0.007 ppm) and Sc (<0.429 ppm) in Heron microbialites were indicative of the absence of contamination by terrigenous detritus. In the latter case, these are not thresholds though. In our study, all the studied microbialite samples showed Zr contents higher than the one indicated by Li et al (2019), ranging between 1.28 ppm and 84.99 ppm but this was not associated with flat REE+Y patterns. Moreover, only three samples (AL2012-17, Pr2014-09 and ATX-2C1-2012) had Th concentrations below the values suggested by Webb and Kamber (2000) and all had Hf contents above 0.007 ppm. We cannot discuss Sc values since the detection limit of the ICP-MS measurements in our study (1 ppm) was above the value indicated by Webb and Kamber (2000).

No positive correlation was detected between the total REE+Y and Al contents of Mexican microbialites with an Al content lower than 0.27 wt.% (r_S=0.39; Fig. SI-3-1). Their total REE+Y content was lower than 3.8 ppm, excluding AlbEsp 2014-01 and Quechulac4B-2012 which had a total REE+Y content superior to some of the "intermediate" microbialite samples moderately affected by detrital contamination. Moreover, these samples showed a higher variability of the Gd, La, Eu and Pr anomalies, Y/Ho ratio and the HREE enrichment (see figures above). This suggests that the detrital contamination has a limited influence on their REE+Y patterns. Similarly, Li et al., (2019) noted that the variability of REE anomalies in marine and lacustrine ooids (Great Bahama Bank and the Great Salt Lake) poorly affected by siliciclastic contamination was higher than in ooids affected by detritism.

The lack of negative correlation between some elements tracing detritism (Zr, Sc, Th, Hf) and Y/Ho has been used by several studies as another indicator of poorly contaminated carbonates (Webb and Kamber, 2000; Bolhar and Van Kranendonk, 2007; Zhao and Zheng 2017). Here, considering the group of authigenic-dominated microbialites, we did not observe significant negative correlations between Y/Ho and Zr, Th, Hf, Ga, Al, and K (r_S<0.58). However, we observed a significant negative correlation between Y/Ho and Rb (r_S=-0.74) and between Y/Ho and Ta (r_S=-0.66). In addition, we observed that the Ce anomaly in authigenic-dominated microbialites was positively correlated with some of the chemical elements tracing detrital contamination (Al [r_S=0.66], Hf [r_S=0.65], Rb [r_S=0.61] and Nb [r_S=0.60]) (Fig. SI-6). The Ce content of microbialites was positively correlated with their Al content for all samples (r_S=0.9). Last, we observed a significant negative correlation between Al content and $(Yb/Nd)_{SN}$ (r_S=0.68;

Fig. SI-3-3). Overall, Rb, Ta and Ce contents, Ce anomaly and $(Yb/Nd)_{SN}$ might be the parameters the most sensitive to detrital contamination in the present study.

Text SI-4. Discussion about the potential origins of REE signatures of Mexican authigenic-dominated microbialites

As mentioned in the main manuscript, REE+Y patterns of Mexican authigenic-dominated microbialites showed (i) a relatively higher proportion of HREE, (ii) relatively high (positive or negative) anomalies in Eu, Ce, La, Gd and Pr and (iii) a high Y/Ho ratio (Text SI-3). By measuring the REE+Y composition of some lake solutions (Table SI-4-1), we could retrieve solid/solution fractionation patterns for these lakes (Fig. SI-4-1).

Aqueous Sample	La	Ce	Pr	Nd	Sm	Eu	Gd	Tb	Dy	Y	Ho	Er	Tm	Yb	Lu
AL2014_3m	<3E-07	<3E-07	<2E-07	9.50E-07	<1.3E-06	1.31E-06	2.55E-06	2.56E-07	1.23E-06	1.40E-06	3.62E-07	<9E-07	2.98E-07	1.51E-06	2.96E-07
Quechulac2014_0m_N	3.35E-06	3.97E-06	6.73E-07	2.94E-06	1.39E-06	6.47E-07	<1.5E-06	2.01E-07	1.10E-06	1.48E-05	2.56E-07	1.28E-06	2.30E-07	9.05E-07	2.14E-07
AlbEsp2014_0m	1.21E-06	< 3E-07	8.33E-07	9.85E-07	1.33E-06	3.80E-06	1.97E-06	3.62E-07	9.61E-07	1.40E-05	3.15E-07	1.51E-06	<2E-07	1.17E-06	2.30E-07
ATX2014_0m	1.88E-06	2.08E-06	5.32E-07	3.08E-06	2.29E-06	1.02E-06	3.08E-06	4.98E-07	2.62E-06	1.32E-05	5.67E-07	1.30E-06	4.63E-07	1.93E-06	3.38E-07
Preciosa2014_0m	5.42E-07	6.86E-07	<2E-07	<7E-07	<1.3E-06	4.42E-07	<1.5E-06	<1.5E-07	8.01E-07	4.30E-06	<2E-07	<9E-07	2.24E-07	7.59E-07	1.39E-07

Table SI-4-1.
REE+Y concentrations (ppm) of some of the aqueous solutions.

Cerium is sensitive to changes in the redox conditions of water because oxidized Ce is tetravalent, less soluble and more easily absorbed onto particles (De Baar et al., 1988; Bolhar and Van Kranendonk, 2007). Negative Ce anomalies (also expressed as $Pr/Pr^*_{SN}>1$) are therefore commonly interpreted as indicative of oxygenated conditions at the time of the deposition (De Baar et al., 1988; Kamber and Webb, 2001). Most of the Mexican authigenic-dominated microbialites showed negative Ce anomalies. The solid/solution fractionation patterns show a high Ce fractionation to the solid (Fig. SI-4-1), which might be well explained by incorporation of detrital particles, even in authigenic-dominated samples (Text SI-3). This suggests that in the absence of detrital contamination, one may expect even stronger negative anomalies. Overall, such negative anomalies are consistent with the oxidized conditions observed at shallow depth in the lakes. However, AL2012-5m showed a marked positive Ce anomaly (Text SI-3). This anomaly could be a record of a poorly oxygenated environment at this depth during microbialite formation. Such an anomaly may record periods of water mixing of the lake in December/January

(corresponding to the sampling period of this sample, *i.e.*, January 2012), when anoxic water from the bottom of Lake Alchichica mixes with top water, resulting in lower oxygen fugacity (Macek et al., 2009). Alternatively, this anomaly may record the input of poorly oxygenated groundwater fluids at or close to the formation site of this sample. No positive Ce anomaly (*i.e.*, indicative of anoxic water conditions) was observed for the Fe-rich microbialites, although they potentially formed with the input of anoxic groundwaters. Biological activity surely impacts the redox state of the pore solution at the lithified biofilm/biofilm interface possibly explaining the lack of Ce-positive anomaly for most of the samples.

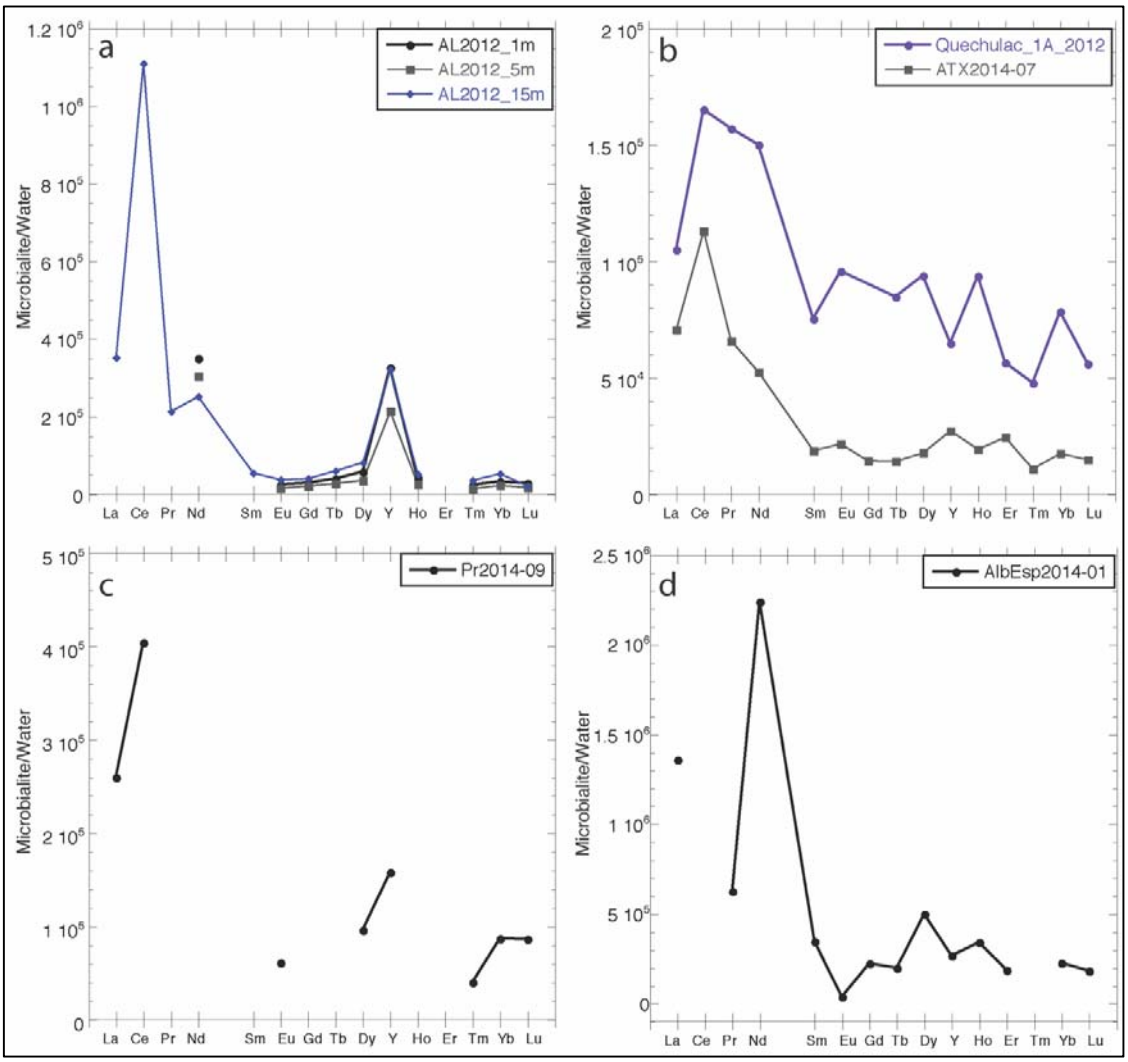

Figure SI-4-1.
REE microbialite/solution fractionation patterns calculated from the analyses of the authigenic-dominated microbialites. The patterns are not flat suggesting fractionation during the incorporation of these elements into the microbialites.

All studied microbialites showed a positive Eu anomaly. Moreover, no strong Eu enrichment of the solid could be seen compared to the solution (Fig. SI-4-1), *i.e.,* water also showed this positive Eu anomaly. The marine positive Eu anomaly is classically interpreted as related to an input of hydrothermal fluids, which have leached basalts under hot and acidic conditions at mid-oceanic ridges (Derry and Jacobsen, 1990; Danielson et al., 1992; Bolhar and Van Kranendonk, 2007). The outflow of underground fluids has been shown to occur at/or close to the location of microbialite formation (Kaźmierczak et al., 2011; Zeyen et al., 2019). In agreement, Lim et al. (2009) and Warden et al. (2019) emphasized the importance of groundwater flow for the formation of microbialites. Other lakes populated by microbialites such as Lake Van, Mono Lake, Lake Walyungup and Great Salt Lake are impacted by groundwater discharge (Kempe et al., 1991; Bischoff et al., 1993; Coshell et al., 1998; Bouton et al., 2016). Moreover, we note that Eu anomalies [Eu/Eu*, Eu* as (0.5Sm+0.5Gd)] were positively correlated with Ca (r_S=0.61), Sr (r_S=0.69), U (r_S=0.59) and to a lesser extent Ba (r_S=0.48) in authigenic-dominated microbialites. Since these elements are preferentially enriched in aragonite (Thompson and Livingston, 1970; Dietzel et al., 2004), this suggests that positive Eu anomalies may be mostly carried by aragonite rather than hydromagnesite or Mg-silicate. Interestingly, the non-living microbialite AL2012-17 combined the highest Eu anomaly (9.03), the highest Gd anomaly (1.81) and the highest Y/Ho ratio (58.00) with the highest Fe concentration (2.49 wt.%) among the studied microbialites. Since Fe enrichment within shallow microbialites might originate from groundwater seepage derived from adjacent Fe-rich volcanic rocks (Zeyen et al., 2019), Eu and Gd positive anomalies and high Y/Ho ratio within microbialites might together be good indicators of seepage of anoxic Fe-bearing groundwater into the lakes.

Last, authigenic-dominated microbialites were enriched in HREE relatively to LREE. Yet, LREE are expected to be scavenged preferentially by the solids because HREE form stronger aqueous complexes with carbonate ions (De Baar et al., 1988, Smrzka et al., 2019). Interestingly, Takahashi et al. (2007) observed a preferential incorporation of HREE *versus* LREE in some biofilms and Takahashi et al. (2005) showed that Tm, Yb and Lu can be particularly highly complexed and concentrated by carboxylate and phosphate groups at the surface of bacterial cells. Similarly, Johannesson et al. (2014) observed a fractionation between Cuatro Cienegas microbialites and ambient continental water with preference for HREE. Such processes may therefore help understanding the HREE enrichment in Mexican microbialites. However, when

assessing the solid/solution fractionation of REE in Mexican lakes, we did not observe a preferential HREE incorporation but a general stronger incorporation of LREE *versus* HREE with some specific strong fractionations of some elements depending on the lakes (Fig. SI-4-1). This suggests that the overall microbialite patterns are controlled by that of the solution. The Y/Ho anomaly was correlated with the Ca content of the microbialites (r_S=0.58) and therefore microbialite samples composed of aragonite showed the highest Y/Ho (from 37.5 to 58.0), while microbialites mainly composed of hydromagnesite showed lower Y/Ho values (from 28.4 to 37.6). The transition metal Y and the lanthanide Ho are often referred to as geochemical twins because they generally show little fractionation upon metamorphic or weathering processes, due to their closely similar chemical properties and nearly identical ionic radii (Leggett, 2017). However, Y strongly fractionates from Ho upon calcite or aragonite precipitation, especially in highly alkaline solutions with a faster uptake of Ho by the solid phase (Qu et al., 2009). From this observation, it could be postulated that massive Ca-carbonate precipitation in Mexican lakes may have resulted in a high increase of the Y/Ho ratio of the epilimnion where microbialites form. Microbialites rich in Ca may form under these conditions, while Mg-rich microbialites may form under conditions where such massive precipitation did not occur. Alternatively, we observed almost systematically a strong Y fractionation between microbialites and the solution, which was not observed for Ho. The molecular mechanisms responsible for this fractionation remain to be understood.

IV. REFERENCES

Álvaro J. J., Ezzouhairi H., Ayad N. A., Charif A., Solá R. and Ribeiro M. L. (2010) Alkaline lake systems with stromatolitic shorelines in the Ediacaran volcanosedimentary Ouarzazate Supergroup, Anti-Atlas, Morocco. *Precambrian Research* **179**, 22–36.

Aminot A. and Kérouel R. (2004) Hydrologie des écosystèmes marins. Paramètres et analyses. 74–78.

Babechuk M. G., Widdowson M., Murphy M. and Kamber B. S. (2015) A combined Y/Ho, high field strength element (HFSE) and Nd isotope perspective on basalt weathering, Deccan Traps, India. *Chemical Geology* **396**, 25–41.

Ball J.W. and Nordstrom D.K. (1991) User's manual for WATEQ4F, with revised thermodynamic data base and text cases for calculating speciation of major, trace, and redox elements in natural waters, *U. S. Geological Survey.*

Barrat J. A., Boulegue J., Tiercelin J. J. and Lesourd M. (2000) Strontium isotopes and rare-earth element geochemistry of hydrothermal carbonate deposits from Lake Tanganyika, East Africa. *Geochimica et Cosmochimica Acta* **64**, 287–298.

Bassetti M.-A., Berné S., Sicre M.-A., Dennielou B., Alonso Y., Buscail R., Jalali B., Hebert B. and Menniti C. (2016) Holocene hydrological changes in the Rhône River (NW Mediterranean) as recorded in the marine mud belt. *Climate of the Past* **12**, 1539–1553.

Bau M. and Dulski P. (1996) Distribution of yttrium and rare-earth elements in the Penge and Kuruman iron-formations, Transvaal Supergroup, South Africa. *Precamb. Res.* **79**, 37–55

Bischoff J. L., Stine S., Rosenbauer R. J., Fitzpatrick J. A. and Stafford Jr T. W. (1993) Ikaite precipitation by mixing of shoreline springs and lake water, Mono Lake, California, USA. *Geochimica et Cosmochimica Acta* **57**, 3855–3865.

Blanc P., Lassin A., Piantone P., Azaroual M., Jacquemet N., Fabbri A. and Gaucher E.C. (2012). Thermoddem: A geochemical database focused on low temperature water/rock interactions and waste materials. *Applied Geochemistry* **27**, 2107-2116.

Bolhar R. and Van Kranendonk M. (2007) A non-marine depositional setting for the northern Fortescue Group, Pilbara Craton, inferred from trace element geochemistry of stromatolitic carbonates. *Precambrian Research* **155**, 229–250.

Bouton A., Vennin E., Boulle J., Pace A., Bourillot R., Thomazo C., Brayard A., Désaubliaux G., Goslar T., Yokoyama Y., Dupraz C. and Visscher P. T. (2016) Linking the distribution of microbial deposits from the Great Salt Lake (Utah, USA) to tectonic and climatic processes. *Biogeosciences* **13**, 5511–5526.

Brecevic L. and Nielsen A.E. (1989) Solubility of amorphous calcium carbonate. *J. Cryst. Growth* **98(3)**, 504-510.

Chahi A. (1997) Textural Transition and Genetic Relationship between Precursor Stevensite and Sepiolite in Lacustrine Sediments (Jbel Rhassoul, Morocco). *Clays and Clay Minerals* **45**, 378–389.

Condie K. C. (1991) Another look at rare earth elements in shales. *Geochimica et Cosmochimica Acta* **55**, 2527–2531.

Corkeron M., Webb G. E., Moulds J. and Grey K. (2012) Discriminating stromatolite formation modes using rare earth element geochemistry: Trapping and binding versus in situ precipitation of stromatolites from the Neoproterozoic Bitter Springs Formation, Northern Territory, Australia. *Precambrian Research* **212–213**, 194–206.

Coshell L., Rosen M. R. and Mcnamara K. J. (1998) Hydromagnesite replacement of biomineralized aragonite in a new location of Holocene stromatolites, Lake Walyungup, Western Australia. *Sedimentology* **45**, 1005–1018.

Danielson A., Möller P. and Dulski P. (1992) The europium anomalies in banded iron formations and the thermal history of the oceanic crust. *Chemical Geology* **97**, 89–100.

De Baar H. J. W., German C. R., Elderfield H. and van Gaans P. (1988) Rare earth element distributions in anoxic waters of the Cariaco Trench. *Geochimica et Cosmochimica Acta* **52**, 1203–1219.

Derry L. A. and Jacobsen S. B. (1990) The chemical evolution of Precambrian seawater: Evidence from REEs in banded iron formations. *Geochimica et Cosmochimica Acta* **54**, 2965–2977.

Dickson A. G. (1981) An exact definition of total alkalinity and a procedure for the estimation of alkalinity and total inorganic carbon from titration data. *Deep Sea Research Part A. Oceanographic Research Papers* **28**, 609–623.

Dietzel M., Gussone N. and Eisenhauer A. (2004) Co-precipitation of Sr2+ and Ba2+ with aragonite by membrane diffusion of CO2 between 10 and 50 °C. *Chemical Geology* **203**, 139–151.

Dostal J. and Chatterjee A. K. (2000) Contrasting behaviour of Nb/Ta and Zr/Hf ratios in a peraluminous granitic pluton (Nova Scotia, Canada). *Chemical Geology* **163**, 207–208.

Dypvik H. and Harris N. B. (2001) Geochemical facies analysis of fine-grained siliciclastics using Th/U, Zr/Rb and (Zr+Rb)/Sr ratios. *Chemical Geology* **181**, 131–146.

Fralick P. W. and Kronberg B. I. (1997) Geochemical discrimination of elastic sedimentary rock sources. *Sedimentary Geology* **113**, 111–124.

Frimmel H. E. (2009) Trace element distribution in Neoproterozoic carbonates as palaeoenvironmental indicator. *Chemical Geology* **258**, 338–353.

Gallois A., Bosence D. and Burgess P. M. (2018) Brackish to hypersaline facies in lacustrine carbonates: Purbeck Limestone Group, Upper Jurassic–Lower Cretaceous, Wessex Basin, Dorset, UK. *Facies* **64**, 12.

Gertsch B., Keller G., Adatte T., Garg R., Prasad V., Berner Z. and Fleitmann D. (2011) Environmental effects of Deccan volcanism across the Cretaceous–Tertiary transition in Meghalaya, India. *Earth and Planetary Science Letters* **310**, 272–285.

Johannesson K. H., Telfeyan K., Chevis D. A., Rosenheim B. E. and Leybourne M. I. (2014) Rare Earth Elements in Stromatolites—1. Evidence that Modern Terrestrial Stromatolites Fractionate Rare Earth Elements During Incorporation from Ambient Waters. In *Evolution of Archean Crust and Early Life* Modern Approaches in Solid Earth Sciences. Springer, Dordrecht. pp. 385–411.

Jones B. F. and Galan E. (1988) Sepiolite and palygorskite. *Reviews in Mineralogy and Geochemistry* **19**, 631–674.

Kamber B. S. and Webb G. E. (2001) The geochemistry of late Archaean microbial carbonate: implications for ocean chemistry and continental erosion history. *Geochimica et Cosmochimica Acta* **65**, 2509–2525

Kamber B. S., Webb G. E. and Gallagher M. (2014) The rare earth element signal in Archaean microbial carbonate: information on ocean redox and biogenicity. *Journal of the Geological Society* **171**, 745–763.

Kaźmierczak J., Kempe S., Kremer B., López-García P., Moreira D. and Tavera R. (2011) Hydrochemistry and microbialites of the alkaline crater lake Alchichica, Mexico. *Facies* **57**, 543–570.

Kempe S., Kaźmierczak J., Landmann G., Konuk T., Reimer A. and Lipp A. (1991) Largest Known Microbialites

Discovered in Lake Van, Turkey. *Nature* **349**, 605–608.

Fukushi K. and Matsumiya H. (2018) Control of Water Chemistry in Alkaline Lakes: Solubility of Monohydrocalcite and Amorphous Magnesium Carbonate in $CaCl_2$ –$MgCl_2$ –Na_2CO_3 Solutions. *ACS Earth Space Chem.* **2**, 735–744.

Larsen R. B. (2002) The distribution of rare-earth elements in K-feldspar as an indicator of petrogenetic processes in granitic pegmatites: Examples from two pegmatite fields in southern Norway. *The Canadian Mineralogist* **40**, 137–152.

Leggett R. (2017) Biokinetics of yttrium and comparison with its geochemical twin holmium. *J. Radiol. Prot.* **37**, 434.

Li F., Webb G. E., Algeo T. J., Kershaw S., Lu C., Oehlert A. M., Gong Q., Pourmand A. and Tan X. (2019) Modern carbonate ooids preserve ambient aqueous REE signatures. *Chemical Geology* **509**, 163–177.

Lim D. S. S., Laval B. E., Slater G., Antoniades D., Forrest A. L., Pike W., Pieters R., Saffari M., Reid D., Schulze-Makuch D., Andersen D. and McKay C. P. (2009) Limnology of Pavilion Lake, B. C., Canada – Characterization of a microbialite forming environment. *Fundamental and Applied Limnology / Archiv für Hydrobiologie* **173**, 329–351.

Macek M., Alcocer J., Vázquez A. L., Martínez-Pérez M. E., Soriano L. P. and Fatjó G. V. (2009) Long term picoplankton dynamics in a warm-monomictic, tropical high altitude lake. *Journal of Limnology* **68**, 183–192.

Nath B. N., Kunzendorf H. and Pluger W. L. (2000) Influence of provenance, weathering, and sedimentary processes on the elemental ratios of the fine-grained fraction of the bedload sediments from the Vembanad Lake and the adjoining continental shelf, southwest coast of India. *Journal of Sedimentary Research* **70**, 1081–1094.

Olivier N. and Boyet M. (2006) Rare earth and trace elements of microbialites in Upper Jurassic coral- and sponge-microbialite reefs. *Chemical Geology* **230**, 105–123.

Parkhurst D.L. and Appelo C.A.J. (2013) Description of input and examples for PHREEQC version 3 – a computer program for speciation, batch-reaction, one-dimensional transport, and inverse geochemical calculations. U.S. geological survey techniques and methods, book 6, chap. A43, pp 497.

Plummer L. N. and Busenberg E. (1982) The solubilities of calcite, aragonite and vaterite in CO2-H2O solutions between 0 and 90°C, and an evaluation of the aqueous model for the system CaCO3-CO2-H2O. *Geochimica et Cosmochimica Acta* **46**, 1011–1040.

Pourmand A., Dauphas N. and Ireland T. J. (2012) A novel extraction chromatography and MC-ICP-MS technique for rapid analysis of REE, Sc and Y: Revising CI-chondrite and Post-Archean Australian Shale (PAAS) abundances. *Chemical Geology* **291**, 38–54.

Qu C., Liu G. and Zhao Y. (2009) Experimental study on the fractionation of yttrium from holmium during the coprecipitation with calcium carbonates in seawater solutions. *Geochemical Journal* **43**, 403–414.

Robie R. A., and Hemingway B. S., (1973) The enthalpies of formation of nesquehonite, MgCO3-3HA and hydromagnesite, 5MgO.4CO2 -5H2O. *U. S. Geological Survey Journal of Research*, **1, 5**, 543-547.

Salminen R., Batista M.J., Bidovec M. et al. (2005) Geochemical atlas of Europe. Part 1: Background information methodology and maps. Geological Survey of Finland. http://www.weppi.gtk.fi/publ/foregsatlas/index.php.

Sarg J. F., Suriamin N., TÌnavsuu-Milkeviciene K. and Humphrey J. D. (2013) Lithofacies, stable isotopic composition, and stratigraphic evolution of microbial and associated carbonates, Green River Formation

(Eocene), Piceance Basin, Colorado. *AAPG Bulletin* **97**, 1937–1966.

Shen, V.K., Siderius, D.W., Krekelberg, W.P., and Hatch, H.W., Eds., NIST Standard Reference Simulation Website, NIST Standard Reference Database Number 173, National Institute of Standards and Technology, Gaithersburg MD, 20899, http://doi.org/10.18434/T4M88Q

Smrzka D., Zwicker J., Bach W., Feng D., Himmler T., Chen D. and Peckmann J. (2019) The behavior of trace elements in seawater, sedimentary pore water, and their incorporation into carbonate minerals: a review. *Facies* **65**, 41.

Solari M. A., Hervé F., Le Roux J. P., Airo A. and Sial A. N. (2010) Paleoclimatic significance of lacustrine microbialites: A stable isotope case study of two lakes at Torres del Paine, southern Chile. *Palaeogeography, Palaeoclimatology, Palaeoecology* **297**, 70–82.

Stoessell R. K. (1988) 25°C and 1 atm dissolution experiments of sepiolite and kerolite. *Geochimica et Cosmochimica Acta* **52**, 365–374.

Takahashi Y., Châtellier X., Hattori K. H., Kato K. and Fortin D. (2005) Adsorption of rare earth elements onto bacterial cell walls and its implication for REE sorption onto natural microbial mats. *Chemical Geology* **219**, 53–67.

Takahashi Y., Hirata T., Shimizu H., Ozaki T. and Fortin D. (2007) A rare earth element signature of bacteria in natural waters? *Chemical Geology* **244**, 569–583.

Testemale D., Dufaud F., Martinez I., Bénézeth P., Hazemann J.-L., Schott J. and Guyot F. (2009) An X-ray absorption study of the dissolution of siderite at 300 bar between 50 °C and 100 °C. *Chemical Geology* **259**, 8–16.

Thompson G. and Livingston H. D. (1970) Strontium and uranium concentrations in aragonite precipitated by some modern corals. *Earth and Planetary Science Letters* **8**, 439–442.

Warden J. G., Coshell L., Rosen M. R., Breecker D. O., Ruthrof K. X. and Omelon C. R. (2019) The importance of groundwater flow to the formation of modern thrombolitic microbialites. *Geobiology* **17**, 536–550.

Weaver C. E. (1967) Potassium, illite and the ocean. *Geochimica et Cosmochimica Acta* **31**, 2181–2196.

Webb G. E. and Kamber B. S. (2000) Rare earth elements in Holocene reefal microbialites: a new shallow seawater proxy. *Geochimica et Cosmochimica Acta* **64**, 1557–1565.

Wollast R., Mackenzie F. T. and Bricker O. P. (1968) Experimental Precipitation and Genesis of Sepiolite at Earth-Surface Conditions. *Am. Miner.* **53**, 1645–1661.

Zeyen N., Benzerara K., Menguy N., Brest J., Templeton A. S., Webb S. M., Gérard E., Moreira D., López-García P., Tavera R. and Morin G. (2019) Fe-bearing phases in modern lacustrine microbialites from Mexico. *Geochimica et Cosmochimica Acta* **253**, 201–230.

Zhang J. and Nozaki Y. (1996) Rare earth elements and yttrium in seawater: ICP-MS determinations in the East Caroline, Coral Sea, and South Fiji basins of the western South Pacific Ocean. *Geochimica et Cosmochimica Acta* **60**, 4631–4644.

Zhao M.-Y. and Zheng Y.-F. (2017) A geochemical framework for retrieving the linked depositional and diagenetic histories of marine carbonates. *Earth and Planetary Science Letters* **460**, 213–221.